Assessing uplift displacement of buried geotechnical structures in liquefied ground during earthquakes

GiChun KANG

Assessing uplift displacement of buried geotechnical structures in liquefied ground during earthquakes

By

GiChun KANG

A thesis submitted for the Degree of Doctor of Engineering
at the Kyoto University

Graduate School of Engineering,
Department of Civil and Earth Resources Engineering
Kyoto University
Kyoto, Japan
February 2010

Abstract

Uplift phenomenon of buried geotechnical structures in liquefied ground has been reported frequently since the 1964 Niigata, Japan, earthquake. After the 2004 Niigata-ken Chuetsu, Japan, earthquake, more than 1,400 manholes were uplifted. Uplifted manholes can be a serious matter because they not only hinder the flow of sewerage systems, as part of lifeline systems, but also disturb traffic flows. Many studies on the uplifting of buried geotechnical structures have been conducted through field investigations, small scale model tests and numerical analyses. Despite intensive research efforts in geotechnical earthquake engineering, practical methods to predict the phenomena and estimate the uplift amount of buried geotechnical structures in liquefied ground have not been established yet. Among the recent researches, the safety factor approach for uplifting is a great accomplishment (Koseki et al., 1997a) and it is currently used in design practice (JRA, 1986). However, factors of the study approach do not give a quantitative estimation of uplift displacement.

The present research is focused on establishing a practical method to assess displacement of manhole uplifts. Firstly, centrifuge studies are conducted to study the mechanisms of uplift behavior and investigate factors affecting the manhole uplift. These test results not only explain the mechanism of the uplift phenomenon but also elucidate that the uplift of the manholes is related to an increase of EPWPR (Excess Pore Water Pressure Ratio) in backfill, and other factors as follows: amplitude of input accelerations, ground water level, relative density of backfill, number of load cycles, manhole length, volume of excavated trench, apparent unit weight of a manhole, soil condition of native ground, and contact condition between the bottom of a manhole and trench.

Secondly, a simplified method is proposed to estimate the uplift displacement of a manhole

and settlement of backfill due to liquefaction. The method is based on the equilibrium of forces acting on a manhole under assumption of no volume change or continuity of liquefied backfill. The validity of the simplified method is examined through the results obtained from the centrifuge model tests. Also, time histories of uplift displacement are simulated by the simplified method using the EPWP measured in centrifuge tests as a component of uplift force acting on a manhole. Test results are confined within the boundary predicted by the simplified method, and this validates the effectiveness of the method. However, the predicted uplift displacement by the simplified method is the maximum uplift displacement and the method is incapable of predicting transient behavior during shaking.

To overcome the limitation of the simplified method, the two dimensional finite element analyses, as a detailed method based on the multiple shear mechanism for soil, are carried out and the results are compared with the centrifuge test data. The numerical analysis is conducted for test cases in which the manhole uplift did not reach the maximum amount and was then overestimated by the simplified method. The computed uplift displacements were consistent with that measured in the centrifuge model tests. However, uplift displacement computed by the numerical analysis is considerably underestimated when the manhole uplift in liquefied ground reached the maximum amount and was consistent with ones predicted by the simplified method. It indicates that the numerical approach is capable within the limit of small uplift displacements.

Then, the methods are applied to the case history data obtained by the Nagaoka city government after the 2004 Niigata-ken Chuetsu, Japan, earthquake to verify the applicability. In the beginning, the database which contains uplift displacement of manholes, location of the manholes, SPT borehole logs and location of SPT borehole is developed. Based on the database, the relationship between uplift displacement and ground water table as a primary

factor is investigated. Then, the simplified and detailed methods are applied to the relationship of the uplifted manholes and ground water table. The results are in good agreement. Also, relationship between uplift displacement and native subsoil material near the ground surface as a secondary factor are investigated through correlation analysis. The secondary factors considered in the investigation are thickness of clay material, SPT blow counts for sand layers and thickness of surface soil. From the correlation analysis, the native subsoil material is found to be related to the uplift amount of the manhole.

Then, based on the results obtained in the present research, it is found that reduction of EPWP is the key to reduce the uplift displacement of a manhole. Therefore, in the final chapter, the effectiveness of the EPWP reduction device as a mitigation measures against uplift is investigated and validated through the centrifuge studies. The performance based on design procedure using the proposed simplified method is also proposed as an application derived from this research activities.

Key words: uplift phenomenon, buried geotechnical structures, liquefied ground, centrifuge studies, primary factor, secondary factor, EPWPR, simplified and detailed method, case history, mitigation measures, and design procedure

Acknowledgments

This dissertation would have never been completed without the support and encouragement from my dear professors and colleagues, to whom I would like to express my gratitude.

First of all, I would like to express my sincere gratitude to my supervisor Professor Susumu Iai and Assistant Professor Tetsuo Tobita for providing excellent guidance for this research and throughout my study at the Kyoto University. Without their guidance and support based on their deep insight and experience in the field, the author would never have been able to finish this dissertation. Their invaluable advice and various teachings were always inspiring me. These memories will always be kept in my mind.

I also wish to thank Professor Fusao Oka and Professor Makoto Kimura for their critical review of the manuscript and constructive suggestions and active discussions as committee members for my doctoral degree. I would like to express my thanks to Yasuhiko Konishi and his staff at Nihon Suido Consultants, Co. Ltd. for their cooperation in providing significant data and information. I want to thank the members of Iai Lab. for their support and friendship; Mamoru Mimura, Associate Professor, Hiroki Shimizu and Kazuhide Tomisaka, Technicians, Waka Yuyama, Secretary, and all students. I received a lot of help and advice from them. I wish to thank Associate Professor T.-H. Kim of the Korea Maritime University for his encouragement and for his helpful comments. He gave me the opportunity to study at Kyoto University.

Last, but not least, I would like to specially dedicate this dissertation to my parents. It is not easy to express the tremendous amount of love and considering that they have given me. Also, I would like to dedicate this dissertation to my brother, sister and my soon to be wife, J.H. Park, for their great support, encouragement and their belief for me.

Table of Contents

List of Figures

List of Tables

1. Introduction

1.1 Background

When the ground is subjected to strong shaking during an earthquake, liquefaction and subsequent ground settlements and/or flow failures which involve extremely large movements of soil masses, may cause serious damage to civil/geotechnical infrastructures. Among those infrastructures, lifeline systems buried underground, such as common utility conduits and sewage systems, are vulnerable to medium to large ground movements. The geotechnical structures buried near the ground surface have a wide range of applications, from small scale pipelines such as means of gas transmission, telecommunications, water supply, and sewerage pipelines, to large scale structures including tunnels for various transportation systems. Serious damage on small scale buried pipelines was observed as early as 1964 in the Niigata, Japan, earthquake and the Alaska, USA, earthquake (Hall and O'Rourke, 1991). Uplift failure of underground oil tanks and wastewater purification tanks were observed after the 1983 Nihonkai-Chubu, Japan, earthquake (Taniguchi and Morishita, 1985), the 1990 Philippine, Luzon earthquake (Hamada, 1991) and 1993 Hokkaido-nasei-oki earthquake (Tokimatsu et al., 1994). A number of concrete sewer pipes suffered longitudinal cracking, and PVC sewer pipes were crushed by a strong seismic motion in Nishinomiya during the 1995 Hyogoken Nanbu, Japan, earthquake (Tohda, 1996). Damage to large underground structures have been reported, for example, the collapse of the Daikai subway station in Kobe after the 1995 Hyogoken Nanbu, Japan, earthquake (Tajimi, 1996), damage to the mountain tunnels in central Taiwan after the 1999 Chi-Chi, Taiwan, earthquake (Wang et al., 2001), and the severe collapse of a highway tunnel after the 1999 Duzce, Turkey, earthquake (O'Rourke et al., 2001), damage to

large underground structures during the 1976 Tangshan, China, earthquake (Wang, 1985) and the 1989 Loma Prieta, USA, earthquake (Schmidt and Hashash, 1998; O'Rourke et al., 1991) has also been reported.

Among the above mentioned buried geotechnical structures, damage to lifeline systems, such as sewage pipes and manholes, buried in liquefiable soil had a severe impact on residents in the affected areas. For example, after the 1995 Hyogoken Nanbu, Japan, earthquake, restoration work to water supply systems took about 10 weeks until full recovery, for gas service about 12 weeks, and for sewerage systems about 15 weeks (Cabinet Office, 2006). Severe damage to sewerage systems had been reported after the 1964 Niigata, Japan, earthquake (OKamoto, 1984). However, at the time, the sewerage treatment systems covered only about 37% of the residential areas in Japan (Konishi et al., 2008), therefore, it might not have been counted as a major problem. In 2006, however, the coverage rate of sewerage treatment systems in Japan has increased on average to 69.3% (JSWA, 2009).

A typical and striking damage pattern on sewerage systems after large earthquakes is uplift of manholes (Fig. 1.1). Ejected manholes block up not only the flow of sewage water but also the traffic flows. About 20 sewerage manholes, whose maximum uplift displacement was about 1.5 m from the ground surface, were uplifted in the 1993 Kushiro-oki, Japan, earthquake (Yasuda and Kiku, 2006; Konishi et al., 2008). In the 1993 Hokkaido-nansei-oki, Japan, earthquake, 55 manholes were uplifted from 10 to 57 cm (JGS, 1997). In the 1994 Hokaido-toho-oki, Japan, earthquake, uplifts of sewerage manholes in several cities were reported (Yasuda and Kiku, 2006). Uplifted sewerage manholes after the 2004 Niigata-ken Chuetsu, Japan, earthquake counted more than 1,400 with maximum uplift displacement of more than 1 m from the ground surface (Fig 1.1) (Yasuda and Kiku, 2006; Konishi et al., 2008). After the earthquake, mitigation of damage on sewerage treatment systems has

recognized as an important societal issue and the Ministry of Land Infrastructure and Transport set up the technical committee to investigate the mechanism of the damage and to select appropriate restoration work (Technical Committee on the Sewer Earthquake Countermeasure, 2005).

Liquefaction of backfill materials in a trench appears to be a major cause of manhole uplifting (Koseki et al., 1997a; Koseki et al., 1997b; Koseki et al., 1998; Yasuda and Kiku, 2006). Figure 1.2(a) shows a typical cross section of a manhole and trench before being hit by large earthquakes. The construction process of sewage manholes and pipes in Japan are as follows: (1) Surface ground is excavated with sheet piles or retaining walls, (2) Manholes and pipes are placed at the bottom of the trench, (3) The trench is backfilled with sandy materials taken from nearby river beds and/or mountains. Due to liquefaction of backfill materials by an earthquake, the manhole system was damaged. Figure 1.2(b) shows schematic view of damage patterns, i.e., uplift of manhole, settlement of backfill, pipe breaks, settlement of pavements near the manhole and along buried pipes, and inward-deformation of trench walls.

Numbers of mitigation measures against manhole uplift for newly constructed ones have been proposed and have already been implemented practically. Mechanisms behind those mitigation measures are to prevent liquefaction by compacting backfill material (Yasuda, 2003), improving backfill material with cement mixed soil (Ishinabe et al., 1999; Yasuda et al., 2001), or to prevent excess pore pressure build-up by leading pressured pore water through valves attached on the side wall of a manhole (Matsushima el at., 2007). Other types of mitigation measures for newly installed manholes are, for example, using soil-bags with backfill (Yoshida et al, 2006), or attaching whoops on a perimeter of a manhole to prevent movements of liquefied soils under a manhole (Kiku et al., 2007). Those mitigation measures proved to be effective after the 2007 Niigataken Chuetsu-oki, Japan, earthquake (Morii and

Nishino, 2008; JGS, 2009).

Development of mitigation measures against uplift for existing manholes is still a remaining and challenging issue. Here, we encounter two major problems: One is the lack of a method to decide which manholes are susceptible to uplifting and require mitigation (economical problem), and the other is how and what type of mitigation measures are to be implemented (technical problem). Seismic guideline (Seismic guidance for mitigation measures against damage to sewerage facilities) (JSWA, 2006) suggests that all the backfill material judged as susceptible to liquefy must be properly treated against liquefaction. However, considering the costs, it may not be a realistic approach. The present study aims to develop and give direction to this issue.

Fig. 1.1 Uplifted manholes and settlements of sidewalk after the 2004 Niigata-ken Chuetsu, Japan, earthquake.

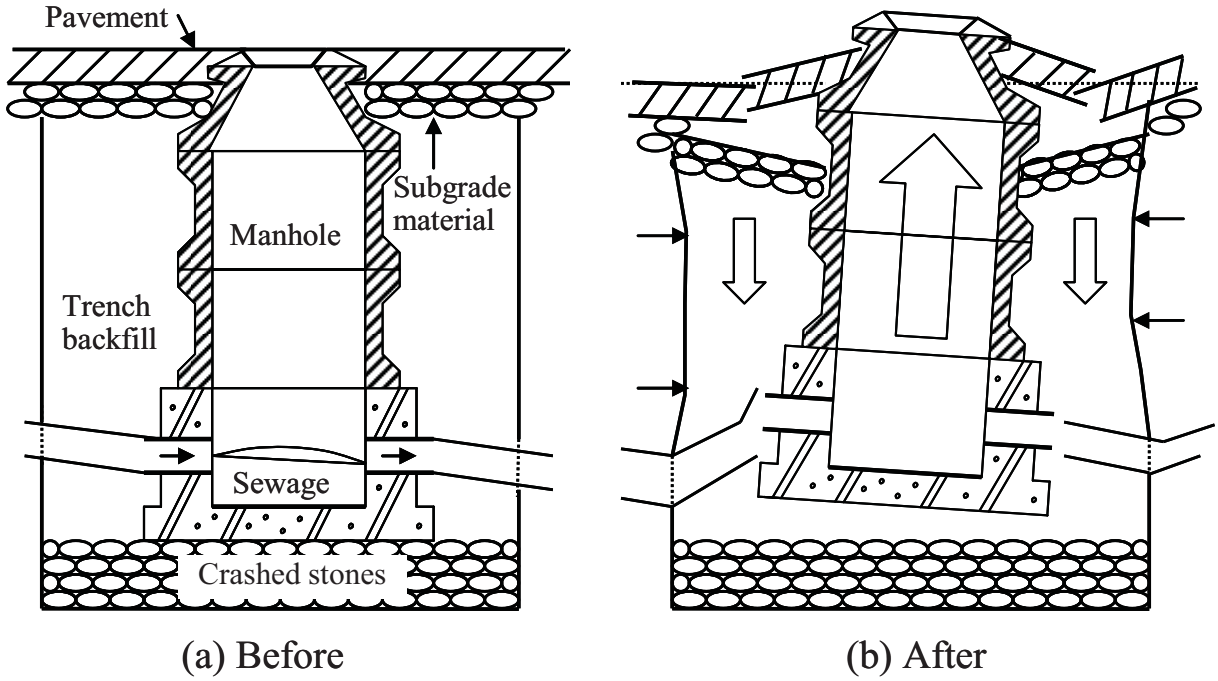

Fig. 1.2 Schematic illustrations of a manhole and trench: (a) before and (b) after being hit by large earthquake.

1.2 Previous researches

The problems of liquefaction received much attention among the geotechnical community and civil engineers after the devastating damage caused by liquefaction during the 1964 Niigata and Alaska earthquakes. Since then, much effort has been made to study the basic mechanism and various aspects of the phenomena and associated problems. Undrained behavior of cohesionless soil under cyclic loadings, or soil liquefaction, has become an active area of research for more than 40 years (Ishihara, 1993). The onset condition of liquefaction was defined and the method of liquefaction analysis has been developed with the accumulation of laboratory and field data (Seed and Idriss, 1971). The volume-change characteristics of sand due to drainage of pore water, which is induced by undrained cyclic loadings, have been studied in laboratory tests (Lee and Albaisa, 1974; Martin, et al., 1975; Tatsuoka et al., 1984;

Nagase and Ishihara, 1988).

Based on these studies, practical methods to estimate the liquefaction-induced settlements of the ground surface were developed (Tokimatsu and Seed, 1987l; Ishihara and Yoshimine, 1992). Mechanism of liquefaction-induced flow failure has been studied with a wealth of field data (O'Rourke and Hamada, 1992) and laboratory experiments focusing on the measurements of residual shear strength (Yasuda et al., 1999). However, estimation of the amount of liquefaction-induced flow has yet been implemented in design practice (Bartlett and Youd, 1995; Bardet et al., 2002). With the advance of computer technologies in the last 40 years, a number of numerical methods based on the mechanics of continuum body to simulate dynamic ground motions under the liquefaction phenomena have been proposed and applied to the simulation of the phenomena with much more complex geometries (Martin et al., 1975; Ishihara and Towhata, 1980; Iai et al., 1992ab; Oka et al., 1999; Yasuda et al., 1999; Elgamal et al., 2003).

With the development of liquefaction studies, large numbers of case histories of damage to underground facilities after large earthquakes have been documented (Duke and Leeds, 1959; Stevens, 1977; Dowding and Rozen, 1978; Owen and Scholl, 1981; Sharma and Judd, 1991; Power et al., 1998; Kaneshiro et al., 2000; JGS, 1994; JGS, 1997 and JGS, 1998). For example, ASCE (1974) reported the damage to water and gas supply, sewer pipeline, channels, etc. in the Los Angeles area after the 1971 San Fernando earthquake, and JSCE (1988) introduced the performance of several underground structures, including an immersed tube tunnel during strong shaking in Japan. Owen and Scholl (1981) updated Dowding and Rozen's (1978) work with 127 case histories of large underground structures such as tunnels. Sharma and Judd (1991) generated an extensive database of seismic damage to underground structures using 192 case histories which confirmed that underground structures suffer appreciably less damage

than surface structures. Power et al. (1998) provided a further update with 217 case histories through statistical studies to correlate the damage level with various seismological parameters, such as magnitude, seismic intensity, epicentral distance or maximum acceleration at ground surface.

Studies on uplifting of buried geotechnical structures have been started by field investigations (Koseki et al., 1997b; KiKu et al., 2004; Yasuda, 2005; Yasuda and Kiku, 2006; Yasuda et al., 2009). Then, experimental studies (Yasuda et al., 1995; Koseki et al., 1997a, Koseki et al., 1998; Orense, et al., 2003; Ling et al., 2003; Iai et al., 2005; Kiku et al., 2007; Cheuk et al., 2008) and analytical and numerical analyses (Wang et al., 1990; Iai and Matsunaga, 1991; Nishio, 1994; JGS, 2003; Ozutsumi, et al., 2003; Venden Berghe et al., 2005; Tateishi et al., 2009; Uno et al., 2009) have been intensively conducted by focusing on the cause of damage and the mechanism of uplift behavior of buried structures due to earthquake-induced liquefaction. Many model tests have been conducted to investigate uplift resistance and the corresponding failure mechanisms (Trautmann et al. 1985; Ng and Springman, 1994; Mohri, 2000; Bransby et al. 2001; White et al. 2001; Chin et al. 2006). Ichii et al. (2008) studied the uplift velocity of buried structures in liquefied ground through a series of shaking table tests to investigate the relationship of the final uplift magnitude and uplift velocity based on the fact that uplift velocity was almost constant in previous model tests. The results revealed the uplift velocity in various soils is dependent on the soil characteristics; especially the effect of fines contents.

The relationships among uplift displacement, amplitude of input motion, thickness of liquefiable layer, and the relative density of soils were studied by Sasaki and Tamura (2002) through centrifuge model tests. They proposed a simplified method to predict uplift displacement of underground structures, in which liquefied soil behaves like a high viscous

liquid. The analytical model consists of the mass of the structure and overburden soil above the structure, buoyant force acting on the structure, and the resistance force from liquefied soil proportional to uplift velocity. The uplift displacement in the analytical model absolutely depends on the empirical parameter (C) which is determined by fitting a series of centrifuge test results as follows:

$$C = 18000(b / h_b)^{1.5}(\rho_{sat} / \rho_m)R^{0.5}F_L \quad (1)$$

where C is resistance coefficient, b is width of structure, ρ_{sat} is density of saturated soil, ρ_m is density of the structure, R is cyclic shear resistance ratio, F_L is liquefaction resistance ratio and h_b is distance from the bottom of structure to the bottom of liquefiable layer.

It is significantly difficult to properly express physical and mechanical properties of soils in the method proposed by Sasaki and Tamura (2002), because the empirical relationship between resistance coefficient, C, and some factors as mentioned above, is a major factor in the proposed method. Also, this empirical relationship has not yet been established to estimate the uplift displacement. Therefore, the results show that sometimes the predicted uplift displacements were 100% smaller or lager than those measured in model tests, and thus it is difficult to predict the uplift displacements in practice due to the critical drawback.

The safety factor approach for uplifting has been developed (Koseki et al., 1997b) and recommended its use in design practice (JRA, 1986). This safety factor is defined based on the equilibrium of vertical forces acting on a manhole, which can be used to evaluate whether the uplift is triggered or not. It is expressed as follows,

$$Fs = \frac{M + R}{U + H} \quad (2)$$

$$U = A \cdot r_u \cdot \sigma'_v \quad (3)$$

$$r_u = F_L^{-p} \quad \text{(if } F_L<1.0 \text{ then } r_u=1\text{)} \quad (4)$$

where, H is the buoyant force due to hydrostatic pressure, R is the frictional resistance force between the side wall of a manhole and backfill. Upon evaluating the frictional force R, the perimeter which is shallower than the ground water level shall be considered, U is the uplift force due to excess pore water pressure caused by liquefaction, M is the mass of a manhole, A is the cross-sectional area of a manhole in the horizontal plane, r_u is the excess pore water pressure ratio, σ_v' is the effective overburden pressure in backfill at the same depth as the bottom of a manhole, F_L is the liquefaction resistance ratio averaged over the depth of a manhole, p is the parameter representing the characteristics of excess pore water pressure generation. Koseki, et al. (1997b) evaluated the uplift behavior by varying the values of the following parameters; Ground water level, excess pore water pressure ratio, the relative density of backfill, and manhole size and material. Among these factors, excess pore water pressure ratio (r_u) is identified as one of the important factors affecting the uplift.

Small scale model tests, numerical studies, and the factor of safety approach thus far have been successfully predicting the triggering of uplift and used widely in practice. However, a method for "quantitative" estimates of the uplift displacements has yet to be established.

1.3 Objectives

The objective of the study is to assess the uplift behavior of geotechnical structures buried near to the ground surface under strong shaking due to large earthquakes. Considering the importance of lifeline facilities, the uplift behaviour of sewerage manholes is investigated in detail through centrifuge studies, numerical analysis, and case histories. Also, a new practical method to predict uplift displacement of a manhole and surface settlements of backfill is developed and validated in the course of the investigation. The basic principal of the proposed method is the same as the evaluation of uplift stability by Koseki, et al. (1997b), and uplift

displacement by proposed simplified method can be estimated by adding an assumption to the method of Koseki, et al. (1997b), which is the volume of the uplifted portion of the manhole above the ground surface is equal to the volume of settled amount measured from the ground surface of backfill. With this simple method, the maximum amount of uplifts can be computed for arbitrary dimensions of a manhole and trench size, and soil properties of backfill material. A performance-based design procedure using the method is proposed as a practical application. One of the drawbacks of this simple method is that, as it gives only the maximum amount of uplifts and settlements, it is incapable of predicting transient behaviors during shaking. To study the transient motions, numerical analysis using the finite element method is conducted in detail with the parameters applied in the centrifuge tests. To validate the application of the methods, they are compared with the field investigation data in Nagaoka city, Niigata Prefecture, Japan. The data has been collected after the 2004 Niigataken Chuetsu, Japan, earthquake. The database, which contains depths of original and disturbed sewerage pipes and manholes and their locations as well as the SPT borehole information, is developed and used intensively to investigate causes of damage to sewerage systems.

1.4 Organization

This thesis is composed of 7 chapters starting from Chapter one as an introduction. Figure 1.3 shows contents and flow of this research.

The geotechnical centrifuge model tests are conducted in Chapter 2 to study the mechanism of the uplift phenomenon and derive the relationship between uplift displacement and some factors affecting the uplift behavior. Factors considered in the experiments are ground water levels, magnitude of input accelerations and number of the load cycles, relative densities of backfill, manhole length, volume of a trench, apparent unit weight of a manhole,

soil conditions of native ground, and soil conditions under manholes.

In Chapter 3, the simplified method based on the equilibrium of forces acting on a manhole under assumption of continuity of liquefied backfill is proposed to estimate the maximum uplift displacements of a manhole and surface settlements of backfill due to liquefied backfill. As a preliminary study, the simplified method is validated through comparisons with the uplift displacement of a well-controlled model tests by using the boiling method. Quantitative relationships between uplift displacement and associated parameters are established by the simplified method. Here the following parameters are considered in relation to the uplifts; the thickness of the non-liquefied layer above the ground water table, excess pore water pressure ratio, unit weight of backfill, and size of the trench. Validity of the simplified method is also examined through the results obtained from the centrifuge model tests. To extend applicability of the method, time histories of uplift displacement are reproduced by substituting the time histories of excess pore water pressure measured in the centrifuge model tests into the model.

To overcome the limitation of the simplified method, in Chapter 4, the two dimensional finite element analyses based on the multiple shear mechanism for soil are performed and the results are compared with the centrifuge test data. The analyses conducted for manhole uplifts in dense backfill (non-liquefiable) and under small amplitudes of input acceleration, whose uplift displacements are overestimated by the simplified method because the manhole does not reach the maximum amount in the centrifuge model tests. Also to investigate the applicability, the numerical analyses are conducted for the saturated backfill whose ground water table coincides with the ground surface.

In Chapter 5, the database which contains the uplift displacement of manholes, location of the manholes, the SPT borehole logs and their locations, is developed from the results of the open-cut surveys conducted by the Nagaoka city government after the 2004 Niigata-ken

Chuetsu, Japan, earthquake. Then, with the database, factors affecting manhole's uplift are investigated. The factors considered in the investigation are ground water table, thickness of clay material, the SPT blow counts for sand layers and thickness of surface soil. Relationships found between the uplift displacements and associated parameters significantly agree with those found in the centrifuge model tests. Then, the methods for prediction of uplift amount are applied to the case history data to see its effectiveness of predicting the real uplift displacements.

Practical applications are discussed in Chapter 6. Based on the results obtained in the present research, it is found that reduction of excess pore water pressure is the key to reduce the uplift displacement of a manhole. Therefore, the effectiveness of the device which reduces excess pore water pressure is investigated and validated through the centrifuge studies. Also, the performance-based design procedure with the simplified method is proposed as an application derived from this research activities.

Finally, conclusions of the dissertation are given in Chapter 7.

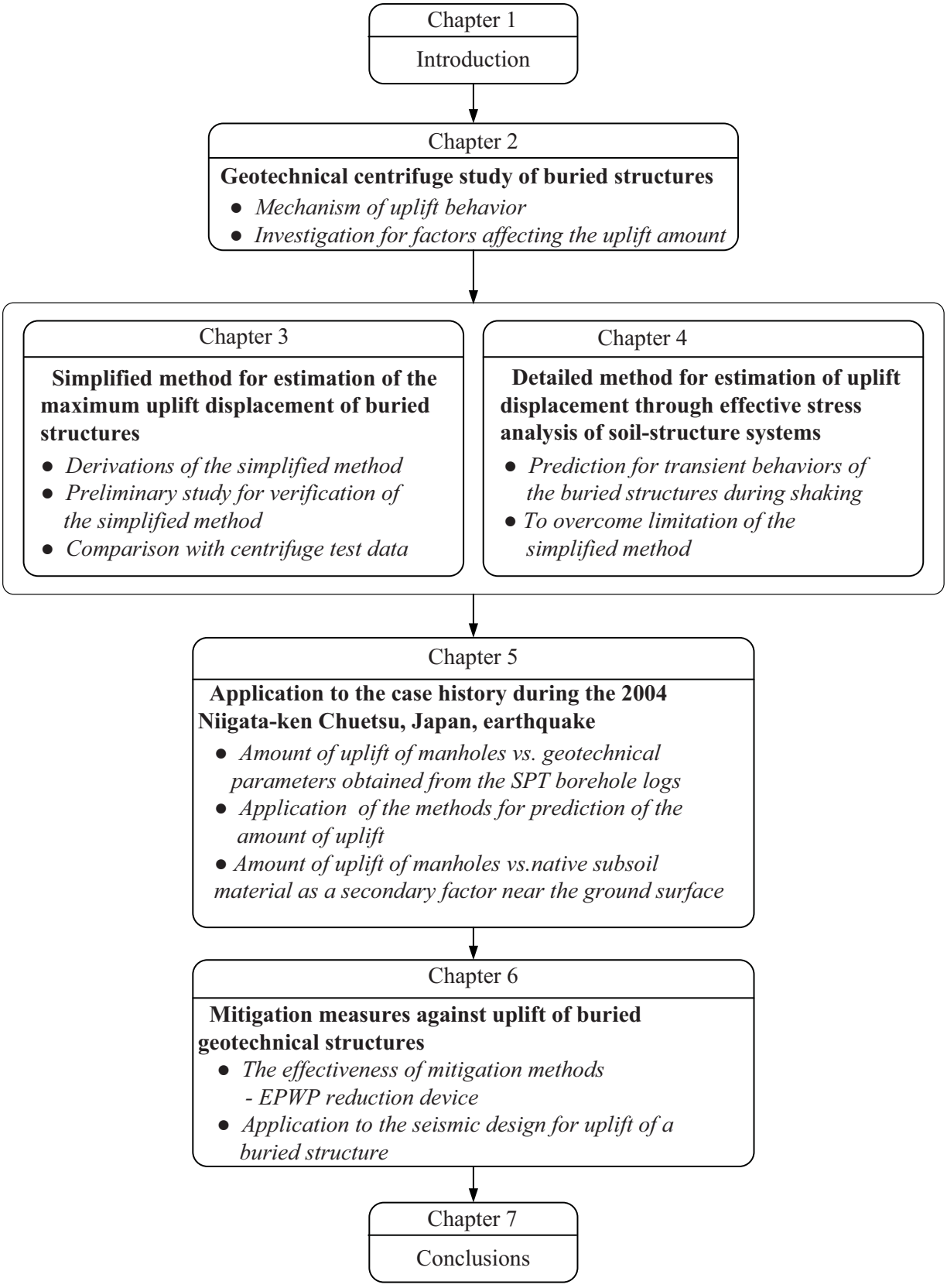

Fig. 1.3 Research framework.

2. Centrifuge studies on uplift mechanism of buried structures in liquefiable soil

2.1 Introduction

A Geotechnical centrifuge has been widely used to perform small-scale model tests of geotechnical structures. In reduced scale, it is able to reproduce the same level of an effective confining stress with a prototype ground. Therefore, the stress-strain response of the prototype ground can be simulated with more accuracy than that of 1 G model tests.

A series of centrifuge tests is conducted to study the uplift mechanism of buried geotechnical structures in liquefied ground. All the tests are conducted with the centrifugal acceleration of 20 G. The scaling law for the centrifuge tests for N G is summarized in Table 2.1.

Table 2.1 Scaling law for the centrifuge tests for N G.

Quantity	Scaling factor (prototype/model)
Length	N
Density	1
Time	N
Frequency	1/N
Acceleration	1/N
Velosity	1
Displacment	N
Stress	1
Strain	1
Stiffness	1
Permeability	N
Pore pressure	1
Fluid pressure	1
EI	N^4
EA	N^2
Bending moment	N^3
Shear	N^2
Axial force	N^2

In terms of the uplift behavior, the effects of excess pore water pressure in the backfill are thought to be one of the most influential parameters (Koseki et al., 1997a, Koseki et al., 1997b, Yasuda and Kiku, 2006). By taking into account the results of previous researches, factors considered in the centrifuge model tests are determined as follows: (1) depth of ground water table, (2) amplitude of input acceleration and number of load cycles, (3) relative density of backfill, (4) apparent unit weight of manhole, (5) manhole length, (6) a cross-sectional area of a trench, (7) condition of native ground and (8) contact condition between the bottom of a manhole and trench. Among these factors, (1) ~ (6) are directly affecting the uplift behavior as a primary factor and (7) and (8) are indirectly affecting the uplift behavior as a secondary factor. To evaluate effectiveness of mitigation measures against uplift which will be discussed in a later chapter, a model manhole with some sort of mitigation measures is shaken simultaneously with normal model manhole (no mitigation measures) which is mainly discussed in this chapter.

2.2 Centrifuge facility in the Disaster Prevention Research Institute, Kyoto University

The geotechnical centrifuge at the Disaster Prevention Research Institute, Kyoto University (DPRI-KU), is employed for a series of tests described in this chapter. The model is scaled down to 1/20. Thus, applied centrifugal acceleration is 20 G (Table 2.1). Figure 2.1 shows the schematic view of the centrifuge facility. It has an in-flight platform radius of 2.5m and a capacity of 24 G-ton. It is equipped with one-dimensional shake table (allowable displacement: ±5 mm) which is operable under the centrifugal accelerations of up to 50 G. It is unidirectionally driven by a servo hydraulic actuator and it is controlled through a laptop

personal computer (PC) on the centrifuge arm. The PC is fixed near to the rotation axis of the centrifuge to minimize the centrifugal force acting on it. It is connected to another PC in the control room by wireless LAN. Another system which controls the data loggers attached on the arm is accessible from another PC in the control room. Counter weight is loaded on the other side of the arm to keep balance during rotation. By the CCD camera mounted on the swinging arm, the lateral side of the model can be monitored through transparent grass wall of the sand box.

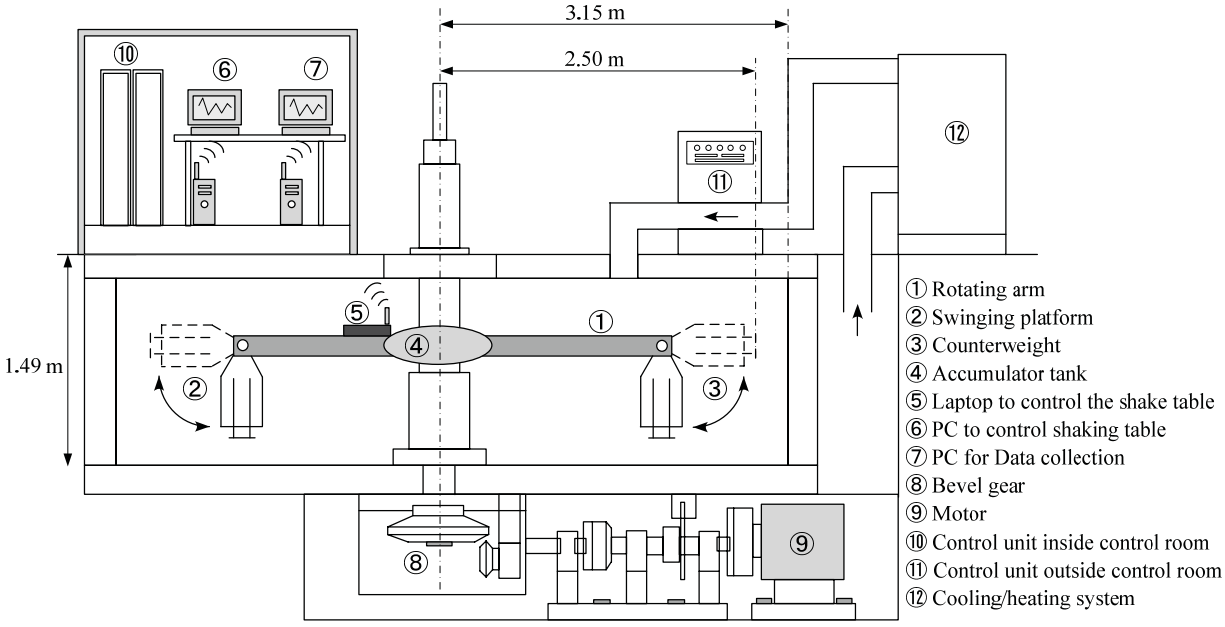

Fig. 2.1 Schematic view for centrifuge facility at the Disaster Prevention Research Institute, Kyoto University (DPRI-KU).

2.3 Model construction procedure

2.3.1 Details of the model manhole with/without mitigation measures

Target manhole, a typical example of a modern manhole in Japan, is the standard No. 1 manhole used (JSWA, 2001) which is made of a hollow cylindrical reinforced concrete (Fig.

2.2). It consists of 5 parts: cap, cylindrical part with inclined wall, vertical wall, body and base slab. Apparent unit weight of the model manhole made of aluminum is taken to be 9.57 kN/m^3, which is slightly larger than that of the standard No.1 manhole shown in Fig. 2.2, 8.25 kN/m^3 (Table 2.2).

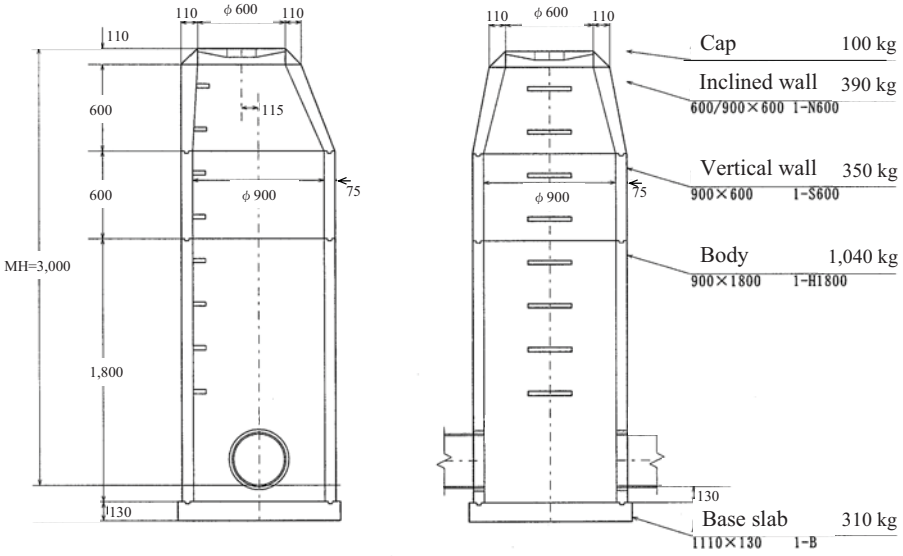

Fig. 2.2 Cross section of the standard No. 1 Manhole (JSWA 2001).

Table 2.2 Model manhole properties.

Aluminum	Unit weight	γ_a	26.5 kN/m^3
Model Manhole	Length		3 m
	Diameter		1.1 m
	Wall thickness		0.1 m
	Mass of sensors installed with manhole		0.67 kN
	Mass of base slab		1.7 kN
	Total weight		27.3 kN
	Volume		2.85 m^3
	Apparent unit weight	γ_m	9.57 kN/m^3
Reinforced concrete	Unit weight	γ_c	23.5 kN/m^3
No.1 Manhole	Length		3 m
	Diameter		1.05 m
	Wall thickness		0.08 m
	Cap		0.92 kN
	Mass of base slab		3.43 kN
	Total weight		20.6 kN
	Volume		2.49 m^3
	Apparent unit weight	γ_m	8.25 kN/m^3

Four types of the manholes (two not equipped with mitigation measures, and two with mitigation measures), which are scaled down to a twentieth of the standard No. 1 manhole (JSWA. 2001), are used in the centrifuge model tests. Figure 2.3 shows the model manholes with and without the mitigation device against uplift behavior used in the tests. The models are with an outer diameter of 55 mm, length of 100 and 150 mm, and a wall thickness of 5 mm in model scale. They are nominally named Model No. 1 to 4 as shown in Fig. 2.3(a) – (d). Model No. 1 is a long manhole (150 mm) and Model No. 2 and 3 are with a mitigation device. Model No.4 is a short manhole (100 mm).

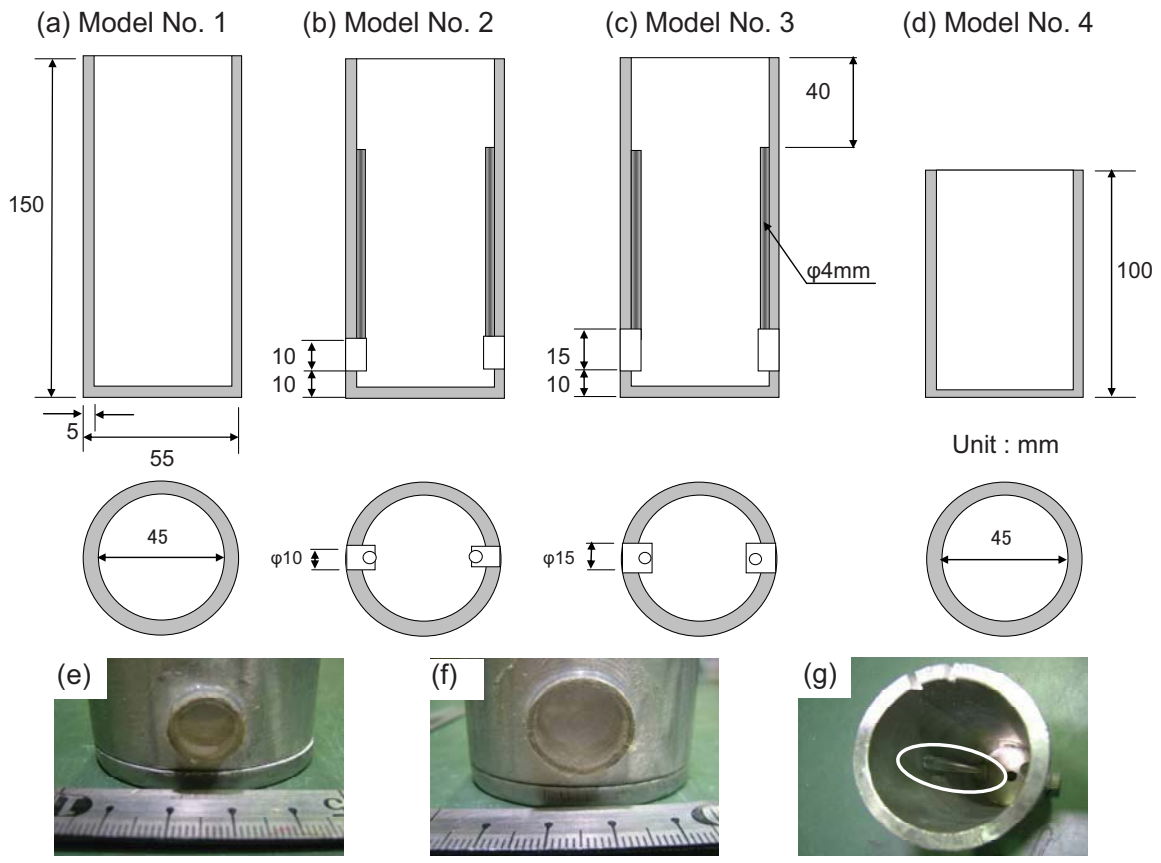

Fig. 2.3 Model manhole and mitigation measures used in the tests; (a) – (d), filtering nets installed Manhole No. 2 (e) and Manhole No. 3 (f), and pipes attached to a device to guide pressurized pore water into the manhole during shaking (g).

The mitigation device consists of a filtering net [Fig. 2.3(b) – (c) and (e) – (f)] which is installed as a part [Fig. 2.3 (b) – (c) and (g)] of the connection of a sewerage pipe and manhole, and a pipe which is installed as a part of filtering nets in the manhole (Konishi et al., 2008).

The mechanism of the mitigation device is as follows: (1) Excess pore water pressure in surrounding ground of the manhole gradually increases during strong shaking, (2) The pressurized pore water is guided into the manhole through the filtering net and pipe due to pressure difference between outside and inside of the manhole. Model No. 2 [Fig. 2.3(b) and (e)] has a pair of the filtering nets with diameter of 10 mm, and Model No. 3 [Fig. 2.3 (c) and (f)] has those of 15 mm in model scale. The length of the pipe which is connected to the filtering nets in the manhole is 100 mm [Fig. 2.3 (b), (c) and (g)]. A stainless mesh filter whose openings are 75 μm is attached to prevent sandy soils from flowing into the manhole.

2.3.2 Preparation of the viscous fluids

Pore fluids having viscosity greater than water are used to accurately satisfy the scaling laws of time relating to diffusion of pore fluid through liquefied soil when modeling dynamic loading events. According to the scaling law of viscosity (Table 2.1), the metolose (Shin-Etsu Chemical Co., Ldt.) is added to tap water to increase the viscosity by 20 times of that of water (20 cSt). The chemical name of the metolose is hydroxypropyl methylcellulose (MC). It is a water-soluble cellulose ether. The metolose used in this study is Type SM-100 in the form of a white powder. The Metolose is a tasteless, odorless, and physiologically harmless (Metolose Brochure 1997). The ability of the Metolose to produce high viscous water without changing other significant fluid parameters such as density or surface tension were tested and approved up to 100 cSt (Dewoolkar et al. 1999). In this study, a 2% solution of Metolose which has an approximate viscosity of 100 cSt at 20ºC was produced several days before model preparation.

This solution was then diluted by adding tap water until the viscosity of 20 cSt is reached. The viscosities of Metolose solutions are measured using rotational 'cup and bob' viscometer (RION, VT-03F). The specification for viscometer can be found in Appendix C. Before model construction, the solution was deaired in a vacuum chamber approximately 24 hours until no air bubbles appeared at the water surface.

2.3.3 Construction of the model ground

Silica sands were used to make the model ground. Physical properties of the sand are listed in Table 2.3, with the grain size distributions curve shown in Fig. 2.4. The soil is classified as "poorly graded sand (SP)" with Gs = 2.66, e_{max} = 1.19, e_{min} = 0.71. The ground model was prepared in a rigid container, with nominal inside dimensions of 0.45, 0.15 and 0.30 m with a transparent side window installed in the container, through which the in-flight model behavior can be monitored.

Table 2.3 Properties of silica sand.

Specific gravity	Gs	2.66	
D_{50}		0.172	mm
D_{10}		0.110	mm
Cofficient of uniformity	C_u	1.727	
Cofficient of curvature	C_g	0.938	
Maximum void ratio	e_{max}	1.19	
Minimum void ratio	e_{min}	0.71	
Wet sand	γ_t	14.8	kN/m^3
Saturated sand	γ_{sat}	18.1	kN/m^3

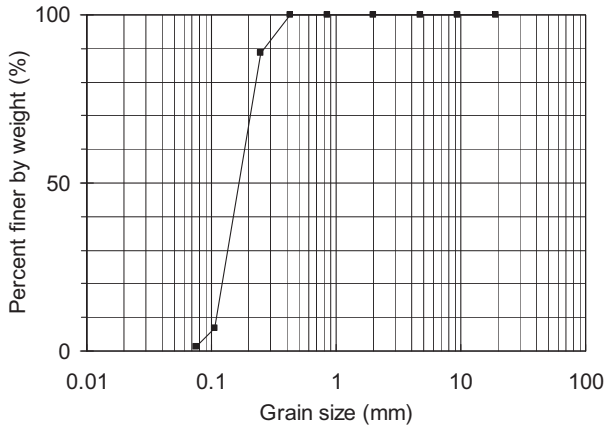

Fig. 2.4 Grain size distribution curve for silica sand used in centrifuge model tests.

Procedure of construction of the model ground is as follows: The native ground layer of relative density, Dr ≈ 85%, was first prepared by compacting moist silica sands up to 200 mm (model scale) from the bottom of the container [Fig. 2.5(a)]. Then, to install the model manholes, the trench with volume 2.3 × 2.3 × 3.2 m^3 was excavated by using an aluminum wall of the same size with the trench in horizontal plane to prevent the excavation wall from collapsing during excavation [Fig. 2.5(b) – (d)]. The manhole was placed on gravel with thickness of 0.2 m at the bottom of the trench [Fig. 2.5(e) – (f) and Fig. 2.6]. The same silica sand as the native ground was water-pluviated in the trench with viscous water to form a loose deposit (Dr ≈ 36%) [Fig. 2.5(g) – (h)].

The permeability of silica sand with the viscous fluid was 3.64×10^{-4} (cm/s) for Dr = 85% and 8.80×10^{-3} (cm/s) for 36%. Because of the permeability difference (2.4 times) between backfill and native ground, seepage of water from the backfill soil to the native ground may be expected to be minor during shaking. Meanwhile, excess pore water pressure can be easily dissipated into the backfill above the water table where soils are inevitably partially saturated before shaking. Special care was taken for saturation of the model ground. After constructing

the model, viscous water was added to assure the full saturation of the native ground as well as backfill so that the water poured in backfill was not absorbed in the native ground.

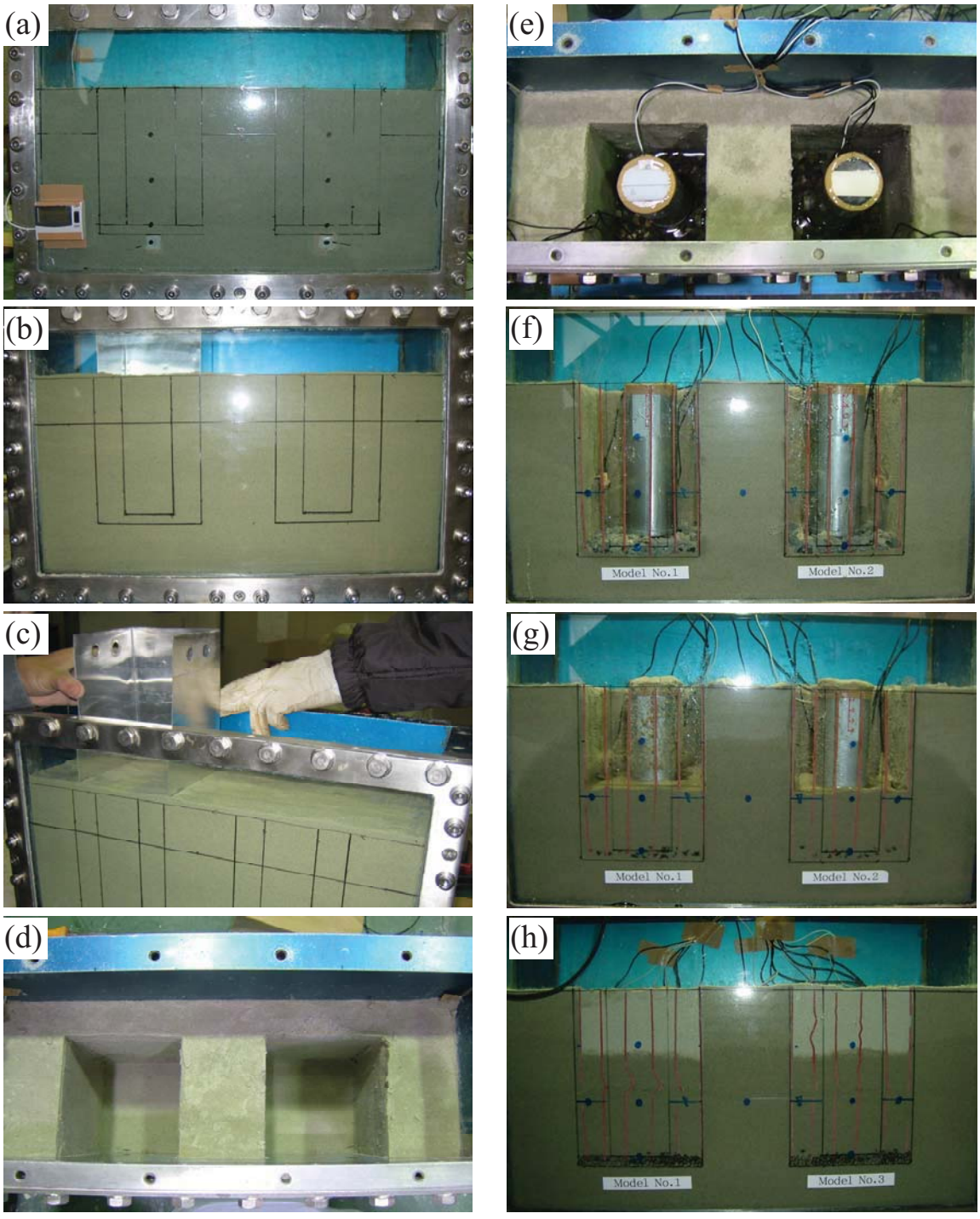

Fig. 2.5 Procedure of construction of model ground.

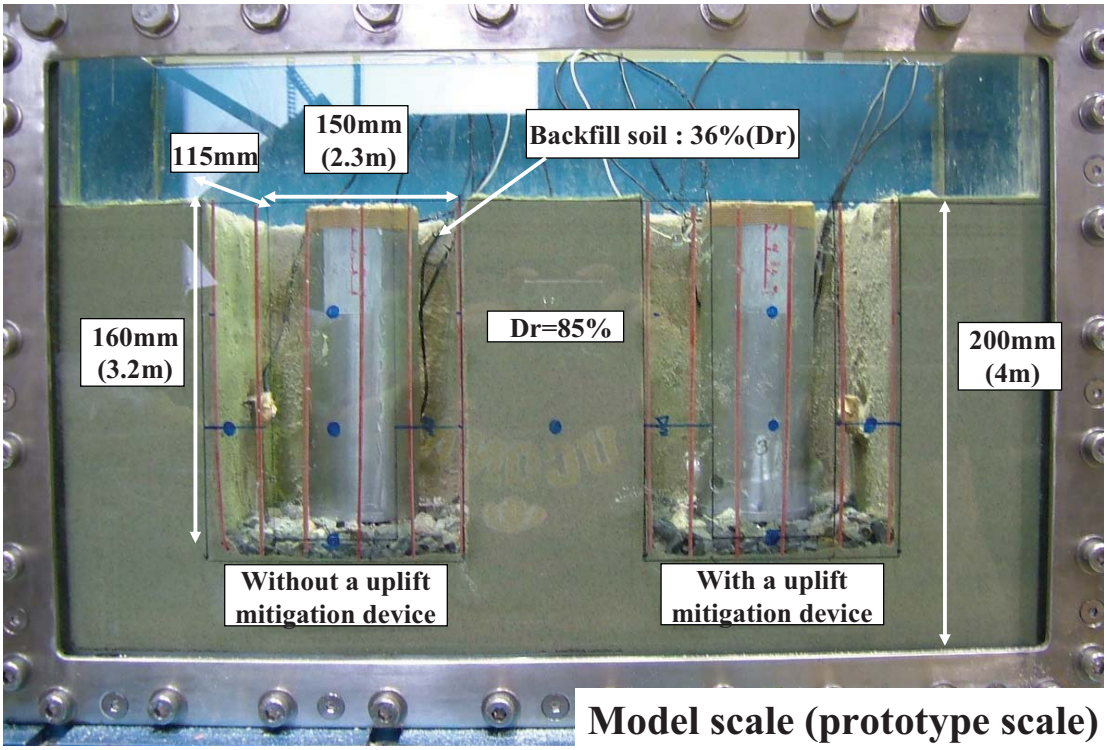

Fig. 2.6 Model manholes installed in the excavated ground before back-filling with loose soils.

2.3.4 Instrumentation and measurement

To monitor dynamic behavior of the model, three types of electronic instruments were used [Fig. 2.7(a) – (c)]: (1) accelerometers (SSK, A6H-50) to record dynamic motions on the ground surface, model manholes and container, (2) pore water pressure transducers (SSK, P306A-2 and P306AV-2) to measure excess pore water pressure in the model, (3) laser displacement transducers (Keyence, LBP-080) to measure the uplift displacement of the manholes. Calibrations factors are taken from the company's specification documents found in Appendix C. Laser displacement sensors were calibrated by using the micrometer. Figure 2.7(a) – (c) shows the general location of instruments for manholes and the model ground. Figure 2.7(a) and (b) corresponds to, respectively, CS2 and CS15 – CS17 (short manholes). Figure 2.7(c) corresponds to test cases except for those of Fig. 2.7(a) and (b).

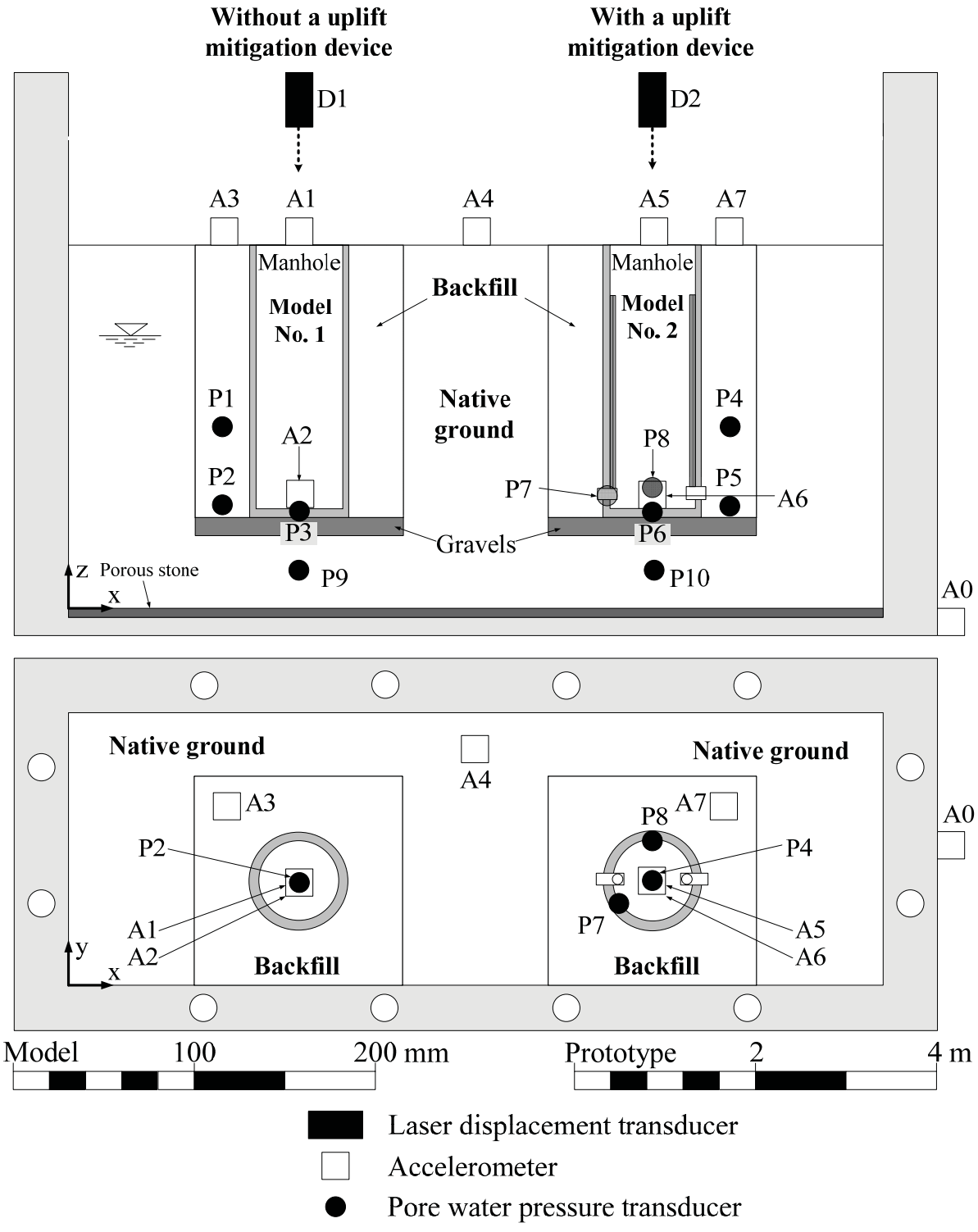

(a) CS2

Fig. 2.7 Centrifuge model test set-up for manholes (cont.).

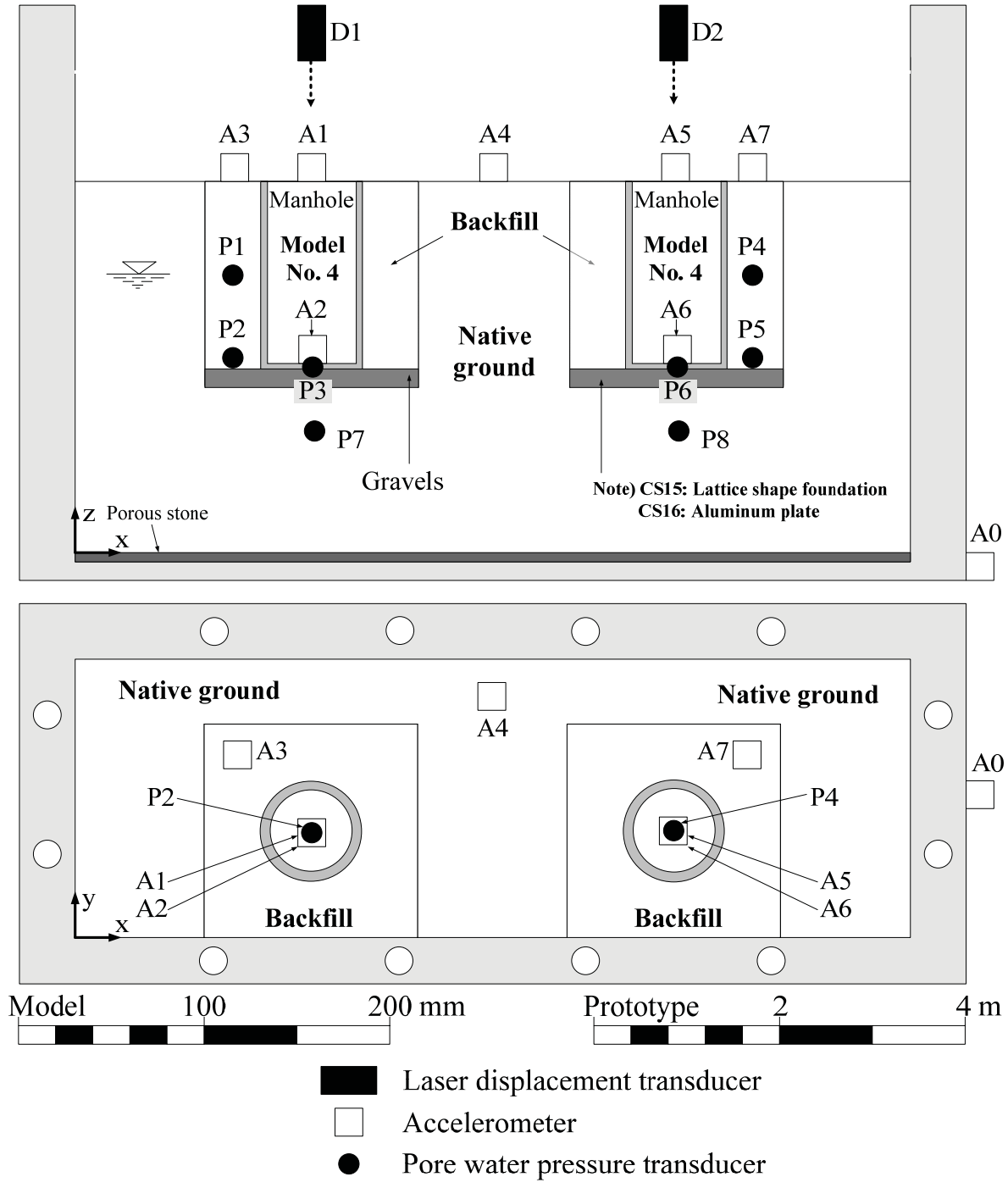

(b) CS15–CS17

Fig. 2.7 Centrifuge model test set-up for manholes (cont.).

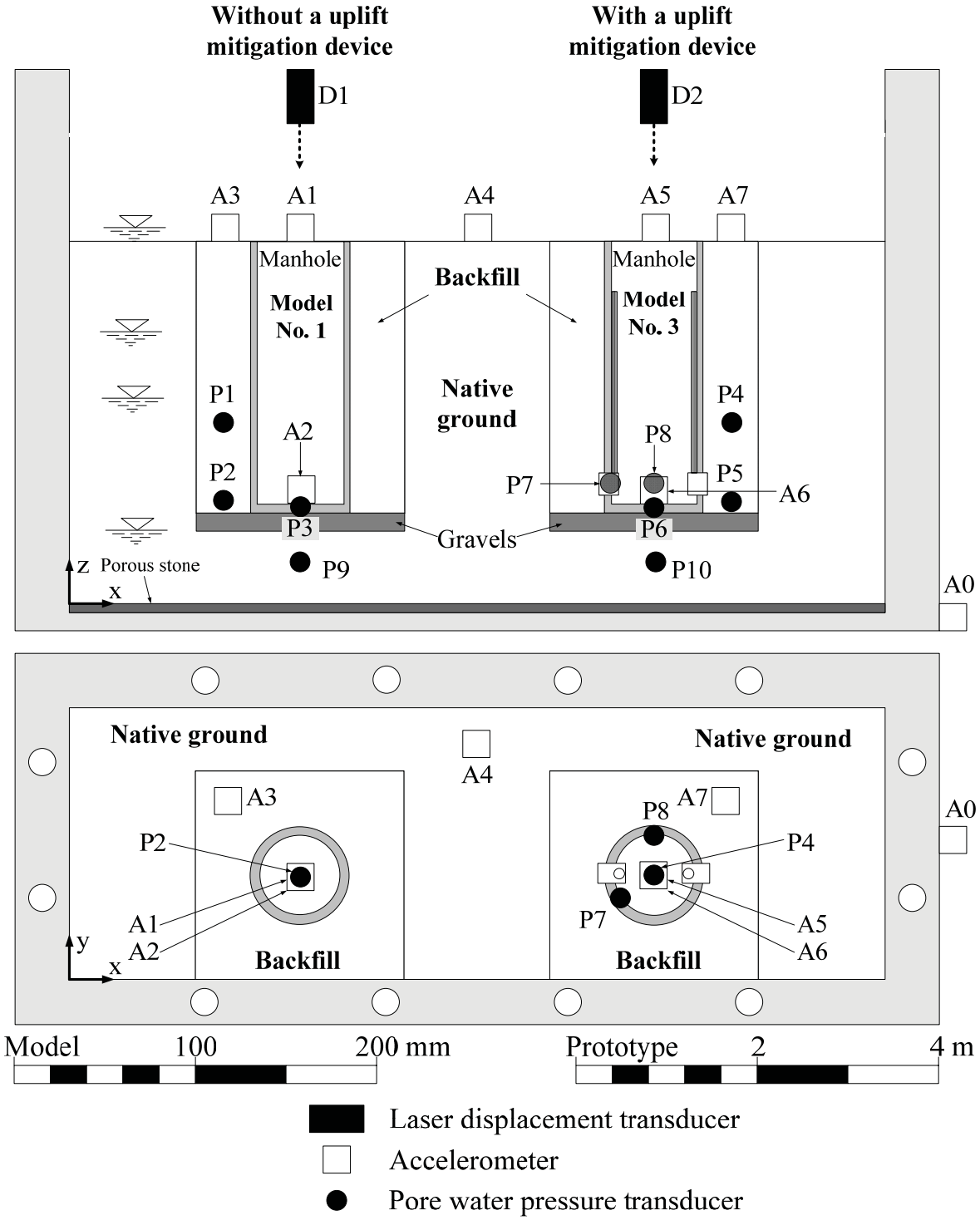

(c) Test cases except for those shown in (a) and (b)

Fig. 2.7 Centrifuge model test set-up for manholes (cont.).

As shown in Fig. 2.7, an accelerometer A0 is installed on the shake table to measure the input acceleration. A1 and A2 (no mitigation measure), and A5 and A6 (with mitigation measures) are installed at the top (A1 and A5) and bottom (A2 and A6) of the manhole. A3 and A7 are installed on the surface of the backfill, and A4 is installed on the native ground surface.

To measure the uplift displacement of the manhole, D1 (no mitigation measure) and D2 (with mitigation measures) whose capacity is ±25mm at a distance of 80 mm from the target are installed as shown in Fig. 2.7.

Ground settlements are directly measured by a ruler (Fig. 2.8) before and after each experiment. Uplift displacements are also measured by a ruler to determine the finial uplift displacement.

Pore water pressure transducers are oriented perpendicular to the direction of shaking to minimize the influence of hydro-dynamic pressures due to shaking. They are attached on the grass wall with double-sided tape. The pore water pressure transducers, P1 (no mitigation measure) and P4 (with a mitigation measures), are located in the backfill at the depth of 2 m from the ground surface. Those of P2 (no mitigation measure) and P3 (with a mitigation measures) are located in the backfill at the same depth (3 m) as the bottom of the manhole. Those of P3 (no mitigation measure) and P6 (with a mitigation measures) are attached from the inside at the bottom of the manhole so that pore water pressure during the uplift can be measured. In order to evaluate the effects of the mitigation device against uplift, P7 is attached just at the side of the filtering net and P8 is installed perpendicular to the filtering net at the back of the manhole at the same depth with P7 as shown in Fig. 2.7(a) and (c). P9 (no mitigation measure) and P10 (with a mitigation measures) are located in the native ground at the depth of 0.4 m below the manholes.

2.4 Test procedures

After confirming that all equipments and sensors are well functioning without any abnormality, centrifugal acceleration was increased gradually up to 20 G. To properly consolidate the model ground before shaking, the model was put under 20 G for 5 minutes. After completion of consolidation of the model ground, the amount of settlements is measured by a ruler to obtain the actual relative density of the ground and the backfill before shaking. Then, centrifugal acceleration is again increased up to 20 G to apply the dynamic motion to the model. The input acceleration is a sinusoidal wave with the maximum amplitude of about 2.05 ~ 7.25 m/s^2 and frequency of 1.25 Hz in prototype scale. The same input acceleration was given to all cases.

Table 2.4 summarizes 22 test cases conducted in this study. The relative density of each case is increased approximately 36% to 39% due to consolidation before shaking as above-mentioned. For convenience, the relative of backfill is considered as 36%. The relative density of backfill in CS22 is changed from 36% to 72% by compaction of backfill as a mitigation measure against the uplift.

Table 2.5 classifies the tests cases with the factors affecting the uplift behavior. In Table 2.5, category (a) investigates the effects for variations of the depth of the ground water table. The ground water table is adjusted from the ground surface to the depth of 3 m. Category (b) investigates the effects of input acceleration. The amplitude of the input accelerations observed on the shake table falls in a range of 2.05 ~ 7.25 m/s^2. Category (c) investigates the effects of variations of the excess pore water pressure ratio in backfill by controlling the relative density of backfill (Dr ≈ 36% to 85%). Categories (d) and (e) investigate the effects of duration of shaking and cross-sectional area of the trench. Categories (f) and (g), respectively, investigate the effects of manhole length (2 m to 3 m) and apparent unit weight of the

Table 2.4 Summary of centrifuge manhole tests.

Test No.	Relative density		Type of model manhole		Length of the manhole		GWL	Amplitude of inpu acceleration	Remarks
	Backfill soil	Native ground	left	right	left	right			
	%	%	No.	No.	m	m	m	m/s^2	
CS1	38.7	85	1	–	3	3	0	6.78	GWL=0 m_saturated
CS2	37.9	85	1	2	3	3	1	7.25	GWL=1 m
CS3	38.7	85	1	3	3	3	1	7.15	GWL=1 m
CS4	38.4	85	1	3	3	3	1.7	7.19	GWL=1.7 m
CS5	37.3	85	1	–	3	3	3	6.60	GWL=3 m_dry
CS6	37.2	85	1	3	3	3	1	2.05	Input motion=2.05 m/s^2
CS7	38.7	85	1	3	3	3	1	4.64	Input motion=4.64 m/s^2
CS8	37.1	37.1	1	3	3	3	1	6.97	Trench=4.5×3.0 m^2
CS9	85	85	1	3	3	3	1	6.47	Dr of backfill ＝85%
CS10	39.4	85	1	3	3	3	1	6.87	Number of cycle load=15cycles
CS11	38.1	85	1	3	3	3	1	6.91	Number of cycle load=60cycles
CS12	38.7	65	1	3	3	3	1	7.05	Dr of native groundl = 65%
CS13	37.3	85	1	3	3	3	1	6.97	Acrylic box
CS14	38	85	1	3	3	3	1	6.89	Native ground = sand mixed clayey material
CS15	38.5	85	4	4	2	2	1	6.89	Left:normal Right:lattice shaped foundation
CS16	38.1	85	4	4	2	2	1	6.51	Left:normal Right:aluminium plate
CS17	39.5	85	4	–	2	2	1	6.63	Left: Liquefiable soil under the manhole
CS18	38	85	1	3	3	3	1	6.95	γ_m = 11.27 kN/m^3
CS19	37.7	85	1	3	3	3	1	7.06	γ_m = 13.08 kN/m^3
CS20	38.1	85	1	3	3	3	1	6.93	γ_m = 15.47 kN/m^3
CS21	38.1	85	1	3	3	3	1	6.62	Connection both manhole and native ground by beam structure
CS22	36→72	85	1	3	3	3	1	6.79	Compaction of backfill

Table 2.5 Classification of test cases for the investigation of the effects on the uplift.

Factors affecting the uplift	Case No.
(a) Ground water depth	1, 2, 3, 4, 5
(b) Amplification of input motion	2, 3, 6, 7
(c) Relative density of backfill	2, 3, 9, 22
(d) Number of load cycles	2, 3, 10, 11
(e) Cross-section area of the trench	2, 3, 8
(f) Manhole length	2, 3, 15, 16
(g) Apparent unit weight of the manhole	2, 3, 18, 19, 20
(h) Condition of native ground	2, 3, 8, 13, 14
(i) Contact condition between the bottom of a manhole and trench	15, 16, 17

Fig. 2.8 Uplifted manhole after shaking (CS2).

manholes. Apparent unit weight of a manhole is the dead-weight of the manhole divided by its volume. Category (h) investigates the effects of conditions of native ground. Dense ground is prepared by compaction up to the relative density of approximately 85% and loose ground with the relative density of 36% is prepared. In CS13, open boxes made of thin acrylic boards (thickness = 1.1 mm) were used as a wall and base of the trench to have perfectly rigid and undrained boundary condition for backfill. Category (i) investigates variation of contact condition between the bottom of a manhole and trench. Four kinds of the conditions are investigated; the manhole is put on a lattice, gravel, aluminum plate to have no gap between the manhole and the base of the trench, and loose liquefiable soil.

The factors considered in categories (a) to (g) are a primary factor directly affecting the uplift behavior of manholes in the trench. On the other hand, factors considered in categories (h) and (i) are a secondary factor accelerating the uplift of the manholes such as squeezing of liquefied native ground.

2.5 Test results

2.5.1 Mechanism of Uplift behavior

In this section, the results of “no mitigation measures” are mainly discussed and the results of “mitigation measures” will be discussed in Chapter 6. Table 2.6 shows the summary of tests results. The uplift displacements were from 0.0 to 1.6 m. The settlements of backfill are from 0.023 to 0.230 m. The maximum uplift displacement is 1.6 m in CS11 in which the number of load cycles as input wave was approximately 60 cycles.

Figures 2.9, 2.10, and 2.11 show the results measured in the centrifuge model tests corresponding to CS3, CS4, and CS9, respectively. The ground water table of CS3 and CS9 is

adjusted to be at 1 m from the ground surface, and that of CS4 is located at 1.7 m from the ground surface. The relative density of backfill in CS3 and CS4 is approximately 36% and that of CS9 is approximately 85%.

Table 2.6 Summary of test results.

Test No.	Type of model manhole		Uplift displacement		Settlement of backfill	
	left	right	left	right	left	right
	No.	No.	m	m	m	m
CS1	1	–	1.100	–	0.183	–
CS2	1	2	0.958	0.922	0.190	0.203
CS3	1	3	0.952	0.773	0.200	0.190
CS4	1	3	0.488	0.377	0.180	0.140
CS5	1	–	0.000	–	0.050	–
CS6	1	3	0.000	0.000	0.073	0.060
CS7	1	3	0.201	0.181	0.175	0.160
CS8	1	3	1.074	0.930	0.217	0.255
CS9	1	3	0.000	0.000	0.018	0.018
CS10	1	3	0.234	0.140	0.168	0.165
CS11	1	3	1.600	1.600	0.220	0.200
CS12	1	3	1.030	0.940	0.170	0.160
CS13	1	3	0.231	0.176	0.230	0.227
CS14	1	3	0.822	0.616	0.205	0.275
CS15	4	4	0.503	0.479	0.200	0.188
CS16	4	4	0.518	0.285	0.150	0.133
CS17	4	–	0.602	–	0.148	–
CS18	1	3	0.574	0.366	0.178	0.195
CS19	1	3	0.421	0.299	0.168	0.123
CS20	1	3	0.131	0.045	0.150	0.120
CS21	1	3	0.700	0.253	0.210	0.195
CS22	1	3	0.129	0.083	0.023	0.083

Indicated by the vertical thick dotted line at 6.5 s in Fig. 2.9 (a) to (j), the manhole starts to lift up (D1) at 6.5 s when the excess pore water pressure in the middle of the backfill [P1: Fig. 2.9(b)] and that of the bottom of the manhole, σ_{vm}', [P3: Fig. 2.9(d)] exceeds the initial effective vertical stress. As shown in Fig. 2.9 (d), manhole starts to lift up slightly later (about 0.5 s) than pore water pressure at the bottom of the manhole (P3) reaches the initial effective

vertical stress. Figure 2.9(d) shows the continuous curve of the effective vertical stress at the bottom of the manhole during the uplift. In this case, the uplift is initiated at the same instance as the excess pore water pressure on the bottom of the manhole exceeded the initial level. Uplifting stops at the end of shaking and a slight downward movement is recoded as shown in Fig. 2.9(a). The excess pore water pressure on the bottom of the manhole is decreased less than the effective vertical stress of the manhole. The peak acceleration on the top of the manhole is slightly larger than that on the bottom as shown in Fig. 2.9(g) – (h). Liquefaction does not occur in the native ground as shown in Fig. 2.9(e) because the excess pore water pressure does not reach the initial effective vertical stress. On the surface of native ground [Fig. 2.9(j)], cyclic mobility is observed after 8 s by strong shake and the maximum acceleration is 17.4 m/s^2.

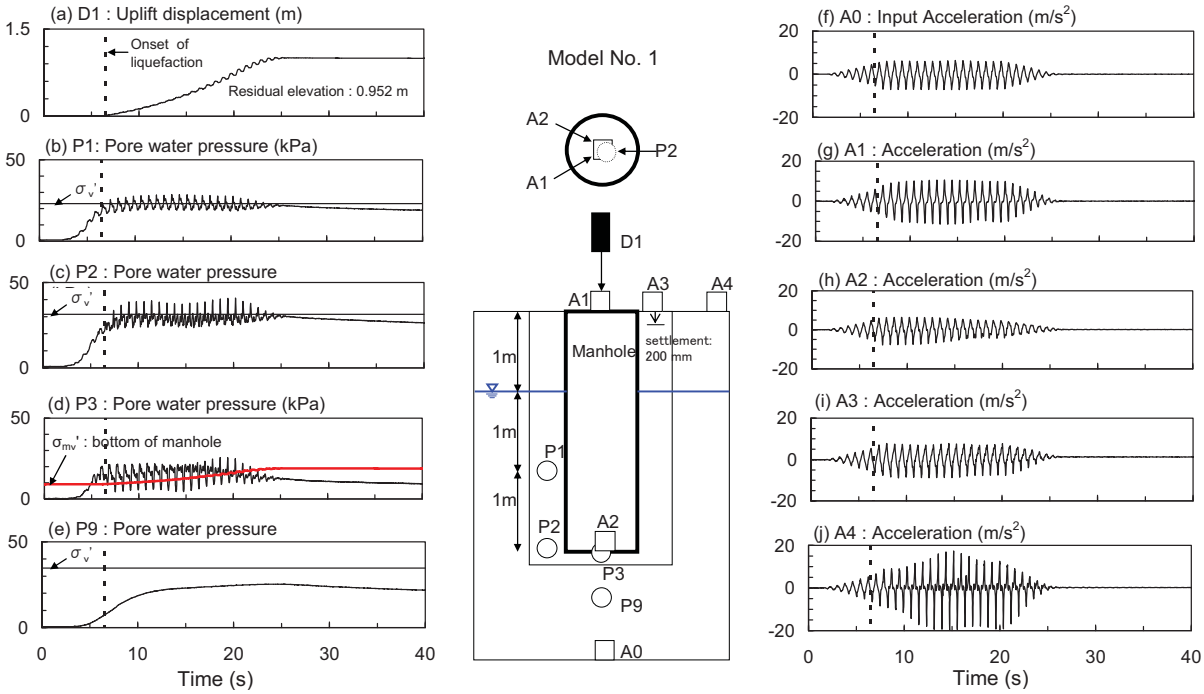

Fig. 2.9 Results of centrifuge model tests for Model No. 1(CS3, G.W.L = −1.0 m).

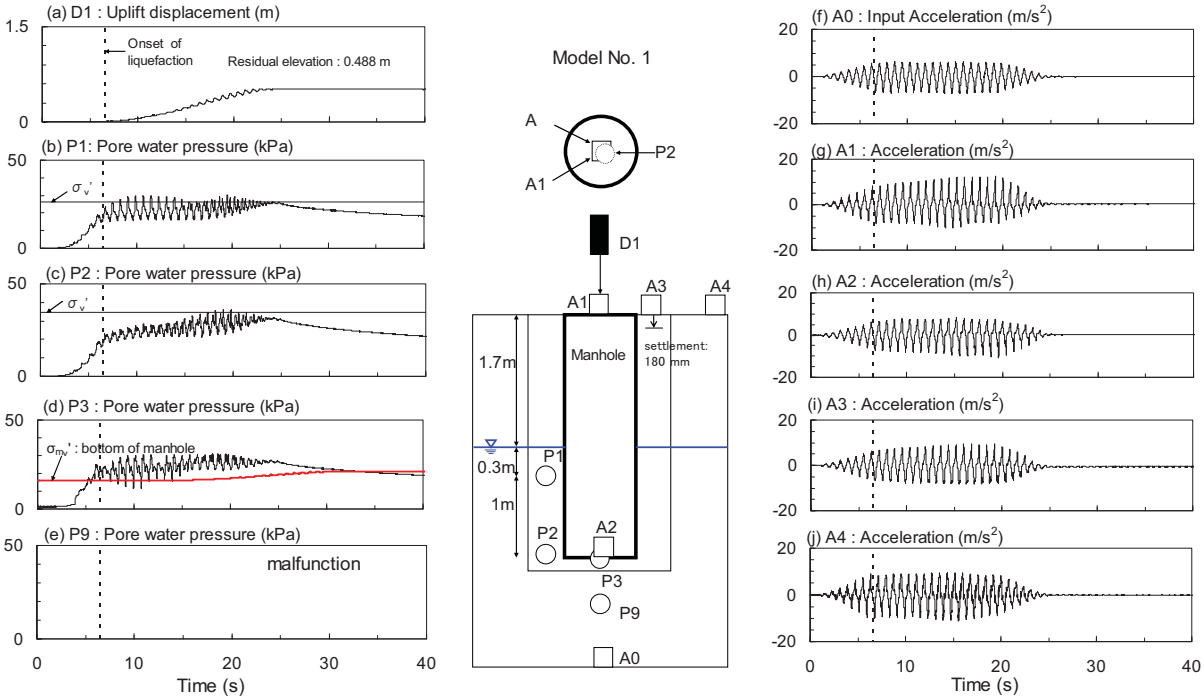

Fig. 2.10 Results of centrifuge model tests for Model No. 1(CS4, G.W.L = −1.7 m).

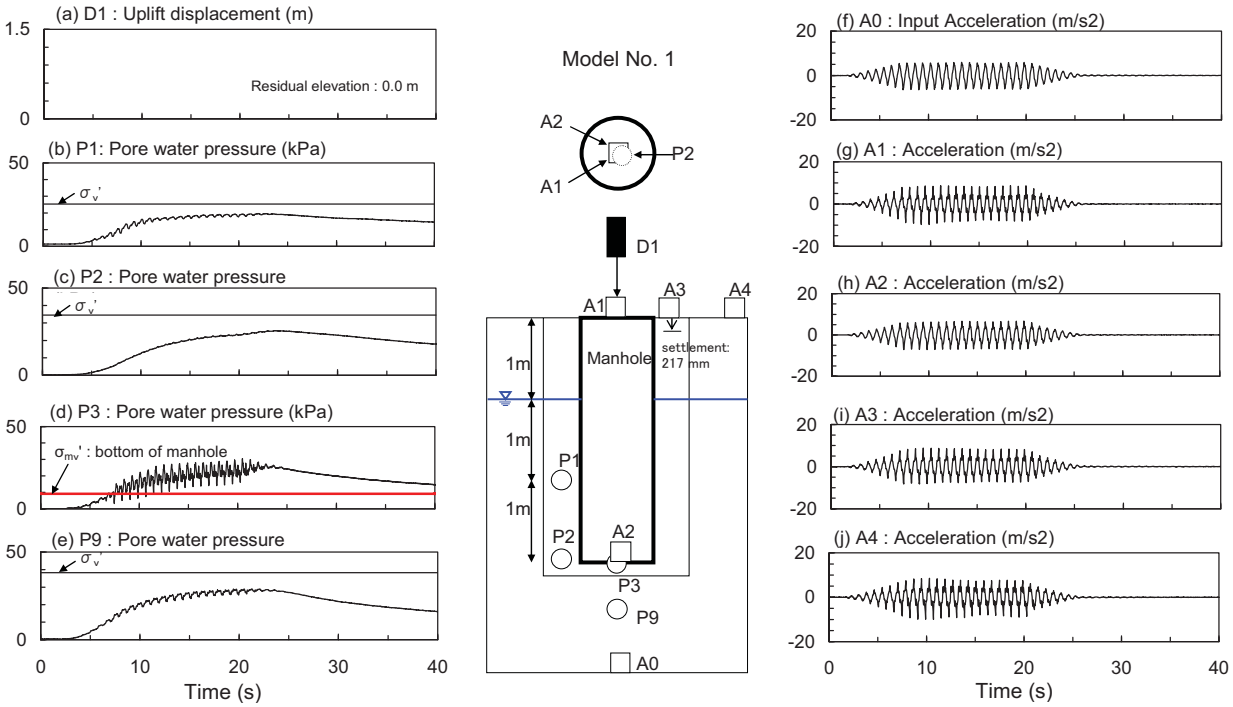

Fig. 2.11 Results of centrifuge model tests for Model No. 1(CS9, Dr of backfill = 85%).

Figure 2.10 is the results for CS4 whose ground water table coincides with 1.7 m from the ground surface. Magnitude of uplift displacement of the manhole with shallow ground water table (1 m) is almost 2 times larger than that of the manhole with deep ground water table (1.7 m) [Fig. 2.9(a) and Fig. 2.10(a)]. Although, the response of excess pore water pressure and accelerations for CS4 is similar to the results of CS3, the excess pore water pressure at depth of 3m from the ground surface is gradually increased in CS4 compared with that in CS3 [Fig. 2.9(c) and Fig. 2.10(c)].

Figure 2.11 shows the dynamic response in dense ground (Dr = 85% for all ground). As shown in Fig. 2.11(b) – (d), the excess pore water pressure at the bottom of the manhole exceeds the initial effective vertical stress, σ_{mv}', however, the manhole does not uplift because backfill is not liquefied. These facts suggest that liquefaction of backfill is a major cause for onset of uplift phenomenon and that frictional resistance force between the side wall of a manhole and backfill play an important part mitigation the uplift.

2.5.2 Uplift behavior of a manhole

To study the uplift behavior of a manhole in detail, acceleration amplification factors and phase differences are examined as shown in Fig. 2.12. The amplification factors are obtained by dividing the peak values of A1 to A4 [A1: top of the manhole, A2: bottom of the manhole, A3: ground surface of backfill, and A4: ground surface of native ground] by corresponding peak values of the input acceleration (A0). While the phase differences are computed from the difference of arrival time of peak accelerations from the corresponding peaks of A0 as in the following equation;

$$\Delta\theta = \frac{t_{An} - t_{A0}}{T} \times 360° \quad (n = 1, 4) \tag{1}$$

where $\Delta\theta$ is phase difference, t_{An} is arrival time of the peak at sensor An (n=1, 4) corresponding to the peak in the input acceleration (A0), and T is the period of input motion (=0.8 s).

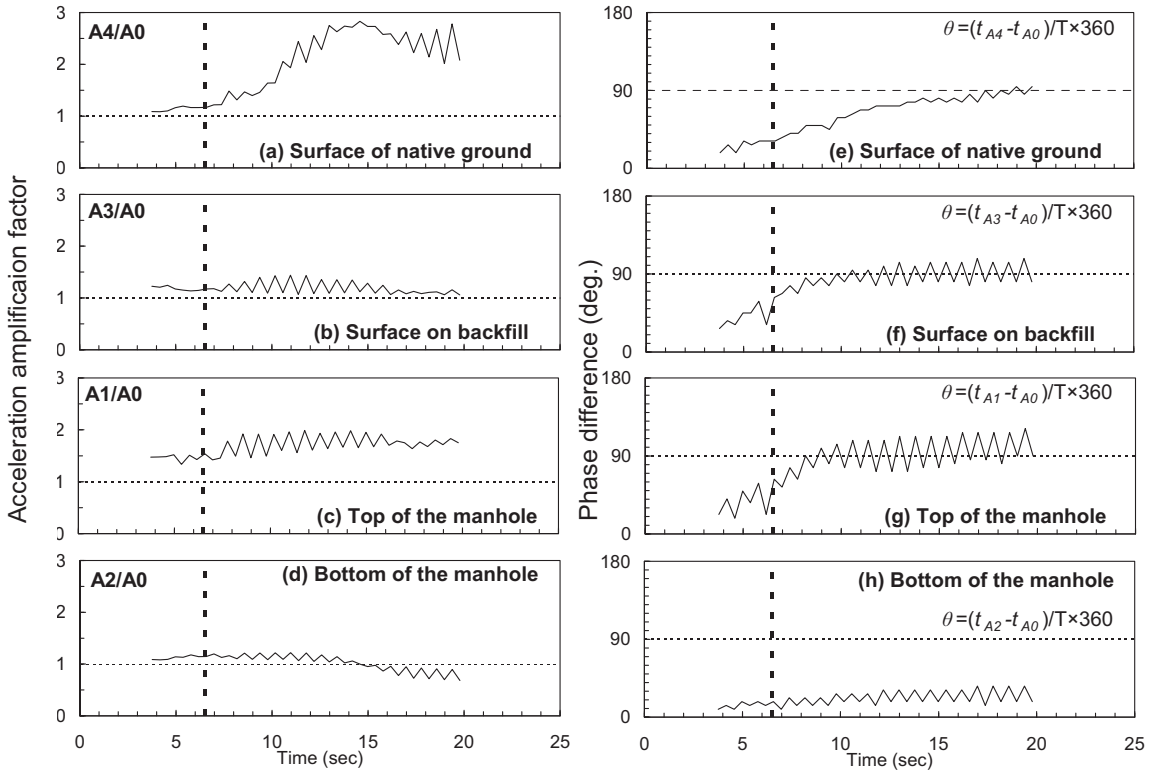

Fig. 2.12 Time history of acceleration amplification factor [(a) to (d)] and phase difference [(e) to (h)] for CS3.

In Fig. 2.12, the vertical thick dotted lines at 6.5 s indicate the initiation of the manhole uplift due to liquefaction of backfill according to build-up of the excess pore water pressure in backfill as shown in Fig. 2.9(b) – (c). In Fig. 2.12(a), amplification of the surface of native ground (A4/A0) is nearly 2.7, while that of the surface of backfill (A3/A0) is gradually decreasing from 1.4 to 1.1 as shown in Fig. 2.12(b). The factor of A1/A0 (top of the manhole/input) is 1.6 times larger than that of A2/A0 (bottom of the manhole/input). Namely,

a larger inertial force is acting at the top of the manhole. This fact represents rocking behavior of the manhole during uplift. Phase difference of the backfill surface keeps to 90° [Fig. 2.12(f)] suggesting complete liquefaction of the backfill. Fig. 2.12(f) and (g) show that the upper part of the manhole is shaken in the same phase with backfill, while, as shown in Fig. 2.12(h), the bottom of the manhole is moving with almost the same phase with the input motion. This also represents rocking behavior of the manhole during uplift.

Figure 2.13 illustrates the relationship between excess pore water pressure and uplift displacement in CS4. Figure 2.13(a) indicates the relationship between uplift displacement and excess pore water pressure at P1 (in backfill) and P3 (at the bottom of the manhole). Figure 2.13(b) shows detailed the relationship when the uplift displacement is in the range of 0.0 to 0.2 m indicated by vertical dotted lines. As shown in this figure, uplift of manholes is increased with the increase of the excess pore water pressure at P1 installed in backfill while the excess pore water pressure at P3 installed on bottom of the manhole is decreased when the manhole is uplifted.

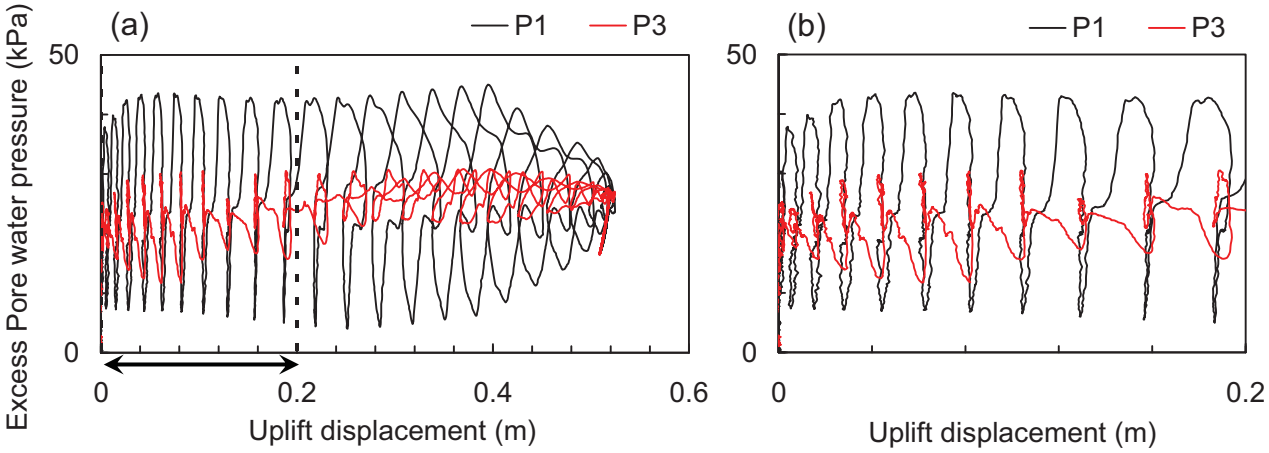

Fig. 2.13 Relationship between uplift displacement and excess pore water pressure for CS4: (a) Uplift displacement vs. EPWP (P1&P3), (b) uplift displacement between 0.04 and 0.2 m vs. EPWP (P1&P2).

Figure 2.14 shows model ground before and after shaking for CS1. In test CS1, colored silica sand is deposited to investigate the behavior of model ground during shaking. Figure 2.14(a) indicates the model ground before shaking. After shaking, the transparent side window installed in the rigid container is removed, and the model ground is cut on the vertical plane at the center of the trench to observe the movement of the ground as shown in Fig. 2.14(b). As shown in Fig. 2.14, liquefied backfill is moving toward the bottom of the manhole with the uplift. On the other hand, native ground is not damaged and is slightly settled toward the trench at the ground surface. The manholes are tilted because the manhole is uplifted enough to exceed its center of gravity.

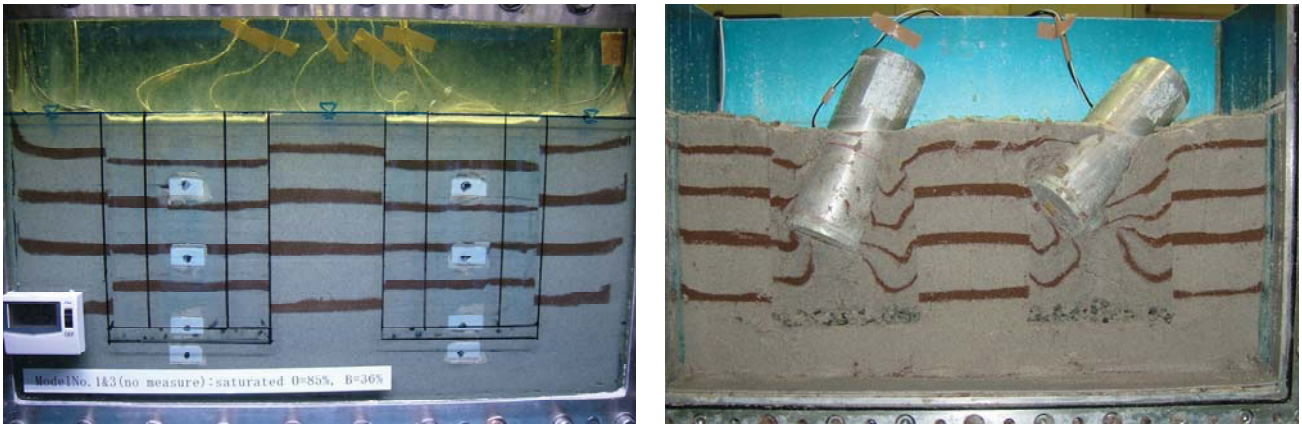

(a) before **(b) after**

Fig. 2.14 Model ground and manholes before and after shaking for CS1. In (b), a trench was cut on the vertical plane to see behavior of surrounding soil.

2.5.3 Relationship between uplift displacement and the depth of ground water depth

The ground water depth is one of the important factors that affect the uplift amount of the manhole. The ground water table ratio (h_w/h) is defined as the ground water table below the ground surface divided by manhole length. The uplift ratio ($\Delta f/h$) and the settlement ratio (Δ

s/*h*) are also normalized by the manhole length (*h* is manhole length, h_w is ground water depth from ground surface, Δs is settlement of backfill and Δf is uplift displacement).

Figure 2.15 shows the relationship between the uplift ratio and ground water table ratio. CS1 – CS5 are results of the manhole with a 3 m length, and CS15 – CS16 are results of the manhole with a 2 m length. Amplitude of input acceleration is in the range of 6.60 ~ 7.25 m/s^2. The maximum uplift displacement (37% of manhole length) occurred in saturated soil below the ground surface. The uplift ratio is decreased with deep ground water depth as shown in Fig. 2.15. At a ground water table ratio of 0.5 (h_w/h), the uplift ratio for CS15 and CS16 (short manhole) is not largely different with that for a long manhole. It indicates that the relationship between the uplift ratio ($\Delta f/h$) and ground water table ratio (h_w/h) does not largely depend on the length of the manhole. The absolute settlement of backfill is also increased with a high ground water table ratio.

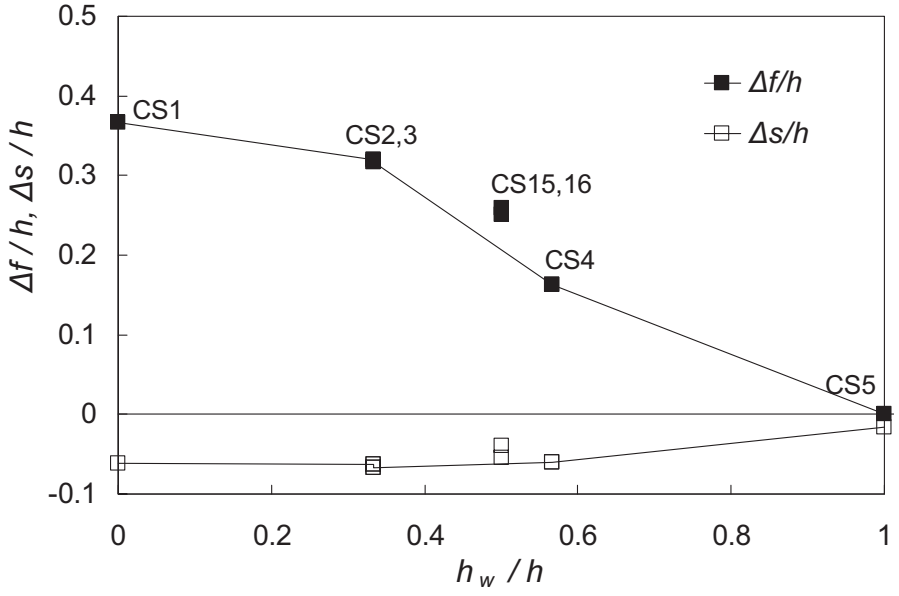

Fig. 2.15 Relationship between uplift ratio and normalized ground water table for CS1–CS5 and CS15 and CS16.

2.5.4 Relationship between uplift displacement and amplitude of input acceleration

Amplitude of input acceleration which can control the excess pore water pressure ratio is also one of the important factors to affect the uplift behavior. Figure 2.16 shows the relationship between uplift ratio and amplitude of input acceleration measured on the shake table. Selected test cases for comparisons are CS2, CS3, CS6 and CS7. Ground water table of selected cases is adjusted at the depth of 1 m from the ground surface. The amplitude of input acceleration is in the range of 2.05 ~ 7.25 m/s^2. The magnitude of the uplift ratio is decreased at small amplitude of the input motions. The maximum uplift ratio (0.32) is observed at the input acceleration of 7.25 m/s^2. The absolute settlement shows a tendency to increase with large amplitude of the input motion.

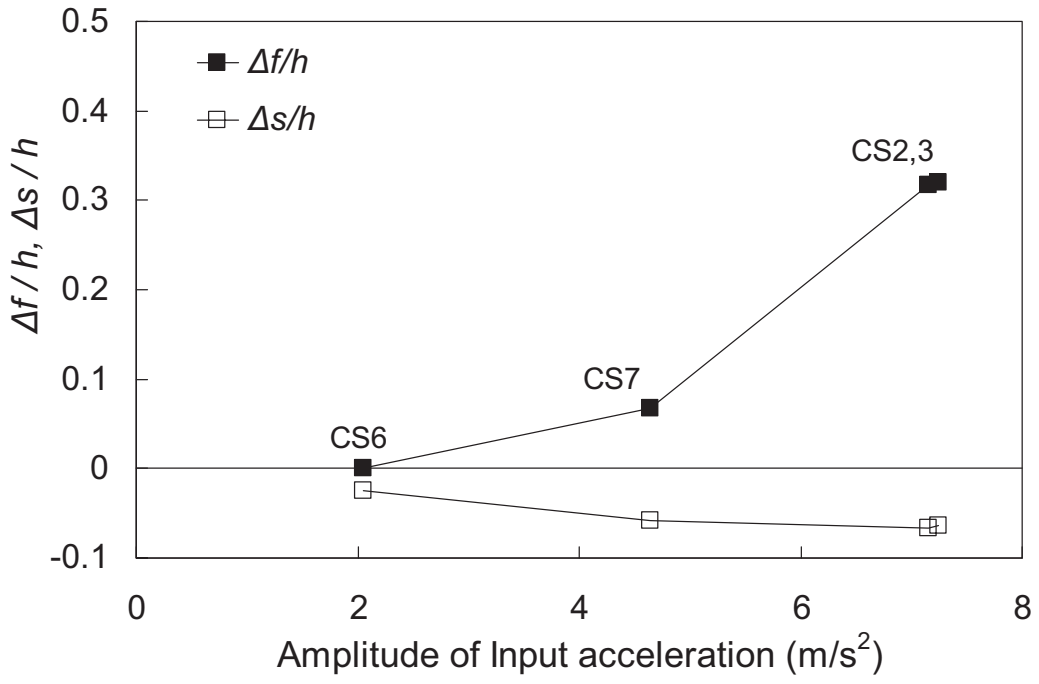

Fig. 2.16 Relationship between uplift ratio and magnitude of input motion for CS2, CS3, CS6 and CS7.

Figure 2.17 shows the relationship between the uplift ratio and the number of load cycles combined with the test results of CS2, CS3, CS10 and CS11. Number of load cycles is in the range of 15 to 60 cycles. In CS11, the uplift displacement is drawn by 1.15 m from the ground surface and the displacement transducer goes out of range during uplifting [Fig. 2.17(b): CS11]. The uplift ratio shows a tendency to increase with large number of load cycles. The manholes stop their lift up when the input wave stops. If the manhole uplift continues with increase of load cycles, it will tilt. The center of gravity for the model manhole (Model No. 1) is located about 1.52 m (proto-type) from the top of the model manhole. Therefore, if the manholes uplifted more than 1.52 m (about 50% for manhole length), the model manhole is tilted as shown in Fig. 2.18. These suggest that duration of liquefaction for a long time due to an increase of the number of load cycles affects the uplift displacement of the manhole.

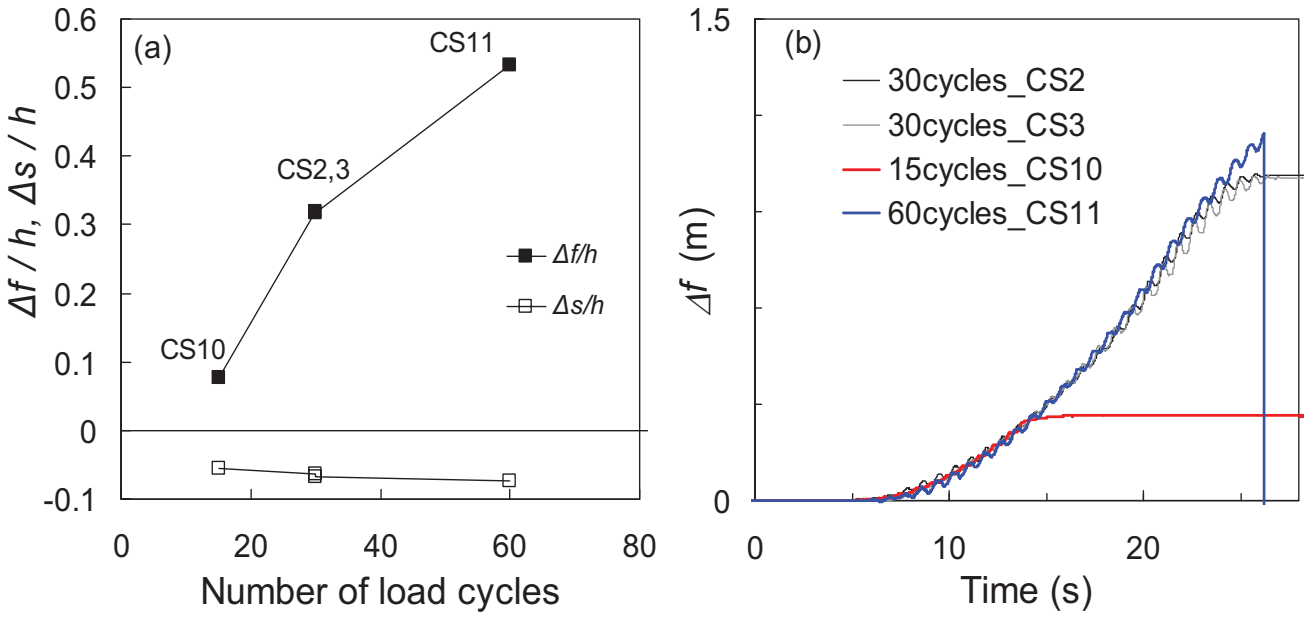

Fig. 2.17 Relationship between uplift ratio and number of load cycle for CS2, CS3, 10 and CS11: (a) $\Delta f/h$, $\Delta s/h$ vs. Number of load cycles, (b) Δf vs. time (s).

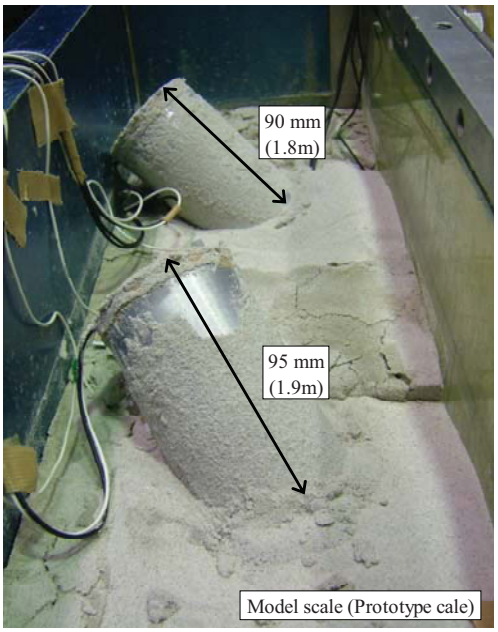

Fig. 2.18 Tilted manhole by duration of load cycles: CS11.

2.5.5 Relationship between uplift displacement and relative density of backfill

Compaction of backfill is thought to be effective to prevent liquefaction during earthquakes (Yasuda, 2003). Here, in this subsection, uplift behavior of manholes in the compacted ground was examined through the centrifuge model tests. Figure 2.19 shows the relationship between uplift ratio and relative density of backfill for CS2, CS9 and CS22 whose ground water table is located at 1 m from the ground surface. As shown in Fig. 2.19, the uplift ratio is decreased with the relative density of backfill because the build-up of excess pore water pressure is restrained in compacted backfill (Dr ≈ 85%) [Fig. 2.11(b) and (c)].

The maximum uplift ratio (0.32) is observed in the ground with the relative density of about 36%. The manhole does not uplift when the relative density of backfill is more than 85%, because the excess pore water pressure in backfill does not reach the initial effective vertical stress. When backfill is compacted by 72%, the uplift ratio is decreased by 0.043. The settlement shows a tendency to decrease with the increase of the relative density of backfill.

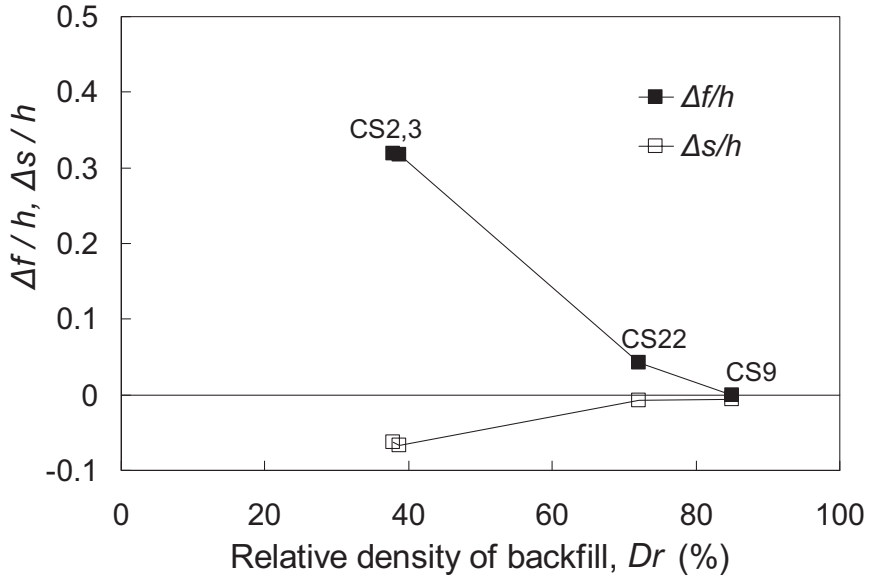

Fig. 2.19 Relationship between uplift ratio and relative density of backfill for CS2, CS3, CS9 and CS22.

2.5.6 Relationship between uplift displacement and cross-sectional area of the trench

Cross-sectional area of the trench will also affect the uplift displacement because liquefaction of backfill in the trench is a major cause for uplift phenomenon. The effect of cross-sectional area of the trench was investigated by the centrifuge model tests.

Figure 2.20 shows the relationship between uplift ratio and cross-sectional area of the trench for CS2, CS3 and CS8 whose ground water table coincides with the depth of 1 m from the ground surface. Cross-sectional area of the trench in horizontal plane for CS2 and CS3 is 2.3×2.3 m^2. In CS8, Trench excavation is not conducted. It means that the rigid container is used as the trench. the cross-sectional area corresponds to nominal inside dimensions of the rigid container (4.5×3.0 m^2). As shown in Fig. 2.20, the uplift ratio is compared with the ratio, *a/d* (= trench width / manhole diameter) and the uplift ratio is increased from 0.32 to 0.36 when

the cross-section of the trench in horizontal plane is increased from 2.09 to 3.34 (*a/d*). It may be that liquefaction occurs widely when loose sand is distributed widely surrounding the manhole. Although, the cross-sectional area of the trench increased about 1.75 times, the uplift ratio only increased about 0.04 (0.12 m). This suggests that the effects of cross-sectional area of the trench against uplift may be small compared with those of ground water table, amplitude of input motion and relative density of backfill. The absolute settlement also shows a tendency to increase with width of trench.

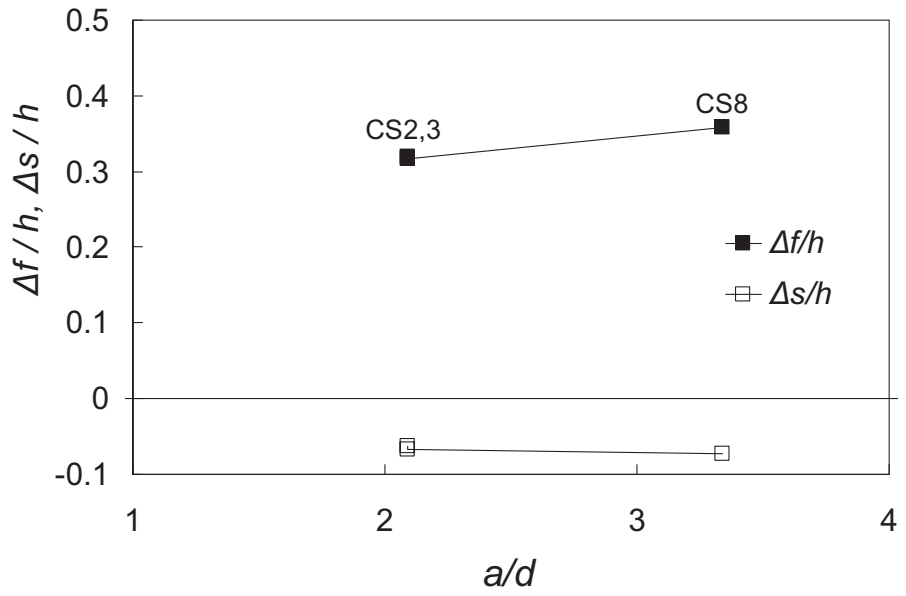

Fig. 2.20 Relationship between uplift ratio and cross-sectional area of the trench for CS2, CS3 and CS8.

2.5.7 Relationship between uplift displacement and manhole length

Manhole length will affect the uplift displacement based on the facts that the apparent unit weight of manholes and the ground water table ratio (h_w/h) are varied by the manhole length.

The effect of the manhole length for uplift displacement was examined through the centrifuge model tests.

Figure 2.21 shows the relationship between uplift ratio and manhole lengths for CS2, CS3, CS15 and CS16. The manhole length in CS2 and CS3 is 3 m, and that of CS15 and CS16 is 2 m. The ground water table for selected test cases coincides with the depth of 1 m from the ground surface. As shown in Fig. 2.21, the uplift ratio is increased from 0.25 to 0.32 when manhole length is increased from 2 m to 3 m. Corresponding uplift displacements are 0.5 m and 0.96 m, respectively. The ground water table ratio (h_w/h) for long manhole becomes smaller than that short manhole and apparent unit weight (γ_m = 9.57 kN/m^3) of the manhole with 3 m length is smaller than that (γ_m = 9.99 kN/m^3) of the manhole with 2 m length. Therefore, the manholes with 3 m length may be easy to uplift compared to the manholes with 2 m length at the same ground water depth. The absolute settlement of backfill is slightly increased with the manhole length.

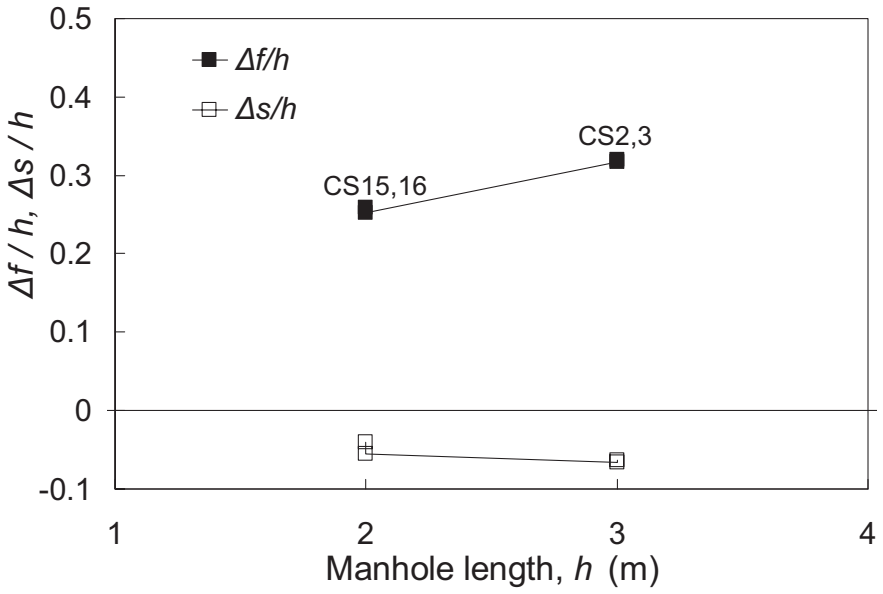

Fig. 2.21 Relationship between uplift ratio and manhole length for CS2, CS3, CS15 and CS16.

2.5.8 Relationship between uplift displacement and apparent unit weight of manhole

The phenomenon of manhole uplift occurs in liquefied ground because the apparent unit weight of the structures becomes smaller than that of the liquefied soil (Koseki et al., 1997b) and the apparent unit weight of the manhole acts as a resistant force against uplift in equilibrium of forces acting on a manhole in liquefied ground. To estimate the effects of the apparent unit weight of the manholes for uplift displacement, a series of centrifuge tests was conducted. The apparent unit weight of manholes is the dead-weight of the manhole divided by its volume. In the centrifuge model tests, the apparent unit weight of the model manholes is increased about 9.57 to 15.47 kN/m^3 by using lead beads as shown in Fig. 2.22, and the apparent unit weight (γ_m) of the manhole is normalized by saturated unit weight of backfill (γ_{sat}) for comparisons. Figure 2.23 shows the relationship between uplift ratio and unit weight ratio (γ_m/γ_{sat}) by using the results of CS2, CS3, CS18, CS19 and CS20. The unit weight ratio for the standard No.1 manhole (Model No. 1) is approximately 0.53. The ground water table for selected test cases coincides with the depth of 1 m from the ground surface. The uplift ratio is decreased by 0.04 from the standard No.1 manhole (0.32) due to an increase in the apparent unit weight of manholes as shown in Fig. 2.23.

In Fig. 2.23, the manhole does not uplift when the apparent unit weight of the manhole equals to the saturated unit weight of backfill. These facts suggest that the manholes may not uplift if the apparent unit weight of the manhole is the same as the saturated unit weight of backfill (γ_{sat}) in the liquefied ground, because the apparent unit weight of the manholes, as a resistance force, is the same as the buoyant force acting on the manhole by the liquefied backfill. The absolute settlement is slightly decreased with an increasing the apparent unit

weight of the manholes because the uplift displacement is decreased.

Fig. 2.22 Lead beads using the centrifuge model tests to increase an apparent unit weight of the manhole.

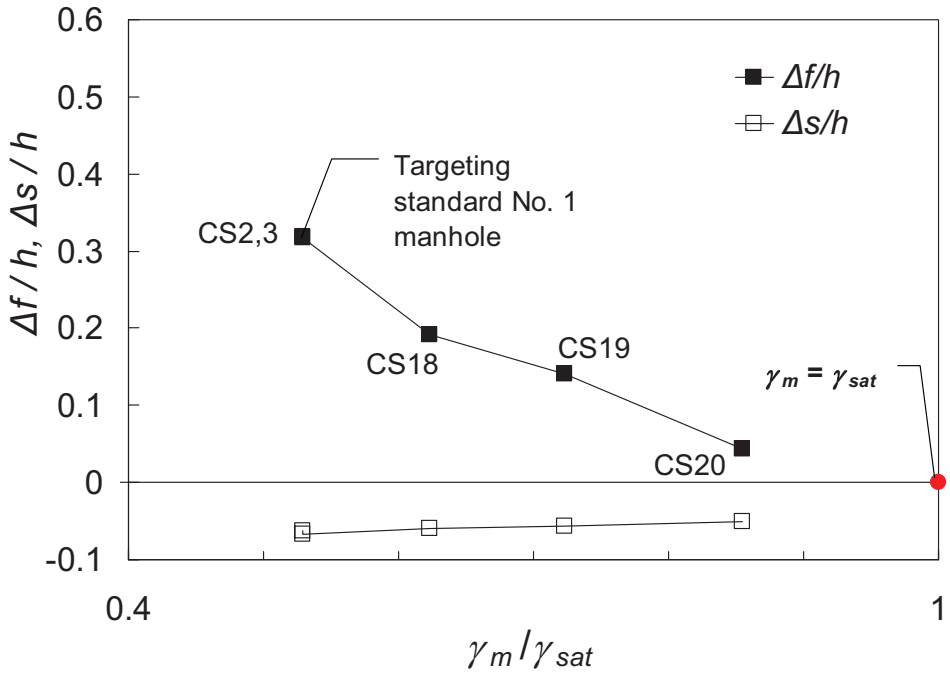

Fig. 2.23 Relationship between uplift ratio and manhole length for CS2, CS3, CS18, CS19 and CS20.

2.5.9 Relationship between uplift displacement and condition of native ground

As a secondary factor affecting the uplift behavior, the effects of native ground were investigated through the centrifuge model tests.

To evaluate the effects of native ground, CS2, CS3, CS8, CS12, CS13 and CS14 tests were conducted. The amplitude of input acceleration for selected test cases is in the range of 6.89 ~ 7.25 m/s^2 and the relative density of backfill is about 36% for all selected test cases. CS2 and CS3 tests were conducted in dense ground with Dr ≈ 85% for native ground. CS8 and CS12 tests were carried out for loose ground with Dr ≈ 36% and medium ground with Dr ≈ 65%, respectively. In CS13, an acrylic box is used as a trench as shown in Fig. 2.24, and CS4 is mixed with sand (85%) and clay (25%) as the native ground. The acrylic box is used to express rigid and undrained boundary condition for backfill during shaking. The sand mixed clay material in CS14 can express the native ground with low permeability and the coefficient of permeability for the sand mixed clay material is 9.81×10^{-5} cm/s which is obtained by a permeability test.

Figure 2.25 shows the results of centrifuge model tests. The maximum uplift ratio (CS8: 0.36) is observed when the native ground is loose sand (Dr ≈ 36%). The uplift ratio is slightly decreased when the native ground consists of dense sand (Dr ≈ 85%). The uplift ratio is small when an acrylic box is used as rigid and undrained boundary condition for backfill. The reason may be that the native ground does not affect the backfill due to the rigid boundary condition caused by the acrylic box. After all, the magnitude of uplift displacement, according to condition of the native ground, is increased in the following sequence: (1) Loose ground with Dr ≈ 36%, (2) Medium ground with Dr ≈ 65 %, (3) Dense ground with Dr ≈ 85%, (4) Sand mixed clay materials with low permeability and (5) rigid and undrained boundary condition for backfill using the acrylic box.

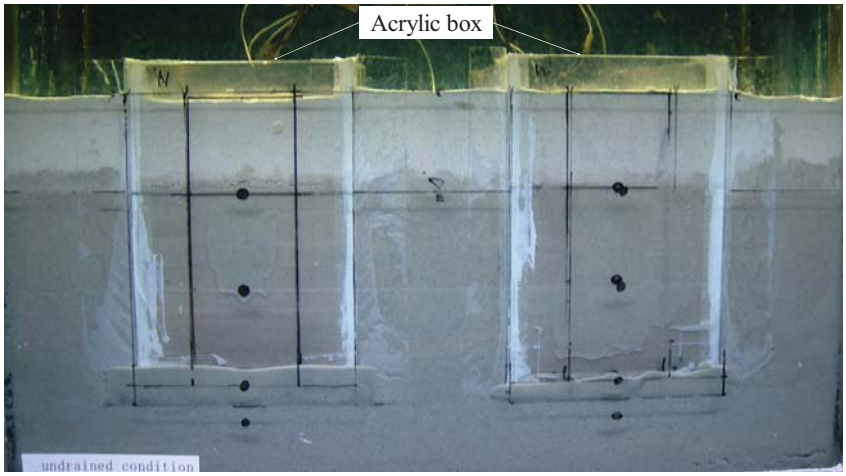

Fig. 2.24 Model manhole for CS13 used acrylic box.

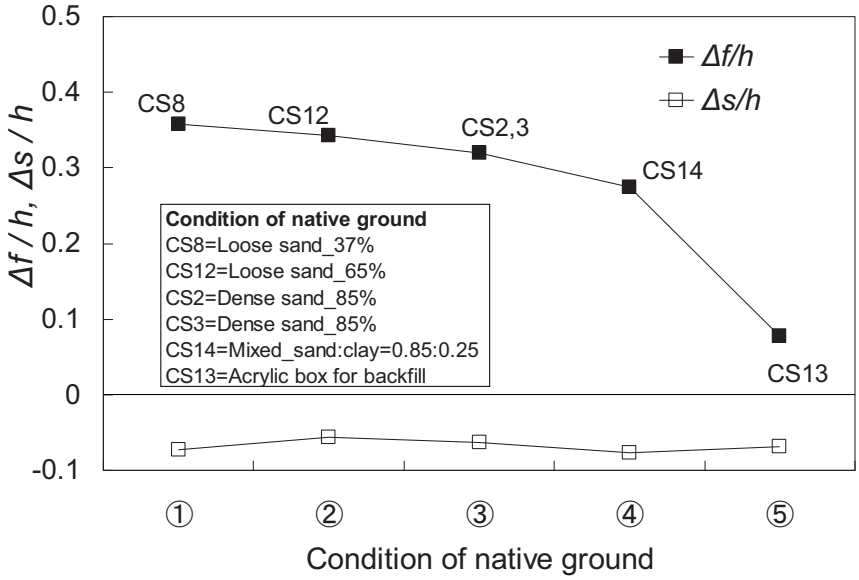

Fig. 2.25 Relationship between uplift ratio and condition of native ground.

To study the uplift behavior of the manhole according to the condition of the native ground in detail, the accelerations measured at the top and bottom of the manhole and on the shake table, and excess pore water pressure measured in backfill (P1) are compared in Fig. 2.26. Left, middle and right rows of Fig. 2.26 correspond to CS8, CS3 and CS13, respectively. As mentioned above, the maximum uplift ratio is observed (Dr of native ground ≈ 36%) in CS8,

and the excess pore water pressure in backfill reaches the initial effective vertical stress at 5 s during shaking [Fig. 2.26(a)]. However, the excess pore water pressure in backfill for CS3 and CS13 reaches the initial effective vertical stress at 6.5 s during shaking [Fig. 2.26(e) and (i)]. This indicates that the liquefaction of the native ground speeds up liquefaction of backfill and that affects the uplift displacement of the manhole.

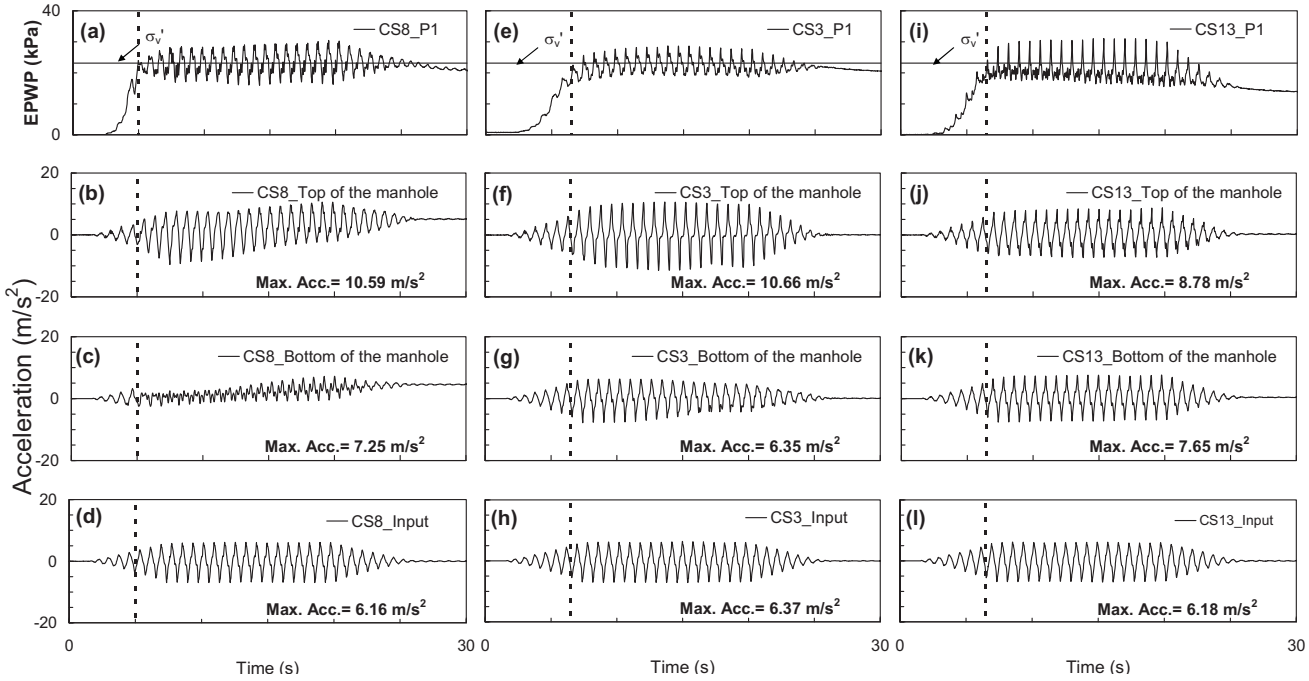

Fig. 2.26 Acceleration measured on the shake table and excess pore water pressure measured at the top and bottom of the manhole; Left row is CS8, middle is CS3 and right is CS13.

The amplitude of the acceleration at the top of the manhole in CS8 is significantly larger than that at the bottom of the manhole [Fig. 2.26(b) and (c)] compared with those in CS3 [Fig. 2.26(f) and (g)]. Namely, a larger inertial force is acting at the top of the manhole during uplift in CS8. This fact represents a rocking behavior of the manhole during uplift. On the other hand, the amplitude of the accelerations at the top and bottom of the manhole for CS13, in which the uplift ratio is the smallest among the selected test cases, is slightly amplified after

liquefaction (6.5 s) compared with the input acceleration and the peaks of acceleration at the top and bottom of the manhole which are almost in the same level [Fig. 2.26(j) – (l)]. These facts also represents that the rocking behavior of the manhole is one of the important causes of the onset of large magnitude of the manhole uplift.

2.5.10 Relationship between uplift displacement and contact condition between the bottom of a manhole and trench

The uplift displacement is also influenced by the contact condition between the bottom of a manhole and trench. Uplift behavior under various contact conditions between manhole and foundation is compared in centrifuge model tests as follows: (1) Aluminum plate is placed at the bottom of the trench. It prevents liquefied sands flowing from the bottom of a manhole as shown in Fig. 2.27 (a), (2) Lattice shaped foundation for partial contact condition as shown in Fig. 2.27(b), (3) Gravel foundation and (4) liquefiable soil. In field construction, manholes are usually put on lattice shaped or gravels foundation.

(a) (b)

Fig. 2.27 Soil condition under the manhole: (a) aluminum plate for perfect contact and (b) lattice shaped foundation for partial contact.

Figure 2.28 shows the uplift ratio for various contact conditions. The minimum uplift ratio is 0.14 (0.29m) and the maximum uplift ratio is 0.30 (0.6 m). The uplift ratio of the manholes in gravel and lattice shaped foundation are nearly at the same level. The magnitude of uplift ratio increases in the following sequence: (1) Aluminum plate, (2) Gravel and lattice shaped foundation and (3) Liquefiable soil. The absolute settlement trends to slightly increase with increasing the uplift displacement.

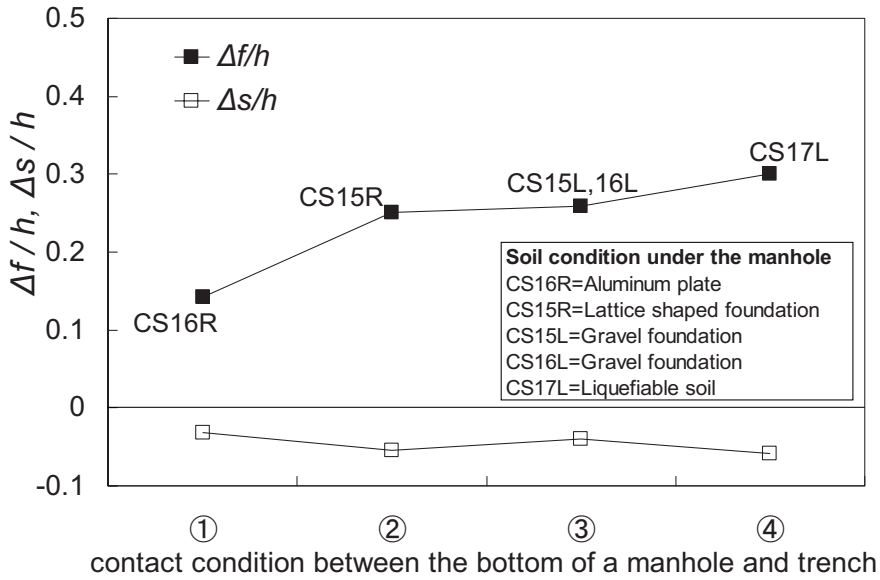

Fig. 2.28 Relationship between uplift ratio and soil condition under the manhole.

2.6 The relationship between uplift displacement and excess pore water pressure ratio

Excess pore water pressure ratio may have a large influence on the uplift displacement of a manhole in liquefied ground (Koseki, et al. 1997b). In this subsection, the relationship between uplift displacement and excess pore water pressure is investigated by comparisons among time histories of the safety factor, uplift displacement, and EPWPR (Excess pore water pressure ratio). Figure 2.29 shows the time histories of the safety factor and EPWPR in

backfill at depth of 2 m from the ground surface during uplifting. EPWPR is measured in centrifuge model tests [P1 of Fig. 2.7] divided by the initial effective vertical stress at the same depth with P1.

The safety factor is evaluated by using Koseki et al. (1997b)' method in which the EPWP (P1) measured in backfill is used as the s shape of EPWPR to evaluate uplift force acting on a manhole. The safety factor is expressed as follows:

$$F_s = \frac{M+R}{U+H} = \frac{\pi\left(d/2\right)^2 \gamma_m(h,\ d)h + \pi d h_w K \sigma_m \tan\delta}{\pi(d/2)^2 r_u \sigma_v{}' + \pi(d/2)^2 \gamma_w (h - h_w)} \tag{2}$$

where h is manhole length, d is diameter of the manhole, h_w is ground water depth in backfill, K is coefficient of lateral earth pressure (= 0.5), σ_m is vertical stress at the middle depth of a manhole above the ground water table to represent average value, δ is friction angle between manhole and backfill (= 10 degree), r_u is excess pore water pressure ratio, σ_v' is effective vertical stress at the depth of the bottom of a manhole, γ_w is the unit weight of water. In evaluating the frictional force R, the section which is shallower than the ground water table was considered. $\gamma_m(h, d)$ is the apparent unit weight of the manhole and the value is evaluated as follows:

$$\begin{aligned} \gamma_m(h,d) &= \frac{W}{V} \text{ (hollow cylindrial aluminium)} \\ &= \frac{\gamma_c \pi \left[\left(\frac{d}{2}\right)^2 - \left(\frac{d-t}{2}\right)^2 \right] h + W_{cap} + W_{base}}{\pi \frac{d^2}{2} h} \end{aligned} \tag{3}$$

where γ_c is unit weight of reinforced concrete, t is wall thickness W_{cap} is weight of manhole cap, W_{base} is weight of base slab.

As shown in Fig. 2.29(a) – (d), the safety factor is more than 1 before shaking, and the value is decreasing to less than 1 when the manholes are uplifted. However, the safety factor

of less than 1 continues despite finishing the uplift, because the safety factor does not consider the apparent unit weight of the uplifted manhole. As indicated by the vertical thick dotted line, the manhole starts to lift up slightly earlier than the pore water pressure in backfill (P1) reaches the initial effective vertical stress, and the uplift displacement is increased with rapid build-up of the EPWPR. Manhole uplift (1.07 m) in Fig. 2.29(a) is initiated at 4.5 s, and manhole uplift (0.20 m) in Fig. 2.29(d) is initiated at 7.5 s. These facts suggest that the triggering condition of manhole uplift can be evaluated by the safety factor and the EPWPR and is one of the important factors affecting the uplift behavior. In Fig. 2.29(e) and (f), although the safety factor is decreased to less than 1 at 9 s, the manhole does not uplift. The reason may be that the frictional force acting on the side of the manholes below the ground water table is neglected even though the backfill is not liquefied.

On basis of these, the EPWPR is one of the important factors affecting the uplift behavior. Thus, to investigate factors affecting EPWPR, it is compared with the uplift ratio. Figure 2.30 shows the time histories of EPWPR in CS1 (G.W.L = 0 m), CS2 (G.W.L = 1 m), CS4 (G.W.L = 1.7 m), and CS5 (G.W.L = 3 m) which are compared in the previous section to investigate the effect of ground water table against uplift behavior. The EPWPR, for convenience, is plotted by using a 2 second moving average filter to remove spikes during shaking. Next, the EPWPR at 7 s after shaking indicated by the vertical dotted line is extracted for each test case as shown in Fig. 2.30. The EPWPR is not increased in CS5 because the ground is dry sand.

Figure 2.31 shows the relationship between EPWPR and uplift ratio for each factor. The EPWPR is increased when the depth of ground water table is shallow, the amplitude of input acceleration is large and the relative density of backfill is large as shown in Fig. 2.31(a) – (c). The EPWPR is slightly increased with wide cross section of a trench. On the other hand, the manhole length and apparent unit weight of a manhole are irrelative to an increase of EPWPR.

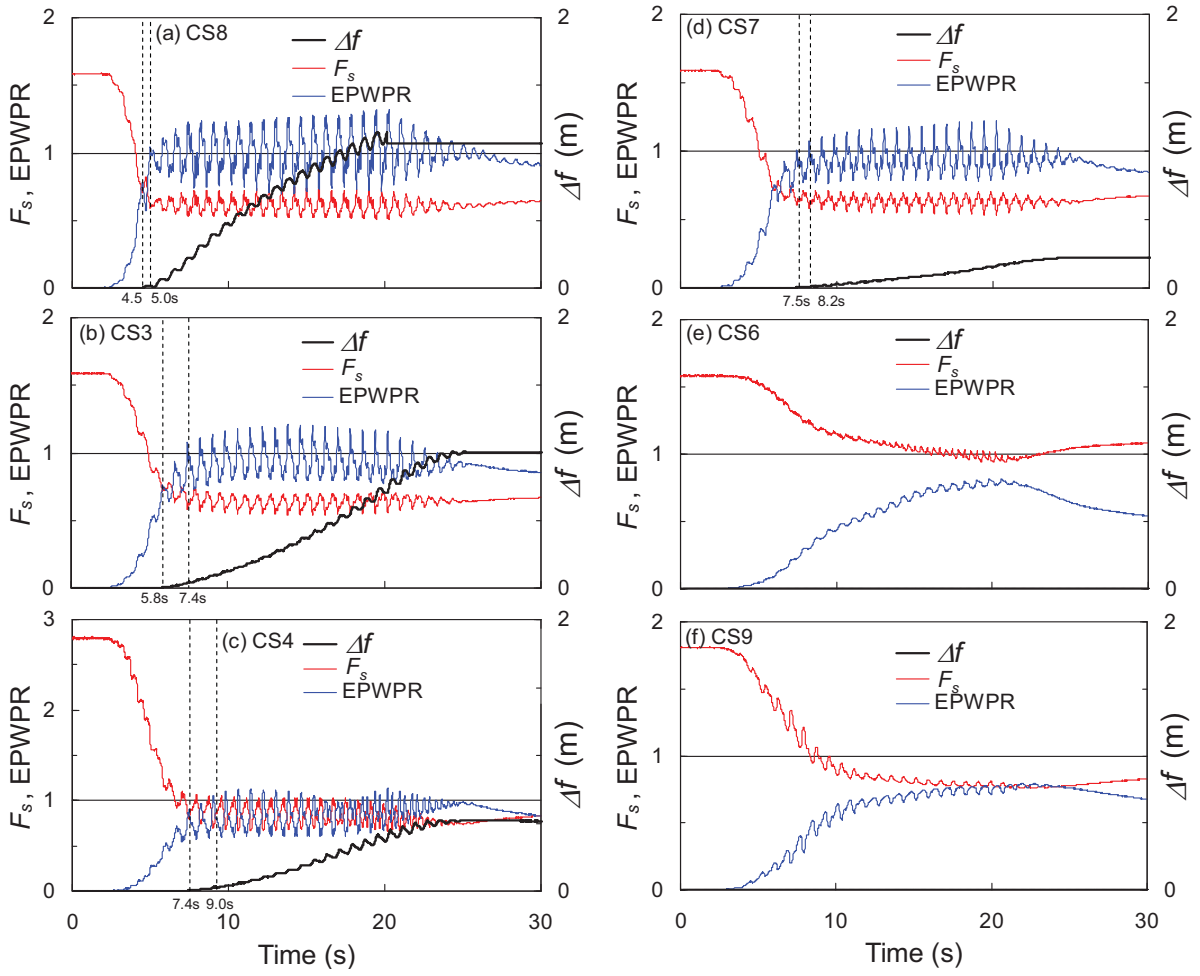

Fig. 2.29 Time histories of uplift displacement, safety factor and excess pore water pressure ratio; (a) CS8, (b) CS3, (c) CS4, (d) CS7, (e) CS6, (f) CS9.

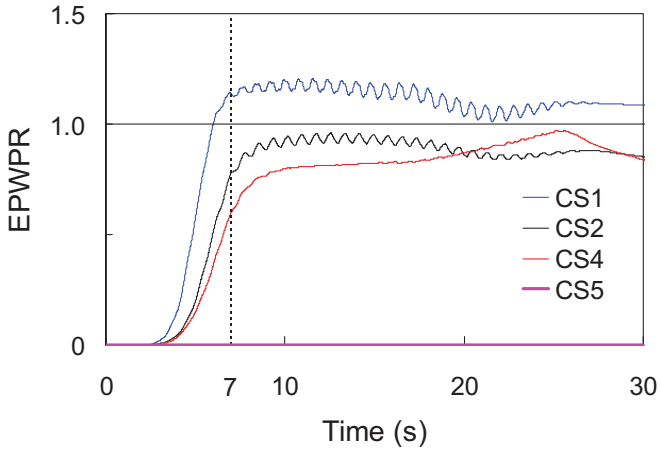

Fig. 2.30 Time histories of excess pore water pressure ratio in CS1, CS2, CS4 and CS5.

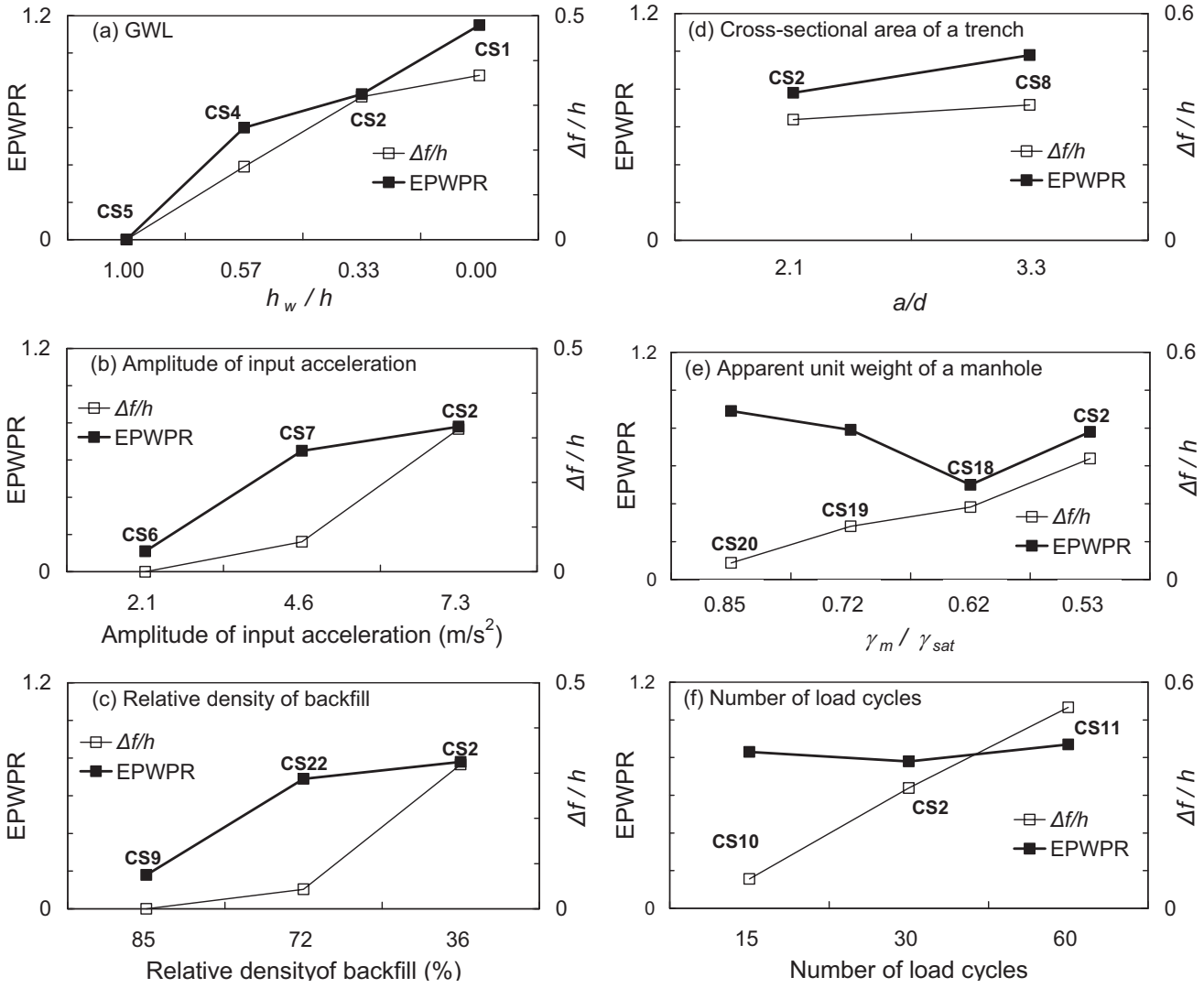

Fig. 2.31 Relationship between EPWPR and uplift ratio for each factor which is investigated in centrifuge model tests; (a) ground water table, (b) amplitude of input acceleration, (c) Relative density of backfill, (d) Cross-sectional area of a trench, (e) manhole length, and (f) apparent unit weight of a manhole.

In the case of the number of load cycles, there is no influence on increase of EPWPR in Fig. 2.32(a). However, the uplift displacement may be increased when the number of load cycles was increased and a high level of EPWPR then continued until the shaking stops as shown in Fig. 2.32(b).

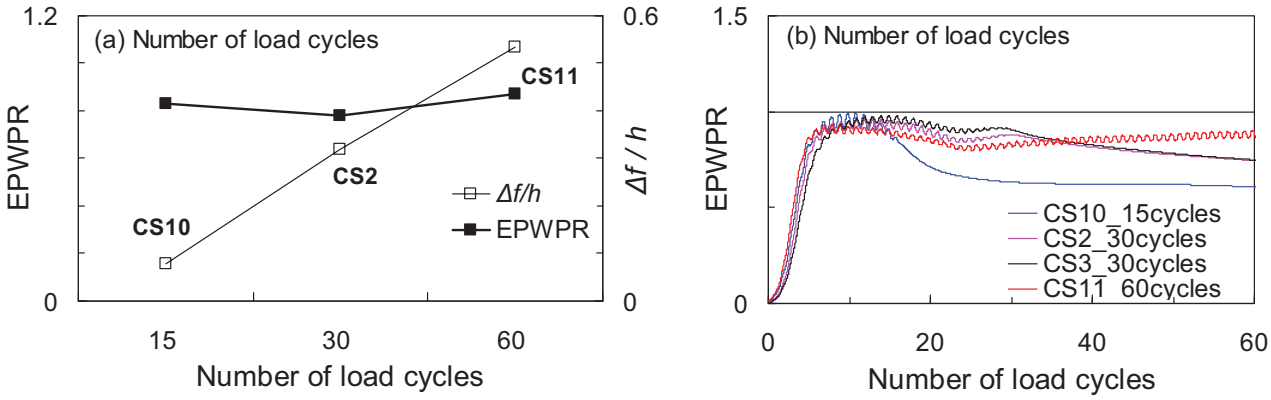

Fig. 2.32 Increase of EPWPR by number of load cycles; (a) relationship between EPWPR and uplift ratio for number of load cycles, (b) time histories of EPWPR according to number of load cycles.

2.7 Summary

Centrifuge experiments were performed to study the mechanism of the uplift behavior of a manhole and investigate the relationship between uplift displacement and factors which have large influence on manhole uplift behavior in liquefiable ground.

The centrifuge model tests not only made clear the mechanism of the uplift phenomenon but also elucidated that the uplift of the manhole was related to some factors as follows: (1) ground water table, (2) amplitude of input motion and number of load cycles, (3) relative density of backfill, (4) cross-sectional area of a trench, (5) manhole length, (6) apparent unit weight of a manhole, (7) condition of native ground, and (8) contact condition between the bottom of a manhole and trench. Among these factors, (1) ~ (6) are directly affecting the uplift behavior as a primary factor, and (7) ~ (8) indirectly affect the uplift behavior as a secondary factor.

The manhole starts to lift up when the excess pore water pressure in the middle of the backfill and that of the bottom of the manhole exceeds the initial effective vertical stress. Once

the manhole is slightly uplifted, liquefied backfill flows toward the bottom of the manhole during uplifting. Also, the rocking behavior of manholes is thought to be one of major causes to lead to large uplift displacement of manholes.

For comparisons between uplift displacement and factors affecting the uplift behavior, the condition of the model test considered as a standard case (CS3) is as follows: ground water table coincides with the depth of 1 m from the ground surface, relative density of backfill is about 36% and relative density of native ground is about 85%, amplitude of input acceleration is about 7.15 m/s^2, number of load cycles is 30 cycles, the ratio (a/d = trench width / manhole diameter) for cross-sectional area of a trench is 2.09, manhole length is 3m, and unit weigh ratio (γ_m/γ_{sat} = apparent unit weight of the manhole/saturated unit weight of backfill) is about 0.53. In this standard case, the uplift ratio ($\Delta f/h$ = uplift displacement/manhole length) is recorded at 0.32 (standard uplift ratio). The relationship between uplift displacement and factors affecting the uplift behavior are derived as follows:

(1) When the ground water table coincides with the ground surface, the uplift ratio is increased by 0.37 from the standard uplift ratio (0.32). When the ground water table is located at the depth of 1.7 m from the ground surface, the uplift ratio is decreased by 0.16 from the standard uplift ratio.

(2) When the amplitude of input acceleration is decreased by 4.64 m/s^2 from the standard case (7.15m/s^2), the uplift ratio is decreased by 0.07 from the standard uplift ratio. When amplitude of input acceleration is decreased by 2.05m/s^2, the manhole is not uplifted because backfill was not liquefied. The uplift ratio is increased by 0.53 from the standard uplift ratio when number of load cycles is approximately 60 cycles. Also, the manholes stop uplifting when the input wave stops. As shaking continues, it will tilt when the uplift displacement exceeds the center of gravity of the manhole.

(3) When backfill is compacted by 72% from the standard case, the uplift ratio is decreased by 0.043 from the standard uplift ratio. When backfill is compacted by 85% from the standard case (36%), the manhole is not uplifted ($\Delta f = 0$) because backfill is not liquefied in the compacted ground.

(4) When ratio (a/d) for the cross-sectional area of a trench in the horizontal plane is increased by 3.34 from the standard case ($a/d = 2.09$), the uplift ratio is increased by 0.36 from the standard uplift ratio. Although the cross-sectional area of the trench is increased about 1.75 times from the standard case, the uplift ratio is only increased about 0.04.

(5) When the manhole length is a 2 m (the standard case (3 m), the uplift ratio is decreased by 0.25 from the standard uplift ratio. Although, the length of manholes is different from each other, the uplift ratio is not largely changed at the same ground water table ratio (h_w/h).

(6) When the unit weight ratio (γ_m/γ_{sat}) is increased by 0.85 from the standard case (0.53), the uplift ratio is decreased by 0.04 from the standard uplift ratio. Also, the manholes may not be uplifted if the apparent unit weight of manhole is the same ($\gamma_m/\gamma_{sat} = 1$) as the saturated unit weight of backfill.

(7) Magnitude of uplift displacement with the condition of the native ground is increased as in the following sequence: (1) Loose ground with Dr ≈ 36%, (2) Medium ground with Dr ≈ 65%, (3) Dense ground with Dr ≈ 85%, (4) Sand mixed clay materials with low permeability, and (5) Rigid and undrained boundary condition for backfill by using the acrylic box.

(8) Magnitude of uplift displacement considering contact condition between the bottom of a manhole and trench is increased as in the following sequence: (1) Aluminum plate, (2) Gravel and lattice shaped foundation and (3) Liquefiable soil.

Among these factors, the most important factors affecting the uplift displacement are ground water table, relative density of backfill and amplitude of input acceleration. The absolute settlement trends to slightly increase with increasing uplift displacement for all test cases.

The triggering condition of manhole uplifts can be evaluated by the safety factor in which the EPWP (P1) measured in backfill is used as the s shape of EPWPR to evaluate uplift forces acting on a manhole in liquefied ground. The uplift displacement is increased with a rapid build-up of the EPWP through relationships among time histories of uplift displacement, safety factor and EPWPR. On the basis of these, the EPWPR is found as one of the important factors affecting uplift behavior. Also, the EPWPR is increased with a shallow ground water table, high amplitude of input acceleration and low relative density of backfill. However, the EPWPR is slightly increased with a wide cross section of a trench, and increase of EPWPR is irrelative to manhole length and apparent unit weight of a manhole. Meanwhile, the uplift displacement is increased when the number of load cycles is increased and a high level of EPWPR then continued until the shaking finished.

3. Simplified method for estimation of the maximum displacement of manhole uplift

3.1 Introduction

Generally speaking, a simplified method based on the equilibrium of vertical forces acting on a manhole and numerical analysis based on the mechanics of a continuum body can be taken to estimate the uplift displacement of the manhole by liquefaction. Also, the prediction methods should be able to consider factors affecting the uplift behavior to provide precise estimates of the uplift displacement. For example, the factors investigated in centrifuge studies were as follows: ground water, amplitude of input acceleration, the relative density of backfill, etc.

The simplified method can only predict the maximum uplift displacement after shaking because of difficulties considering uplift behavior of buried manholes in completely liquefied ground. On the other hand, the numerical analysis by the finite element method can predict transient behavior during shaking as well as the maximum uplift displacement after shaking.

In this chapter, a simplified method for quantitative estimation of the maximum uplift displacement is proposed and discussed. With the assumption that the volume of the trench is continuity, a preliminary study for verification of the simplified method is performed through comparison with results of a simple model test by using the boiling method. In this study it is assumed that the volume in the trench is continuity. To verify the validation or application of the proposed method, in addition, the predicted uplift displacements by the simplified method are compared with those obtained from the centrifuge model tests.

3.2 Derivation and behavior of the simplified method

The mechanism of uplift behavior of buried manholes is explained as follows: First, the uplifting force is initiated by the increase in excess pore water pressure due to the liquefaction of backfill caused by strong shaking. Once the manhole is slightly uplifted, liquefied backfill flows beneath a manhole. Uplifting continues until equilibrium is reached among the uplifting force, the weight of the manhole, friction, and resistance from the sewage pipes connected to a manhole. Based on this equilibrium, the safety factor against uplift is derived. Koseki et al. (1997b) examined the relationship between the safety factor and the uplift displacement of box-type structures and manholes. They concluded that uplift of underground structures continues when the safety factor is almost equal to or less than 1.0, and the safety factor can be used to evaluate whether manhole uplift is triggered or not. This factor, however, only yields the triggering condition of manhole uplift and is incapable of predicting the amount of uplift.

3.2.1 Derivation

A new simple and quantitative method for estimation of the maximum uplift displacement is proposed based on the above-mentioned equilibrium of forces acting on a buried manhole. The simplified method can consider important factors affecting the uplift behavior investigated through centrifuge model tests as follows; excess pore water pressure ratio, ground water table, unit weight of backfill (the relative density), apparent unit weight of a manhole, manhole size (length and diameter), and cross-sectional area of a trench.

To derive the simplified method for quantitative estimation of uplift displacement, another condition to be assumed is the continuity of the volume between the uplifted portion of the manhole and ground settlement of backfill. The method aims to estimate the maximum uplift

displacement of a manhole and settlement of backfill, i.e., the amount of the uplift and the settlement of backfill at the final state.

On deriving the method, the following assumptions are made: (1) no volume change in the trench during the uplifting, (2) undrained condition of the trench during liquefaction of backfill, i.e., no volume change is allowed in the backfill material of the trench, (3) ground water depth is kept constant in the backfill because the duration of uplifting may be short enough for the ground water to permeate into the ground above the water table, (4) uniform settlement of backfill in the trench, (5) pipes attached to the manhole are neglected for simplicity, and (6) no tilting of the manhole.

Among these assumptions, undrained condition (2) is rather a strict restriction. In reality, backfill is consolidated due to dissipation of excess pore water, and the change of volumetric strain due to the consolidation is estimated as large as 5 to 6 % (Ishihara and Yoshimine, 1992). This amount may be negligible compared to the one caused by the uplift of a manhole.

An idealized diagram of a manhole and trench is shown in Fig. 3.1. The manhole is simplified as a hollow cylinder whose height and diameter are, respectively, h and d. It is installed in a trench whose cross-section in horizontal plane is a square of side a. Ground water depth is specified by h_w. As shown in the following formulation, the depth of a trench becomes irrelevant to the amount of uplift and settlements of backfill.

From the assumptions given above, the volume of the uplifted portion of the manhole above the original ground surface is equal to the amount of the settled volume measured from the original ground surface of backfill. Let Δf and Δs be, respectively, the uplift displacement of the manhole and settlement of the backfill. Then, equating these volumes, the relationship can be obtained as follow:

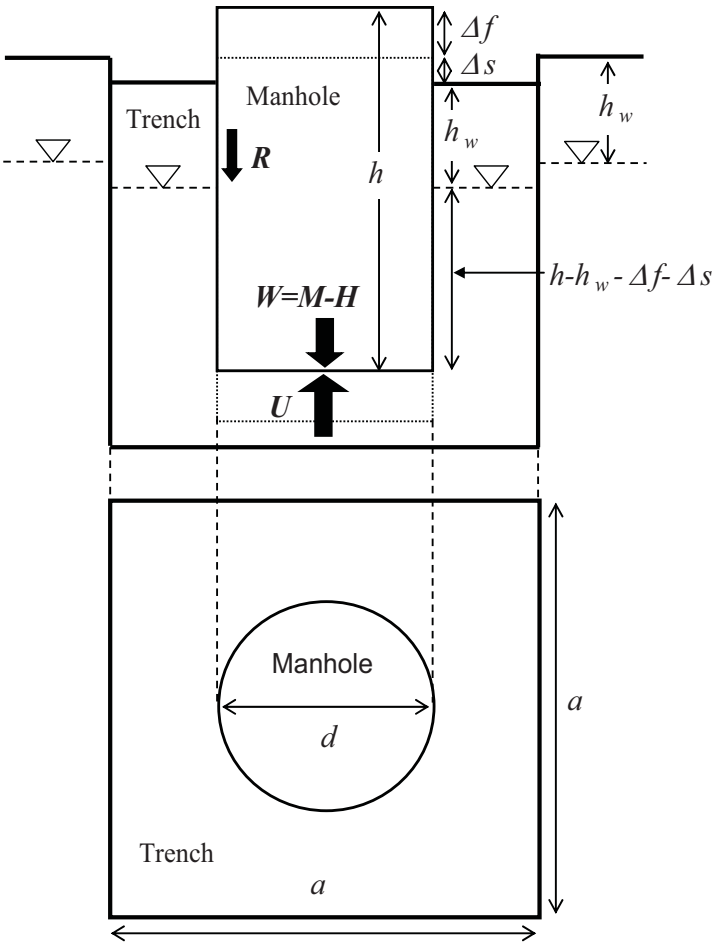

Fig. 3.1 Idealized diagram of a manhole and trench.

$$\pi\left(\frac{d}{2}\right)^2 \Delta f = \left\{a^2 - \pi\left(\frac{d}{2}\right)^2\right\}\Delta s \qquad (1)$$

Solving Eq. (1) for Δf gives

$$\Delta f = \left\{\frac{1}{\pi}\left(\frac{2a}{d}\right)^2 - 1\right\}\Delta s \qquad (2)$$

Next, the condition of manhole uplift is considered. Forces acting on the manhole are the buoyant weight of the manhole, $W=M - H$ where M is the weight of the manhole and H is the

buoyant force due to a hydrostatic pressure, the frictional force acting at the side of the manhole, *R*, and the uplift force due to the excess pore water pressure, *U*. During the uplifting of a manhole, the following inequality holds:

$$M + R \le U + H \tag{3}$$

From Eq. (3), the safety factor against uplift, *S*, can be derived as follows (Koseki, et al., 1997b):

$$F_s = \frac{M + R}{U + H} \tag{4}$$

The force due to the buoyant weight of the manhole is given as

$$W = M - H = \pi \left(\frac{d}{2} \right)^2 \sigma_{vm}' = \pi \left(\frac{d}{2} \right)^2 \left\{ \gamma_m(h,\ d)h - \gamma_w(h - h_w - \Delta f - \Delta s) \right\} \tag{5}$$

where $\gamma_m(h, d)$ is the apparent unit weight of the manhole, which is a function of the manhole length, *h*, and diameter, *d*, and γ_w is the unit weight of water.

If it assumes that the frictional force on the side of the manhole acts only above the ground water table and that the frictional force due to liquefied backfill is neglected, then

$$R = \pi d h_w \sigma_r = \pi d h_w K \sigma_m \tan\delta \tag{6}$$

where *K* is the coefficient of lateral earth pressure, σ_r is normal stress acting on the lateral side of a manhole above the ground water table, σ_m is vertical stress at the middle depth of a manhole above the ground water table to represent average value, and δ is the angle of friction between the manhole and backfill. The uplifting force is expressed as a function of the effective vertical stress at the same depth as the manhole base in the backfill,

$$U = \pi \left(\frac{d}{2} \right)^2 r_u(\gamma_t h_w + \sigma_v') = \pi \left(\frac{d}{2} \right)^2 r_u \left\{ \gamma_t h_w + \gamma'(h - h_w - \Delta f - \Delta s) \right\} \tag{7}$$

where γ_t is the unit weight of backfill above the groundwater table, $\gamma' = \gamma_{sat} - \gamma_w$ is the submerged unit weight of backfill, σ_v' is effective vertical stress at the depth of the bottom of a manhole in the backfill and r_u is excess pore water pressure ratio.

To formulate the uplift displacement of the manhole and settlement of backfill soil, substitute Eqs. (5) to (7) into Eq. (3), and solve for the sum of uplift displacements and settlements, $\Delta f + \Delta s$:

$$\Delta f + \Delta s = \left(1 - \frac{\gamma_m(h,\ d)}{r_u\gamma' + \gamma_w}\right)h - \left(1 - \frac{r_u\gamma_t}{r_u\gamma' + \gamma_w}\right)h_w - \frac{R}{r_u\gamma' + \gamma_w}\frac{1}{\pi}\left(\frac{2}{d}\right)^2 \tag{8}$$

Then, removing Δf from Eqs. (8) and (2), the maximum settlement of backfill is given by

$$\Delta s = \pi\left(\frac{d}{2a}\right)^2 \left\{\left(1 - \frac{\gamma_m(h,\ d)}{r_u\gamma' + \gamma_w}\right)h - \left(1 - \frac{r_u\gamma_t}{r_u\gamma' + \gamma_w}\right)h_w - \frac{R}{r_u\gamma' + \gamma_w}\frac{1}{\pi}\left(\frac{2}{d}\right)^2\right\} \tag{9}$$

Substituting Eq. (9) into Eq. (8), the maximum uplift displacement of a manhole is obtained:

$$\Delta f = \left\{1 - \pi\left(\frac{d}{2a}\right)^2\right\}\left\{\left(1 - \frac{\gamma_m(h,\ d)}{r_u\gamma' + \gamma_w}\right)h - \left(1 - \frac{r_u\gamma_t}{r_u\gamma' + \gamma_w}\right)h_w - \frac{R}{r_u\gamma' + \gamma_w}\frac{1}{\pi}\left(\frac{2}{d}\right)^2\right\} \tag{10}$$

Now let us simplify Eq. (10) under the following conditions:

(1) Ground water level is at the ground surface (h_w = 0.0 m)

(2) Backfill is totally liquefied (r_u = 1.0)

(3) Cross-sectional area of the trench is large ($a = \infty$)

Then, Eq. (10) is simplified to

$$\Delta f = \left(1 - \frac{\gamma_m(h,\ d)}{\gamma_{sat}}\right)h \tag{11}$$

From Eq. (11), the maximum uplift displacement is expressed as a function of the ratio of the apparent unit weight of the manhole and the saturated unit weight of backfill. This equation may give us some insights into the phenomena and can be used as an initial estimate of the uplift displacement. The maximum uplift displacement by the simplified method is about 50 % of the manhole length when the properties of soil and manholes used in centrifuge model tests are adopted.

3.3 Preliminary study for verification of the simplified method through static 1G model tests

The simplified method is validated through comparisons with the uplift displacement of a well-controlled model tests by using the boiling method as a preliminary study. Figure 3.2(a) shows the schematic view which can illustrate the test procedure. Figure 3.2(b) and (c) is the manholes before and after the tests. The values of parameters used to predict the maximum uplift displacement are summarized in Table 3.1. A total of 6 tests are conducted as summarized in

Table 3.2. Diameter of the model manhole made of aluminium cylinder is 55 mm and length of manhole models is either 150 or 100 mm. It corresponds to model manhole No.1 and No. 4 used in centrifuge modeling tests of Chapter 2. The model manhole was placed in the cylindrical container whose diameter and depth were, respectively, 88 mm and 200 mm (Fig. 3.2). This container is regarded as a trench.

The procedure of the test is as follows: Firstly, the model manhole was placed in the empty container. Then, silica sands were poured in the air as a backfill. To simulate liquefaction in the backfill, normal water was slowly injected through a valve located at the bottom of the container. The height of sands before uplifting of the manhole was 200 mm which gives 40 % of the relative density. Maximum uplift displacement of the cylinder and the amount of the settlement were measured by a ruler as shown in Fig. 3.2 (b) and (c).

Because horizontal section of the model trench is not square but circular, Eq. (1) is modified as follows:

$$\pi\left(\frac{d}{2}\right)^2 \Delta f = \frac{\pi}{4}\left\{a^2 - d^2\right\}\Delta s \qquad (12)$$

where d is the diameter of the model trench.

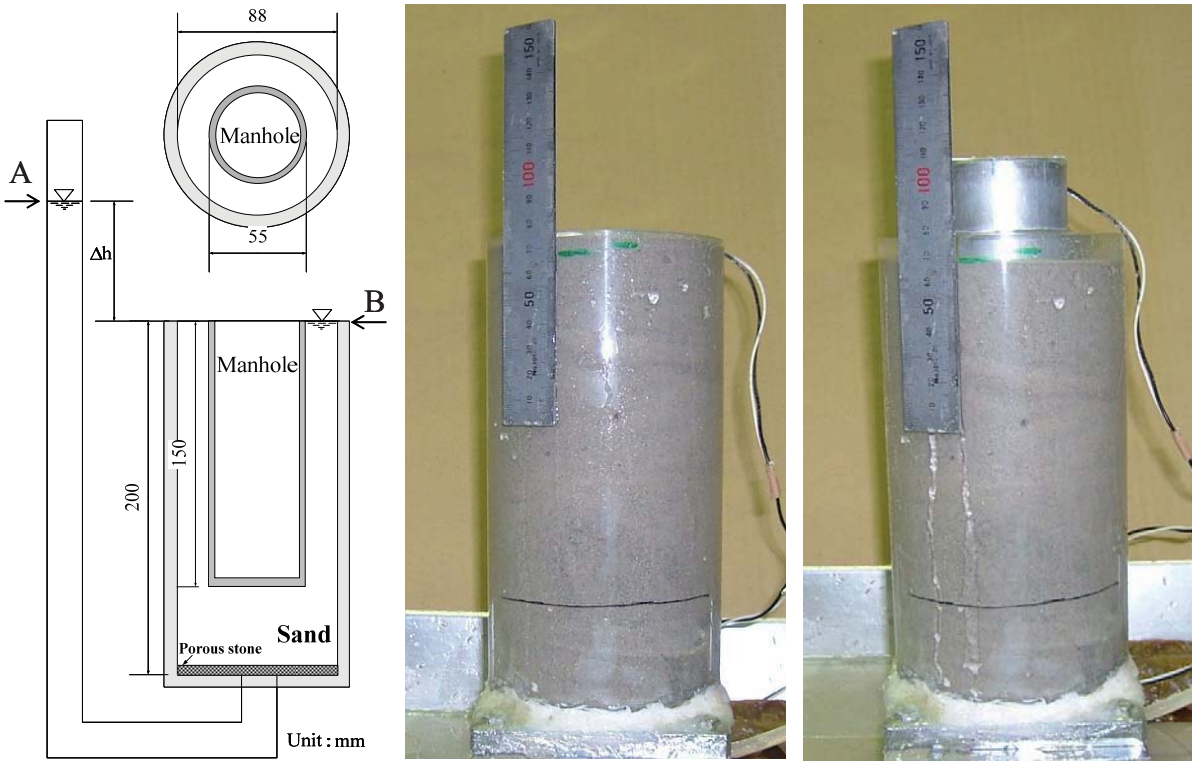

Fig. 3.2 Schematic view of a simple test to verify the propose method: (a) Schematic view (b) before the test and (c) after the test.

Solving Eq. (12) for Δf gives

$$\Delta f = \left\{ \left(\frac{a}{d} \right)^2 - 1 \right\} \Delta s \tag{13}$$

The following relationships are used for the estimate for surface settlements,

$$\Delta s = \left(\frac{d}{a} \right)^2 \left\{ \left(1 - \frac{\gamma_m(h,\, d)}{r_u \gamma' + \gamma_w} \right) h - \left(1 - \frac{r_u \gamma_t}{r_u \gamma' + \gamma_w} \right) h_w - \frac{R}{r_u \gamma' + \gamma_w} \frac{1}{\pi} \left(\frac{2}{d} \right)^2 \right\} \tag{14}$$

And for uplifts,

$$\Delta f = \left\{1-\left(\frac{d}{a}\right)^2\right\}\left\{\left(1-\frac{\gamma_m(h,\ d)}{r_u\gamma'+\gamma_w}\right)h-\left(1-\frac{r_u\gamma_t}{r_u\gamma'+\gamma_w}\right)h_w-\frac{R}{r_u\gamma'+\gamma_w}\frac{1}{\pi}\left(\frac{2}{d}\right)^2\right\} \quad (15)$$

Table 3.2 shows the summary of test results, and predicted maximum uplift displacement of the manhole and the maximum settlement of backfill are derived by Eqs. (14) and (15). The measured maximum uplift displacements are 44 mm for the manhole with 150 mm length and 28 mm for the manhole with 100 mm length.

Table 3.1 Parameters for the backfill, manhole and trench used in the centrifuge experiments (Prototype scale).

Backfill	Max. void ratio	e_{max}	1.19	
	Min. void ratio	e_{min}	0.71	
	Density	G_s	2.66	
	Wet sand	γ_t	14.8	kN/m^3
	Saturated sand	γ_{sat}	18.1	kN/m^3
	Friction angle b/w concrete and soil	δ	10.0	deg
	Diameter of a trench (Preliminary study)	a	8.8	cm
	Width of a trench (Centrifuge study)	a	2.3	m
Manhole	Length	h	3.0	m
	Diameter	d	1.1	m
	Apparent unit weight of a manhole	γ_m	9.57	kN/m^3

Table 3.2 Summary of test results and predicted uplift displacement and settlement.

Model type	Manhole Length	Measured uplift displacement	Measured settlement of backfill	Predicted uplif displacement	Predicted settlement of backfill
	mm	mm	mm	mm	mm
Model manhole No.1	150	40 43 44	19 19 18	43.1	27.6
Model manhole No.4	100	28 25 27	11 11 11	27.4	17.5

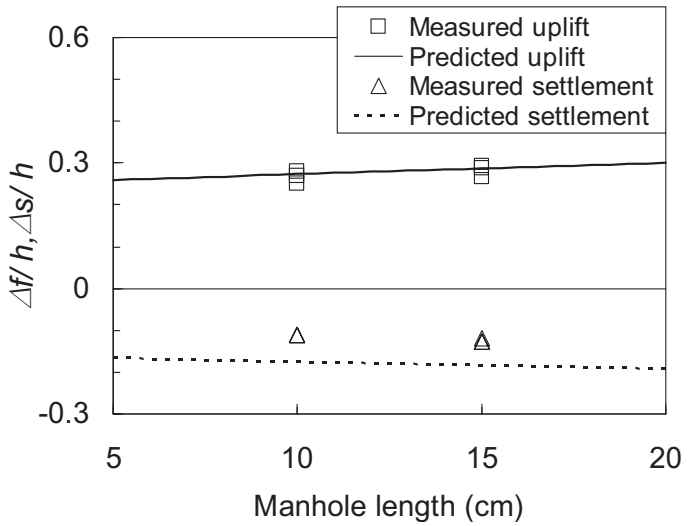

Fig. 3.3 Comparison between measured and predicted maximum uplift displacement and settlement of soil surrounding manhole.

Figure 3.3 shows the comparison between measured and predicted maximum uplift displacements and settlements of soil around the manhole. Just before the sand-boils, the cylinder started uplifting and reached the uplift displacement of 40 mm (Fig. 3.3) which was exactly anticipated by the proposed method, Eq. (14). After shutting off the injection of water, the model manhole was not sunk, indicating the state of equilibrium between the model manhole and backfill material. For settlements, however, the measured amounts were smaller than predicted ones for both cases of manhole length (Fig. 3.3). Although it takes time for consolidation of backfill, the settlement was measured right after tests. As mentioned earlier, "ground water depth is kept constant in the backfill" was assumed to derive from the simplified method, however, the assumption is not admitted in this simple model test. Thus, the discrepancy between measured and predicted settlements of backfill is found. This might be attributed to the boiling method which made backfill be loosely deposited. By the well-controlled small scale experiments as described above, the applicability of the method was examined and verified.

3.4 Uplift behavior of the manhole by the simplified method

3.4.1 Effects of excess pore water pressure ratio

The method enables us to evaluate the amount of uplift of a manhole and settlement of backfill as a function of excess pore pressure ratio, r_u. However, predicted uplift displacement has negative value when the ratio, r_u, is small. It indicates that the manhole is settled under a low r_u in the simplified method. Therefore, the minimum value of excess pore water pressure ratio has to be investigated so that the uplift displacement becomes a positive value. If it is regarded as an infinitely large cross-sectional area of a trench ($a \rightarrow \infty$), Eq. (10) has to be larger than zero as follows:

$$\left\{\left(1-\frac{\gamma_m(h,\ d)}{r_u\gamma'+\gamma_w}\right)h-\left(1-\frac{r_u\gamma_t}{r_u\gamma'+\gamma_w}\right)h_w-\frac{R}{r_u\gamma'+\gamma_w}\frac{1}{\pi}\left(\frac{2}{d}\right)^2\right\}\geq 0 \qquad (16)$$

Then, Eq. (16) is simplified to

$$r_u \geq \frac{(\gamma_m-\gamma_w)h+\gamma_w h_w+\frac{R}{\pi}\left(\frac{2}{d}\right)^2}{(\gamma' h-\gamma' h_w+\gamma_t h_w)} \qquad (17)$$

Figure 3.4 shows the normalized maximum uplift displacement versus the normalized ground water depth. The length of the manhole, h, is employed for the normalization. Values of parameters to be inputted into Eqs. (8) to (10) are summarized in Table 3.1. These parameters are taken from the centrifuge experiment in a previous chapter. Curves in Fig. 3.4 illustrate the estimated amount of uplift [Fig. 3.4(a)], settlement [Fig. 3.4(b)], and total vertical displacement [Fig. 3.4(c)] for a given excess pore pressure ratio with variation of normalized ground water depth, h_w/h. The minimum excess pore water pressure ratio, in which the uplift displacement becomes a positive value, correspond to 0, 0.13, 0.36, 0.52, 0.60 and 0.75 for each h_w/h satisfying Eq. (17) as shown in Fig. 3.4(a). The minimum excess pore water pressure ratio is

increased when the ground water table is deep.

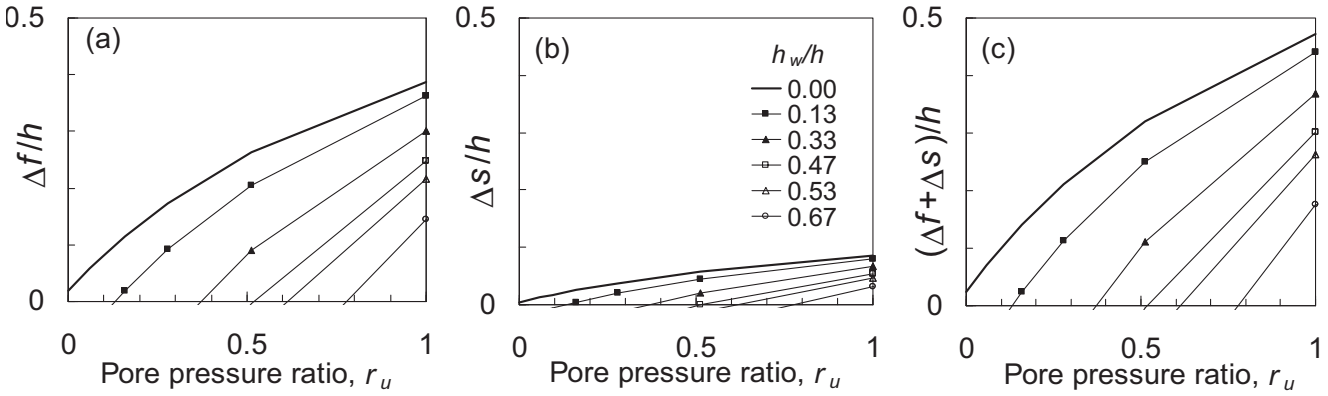

Fig. 3.4 Excess pore water pressure ratio (r_u) and the normalized ground water depth (h_w/h), versus (a) normalized uplift, $\Delta f/h$, (b) normalized settlement, $\Delta s/h$, and (c) normalized total displacement, $(\Delta f + \Delta s)/h$.

In Fig. 3.4, if the ground water table coincides with the surface of backfill ($h_w/h = 0.0$) and excess pore pressure ratio is 0.5, then the maximum uplift displacement of a manhole is expected to be about 25% of the manhole length [thick solid line in Fig. 3.4(a)]. Note that in Eqs. (9) and (10), the side frictional force of a manhole below the ground water table is assumed to be zero. This assumption may give an overestimation of the uplift, or excessively safe-side estimation. For a more precise prediction, a study on the effects of side friction in liquefied ground may be required. Another assumption to be considered here is that the drainage is not admitted at the surface of the backfill soil. If the drainage is admitted from the surface of backfill, the estimated uplift displacement may be reduced. This condition can be achieved in reality if excess pore water pressure is dissipated from gaps between the manhole and pavements spread over the backfill soil.

3.4.2 Effects of friction and unit weight of backfill

The simplified method can consider the effects of the frictional resistance force between the side wall of a manhole and backfill during the uplifting as a parameter *R*. As mentioned earlier, in evaluating the frictional force, *R*, the section which is shallower than the ground water table was considered. The relationships are shown in Fig. 3.5. Figure 3.5(a) is the case with no frictional force ($\delta = 0$), while the curves in Fig. 3.5(b) are with frictional force ($\delta = 10$). In Fig. 3.5, curves relative to various unit weights of non-liquefiable soil of backfill above the ground water table are also plotted for comparisons.

With the frictional force at the side of the manhole, the uplift displacement is slightly reduced compared to the case of no frictional force. When the ground water table is deep (h_w/h is large), the uplift displacement decreases. The uplift displacement is also increasing with the increase in unit weight of non-liquefiable backfill above the ground water table.

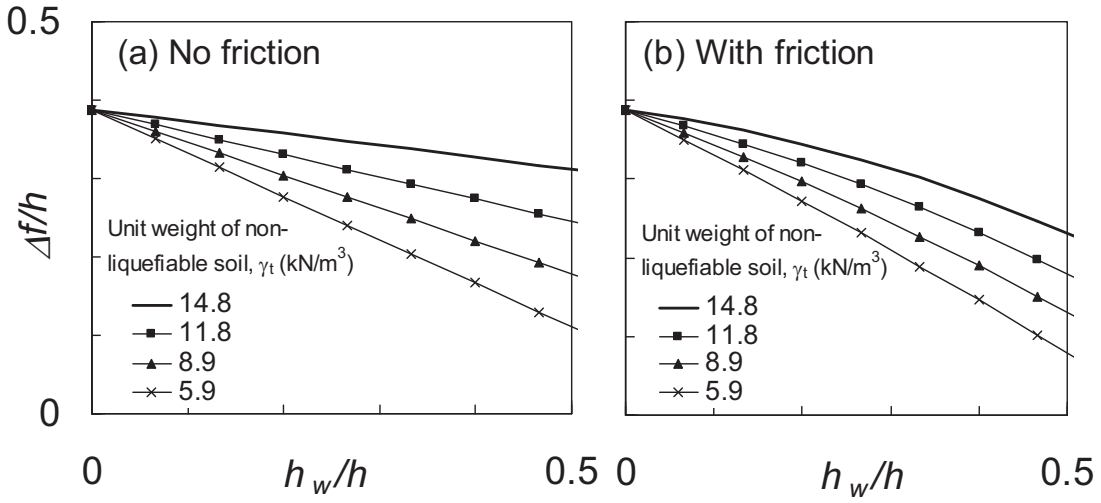

Fig. 3.5 Normalized uplift amount, $\Delta f/h$, versus normalized groundwater depth, h_w/h: (a) No frictional force at the side of a manhole is assumed (δ= 0 deg.); (b) Frictional force (δ= 10 deg.) assumed.

3.4.3 Effects of cross-sectional area of the trench

In reality, the surface ground is excavated to install manholes and pipes. Under the construction, the trench size on the horizontal cross-section is about 2 times of manhole diameter to minimize the working space in a trench thus reducing construction costs. Based on the facts that liquefaction of backfill in the trench appears to be a major cause of manhole uplifting (Koseki et al., 1997a; Koseki et al., 1997b; Yasuda and Kiku, 2006), the trench size must affect the uplift displacement of buried manholes. Also, in a previous chapter (centrifuge studies), the cross-sectional area of the trench was revealed to be one of the important factors affecting the uplift displacement. This factor could not be considered in the safety factor approach of previous research (Koseki et al., 1997b).

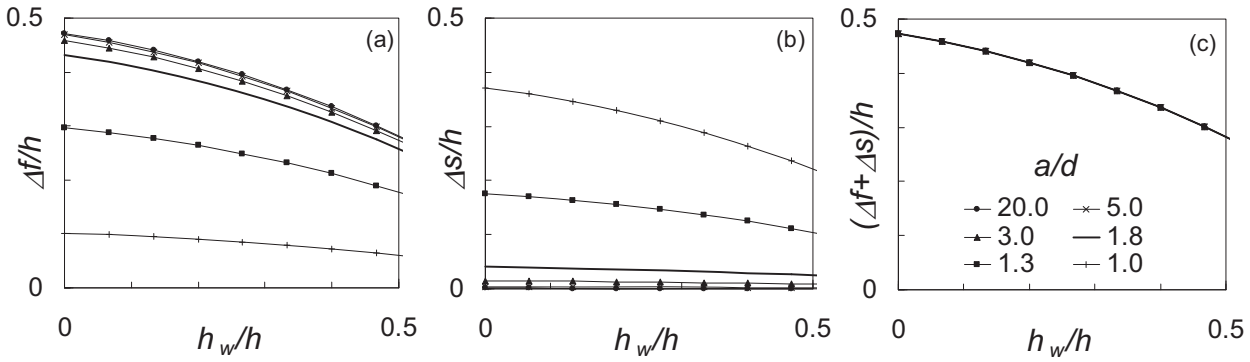

Fig. 3.6 Effects of the ratio of the normalized trench, a/d (=trench width / manhole diameter), on estimated relationships of normalized groundwater depth, hw/h, versus (a) normalized uplift, Δf/h, (b) normalized settlement, Δs/h(c) normalized total displacement, *(Δf + Δs)/h.*

The proposed relationship in Fig. 3.6(a) shows more uplift displacements with an increase in cross-sectional area. The uplift displacement has been converging when the ratio of a cross-sectional area was more than 5 (*a*/*d*) [Fig. 3.6(a)]. However, the settlement is decreased

with the increase in cross-sectional area. Although, the settled depth from the original ground surface in a wide cross-sectional area is smaller than that of a small cross-sectional area, settled volume is larger than that of a small cross-sectional area. Total vertical displacement which is the top of the manhole to backfill surface is constant. It indicates that the total vertical displacement is related to ground water depth and is independent from the cross-sectional area.

3.5 Comparison with centrifuge test data

To verify the validation or application of the proposed method, the predicted uplift displacements by the simplified method are compared with those obtained from centrifuge model tests. The parameters used as an input of the proposed method are summarized in Table 3.1. Table 3.3 indicates the test cases selected from the centrifuge model tests for the comparisons. Test cases including parameters irrelevant to uplift displacement predicted by the simplified method such as condition of the native ground and the contact condition between the bottom of a manhole and trench were excluded. Among the test data, only results of no mitigation measures (Model No. 1 and 4) are employed. Also, detailed data for selected test cases are represented in appendix A.

3.5.1 Comparison for effect by excess pore water pressure ratio

In previous chapters, the depth of ground water table, amplitude of input acceleration, the relative density of backfill were identified as major factors affecting the increase in excess pore water pressure ratio during strong shaking. Also, the increase in excess pore water pressure ratio affected the uplift displacement of a manhole. Therefore, predicted uplift displacement by the simplified method is compared with centrifuge test data to investigate

whether the simplified method can estimate the uplift displacement when various excess pore water pressure ratios are considered. The excess pore water pressure ratio, r_u, measured in centrifuge model tests is substituted for the simplified method in Eq. (10). The maximum excess pore water pressure filtered by a 2 second moving average to remove a spike during shaking is employed. Selected test cases are CS2, CS3, CS6, CS7, CS9 and CS22 as shown in Table. 3.3. The relative density of backfill for each case is targeting 36% except for CS9 and CS22, and the ground water table coincides with 1 m from the ground surface. In prediction, the relative density of 36% for backfill is used. Therefore, predicted uplift displacement for CS9 (relative density for backfill = 85%) and CS22 (relative density for backfill = 72%) may has some discrepancies because the unit weight of backfill for CS9 and CS22 will be increased due to increase of relative density. Amplitude of input acceleration is in the range of 2.05 ~ 7.25 m/s^2. The results are shown in Fig. 3.7. As shown in this figure, the predicted uplift

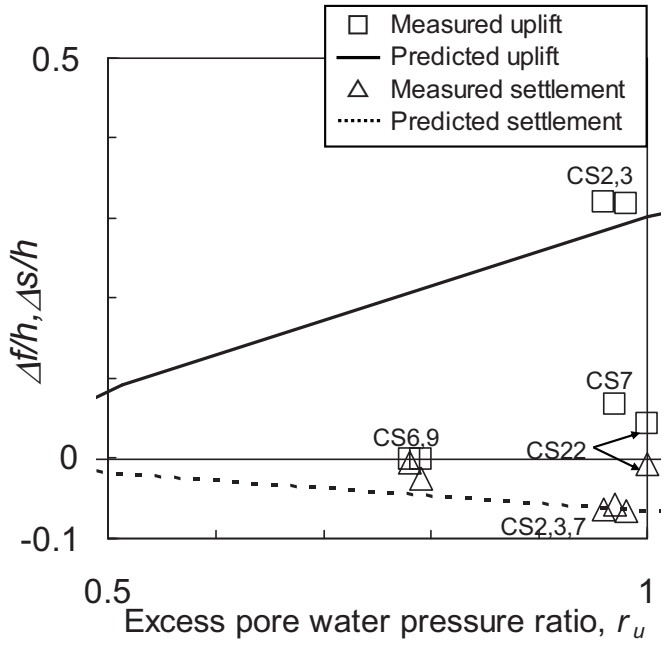

Fig. 3.7 Predicted and measured normalized uplift displacements of a manhole and settlement of backfill soils versus relative density of backfill.

Table 3.3 Test cases selected from the centrifuge model tests for the comparisons.

Test No.	Relative density		Model manhole type		Length of the manhole		GWL	Amplitude of inpu acceleration	Remarks
	Backfill soil	Original subsoil	left	right	left	right			
	%	%	No.	No.	m	m	m	m/s^2	
CS1	38.7	85	1	–	3	3	0	6.78	GWL=0 m_saturated
CS2	37.9	85	1	2	3	3	1	7.25	GWL=1 m
CS3	38.7	85	1	3	3	3	1	7.15	GWL=1 m
CS4	38.4	85	1	3	3	3	1.7	7.12	GWL=1.7 m
CS6	37.2	85	1	3	3	3	1	2.05	Input motion=2.05 m/s^2
CS7	38.7	85	1	3	3	3	1	4.64	Input motion=4.64 m/s^2
CS8	37.1	37.1	1	3	3	3	1	6.97	Trench=4.5×3.0 m^2
CS9	85	85	1	3	3	3	1	6.47	Dr of backfill ＝85%
CS10	39.4	85	1	3	3	3	1	6.87	Number of cycle load=15cycles
CS15	38.5	85	4	4	2	2	1	6.89	Left:normal Right:lattice shaped foundation
CS16	38.1	85	4	4	2	2	1	6.51	Left:normal Right:aluminium plate
CS18	38	85	1	3	3	3	1	6.95	γ_m = 11.27 kN/m^3
CS19	37.7	85	1	3	3	3	1	7.06	γ_m = 13.08 kN/m^3
CS20	38.1	85	1	3	3	3	1	6.93	γ_m = 15.47 kN/m^3
CS22	36->72	85	1	3	3	3	1	6.79	Compaction of backfill

displacements are significantly overestimated in dense ground [CS9: Dr = 85% and CS22: Dr = 72%] and small amplitudes of input acceleration [CS6: Max. amplitude of input Acc. = 2.05 m/s^2, CS7: Max. amplitude of input Acc. = 4.64m/s^2]. The reason is that the manhole uplift in these cases does not reach the maximum amount. However, measured uplift displacement and settlement of backfill is under predicted by the simplified method and the manhole uplift may reach the predicted uplift displacement if larger amplitudes of input acceleration are applied. It indicates that the proposed method is reasonable to estimate the maximum uplift displacement.

3.5.2 Comparison for effect by the depth of ground water table

For comparison, the test cases selected from the centrifuge model tests are CS1, CS2, CS3, CS4, CS15 and CS16 as shown in Table 3.3. The length of the manhole used in CS1 to CS4 is 3 m and that in CS15 and CS16 is 2 m as shown in Table 3.3. In each test, the model is prepared carefully so that every experiment has the same initial condition. Maximum peak accelerations measured in each case are in the range of 6.78 ~ 7.25 m/s^2. The relative density of backfill is 36% and that of the native ground is 85% for selected test cases. Figure 3.8 shows a comparison between measured and predicted uplift ratios for the ground water table ratio h_w/h. In Fig. 3.8, thick solid line indicates predicted uplift and settlement ratio for the manhole with 3 m length and dotted line indicates predicted uplift and settlement ratio for the manhole with 2 m length. As shown in Fig. 3.8, measured data is confined with predicted uplift and settlement. However, the predicted uplift ratio ($\Delta f/h$) for CS2 and CS3 is slightly underestimated compared with the measured one. The measured uplift ratio for CS15, CS16 and CS4 are slightly plotted below the predicted line. Overall performance of the proposed method is fairly good considering that all the data are plotted within the predicted boundary of the maximum uplift and settlements.

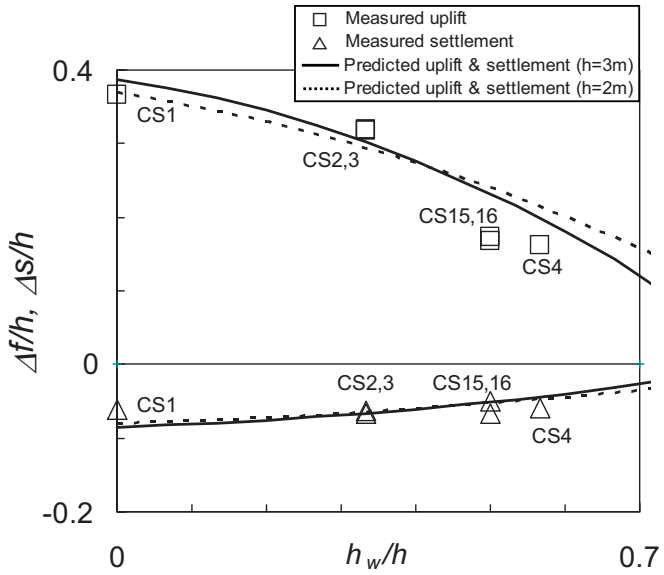

Fig. 3.8 Predicted and measured normalized uplift displacements of a manhole and settlement of backfill soils versus normalized groundwater depth.

3.5.3 Comparison for effect by relative density of backfill

For comparison, the test cases selected from the centrifuge studies of Chapter 2 are CS2, CS3, CS9 and CS22. Unit weight of backfill is calculated from each relative density because there is no term for the relative density for soils in the simplified method as follows:

$$\gamma_t = \frac{(Gs + Se)\gamma_w}{1+e} \tag{18}$$

where γ_t is wet unit weight of soil, Gs is specific gravity, S is degree of saturation, e is void ratio, γ_w is unit weigh of water. Degree of saturation (S) is assumed 30% and the void ratio (e) is given by:

$$e = e_{\max} - (e_{\max} - e_{\min})Dr \tag{19}$$

where e_{max} is maximum void ratio, e_{min} is minimum void ratio, Dr is relative density of soil. Then the unit weight of soil can be derived by substituting Eq. (19) into Eq. (18).

Figure 3.9 shows comparisons between measured and predicted uplift ratio for the relative

density of backfill. Every experiment for selected cases has the same initial condition except for the relative density of backfill. As shown in this figure, predicted uplift ratio is slightly increased with the relative density of backfill. However, measured uplift displacement is significantly decreased when the relative density of backfill is small as in the following sequence; CS2 and CS3 (Dr=36%), CS22 (Dr=72%), and CS9 (Dr=85%). In the prediction, the maximum uplift displacement is assessed under the assumption of a complete liquefaction condition for backfill (r_u = 1). Then, the result shows a large magnitude of manhole uplift in compacted backfill due to a large buoyant force by liquefied backfill with a large unit weight. However, the uplift ratio measured in centrifuge model tests did not yet reach the maximum amount. If a large amplitude of input acceleration was applied and backfill was completely liquefied, the uplift ratio may then reach the predicted uplift ratio. The settlement ratio ($\Delta s/h$) shows the same tendency to be found on the uplift ratio. The measured settlement ratio is also small in dense ground (Dr = 72 ~ 85%).

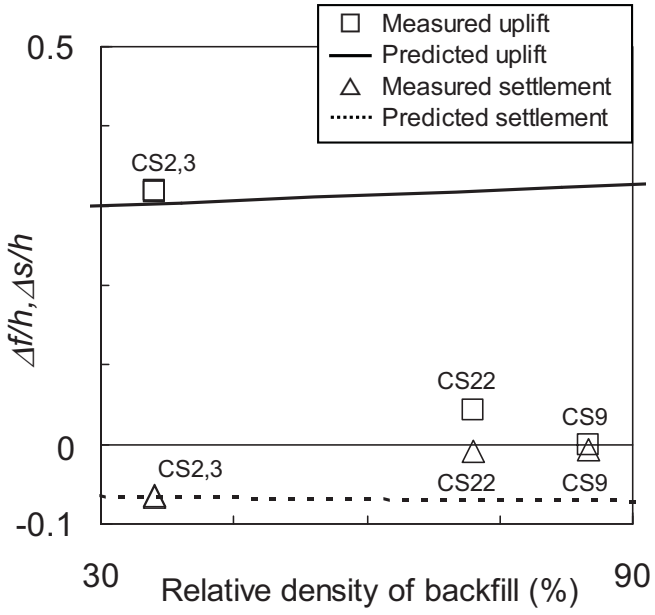

Fig. 3.9 Predicted and measured normalized uplift displacements of a manhole and settlement of backfill soils versus relative density of backfill.

3.5.4 Comparison for effect by cross-sectional area of a trench

For comparison, the test cases selected from the centrifuge studies of Chapter 2 are CS2, CS3 and CS8. Figure 3.10 shows predicted and measured uplift ratio of a manhole and settlement ratio of backfill versus the cross-sectional area of a trench. The cross-sectional area is 2.3 × 2.3 m^2 for CS2 and CS3, and 4.5 × 3.0 m^2 for CS8. Every experiment for selected cases has the same initial condition except for the cross-sectional area of the trench as shown in Table 3.3. Predicted and measured uplift ratio ($\Delta f/h$) is increased with the increase in cross-sectional area of the trench (a/d). Predicted settlement ratio ($\Delta s/h$) is decreased with the increase in the cross-sectional area of the trench. In the prediction, the settlement of backfill may be small in wide cross-section because the settled volume of the trench is larger than that of small cross-section. However, measured settlement of backfill is slightly increased with the

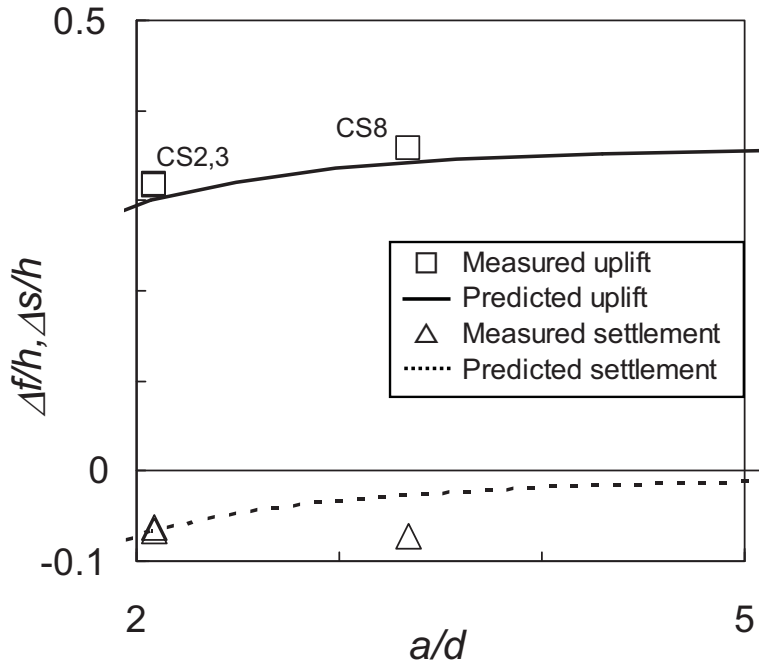

Fig. 3.10 Predicted and measured normalized uplift displacements of a manhole and settlement of backfill soils versus cross-sectional area of the trench.

increase in the cross-sectional area. Among assumptions in the proposed method, the undrained condition is rather a strict restriction. In reality, backfill is consolidated during and after shaking because of excess pore water dissipation. Overall performance of the proposed method is fairly good considering that all the data are consistent with the predicted the maximum uplift ratio.

3.5.5 Comparison for effect by apparent unit weight of a manhole

For comparison, the test cases selected from the centrifuge studies of Chapter 2 are CS2, CS3 and CS18, CS19 and CS20. The apparent unit weight of the model manholes is increased about 9.57 to 15.47 kN/m^3 and the apparent unit weight (γ_m) of the manhole is normalized by saturated unit weight of backfill (γ_{sat} = 18.1 kN/m^3). Every experiment for selected cases has

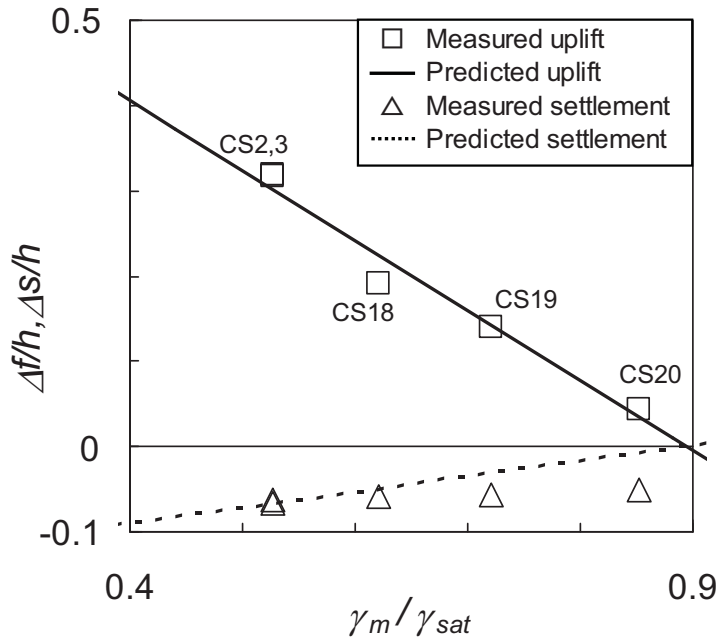

Fig. 3.11 Predicted and measured normalized uplift displacements of a manhole and settlement of backfill soils versus an apparent unit weight ration (γ_m/γ_{sat}).

the same initial condition except for the apparent unit weight of the manhole as shown in Table 3.3. Figure 3.11 shows predicted and measured uplift ratio and settlement ratio versus apparent unit weight of the manhole. As shown in this figure, predicted and measured uplift ratio ($\Delta f/h$) is decreased with the increase in the unit weight ratio (γ_m/γ_{sat}). Predicted settlement ratio ($\Delta s/h$) is decreased with the increase in the unit weight ratio (γ_m/γ_{sat}). Meanwhile, a reduction in the measured settlement ratio is smaller than that predicted because backfill is actually consolidated due to excess pore water dissipation. The measured and predicted uplift displacements calculated by the simplified method are fairly in agreement.

3.6 Derivation of uplift force using centrifuge test data

In order to extend validation of the simplified method, time histories of uplift displacement is estimated by using centrifuge test data. As mentioned earlier, the simplified method can only estimate the maximum uplift displacement when the excess pore water pressure ratio, r_u, is 1 (complete liquefaction). However, if time histories of the excess pore water pressure ratio or the uplift force are known during uplifting, the uplift displacement can be expressed by the simplified method.

Time histories of uplift displacement by the simplified method can be derived by using the pore water pressure measured in centrifuge modeling tests. For performing this, the excess pore water pressures measured in backfill and on the bottom of the manhole were used. The excess pore water pressures in backfill were measured at the depth of 2 m and 3 m from the ground surface. The excess pore water pressures measured in backfill are directly substituted for the term of r_u in Eq. (7) ($r_u = U_m/\sigma_0'$, U_m is the excess pore water pressure measured in centrifuge model tests, and σ_0' is initial effective stress at the same depth with the pore water pressure transducer). The excess pore water pressures measured on the bottom of the manhole

are substituted for modified Eq. (7) as a term of uplift force acting on the base of manhole, *U*.

3.6.1 Uplift force using excess pore water pressure measured in backfill

Figure 3.12 shows a diagram of a manhole and trench with the location of excess pore water pressure transducers. As mentioned above, P1 and P2 [Fig. 3.13(a) and (b)] are measured in backfill. In Fig. 3.13, the peak values of P2, which are installed at the same depth with the manhole bottom, are larger than that of P1, which are installed at the depth of 2 m from the ground surface in backfill. To plot time histories of uplift displacement by the simplified method, the ratio, r_u ($=U_m/\sigma_0'$), is directly applied to Eq. (7).

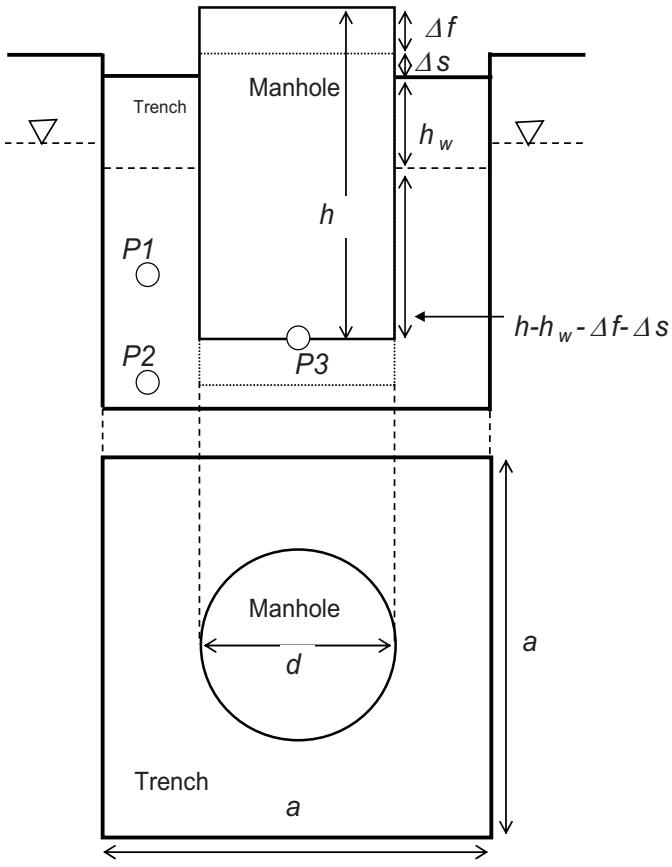

Fig. 3.12 Idealized diagram of a manhole and trench, and location of pore water transducers.

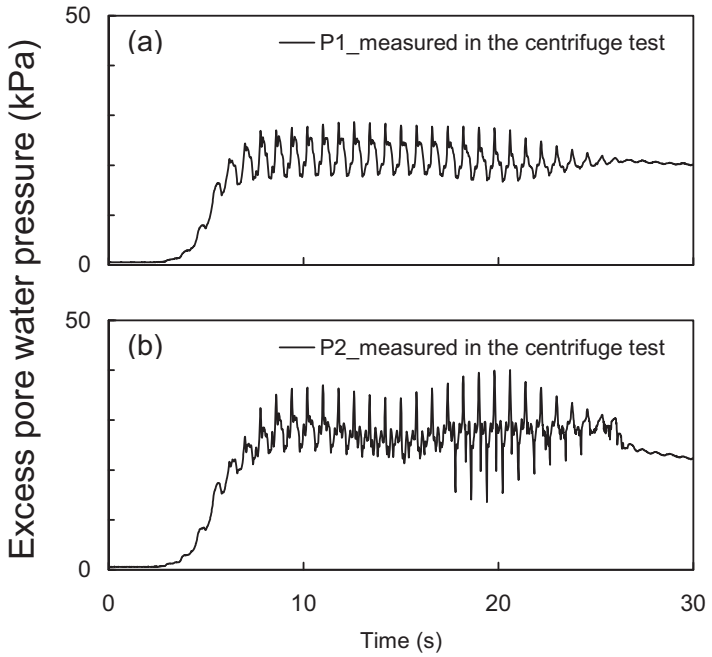

Fig. 3.13 Excess pore water pressure measured in backfill for CS2: (a) P1, (b) P2.

3.6.2 Uplift force using excess pore water pressure measured on the bottom of manhole

The uplifting force acting on the bottom of a manhole in liquefied ground can be expressed by using the excess pore water pressure measured on the bottom of the manhole in the centrifuge modeling tests as shown in Fig. 3.12 (P3). Figure 3.14 indicates a modified diagram of a manhole and trench to estimate the uplift force, *U*. The uplift force, *U*, is evaluated from the excess pore water pressure (Δu) acting on the bottom of a manhole and the cross-sectional area (A) of the manhole on the horizontal plane and Δu is considered as excess pore water pressure excluding hydrostatic pressure. The excess pore water pressure, u_m', measured on the bottom of the manhole does initially not include the hydrostatic pressure because the transducers are configured to zero before shaking. However, the transducers measured not only the excess pore water pressure but also the hydrostatic pressure after shaking. The

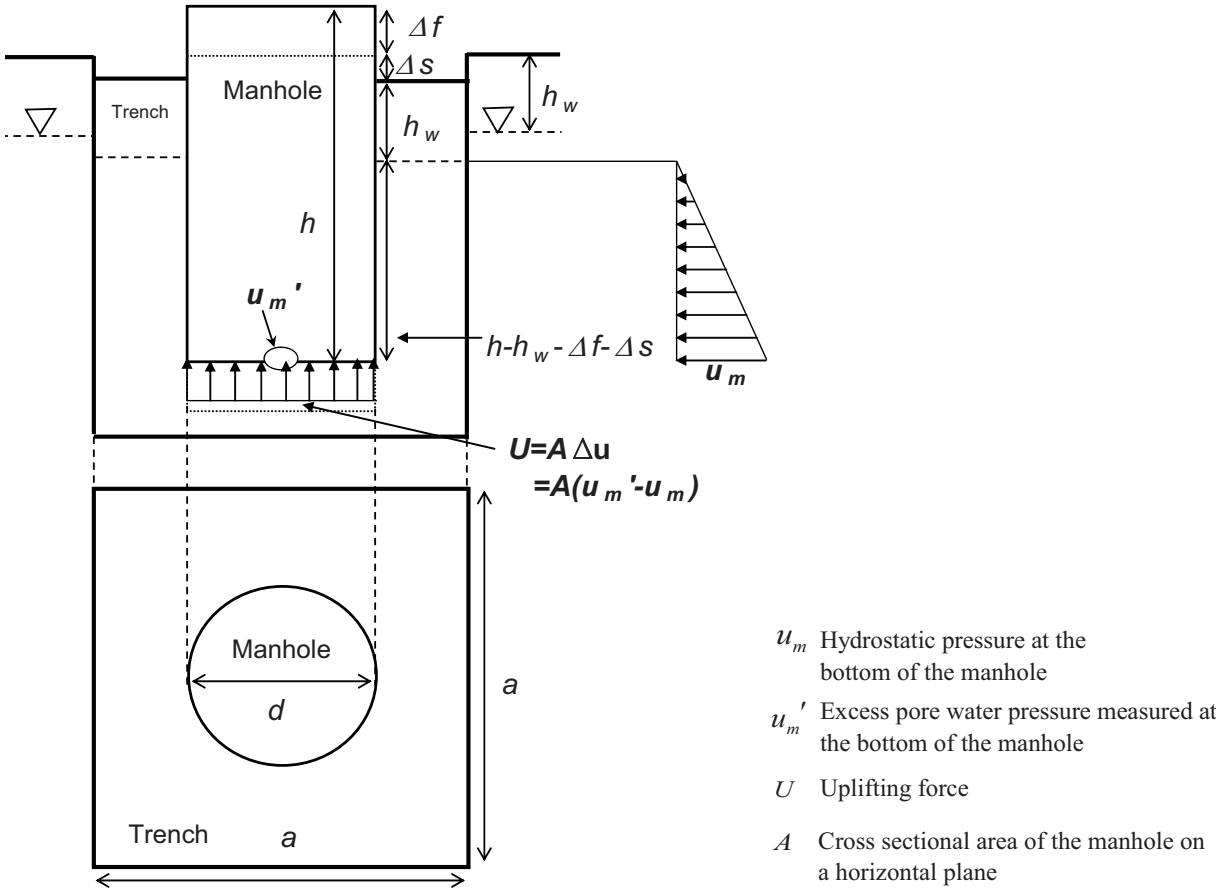

Fig. 3.14 Modified diagram of a manhole and trench to estimate the uplift force, *U*.

hydrostatic pressure acting on the bottom of the manhole needs to be calculated considering the uplift displacement because the hydrostatic pressure is changing with the manhole uplift. The hydrostatic pressure acting on the bottom of the manhole can be calculated as follows:

$$u_m = \gamma_w (h - h_w - \Delta f - \Delta s) \tag{20}$$

Δf is measured in the centrifuge modeling tests. However, Δs is measured by a ruler before and after every test. If the assumption that the volume of the uplifted portion of the manhole is equal to the amount of settled volume of backfill is used again, the settlement of backfill, Δs, in Eq. (1) can be calculated as follows:

$$\Delta s = \frac{\Delta f \pi \left(\frac{d}{2}\right)^2}{a^2 - \pi \left(\frac{d}{2}\right)^2} \tag{21}$$

Then, substituting measured uplift displacement, Δf, into Eq. (21), the settlement of backfill, Δs, can be evaluated and the excess pore water pressure, Δu, acting on the bottom of the manhole is also derived as follows:

$$\Delta u = u_m{}' - u_m \tag{22}$$

Figure 3.15 shows the excess pore water pressures acting on the bottom of the manhole base. Blue line indicates the hydrostatic pressure (u_m) and red line indicates the excess pore water pressure (u_m') measured on the bottom of the manhole during shaking. The hydrostatic pressure is decreasing with the manhole uplift because overburden of soils at the location of the bottom of the manhole is decreased with the uplift. After the uplifting, the hydrostatic pressured is constant. The excess pore water pressure (Δu) acting on the bottom of the manhole is expressed as a subtraction of these two pore water pressures as shown in Fig. 3.15.

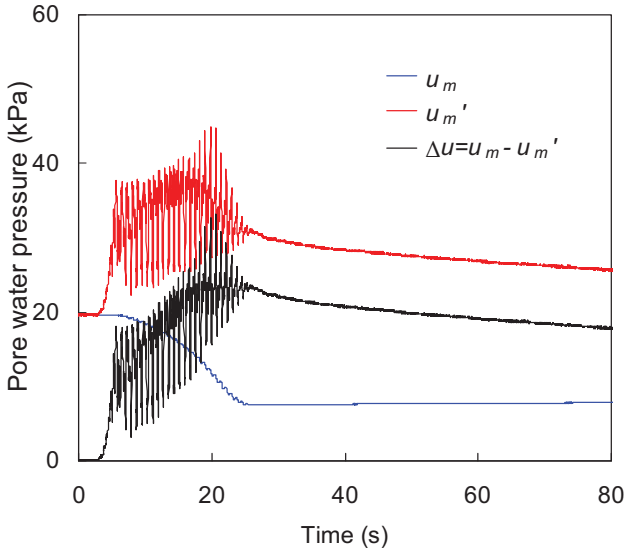

Fig. 3.15 Pore water pressure acting on the bottom of the manhole for CS2.

The uplift force, U, can be derived by modifying Eq. (7) as follows:

$$U = \pi\left(\frac{d}{2}\right)^2 \Delta u = \pi\left(\frac{d}{2}\right)^2 (u_m' - u_m) \tag{23}$$

Then, the maximum uplift displacement of a manhole is obtained, Δf:

$$\Delta f = \left\{1 - \pi\left(\frac{d}{2a}\right)^2\right\}\left\{\left(\frac{\Delta u}{\gamma_w}\right) + \left(1 - \frac{\gamma_m}{\gamma_w}\right)h - h_w - \frac{R}{\gamma_w}\frac{1}{\pi}\left(\frac{2}{d}\right)^2\right\} \tag{24}$$

3.7 Estimation of time histories of uplift displacement

3.7.1 Estimation by using excess pore water pressure in backfill

Time histories of uplift displacement can be estimated by substituting the excess pore water pressure measured in backfill (P1) into Eq. (10). Figure 3.16 shows the comparison with measured and predicted uplift time histories for CS2, CS4, CS6, CS7, CS9, CS10, CS15, and CS19. Detailed briefs of each test case are summarized in Table 3.3. In CS2, the ground water table is located at the depth of 1 m from the ground surface and amplitude of input acceleration is 7.25 m/s^2. In CS4, the ground water table coincides with the depth of 1.7 m from the ground surface. In CS6 and CS7, amplitudes of input acceleration are 2.05 m/s^2 and 4.64 m/s^2, respectively. In CS9, backfill was compacted by 85%. In CS10, number of load cycles is 15cycles. In CS15, the short manhole with 2 m length was used. In CS19, apparent unit weight of a manhole was increased by 13.08 kN/m^3. In Fig. 3.16, thin gray line indicates time history of the uplift displacement predicted by the simplified method. Predicted uplift displacement is largely moving up and down because the predicted uplift displacement depends on the excess pore water pressure measured in the centrifuge model tests. Thus, predicted uplift displacement is plotted by using a 2 second moving average filter as a red line

indicated in Fig. 3.16. Blue line indicates the uplift displacement measured in centrifuge model tests and dotted line indicates the predicted uplift displacement when backfill soil is completely liquefied ($r_u = 1$).

In CS2, CS4, CS15 and CS19, the measured and predicted maximum uplift displacements are in the same level. However, the predicted maximum uplift displacements are overestimated in CS6, CS7, CS9 and CS10. These facts suggest that the simplified method tends to overestimate the uplift displacement when the uplift displacement of manholes was small such as those of CS6, CS7, CS9 and CS10. It indicates that the uplift did not reach the maximum amount. In CS2, CS7, CS10, CS15 and CS19, the predicted uplift displacement reaches the maximum amount much faster than the measured one. In measured data, the manhole starts to lift up when the excess pore water pressure in the backfill exceeds the initial effective vertical stress as shown in Fig. 2.9 – 2.10 of Chapter 2. On the other hand, in prediction, the manhole uplift is rapidly increased with the increase in the excess pore water pressure or the ratio, r_u, and the uplift displacement reaches at the maximum level when the excess pore water pressure in the backfill exceeds the initial effective vertical stress. The predicted uplift displacement is rather decreasing after shaking because pore water pressure used as an input of the simplified method is dissipated.

After all, the uplift displacement predicted by the simplified method reaches the maximum amount when the manhole uplift is initiated in the centrifuge model tests as shown in Fig. 3.16. However, the predicted maximum uplift displacements are in agreement compared with those measured in centrifuge model tests. It indicates that the verification of the simplified method was made. In appendix B, comparisons between measured and predicted uplift displacements for all test cases are presented.

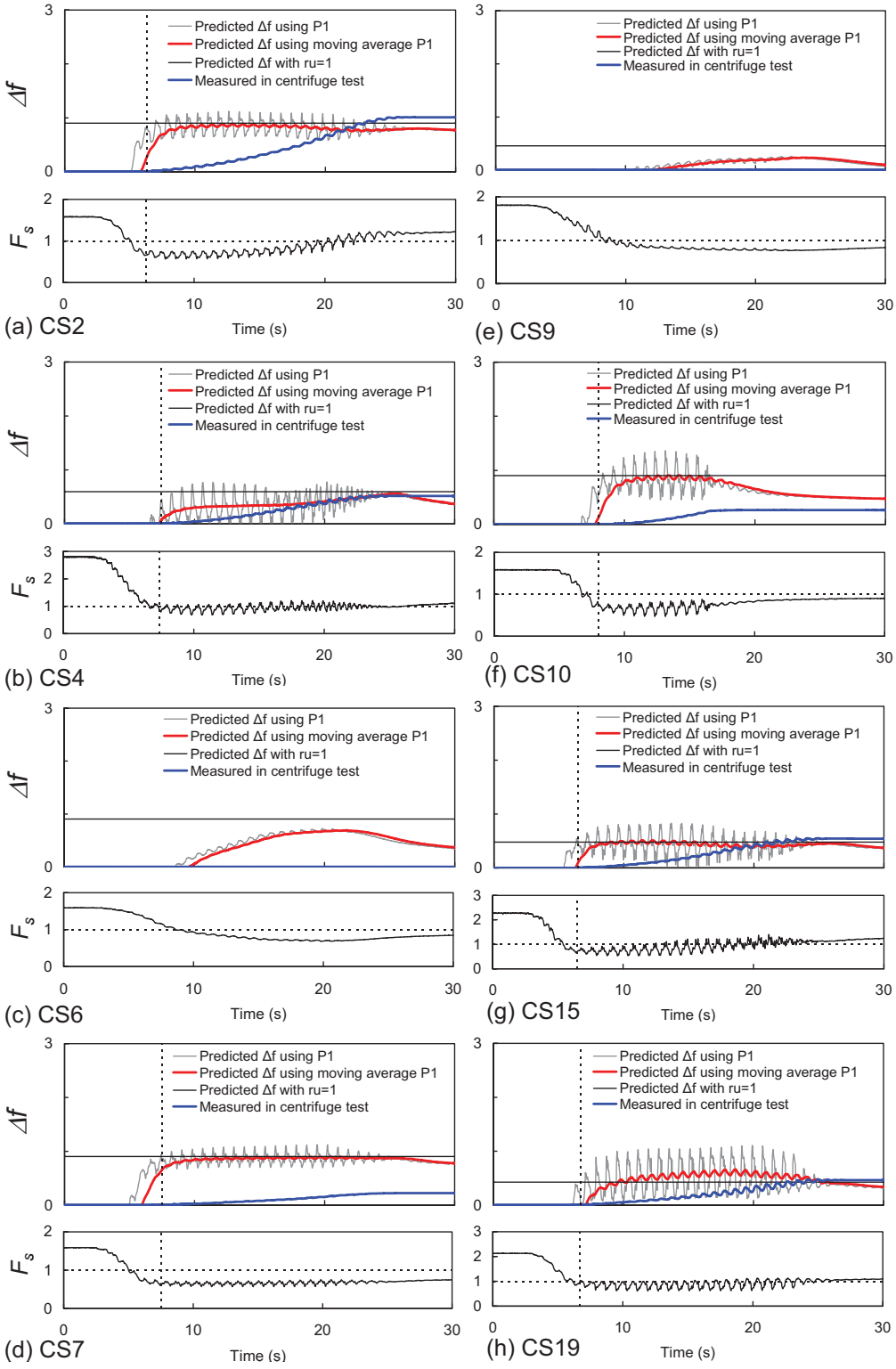

Fig. 3.16 Comparisons between measured and predicted uplift time histories using excess pore water pressure measured in backfill, and safety factor; (a) CS2, (b) CS4, (c) CS6, (d) CS7, (e) CS9, (f) CS10, (g) CS15, and (h) CS19.

To evaluate the triggering of manhole uplift by the simplified method, the safety factor is plotted as shown in Fig. 3.16. The safety factor is expressed as Eq. (5), and solving by substituting parameters, F_s:

$$F_s = \frac{M+R}{U+H} = \frac{\pi\left(d/2\right)^2 \gamma_m(h,\ d)h + R}{U + \pi(d/2)^2 \gamma_w(h - h_w - \Delta f - \Delta s)} \tag{25}$$

In Eq. (25), the terms of the hydrostatic pressure and uplift force are different with the safety factor by Koseki, et al. (1997b) mentioned in Chapter 2. As mentioned above, in order to evaluate the uplift force (U), the excess pore water pressure measured in backfill is substituted into Eq. (7) as a shape of the ratio, r_u, or the excess pore water pressure measured on the bottom of a manhole is substituted into Eq. (23).

The safety factor is larger than 1 before shaking, and the manhole starts to lift up slightly later than the safety factor reached 1 as shown in Fig. 3.16. The safety factor is increasing until larger than 1 after shaking in CS2, CS4, CS15 and CS19, again, because the simplified method considered equilibrium of forces during the uplifting. Figure 3.16(c) and (e) shows time histories of the safety factor for CS6 (small amplitude of input acceleration = 2.05 m/s^2) and CS9 (relative density of backfill ≈ 85%) and the safety factor is decreasing to less than 1, however, the manhole did not uplift. The reason may be that the frictional force acting on the side of the manholes below ground water table is neglected even though backfill is not liquefied (Fig. 2.29 in Chapter 2).

3.7.2 Estimation by using excess pore water pressure on the bottom of the manhole

Using the excess pore water pressure measured on the bottom of the manhole in centrifuge model tests, the uplift force can be estimated as shown in Fig. 3.15 and the uplift force is introduced to the simplified method through Eq. (24). The uplift displacements predicted by

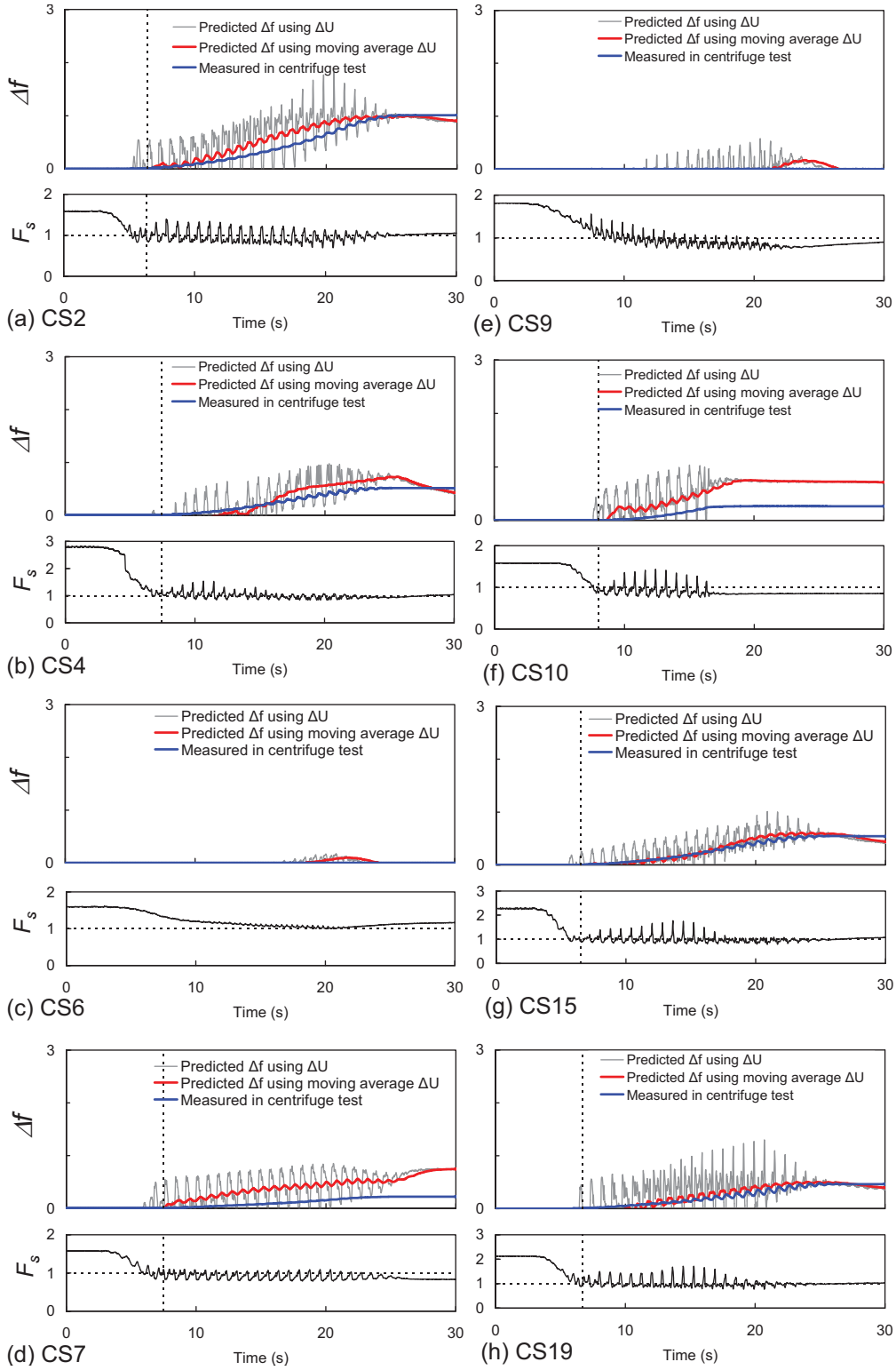

Fig. 3.17 Comparisons between measured and predicted uplift time histories using excess pore water pressure measured on the bottom of the manhole, and safety factor; (a) CS2, (b) CS4, (c) CS6, (d) CS7, (e) CS9, (f) CS10, (g) CS15, and (h) CS19.

the simplified method are gradually increased with those measured in centrifuge model tests as shown in Fig. 3.17. In CS2, CS4, CS15 and CS19, the measured and predicted maximum uplift displacements are in the same level and the time histories as the uplift by the simplified method is in sufficiently good agreement compared with those measured in the centrifuge model tests. Especially, the comparisons perfectly agree in CS15 and CS19 except for a transient amplitude of the uplift displacement. On basis of the facts that the uplift displacements by the simplified method are gradually increased with those measured in centrifuge model tests and the maximum uplift displacements measured in centrifuge model tests are plotted under the predicted boundary, the validity of the new method is proved through the comparisons with time histories of the manhole uplift. However, the predicted uplift displacements are still overestimated in CS6, CS7, CS9 and CS10.

The safety factor is larger than 1 before shaking, and the manhole starts to lift up when the safety factor almost reached to 1 as shown in Fig. 3.17. The safety factor is increasing until almost 1 after the shaking in CS2, CS4, CS9, CS15 and CS19, again. These facts indicate that the triggering of manhole uplift can be evaluated by the simplified method.

3.8 Summary

A new method is proposed to estimate the maximum uplift displacement of a manhole and settlement of backfill in liquefied ground. The method was derived based on the equilibrium of forces acting on a manhole in liquefied ground. Forces acting on the manhole are the dead weight of the manhole and the frictional force between the manhole and backfill above ground water table as downward force, and hydrostatic pressure and the uplift force due to liquefied backfill as upward forces. Basic assumptions include no volume change or continuity of liquefied backfill during uplift of a manhole by neglecting the minor effect of consolidation,

and same ground water depth during uplift.

Preliminary study for verification of the simplified method was performed through a comparison with results of model test by using the boiling method. The predicted maximum uplift displacement of the manhole is significantly at the same level compared with the measured.

Quantitative relationships between uplift displacement and the thickness of the non-liquefied layer above the ground water table, the unit weight of backfill, and the width of the trench were derived from the simplified method. The uplift displacements by the simplified method show a tendency to increase with shallow ground water table, small unit weight of backfill and wide cross-sectional area of the trench. Also, the maximum uplift displacement by the simplified is about 50 % of manhole length when properties of soil and manholes used in centrifuge model tests were introduced under some assumptions as follows; ground water level coincides with the ground surface (h_w = 0.0 m), backfill is totally liquefied (r_u = 1.0) and cross-sectional area of the trench is large ($a = \infty$).

To verify the validation or application of the proposed method, predicted uplift displacements by the simplified method were compared with those obtained from centrifuge model tests. The predicted uplift displacements were significantly overestimated in dense ground and small amplitude of input acceleration. The reason is that the manhole uplift in these cases does not reach the maximum amount. However, measured uplift displacement and settlement of backfill was under predicted by the simplified method.

To extend the verification of the simplified, time histories of uplift displacement were estimated by using centrifuge test data. Although, the simplified method could not estimate the time histories of the uplift displacement when excess pore water pressure measured in backfill was used as an input data, the measured and predicted maximum uplift displacements were at

the same level. When the excess pore water pressure measured on the bottom of the manhole in the centrifuge model tests was introduced in the simplified method, the time histories of the uplift displacement by the simplified method were sufficiently good compared with those measured in the centrifuge model tests and the measured maximum uplift displacements were under predicted ones. However, the simplified method tends to overestimate the uplift displacement when the manhole uplift did not reach the maximum amount, i.e., the uplift displacement of manholes was small. These facts suggest that the validity of the new method which aims to estimate the maximum uplift amount of a manhole in liquefied ground was verified through the comparisons with centrifuge test data.

To evaluate the triggering of manhole uplift by the simplified method, the safety factor was plotted by using excess pore water pressure measured in centrifuge model tests. The safety factor was larger than 1 before shaking, and the manhole started to lift up when the safety factor almost reached to 1. Also, the safety factor went back to 1 after the shaking because the simplified method considered equilibrium of forces during the uplifting. These facts indicate that the triggering of manhole uplift can be evaluated through the safety factor by the simplified method.

4. Detailed method for estimation of uplift displacement through effective stress analysis of soil-structure systems

4.1 Introduction

In a previous chapter, the maximum uplift displacements predicted by the simplified method are overestimated when the uplift displacement does not reach the maximum amount due to build-up of a low excess pore water pressure ratio. In other words, the simplified method can provide more precise estimates of the uplift displacement when a high excess pore water pressure ratio builds up in backfill during shaking and the uplift displacement reaches the maximum amount.

In order to overcome the limitation of the simplified method for estimation of uplift displacement of buried structures, the two dimensional effective stress analyses based on the multiple shear mechanism for soil are performed and the results are compared with the centrifuge test data. In the numerical approach, based on mechanics of continuum body, it is possible to evaluate both failure modes and the extent of displacement/stress/ductility/strain subjected to the complex soil-structure interaction. Also, the effective stress analysis can estimate transient behaviors of the manhole uplift as well as the maximum uplift displacement during shaking. The analysis is conducted for the above-mentioned cases which the uplift displacement did not reach the maximum amount, such as uplift behavior under small amplitude of input acceleration, small number of load cycles, or uplift behavior in compacted ground. To investigate the applicability, the numerical analysis is also conducted when the uplift displacement reaches the maximum amount, such as uplift behavior in saturated soil below the ground surface and under large amplitude of input acceleration as an input wave.

4.2 Numerical modeling

4.2.1 Outline of effective stress analysis method, FLIP

A program FLIP (Finite element analysis program for Liquefaction Process) based on effective stress analysis method (Iai et al., 1992a) was used to analyze the seismic response of a buried structure. The effective stress model for soils is the multiple shear mechanism model (Iai et al., 1992a). The model was originally proposed by Towata and Ishihara (1985). As shown in Fig. 4.1, this model is represented by a movable point located within the circular fixed boundary defined in shear strain space and connected to the boundary with an infinite number of virtual springs. Each spring corresponds to a virtual simple shear mechanism having a various orientation. The relationship between force and displacement of each spring follows the hyperbolic type load displacement relationship. The displacement of the movable point from the center represents the mobilized shear strain and the resultant of forces acting on the point represents the shear stress induced in the soil.

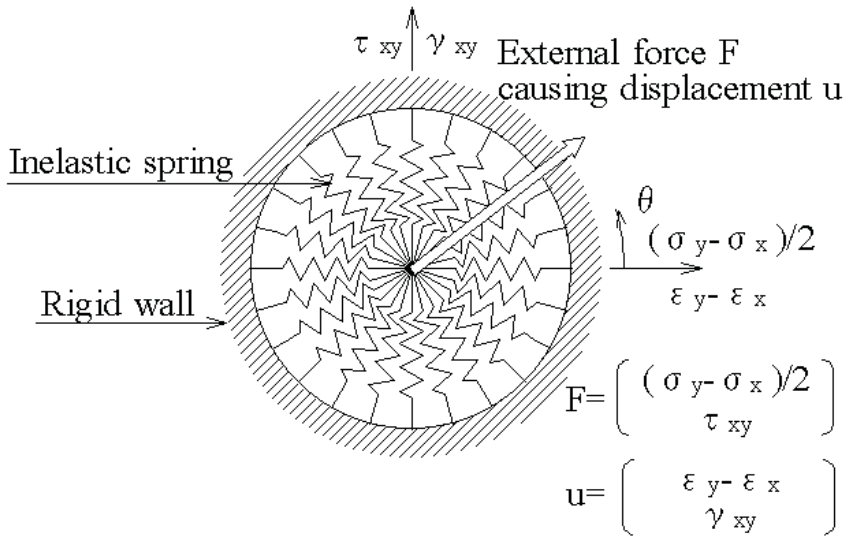

Fig. 4.1 Schematic view of multi-spring model (Towata and Ishihara, 1985).

With the effective stress and strain vectors in plane strain condition expressed as

$$\left\{\sigma'\right\}^T = \left\{\sigma'_x \quad \sigma'_y \quad \tau_{xy}\right\} \tag{1}$$

$$\left\{\varepsilon\right\}^T = \left\{\varepsilon_x \quad \varepsilon_y \quad \gamma_{xy}\right\} \tag{2}$$

the basic form of the constitutive relation is given by

$$\left\{d\sigma'\right\} = [\boldsymbol{D}](\{d\varepsilon\} - \{d\varepsilon_p\}) \tag{3}$$

in which

$$[\boldsymbol{D}] = \boldsymbol{K}\{\boldsymbol{n}^{(0)}\}\{\boldsymbol{n}^{(0)}\}^T + \sum_{i=1}^{I} \boldsymbol{R}_{L/U}^{(i)}\{\boldsymbol{n}^{(i)}\}\{\boldsymbol{n}^{(i)}\}^T \tag{4}$$

where $\{\sigma'\}$ is effective stress vector, $\{\varepsilon\}$ is strain vector, $\{d\sigma'\}$ is effective stress increment vector, $\{d\varepsilon\}$ is strain increment vector, $\{d\varepsilon_p\}$ is volumetric strain increment vector due to the dilatancy, $\boldsymbol{K}$ is rebound modulus, $\boldsymbol{R}_{L/U}^{(i)}$ is tangential shear modulus.

In this relation, the term $\{d\varepsilon_p\}$ in Eq. (3) represents the additional strain increment vector to take the dilatancy into account and is given from the volumetric strain increment due to the dilatancy, $d\varepsilon_p$, as

$$\left\{d\varepsilon_p\right\}^T = \left\{d\varepsilon_p/2 \quad d\varepsilon_p/2 \quad 0\right\} \tag{5}$$

The first term in Eq. (4) represents the volumetric mechanism with rebound modulus $\boldsymbol{K}$ and the direction vector is given by

$$\left\{\boldsymbol{n}^{(0)}\right\}^T = \left\{1 \quad 1 \quad 0\right\} \tag{6}$$

The second term in Eq. (4) represents the multiple shear mechanism. Each mechanism I = 1,⋯ , I represents a virtual simple shear mechanism, with each simple shear plane oriented at an angle $\theta_i/2$ relative to the x axis. The tangential shear modulus $\boldsymbol{R}_{L/U}^{(i)}$ represents the

hyperbolic stress strain relationship with hysteresis characteristics. The direction vectors for the multiple shear mechanism in Eq. (4) are given by

$$\left\{\boldsymbol{n}^{(i)}\right\}^T = \left\{\cos\theta_i \quad -\cos\theta_i \quad \sin\theta_i\right\} \quad (\text{for } i=1, \cdots, I) \tag{7}$$

in which

$$\theta_i = (i-1)\Delta\theta \qquad (\text{for } i=1, \cdots, I) \tag{8}$$

$$\Delta\theta = \pi / I \qquad (\text{for } i=1, \cdots, I) \tag{9}$$

The loading and unloading for shear mechanism are separately defined for each mechanism by the sign of $\{n^{(i)}\}^T\{d\varepsilon\}$. This multiple shear mechanism takes into account the effect of rotation of principal stress axis directions, the effect of which is known to play an important role in the cyclic behavior of the anisotropically consolidated sand (Iai et al., 1992b)

The excess pore water pressure is generated as a function of cumulative shear work. Effect of positive dilatancy is also included for taking into account the cyclic mobility behavior using the concept of liquefaction front, as shown in Fig. 4.2, by the following function:

$$S = S_0 \qquad (\text{if} \quad r < r_3)$$

$$S = S_2 + \sqrt{(S_0 - S_2)^2 + [(r - r_3)/m_1]^2} \qquad (\text{if} \quad r > r_3) \tag{10}$$

in which

$$r_2 = m_2 S_0 \tag{11}$$

$$r_3 = m_3 S_0 \tag{12}$$

$$S_2 = S_0 - (r_2 - r_3)/m_1 \tag{13}$$

and S_0 is a parameter to be defined by a function of shear work; m_1 is inclination of failure line, defined by the shear resistance angle ϕ_f' as $m_1 = \sin\phi_f'$; m_2 is inclination of the phase transformation line, defined by the phase transformation angle ϕ_p' as $m_1 = \sin\phi_p'$; and $m_3 = 0.67$

m_2. The auxiliary parameter m_3, introduced for ensuring the smooth transition from one zone to the other, is determined as balance of the smoothness and the realistic stress path shape.

In Fig. 4.2, S is a state variable ($S = \sigma_m' / \sigma_{m0}'$) under undrained condition with a constant total confining pressure, and r is the shear stress ratio ($r = \tau / \sigma_{mo}'$). The initial effective mean stress and the deviatoric stress is defined by $\sigma_{m0}' = (\sigma_{x0}' + \sigma_{y0}')/2$ and $\tau = (\sigma_1' - \sigma_3')/2 = \sqrt{\tau_{xy}^2 + [(\sigma_x' - \sigma_y')/2]^2}$. The model can simulate the rapid or gradual increase in cyclic strain amplitude of the order of several percent under undrained cyclic loading. The program has been verified in many numerical simulation works of structure damage induced by earthquakes and liquefaction (Sawada et al., 2000; Ozutsumi et al., 2002; Iai et al., 2005).

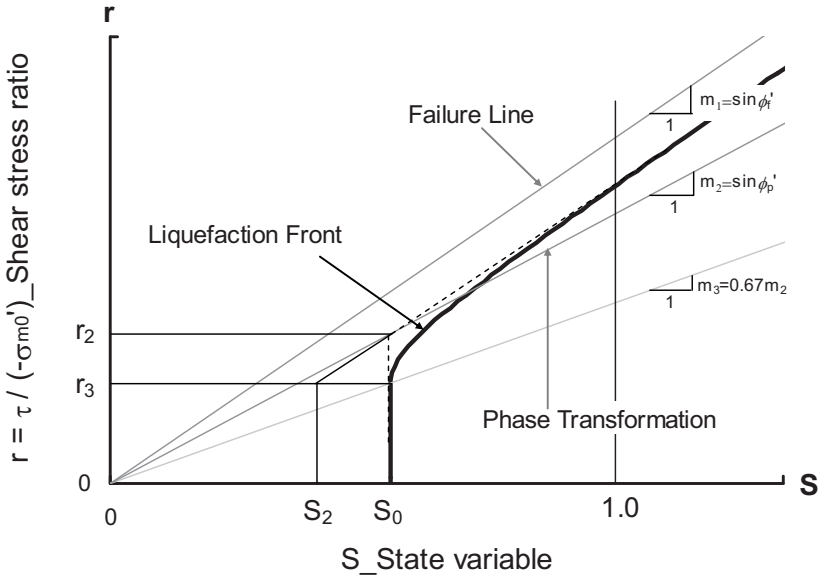

Fig. 4.2 Schematic view of liquefaction front, state variable S and shear stress ratio r (Iai et al. 1992a).

4.2.2 Simulation conditions and parameters

The finite element mesh used in the analysis is shown in Fig. 4.3. The mesh was targeting

to the centrifuge model tests conducted in Chapter 2. For comparisons with the centrifuge data, the locations of instruments are indicated in Fig. 4.3. A1 ~ A3 are to record dynamic motions on the ground surface and model manhole. P1~P3 are to measure excess pore water pressure in the ground. The manhole structures were modelled using linear elastic solid elements. Modelling parameters are defined in Table 4.1 to Table 4.3. As shown in Table 4.1, the parameters of a hollow cylinder (sewerage manhole) are adopted as standard values of aluminium materials used in the centrifuge model tests (National Astronomical Observatory of Japan, 2003). While mass density of aluminium is 2.7 t/m^3, density of the manhole structure is decreased by 0.976 t/m^3 because the inside of a hollow cylinder is empty.

Table 4.1 Model parameters for hollow cylinder.

Young's modulus E (kPa)	Poisson ratio v	Mass density ρ (t/m^3)
7.03×10^7	0.345	0.967

Table 4.2 Soil model parameters for the analysis.

Soil type	Density	Parameter for deformation characteristic					
		Elastic tangent shear modulus	Elastic tangent bulk modulus	Reference mean effective stress	Inernal friction angle	Cohesion	Max. damping ratio
	ρ (t/m^3)	G_{ma} (kPa)	K_{ma} (kPa)	σ_{ma}' (kPa)	ϕ_f (°)	c (kPa)	h_{max}
Native ground	1.93	9.39×10^4	2.45×10^5	98	40.04	0	0.24
Backfill	1.82	5.25×10^4	1.37×10^5	98	38.09	0	0.24

Table 4.3 Model parameters for liquefaction properties.

Soil type	Parameter for liquefaction characteristic					
	Phase trans. Angle	Parameters for dilatancy				
	ϕ_p (°)	S_1	w_1	p_1	p_2	c_1
Native ground	28	0.005	10.0	0.65	0.40	3.00
Backfill	28	0.005	1.90	0.35	1.05	1.78

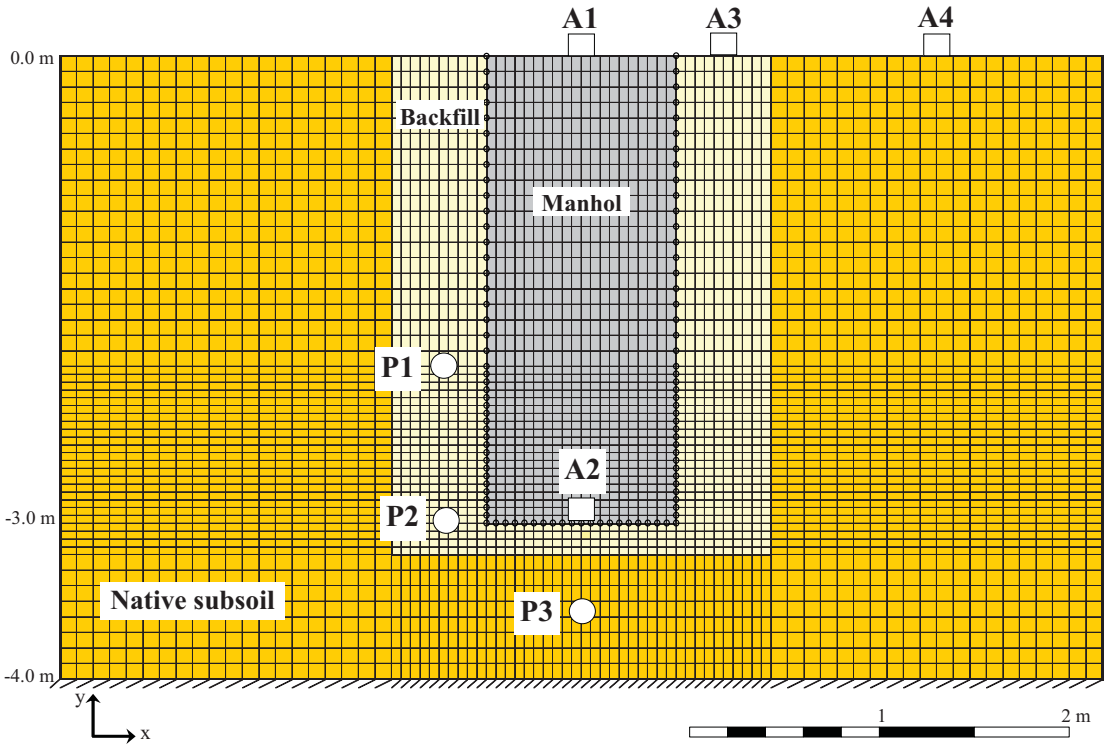

Fig. 4.3 Mesh, boundary, element type for numerical modeling.

A series of laboratory tests was conducted to determine physical and mechanical properties of the sand. Angle of internal friction ϕ_f was determined by isotropically consolidated

undrained triaxial test ($\overline{\text{CU}}$) which was performed on loose (Dr = 45%) and dense (Dr = 75%) sand. The effective stress paths in terms of q [= (σ'_v–σ'_h)] and p' [= (σ'_v+2σ'_h)/3, σ'_v: effective vertical stress and σ'_h: effective horizontal stress] from all the consolidated undrained triaxial tests are depicted in Fig. 4.4. A dotted line was fitted to the data set of (p', q) that corresponded to the critical state of each triaxial test as shown in Fig. 4.4 (a) and (b). The slope of this fitted line was referred to as M. M values are 1.55 and 1.64 for loose and dense sand. These M [= 6sinϕ_f / (3-sin ϕ_f)] values should correspond to angles of internal friction (ϕ_f) of 38.09º and 40.04°, respectively.

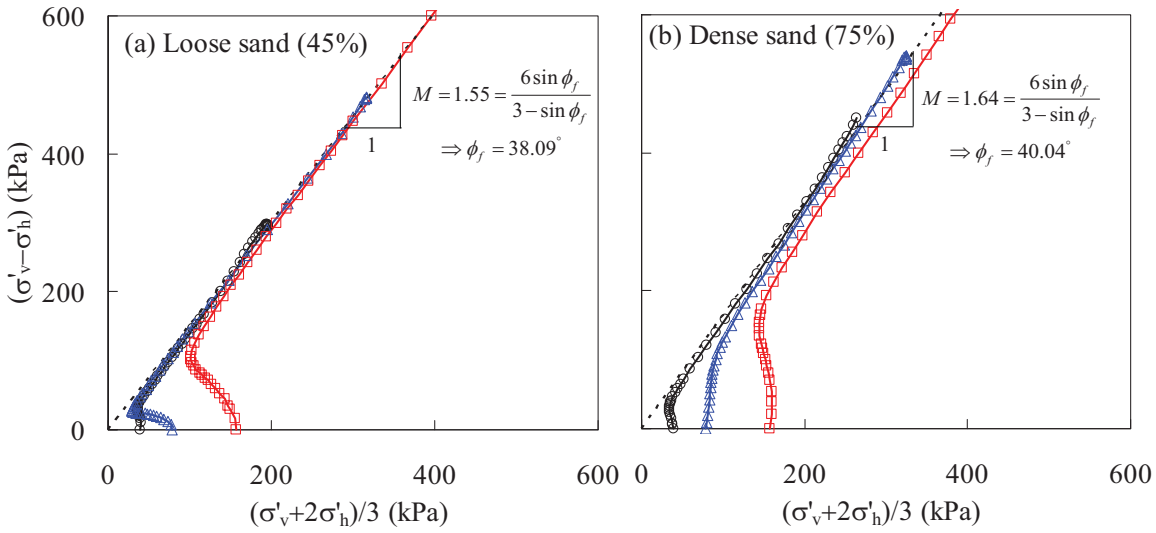

Fig. 4.4 Effective stress paths from tests; (a) loose sand, (b) dense sand.

A series of cyclic triaxial tests was performed to estimate liquefaction resistance for loose and dense sand, isotropically consolidated at confined pressure of 98 kPa. To simulate the uplift behavior of a manhole, the maximum shear modulus for soils was employed in stress-strain curves by the cyclic triaxial tests as shown in Fig. 4.5. The liquefaction resistance values were

measured using stress controlled cyclic triaxial tests where the soil specimen was consolidated under isotropic effective confining stress σ_c' and then subjected to a cyclic deviator stress, σ_d in axial direction. A series of cyclic triaxial tests was performed with various $\sigma_d/2\sigma_c'$ values for loose (36%) and dense (85%) sand. Figure 4.6 depicts the cyclic stress ratio versus N_c from cyclic triaxial tests with computed one. The computed liquefaction resistance curves obtained by applying cyclic stress loading upon one element for the same sand are shown in Fig. 4.6. The onset condition of liquefaction or cyclic softening is specified in terms of the magnitude of a cyclic stress ratio required to produce 5% DA (Double Amplitude) axial strain in 20 cycles of the uniform load application. Table 4.3 shows model parameters of the analysis of undrained cyclic loading.

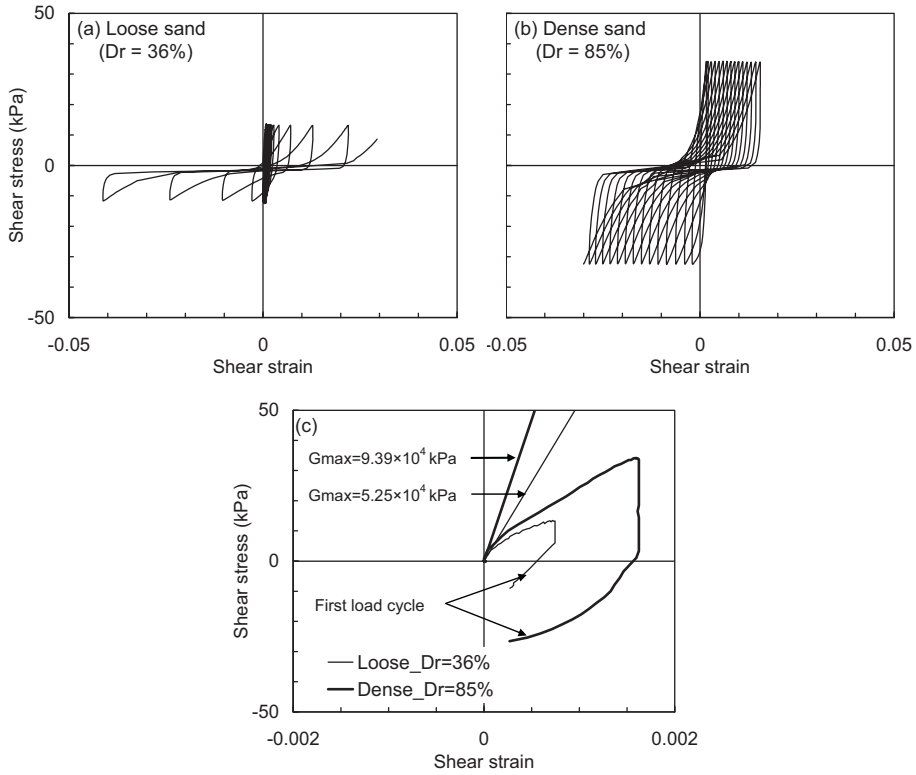

Fig. 4.5 Stress-strain curve measured in cyclic triaxial tests: (a) loose sand, (b) dense sand, (c) determination of G_{max}.

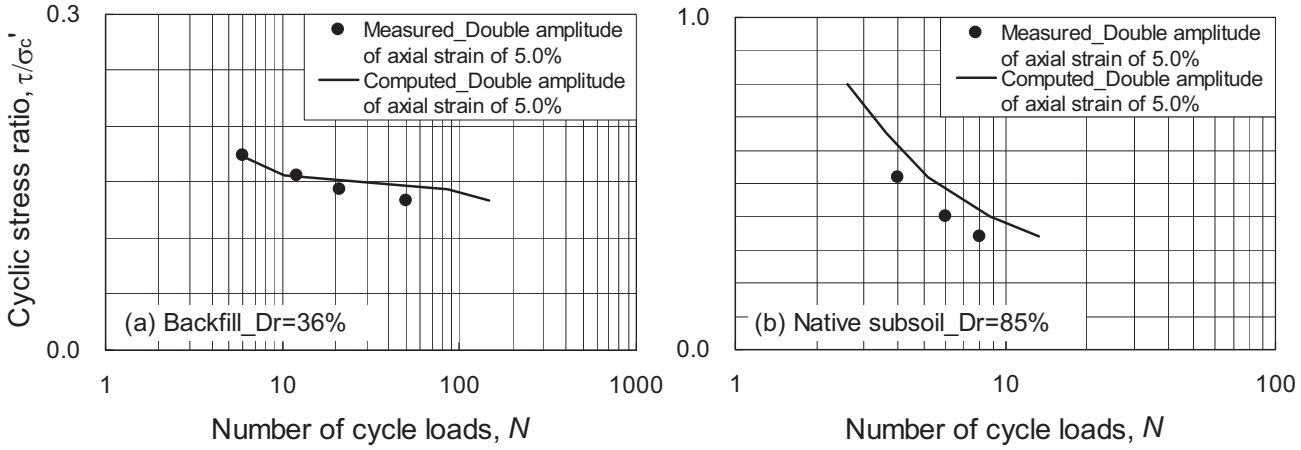

Fig. 4.6 Computed and liquefaction resistance curves measured in cyclic triaxial tests, (a) Loose sand (Dr≈36%), (b) Dense sand (Dr≈85%).

4.3 Initial and Boundary condition

4.3.1 Initial condition

Before the earthquake response analysis, a static analysis was conducted with gravity to simulate the initial stresses acting on the ground before the earthquake. The same constitutive model was used as in the earthquake response analysis.

A more realistic static analysis could be conducted by closely simulating the actual steps taken in the construction of the buried structure; i.e. by simulating the processes of the excavation, insertion of the structure and backfilling and, if any, the effect of pre-stress histories in the ground, due to the previous earthquakes. These steps, if taken, will be so complicated that the static analysis itself can become a major research problem. In the present analysis, such a complication is avoided because the main target is on the earthquake response analysis. For the simulation of uplift behavior of a buried structure, the static analysis with gravity is under an unstable condition because the apparent unit weight of the manhole structure proposed in this study is smaller than that of water. Therefore, a special step needs to

ensure the stability of the numerical solution process by controlling mass density of soil and structure. Three steps were used to conduct the analysis of uplift behavior for a buried structure as follows:

(1) static analysis under dry ground.

[mass density of manhole = ρ_m, mass density of soil = ρ_d]

(2) static analysis considering hydrostatic pressure by water in the ground.

[mass density of manhole = $-\rho_w$, mass density of soil = $-(1-n_s)\rho_w$]

(3) earthquake response analysis under undrained condition.

[mass density of manhole = ρ_m, mass density of soil = ρ_{sat}]

where ρ_m is mass density of manhole structure, ρ_d is dry density of sands, ρ_{sat} is saturated density of soils, and ρ_w is density of water. n_s is porosity of sands. $-(1-n_s)\rho_w$ indicates water pressure acting ON soil particles.

4.3.2 Boundary condition

The numerical model dimensions were set as the prototype scale in the centrifuge model test. For the solid phase, to have boundary conditions similar to the rigid container, displacement degrees of freedom at the base were fixed both horizontally and vertically. Although, lateral displacement was fixed at the side boundary condition in the centrifuge model test, the manhole as well as backfill in the trench was intensively shaking in three dimensional modes. Thus, in the two dimensional analysis, lateral displacement at side boundaries are set to be equal for each node with the same depth to reproduce the shear behavior of backfill in the trench. The double nodes with the same coordinate, but different node number, are assigned to the bottom and sides of the manhole structure and neighboring soil node. Double nodes are assumed as no friction between the manhole and the neighboring

soils, and lateral displacements of double nodes are set to be equal. Joint elements can be employed to consider the friction between the manhole and backfill. However, no friction was adopted between double nodes on the manhole and backfill elements because the objective in this analysis is to simulate transient behavior of manhole uplift and it is difficult to determine the properties of joint elements considering the complex soil-structure interaction. Therefore, the major approximations and assumptions made in the present study are

(1) simulating the initial stress conditions by the two steps gravity analysis,

(2) imposing the undrained conditions on the sand,

(3) assuming no frictions between the soil and the structures, and

(4) simulating the manhole structures by the linear plane element in the two dimensional analysis

4.4 Input motion and time integration

With these initial and boundary conditions, the earthquake response analysis was conducted on the buried manhole structure. The actual input motions measured on the base plate of the shaking table in the centrifuge model tests, as shown in Fig. 4.10, are employed to the bottom boundary of the analytical model. Maximum amplitudes of input acceleration are in the range of 2.05 ~ 7.25 m/s^2. The input motion is a sinusoidal with frequency of 1.25 Hz.

The dynamic analysis for uplift behavior of buried structures was conducted under the undrained conditions (Zienkiewicz et al., 1982). The numerical integration was done by the Wilson-θ method (θ = 1.4) using a time step of 0.01 seconds. Rayleigh damping (α = 0 and β = 0.0005) which was proportionally decreasing with the degree of cyclic mobility was used to ensure the stability of the numerical solution process.

4.5 Comparison of soil behavior between 2 and 3 dimensions for as a preliminary study

The application of numerical simulation employed in this chapter is limited to the two dimensional boundary value problems. However, in reality, the simulation cannot be permitted as two dimensional mechanisms because the uplift behavior of a buried structure needs to be considered as three dimensional mechanisms. Effects of the soils of the front and back for the manhole during shaking are neglected in two dimensional analyses. Therefore, behavior of the soils in three dimensional mechanisms is examined by cyclic simple shear for one soil element below the manhole, under an undrained condition, as a preliminary study.

The soil below the manhole may be put into the stress state of a tension shear during an earthquake because the apparent unit weight of the manhole is smaller than that of backfill. Horizontal earthquake shaking will then cause cyclic simple shear in this soil element. Then, the manhole will be uplifted with a stretching of this soil element due to the stress state of a tension shear. In order to compare behavior of soil elements between 2 and 3 dimensions, the undrained cyclic simple shearing of initially anisotropically consolidated sand was analyzed. In this analysis, the soil element was, first, consolidated with $\sigma'_h - \sigma'_v$ = 4.5 kPa. This is to simulate the soil condition beneath the manhole before shaking. The initial axial stress difference was kept unchanged throughout the cyclic shearing. A cyclic simple shear with an amplitude of τ_{xy} = 1.5 kPa is applied to the simulation.

The results are shown in Fig. 4.7. As shown in this figure, the computed results of the two dimensional model are similar to those of the three dimensional model. Axial strain difference (42%) in three dimensional condition is larger than that (36%) of two dimensional condition. The facts suggest that the soil element is more stretched in three dimensional

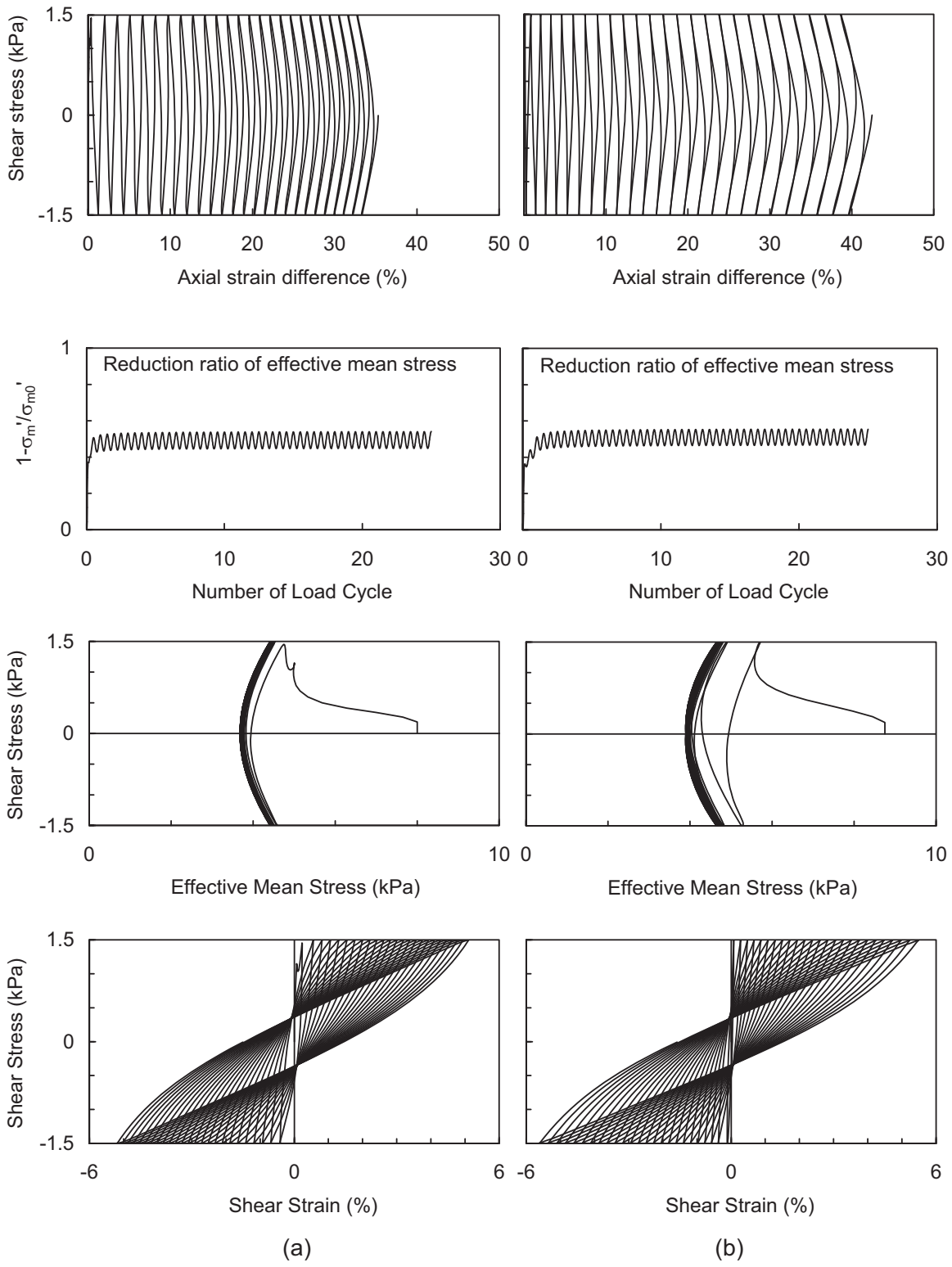

Fig. 4.7 Computed results for cyclic simple shear under undrained: (a) 2 dimensional model, (b) 3 dimensional model.

conditions and then the uplift of buried structures may be increased more than that in two dimensional conditions. Fig. 4.8 shows comparison of axial strain between the two and three dimensional conditions for the soil element beneath the manhole. Axial strain in the three dimensional models is 1.34 times larger than that in the two dimensional models when axial strain difference is in the same level. The facts suggest that uplift of manhole structures in the three dimensional models may be 1.34 times larger than that in the two dimensional models.

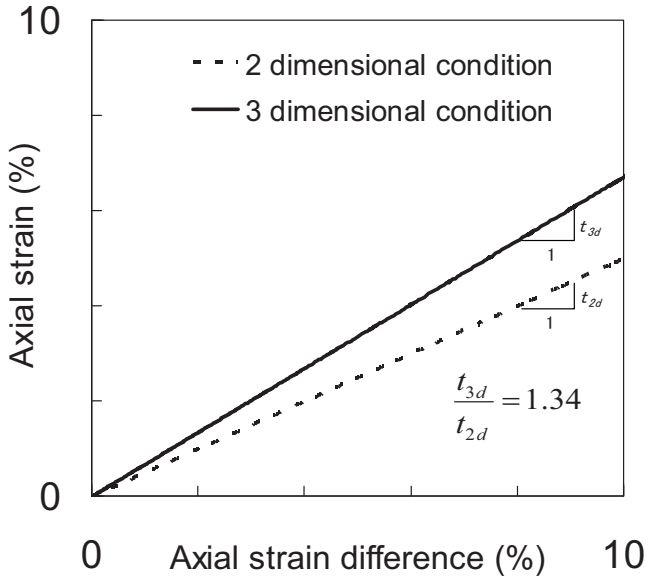

Fig. 4.8 Comparison of axial strain difference between 2D and 3D.

4.6 Results and comparison

In this section, the two dimensional effective stress analyses are carried out to overcome the limitations in the simplified method. From the results of the centrifuge model tests, the simplified method, which aims to estimate the maximum uplift amount of a buried structure in liquefied ground, tends to overestimate the uplift displacement when the uplift displacement does not reach the maximum amount. The simulation cases considered in the numerical

analysis, are small amplitude of input acceleration or small number of load cycles as an input wave, and compacted backfill. To verify the applicability of the numerical approach, the numerical analysis is also conducted for some cases where the manhole uplift was expected to reach the maximum amount in the centrifuge model tests, such as uplift behavior of a manhole in saturated soil below the ground surface and under large amplitude of input acceleration as an input wave. The results are compared with the centrifuge test data.

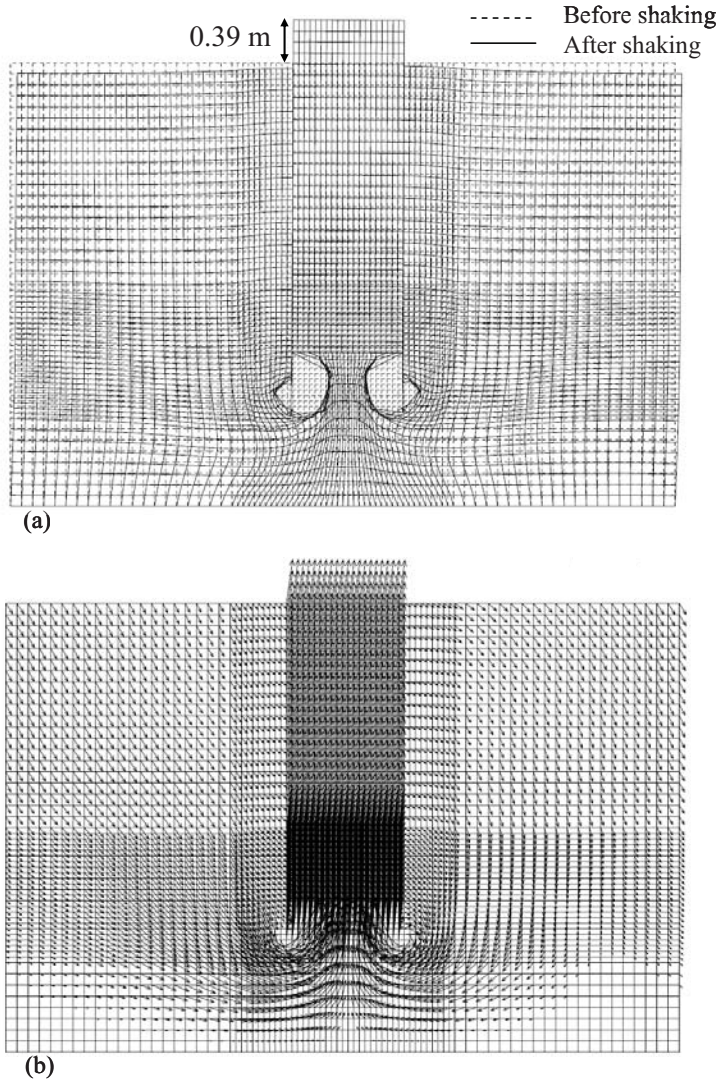

Fig. 4.9 Computed deformation of the manhole at the end of shaking for saturated soil below the ground surface: (a) Mesh deformation, (b) Displacement vectors.

Figure 4.9 shows computed deformation of the manhole at the end of shaking for saturated soil below the ground surface. The maximum uplift displacement at the top of the manhole gradually is accumulated and reached about 0.39 m. Uplift behavior of the manhole by the numerical analysis can be expressed, but the liquefied backfill soil is difficulty flowing toward the bottom of the manhole during the uplifting as shown in Fig. 4.9. Although, the displacement vectors look toward the bottom of the manhole [Fig. 4.9(b)], the soil element did not move toward the bottom of the manhole [Fig. 4.9(a)]. The uplift behavior in the numerical analysis may have resulted from analytical problems considering the behavior of soils in a small strain domain or the finite element method.

4.6.1 Comparison for effect of amplitude of input motion against uplift displacement

The uplift displacement predicted by the simple method was considerably overestimated using small amplitude of input acceleration as the input acceleration in a previous chapter. Then, the uplift behavior of a manhole due to various amplitude of input accelerations is investigated by the numerical analysis to make up for the limitation of the simplified method and the results are compared with centrifuge test date. The maximum accelerations considered in the numerical analysis as an input data are 2.05, 4.64 and 7.15 m/s^2 which were measured on the base plate of the shaking table in the centrifuge model tests as shown in Fig. 4.10. The ground water depth coincides with the depth of 1 m from the ground surface.

The measured and computed time histories of uplift displacements at the top of the manhole, acceleration and excess pore water pressure of sand deposits are shown in Fig. 4.11 to 4.13. Figure 4.11 corresponds to CS6 of centrifuge model tests mentioned in Chapter 2

whose amplitude of input acceleration is 2.05 m/s^2. Figures 4.12 and 4.13 are compared with results of CS7 and CS3 of centrifuge model tests. Conditions of the soil and manhole for simulations by the numerical analysis are consistent with those used in the centrifuge model tests.

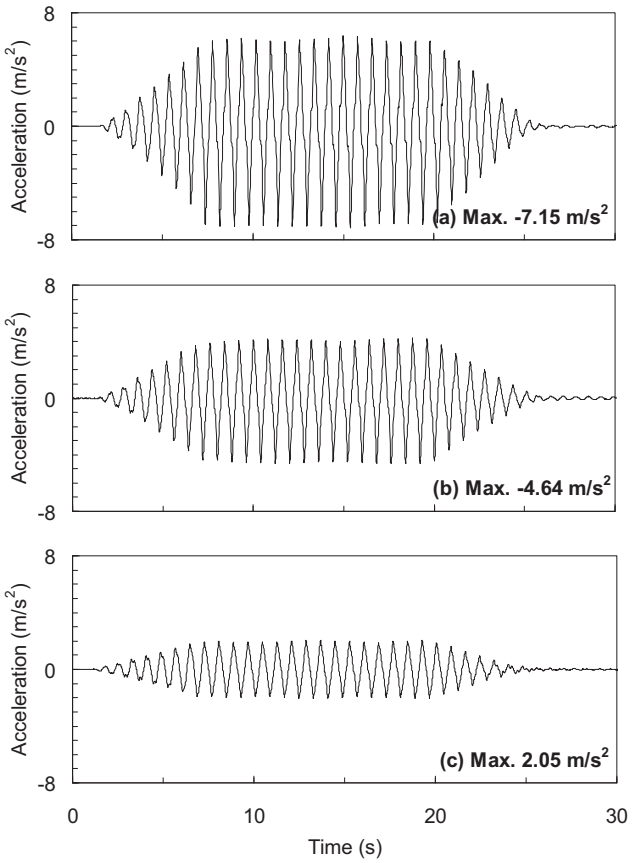

Fig. 4.10 Input motions for numerical simulation: (a) Max. Acc. -7.15 m/s^2, (b) Max. Acc. -4.64 m/s^2, (c) Max. Acc. 2.05 m/s^2.

Under the small amplitude of the input acceleration in Fig. 4.11, the manhole is not uplifted in the centrifuge model test because backfill is not liquefied during shaking [Fig. 4.11(b) and (c)], however, the manhole is uplifted about 0.04 m in numerical analysis. In the

numerical analysis, the manhole starts to lift up when excess pore water pressure in the middle of the backfill reaches about 100 % of the initial effective vertical stress at 6 seconds. In Fig. 4.12, similar behavior is also found between measured and computed uplift behavior of the manhole, however, the manhole in the numerical analysis is uplifted slightly faster than that of the centrifuge model test. In the numerical analysis, the excess pore water pressure in the middle of the backfill reaches about 100 % of the initial effective vertical stress at 5 seconds whereas the excess pore water pressure in the middle of backfill in the centrifuge model test reaches the initial effective vertical stress at 7 seconds. The uplift displacements are 0.14 and 0.18 m for computed and measured, respectively. Computed acceleration responses at the surface of the backfill, native ground, and the top of the manhole are smaller than that measured in the centrifuge model tests.

Under the strong shaking, computed uplift displacement (0.197 m) is underestimated compared with measured one (0.952 m) as shown in Fig. 4.13. The uplift is actually accelerated by moving the liquefied backfill soils laterally toward the bottom of the manhole during shaking based on the fact that the slopes (uplift speed) of the measured uplift time histories are rapidly increased after 10 seconds as shown in Fig. 4.13(a). However, the slopes (uplift speed) of the computed uplift time histories are gradually decreased after 10 seconds. It indicates that liquefied backfill soil is difficulty flowing toward the bottom of the manhole with the uplift of the manhole in the numerical analysis.

Figure 4.14 shows comparisons among measured and predicted uplift displacements by the simplified method and numerical analysis, respectively, for various amplitudes of input accelerations. Computed uplift displacements in the three dimensional models are to multiply results of the two dimensional model by 1.34 as above mentioned. The uplift displacement predicted by the simplified method is constant at the magnitude of 0.9 m because the method

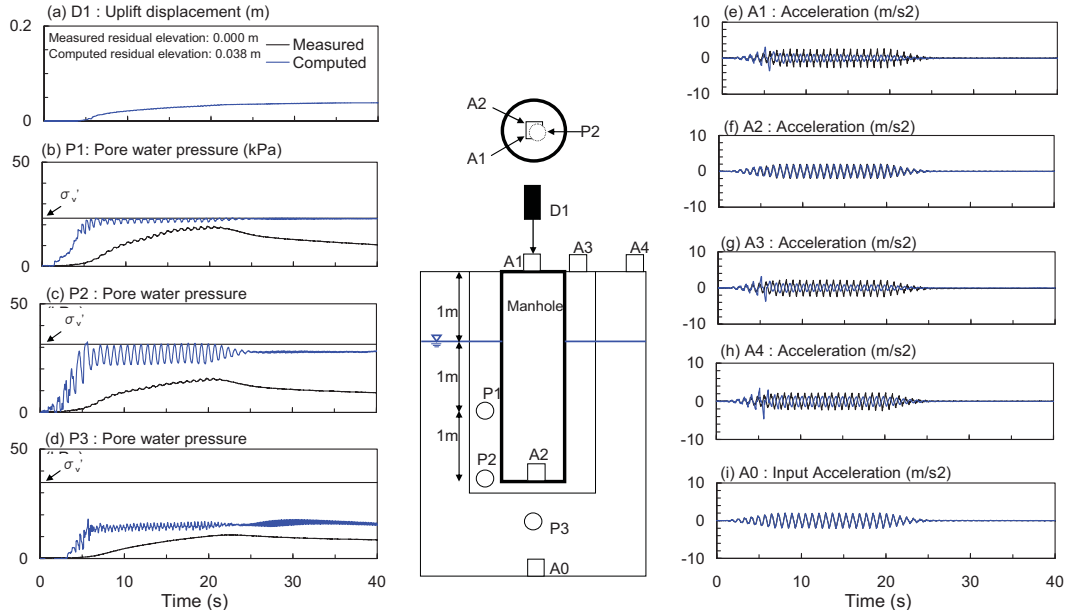

Fig. 4.11 Measured and computed response for input motion of 2.05 m/s^2: (a) uplift displacement of the manhole, (b) – (d) excess pore water pressure, and (e) – (i) accelerations

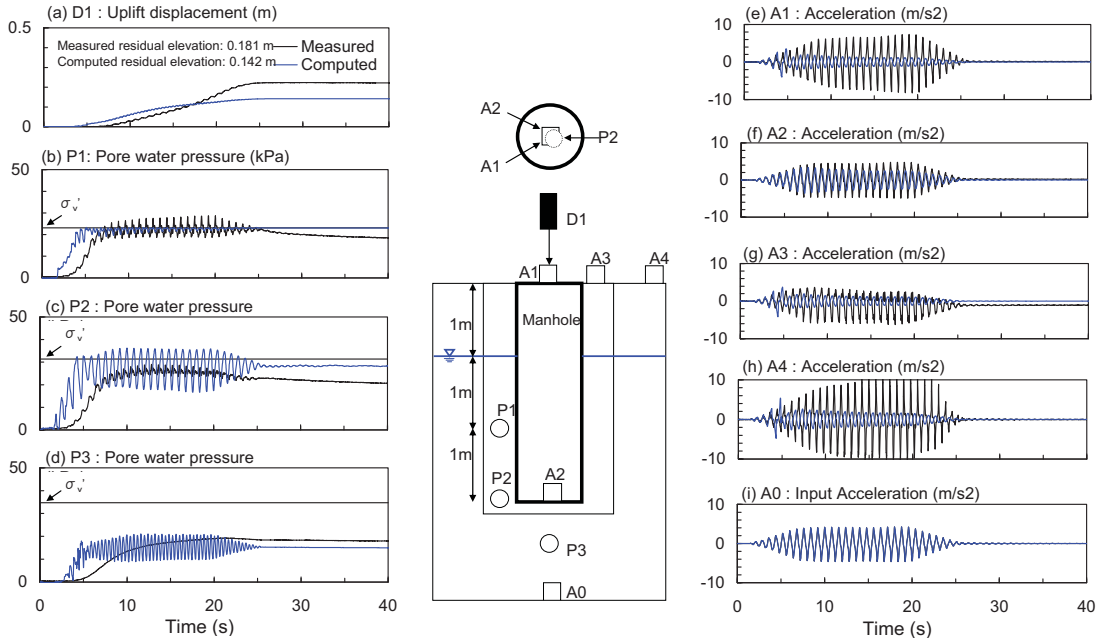

Fig. 4.12 Measured and computed response for input motion of 4.64 m/s^2: (a) uplift displacement of the manhole, (b) – (d) excess pore water pressure, and (e) – (i) accelerations.

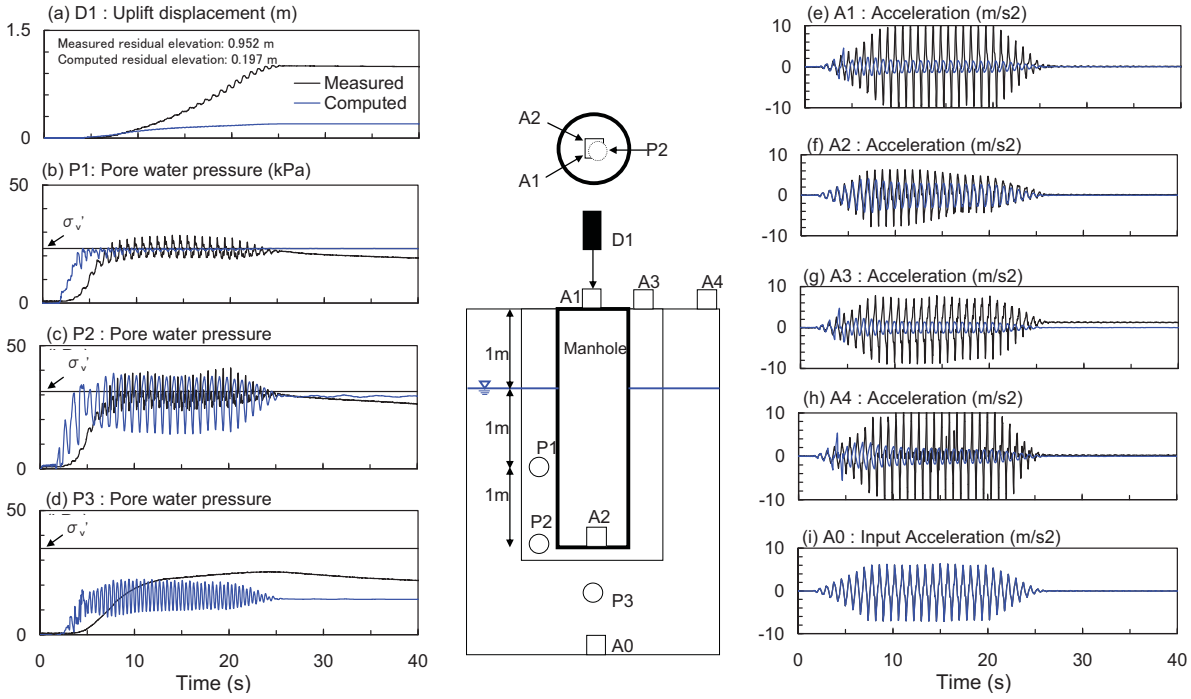

Fig. 4.13 Measured and computed response for input motion of 7.15 m/s^2: (a) uplift displacement of the manhole, (b) – (d) excess pore water pressure, and (e) – (i) accelerations.

is irrelevant to the amplitude of input acceleration. The uplift displacement predicted by the simplified method is significantly overestimated at relatively small amplitude of the input acceleration (2.0 ~ 4.64 m/s^2), whereas the uplift displacements computed by the numerical analyses in the two and three dimensional conditions are fairly good at the input accelerations of less than 4.64 m/s^2 as shown in Fig. 4.14. At large amplitude of the input acceleration (7.15 m/s^2), the uplift displacement predicted by the simplified method is fairly good compared with those of the numerical analysis in the two and three dimensional conditions. In other words, the uplift displacement computed by numerical analysis is about 4.8 times smaller than that of measured in the centrifuge model tests when large amplitude of the input acceleration (7.15 m/s^2) was applied to the numerical analysis.

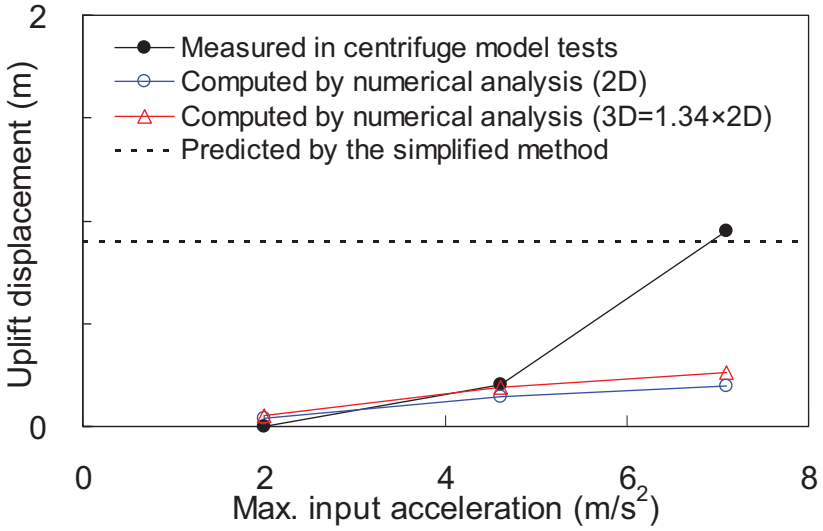

Fig. 4.14 Measured and computed uplift displacement for maximum amplitude of input accelerations.

4.6.2 Comparison for effect of number of load cycles against uplift displacement

The numerical analysis is conducted when number of load cycles of the input acceleration is small and the results are compared with centrifuge test date. The maximum peak acceleration as an input data is 6.87 m/s^2 which was measured on the base plate of the shaking table in centrifuge model tests [Fig. 4.15(i)]. The ground water depth coincides with the depth of 1 m from the ground surface.

Figure 4.15 shows comparisons between measured and computed uplift behavior of the manhole. Measured maximum uplift displacement is 0.234 m. Computed uplift displacement by numerical analysis in the two dimensional conditions is 0.154 m and the uplift displacement considering the three dimensional conditions is 0.207 m. Although, computed uplift displacement by the numerical analysis is slightly smaller than that measured in the centrifuge model test, the ability of the numerical analysis to estimate the uplift displacement of the manhole under small number of load cycles is verified.

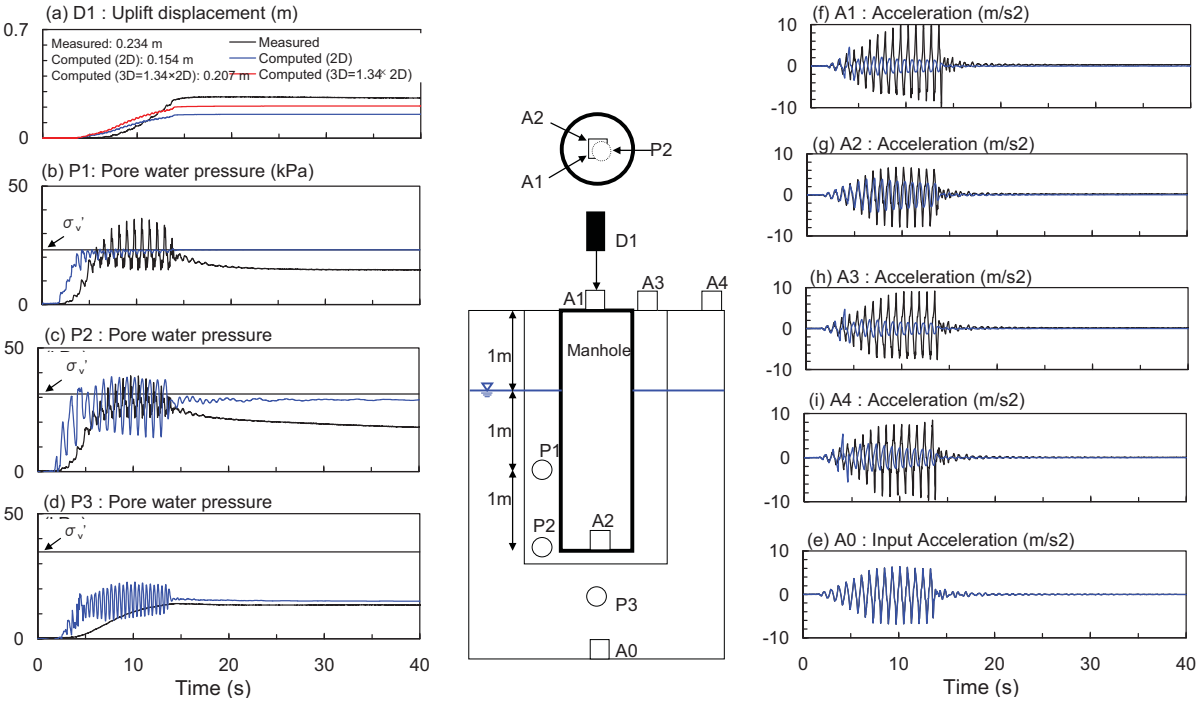

Fig. 4.15 Measured and computed when number of load cycles is small: (a) uplift displacement of the manhole, (b) – (d) excess pore water pressure, and (e) – (i) accelerations.

4.6.3 Comparison for effect of compacted ground against uplift displacement

The numerical analysis was conducted for uplift behavior of a manhole in dense ground. The maximum peak acceleration as an input data is 6.5 m/s^2 which was measured on the base plate of the shaking table in centrifuge model tests [Fig. 4.16(i)]. The ground water depth is located at the depth of 1 m from the ground surface. In the numerical analysis, the uplift behavior of the manhole in dense ground is simulated by considering non-liquefiable ground. It indicates that a zero value is set at parameters for liquefaction properties shown in Table 4.3.

Figure 4.16 shows a comparison between measured and computed uplift behavior of the manhole. In Fig. 4.16(b), the excess pore water pressure in the middle of backfill does not reach the initial effective vertical stress in measured and computed one. In results of centrifuge

model tests of Fig. 4.16(g) and (h), accelerations on the ground surface of backfill and native ground are largely amplified compared with amplitude of the input acceleration. However, in results of the numerical analysis, amplitude of accelerations on the ground surface of backfill and native ground in the numerical analysis is almost at the same level compared with the amplitude of the input acceleration. The maximum uplift displacement measured in the centrifuge model test is 0.00 m. The maximum uplift displacements computed in the two and three dimensional conditions are 0.025 m and 0.033 m, respectively. Comparison between measured and computed uplift displacements of the manhole in dense ground shows good agreement with each other. This fact suggests that it is possible to estimate the uplift behavior of a manhole in dense ground by the numerical analysis.

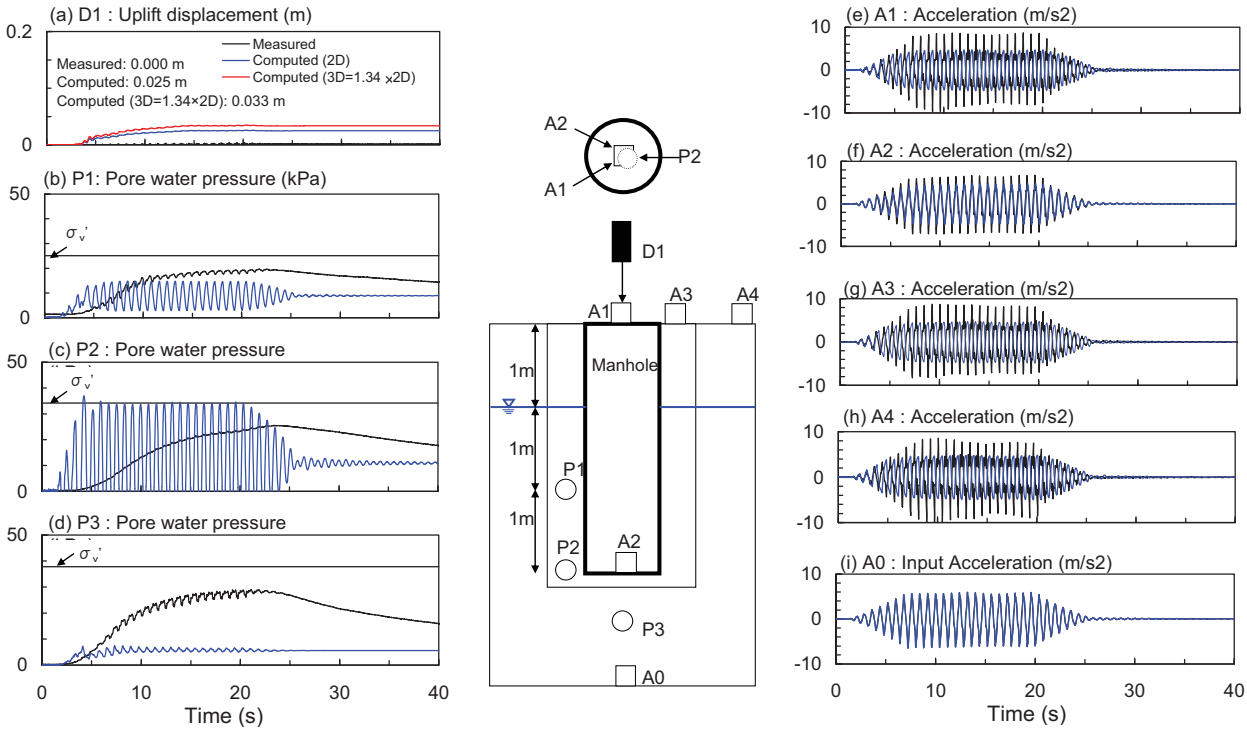

Fig. 4.16 Measured and computed response in non- liquefiable ground: (a) uplift displacement of the manhole, (b) – (d) excess pore water pressure, and (e) – (i) accelerations.

4.6.4 Comparison for saturated soil below the ground surface

In previous sections, the numerical approach by the finite element method can overcome the limitation of the simplified method by simulating the uplift displacement of the manhole when amplitude of input acceleration was small or number of load cycles was short as the input motion, and backfill was sufficiently compacted. To investigate the applicability, the numerical analysis was also conducted for the saturated soils whose ground water table coincides with the ground surface and the results are compared with centrifuge test date. The maximum acceleration as an input data is 6.78 m/s^2 measured on the base plate of the shaking table in centrifuge model tests [Fig. 4.17(i)].

Figure 4.17 shows comparisons between measured and computed uplift behavior of the manhole. In Fig. 4.17(b) and (c), the manhole starts to lift up when excess pore water pressure in the middle of backfill reached about 100% of the initial effective vertical stress at about 5 seconds in the measured and computed one. In Fig. 4.17(e) and (f), the amplitude of the acceleration at the top of the manhole [Fig. 4.17(e)] is significantly smaller than that of the bottom of the manhole [Fig. 4.17(f)] in the measured and computed. Also, the amplitudes of accelerations on the ground surface of backfill and native ground by numerical analysis are significantly smaller than those measured in the centrifuge model tests. The maximum uplift displacement measured in the centrifuge model tests is 1.10 m. The maximum uplift displacements computed by numerical analysis in the two and three dimensional conditions are 0.391 m and 0.524 m, respectively. The uplift displacement computed by numerical analysis is about 2 times smaller than that measured in the centrifuge model tests. This fact indicates that numerical analysis tends to underestimate the uplift displacement of the manhole when a high magnitude of uplift displacement occurred, such as a large amplitude of input acceleration [Figs. 4.13 and 4.14] or the saturation of soils below the ground surface.

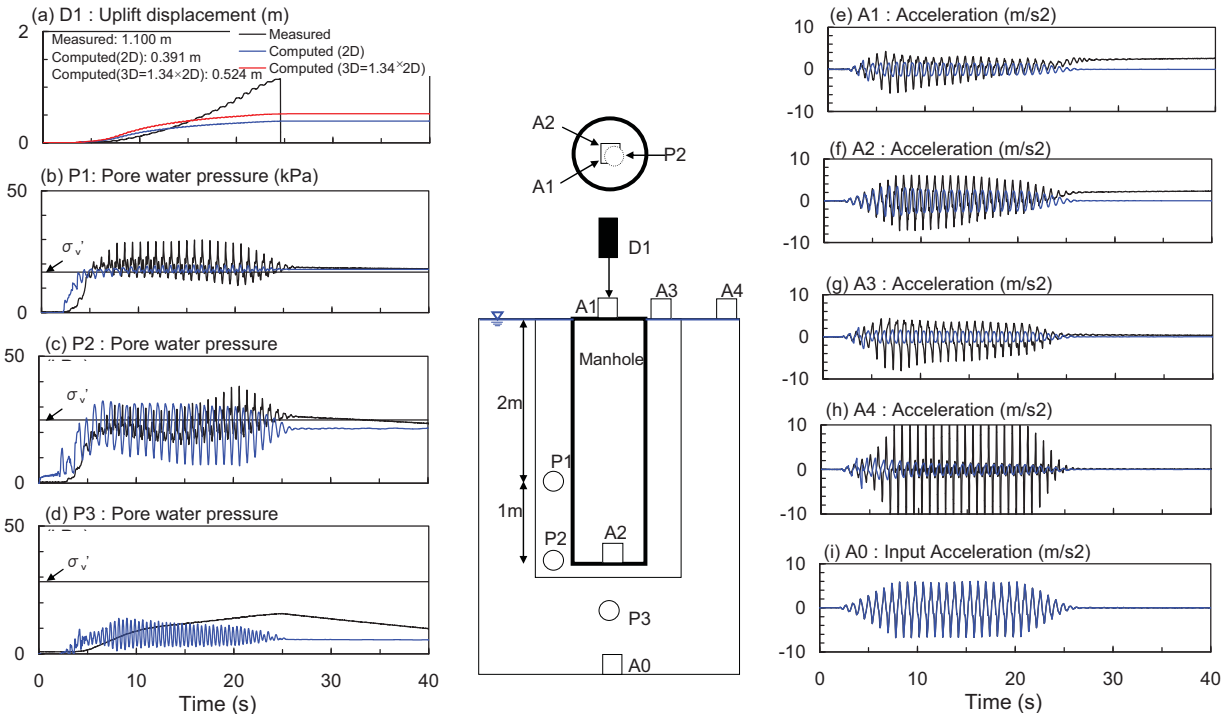

Fig. 4.17 Measured and computed response in saturated soil below the ground surface: (a) uplift displacement of the manhole, (b) – (d) excess pore water pressure, and (e) – (i) accelerations.

4.7 Summary

Two dimensional effective stress analyses were conducted to overcome the limitation of the simplified method which significantly overestimates the uplift displacement of a manhole in liquefied ground when amplitude of input acceleration is small or number of load cycles is short, and backfill is sufficiently compacted. The effective stress analysis based on mechanics of a continuum body can estimate transient behaviors of a manhole during shaking as well as the maximum uplift displacement. Also, it is possible to evaluate both failure modes and the extent of displacement/stress/ductility/strain subjected to the complex soil-structure interaction. The results of the analysis were compared with centrifuge test data.

Before performing the numerical analysis for uplift behavior of the manholes, the behavior of the soils in the three dimensional conditions is examined by applying cyclic simple shear to a soil element below the manhole under an undrained condition as a preliminary study because the uplift behavior of a buried structure needs to be considered as three dimensional mechanisms. The results show that the uplift of manhole structures by the three dimensional models may be 1.34 times larger than that in the two dimensional models based on the fact that the axial strain of the soil element below the manhole in the three dimensional conditions was 1.34 times larger than that in the two dimensional conditions when the axial strain difference was at the same level.

In order to overcome the limitation of the simplified method, conditions of the model tests selected from the centrifuge model tests are as follows: (1) Ground water table coincides with the depth of 1 m from the ground surface, relative density of backfill and native ground is about 36% and 85%, respectively, and amplitudes of input acceleration are 2.05 m/s^2 and 4.64 m/s^2 with load cycles of 30. (2) Amplitude of input acceleration is 6.87 m/s^2 with load cycles of 15 under the same test condition with (1). (3) Amplitude of input acceleration is 6.9 m/s^2, relative density of backfill is 85% and other test conditions are the same with (1).

The uplift displacements computed by the numerical analysis in the two and three dimensional conditions (1.34×2D) are consistent with those measured in the centrifuge model tests under the input acceleration of 2.05 m/s^2 and 4.64 m/s^2. When the number of load cycles of 15, as the input wave were applied, the computed uplift displacement (0.207 m) was slightly smaller than that (0.234 m) of the measured displacement in the centrifuge model test. However, the ability of the numerical analysis to estimate the uplift displacement of the manhole was verified. Also, results by numerical analysis, when the ground was significantly compacted (85%), show that backfill was not liquefied and the uplift displacements were

0.025 m in the two dimensional conditions and 0.033m in the three dimensional conditions (1.34×2D). These facts indicate that numerical analysis can estimate the uplift displacement of manholes in compacted ground.

However, the uplift displacement by the numerical analysis was about 4.8 times smaller than that measured in the centrifuge model tests when amplitude of input acceleration was increased by 7.15 m/s^2 from the test condition (1). When the ground water table coincides with the ground surface and amplitude of input acceleration is increased by 6.8 m/s^2 from the test condition (1), the uplift displacement was about 2 times smaller than that measured in the centrifuge model tests. These facts indicate that numerical analysis tends to underestimate the uplift displacement of the manhole when a high magnitude of uplift displacement is occurred such as large amplitude of input acceleration or the saturated backfill whose ground water table coincides with the ground surface.

On the basis of the above-mentioned discussion, the ability of the numerical analysis to estimate transient behaviors of the manhole uplift during an earthquake and to overcome the limitation of the simplified method was verified through the results in a series of two dimensional effective stress analyses.

5. Application to the case history during the 2004 Niigata-ken Chuetsu, Japan, earthquake

5.1 Introduction

The main objective in this chapter is to verify the application of the methods for estimation of uplift amount of the manholes proposed in this study by applying them to the case histories of an earthquake. In accordance with this, factors affecting the uplift behavior are investigated. The factors considered in the investigation are the depth of ground water table as a primary factor and the native subsoil material near the ground surface such as SPT blow counts, thickness of clay layer, and thickness of surface soil (embankment and reclamation) as a secondary factor.

The Niigata-ken Chuetsu, Japan, earthquake of 23 October 2004 (Mw=6.6) was the most significant earthquake since the 1995 Hyogoken-Nambu, Japan, earthquake. The damages occurred mainly due to affected sewer pipelines. More than 1,450 buried sewerage structures, known as manholes, were disturbed. The maximum uplift displacement of the manhole was about 1.5 m as shown in Fig. 5.1. A car collided with an uplifted manhole in Nagaoka city as shown in Fig. 5.2.

Prior to the restoration works after the earthquake, the open-cut surveys were conducted to investigate severe damage to sewer systems by the Nagaoka city government. Based on the results, the database which contains uplift displacement of manholes, location of the manholes, the SPT borehole logs and their locations, was developed. Then, with the database, the effect of the ground water table, as a primary factor affecting manhole uplift, were investigated through analyzing the relationship between the uplift displacement of manholes and the SPT borehole

logs. Although conditions of backfill are also primary factors to affect uplift phenomenon of buried structures, it is difficult to investigate the soil conditions of backfill in the field before earthquakes. Using the relationship between the uplift displacement and the depth of THE ground water table, the methods for estimation of uplift amount are applied to the case history data to verify its effectiveness of predicting the real uplift displacements. Finally, the factors affecting manhole uplift as a secondary factor, which is the native subsoil material near the ground surface, is investigated through correlation analysis.

Fig. 5.1 Uplifted manhole after the 2004 Niigata-ken Chuetsu, Japan, earthquake.

Fig. 5.2 Car collided with uplifted manhole in Nagaoka city after the 2004 Niigata-ken Chuetsu earthquake, Japan (Technical Committee on the Sewer Earthquake Countermeasures, 2005).

5.2 Observed uplift behavior of buried geotechnical structures in Nagaoka, Japan, during the 2004 Niigata-ken Chuetsu earthquake

5.2.1 Subsurface soil condition and general description

Nagaoka city has an area of 841 km^2 and population is about 194,414 people. The affected region (Nagaoka city) is characterized by low hills in upland terrain and multiple river valleys in the lowland areas. The Shinano River, which caused tremendous damage to many types of structures and the ground due to liquefaction in Niigata city in the 1964 Niigata earthquake, flows north along the western margin of the hills towards the cities of Nagaoka and Niigata, whereas the Uono River flows west through the affected region and joins the Shinano River at Kawaguchi. The surrounding Uonuma hills consist of Neogene (mostly Pliocene) and late Pleistocene sedimentary deposits, with Pleistocene terrace deposits at the margins of the river valleys (Yanagisawa et al. 1986). The terrace deposits and alluvium within the river valleys are predominantly gravel, with some sand and silt. Comparing the liquefaction observations with geologic maps of the Nagaoka areas (Kobayashi et al. 1991), the results indicate that liquefaction was concentrated in the alluvial deposits (floodplains) of the Shinano and Uono Rivers. Investigated areas where liquefaction was not observed tend to be terrace and alluvial fan deposits. Rarely was liquefaction observed in urban areas (Rathje et al. 2006, Yanagisawa et al. (1986)).

The largest city significantly affected by the earthquake was Nagaoka city, where about 1,000 buildings were completely destroyed. Roads and highways sustained damage at over 6,000 locations; rail lines, water systems, and wastewater systems sustained major damage (Scawthorn et al. 2006). Damage to sewerage systems occurred mainly due to disrupted sewer pipelines.

Table 5.1 Cities and town where sewage pipes or manholes were damaged during the 2004 Niigata-ken Chuetsu, Japan, earthquake. (Konish et al. 2008)

Municipality	Length of sewage system (km)	Damaged length (km)	Number of uplifted manholes	Number of cave-in road
Niigata Prefecture	61.3	0.5	51	130
Nagaoka City	1258.0	62.9	436	3685
Kashiwazaki City	421.5	3.9	12	230
Ojiya City	182.8	31.1	400	349
Tochio City	135.1	2.5	9	20
Mitsuke City	195.0	0.2	64	315
Koshiji Town	83.7	4.7	93	157
Mishima Town	58.7	1.8	5	16
Yoita Town	56.0	5.1	88	187
Washima Village	37.7	6.1	36	114
Izumozaki Town	39.6	3.1	5	22
Oguni Town	61.3	9.6	158	107
Toukamachi City	198.1	2.9	10	110
Kawaguchi Town	43.0	9.3	24	93
Kawanishi Towon	29.3	2.4	0	1
Horinouchi Town	75.1		37	93
Sumon Village	48.6	4.3	9	178
Koide Town	88.5		5	19
Yahiko Village	100.2	0.0	0	3
Tsunan Town	59.0	1.5	0	20
Nakanoshima Town	33.3	0.0	0	19
Nishiyama Town	25.8	0.3	8	2
Others			3	38
Total	3291.6	152.2	1453	5908

In Table 5.1, more than 1,400 manholes were disturbed and total damaged length was 152 km. The total loss of sewage facilities was valued at 20.6 billion yen. The maximum distance from the epicenter to a damaged town was about 30 km. The most severely damaged areas were in Nagaoka city, Ojiya city and Kawaguchi Town. The maximum surface accelerations recorded in these cities and this town was about 5.4 to 17 m/s^2. In Nagaoka city, the number of uplifted manholes was 436 and damaged length was 62.9 km out of 1,258 km of sewerage pipelines in the city.

5.2.2 Damage investigation by an open-cut survey

Detailed damage investigation is conducted by open-cut and level survey as shown Fig. 5.3. The survey compiled valuable datasets for sewerage pipeline damage due to liquefaction during the earthquake. The main feature of the collected data includes locations of damaged sections and inclination of pipes before and after the earthquake. Uplift displacements of manholes and pipes were directly measured by leveling. As shown in Fig. 5.4, damage datasets used in this study are concentrated to the eastern part from the Shinano River. Yellow circles indicate the damaged manhole and black triangles are exiting SPT boreholes. The total number of manholes is 2,124. The affected areas are selected by two zones (Zone 1 and Zone 2) where damage of the sewer manhole is gathered with SPT boreholes as shown in Fig. 5.4.

Fig. 5.3 Open-cut and level survey carried out before the restoration in Nagaoka (Nagaoka city government).

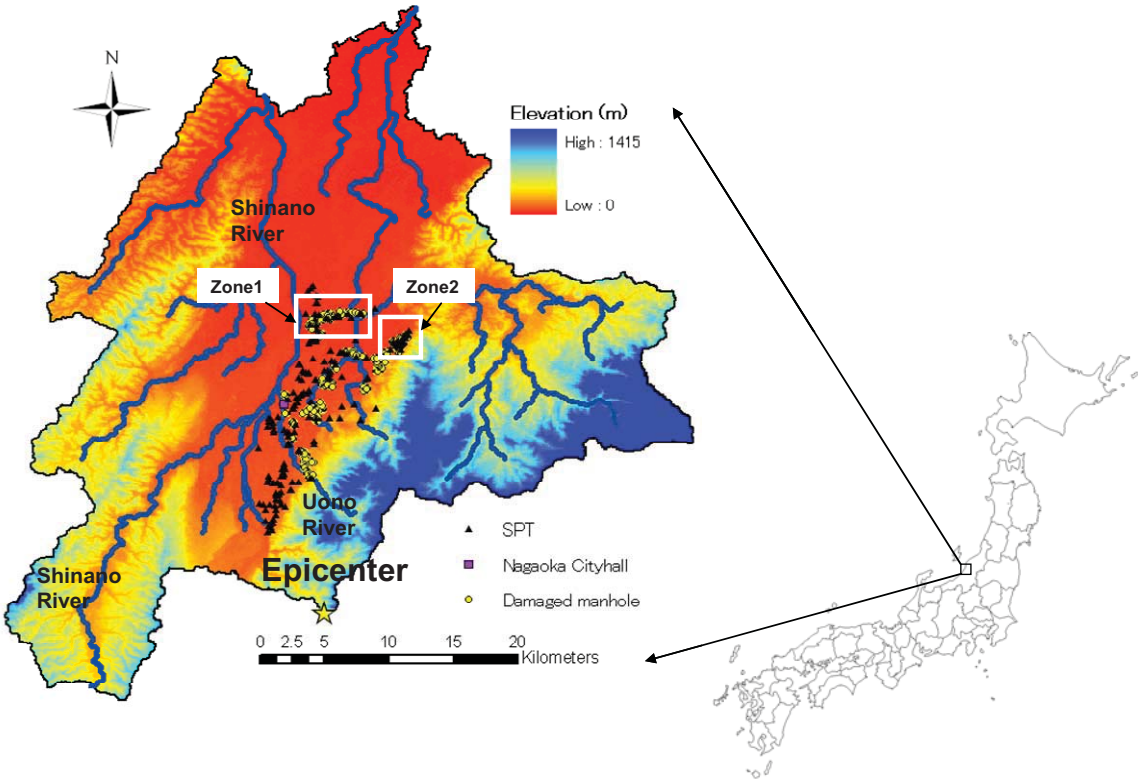

Fig. 5.4 Nagaoka city

Figure 5.5 shows the grain size distribution curve of backfill taken in Nagaoka city during the open-cut survey. The soil is classified as "poorly graded sand (SP)" with Gs = 2.67, e_{max} = 0.99, e_{min} = 0.59. For its ease of handling, this type of backfill material is pervasive in a utility trench in the cohesive native ground in Nagaoka city.

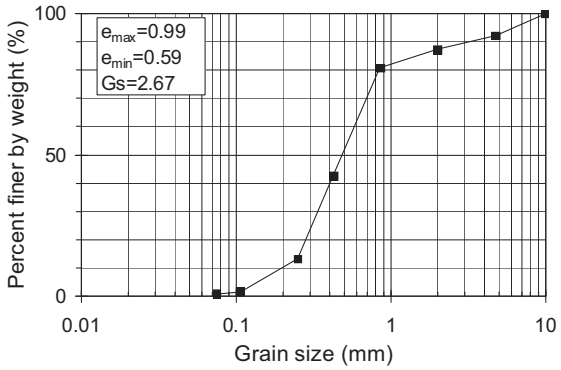

Fig. 5.5 Grain size distribution curve of backfill material in Nagaoka.

5.2.3 Study area and observed manhole uplift

In this chapter, two zones are selected as a study area in Nagaoka city. One is located at near the Shinano River (Plain field_Zone1) with an elevation of 15 m ~ 20 m. The other is located at the foot of the mountain (Foot of mountain_Zone2) with an elevation of 20 m ~ 40 m.

Table 5.2 shows the results of the damage investigation in selected zones which include total extension, number of manholes and maximum uplift of manholes and pipes. Total extension of sewerage systems is 4.8 km and number of manholes is 173 in Zone 1. In Zone 2, total extension is 2.2 km and number of manholes is 101. Number of existing SPT borehole is 28 and 17, respectively.

Table 5.2 Results of the damage investigation in selected zones.

	Total extension (m)	Number of manholes	Max. uplift		Number of SPT borehole
			manholes (m)	pipes (m)	
Zone 1	4,800	173	0.432	1.670	28
Zone 2	2,200	101	0.528	1.062	17
Total	7,000	274			45

Plain field (Zone 1)

Zone 1 shown in Fig. 5.4, which includes a total of 173 manholes (Table 5.2) is located in a plain field about 20 km north of the epicenter. Figure 5.6 shows a summary of the investigation in Zone 1. Red solid circles indicate uplifted manholes, yellow solid circles indicate settled manholes, and blue solid circles indicates no damage manholes and black solid triangles indicate locations of SPT borehole in the native ground. The number of SPT boreholes is 28. Manholes were not uplifted in the eastern part of the figure, which is located

at about 4 km from Shinano River, because these are located in protected lowlands surrounded by rice fields.

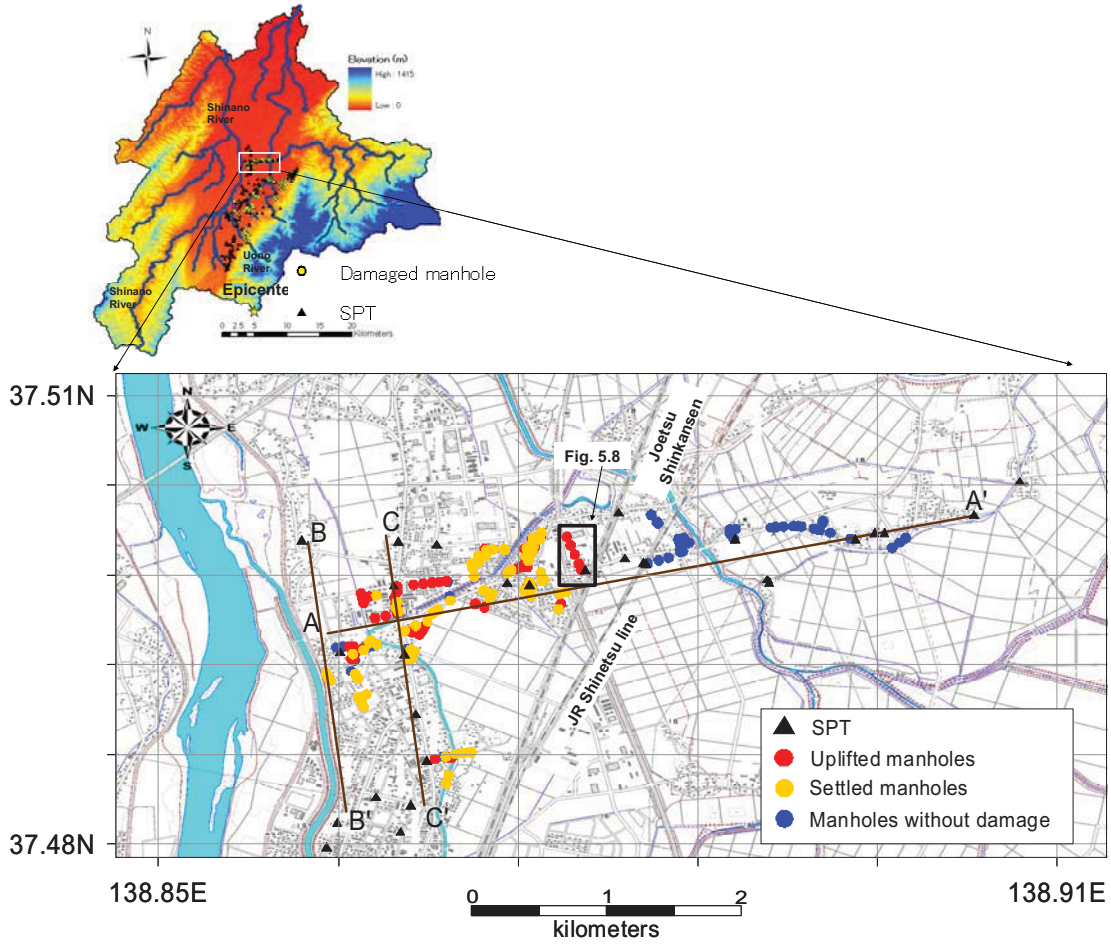

Fig. 5.6 Zone 1 (Plain field) in Nagaoka.

Uplifted and settled manholes were concentrated near the Shinano River, where loose sands with SPT blow counts of less than 10, are dominant in native ground which caused damage due to liquefaction in Niigata city in the 1964 Niigata earthquake. It indicates that liquefaction of the native ground may instigate the uplift of buried manholes. Figure 5.7 shows a histogram of the magnitude of the manhole uplifts in Zone 1. In this figure, 31% of manholes are uplifted by 0.432 m. 44% are settled and in 25% there is no damage.

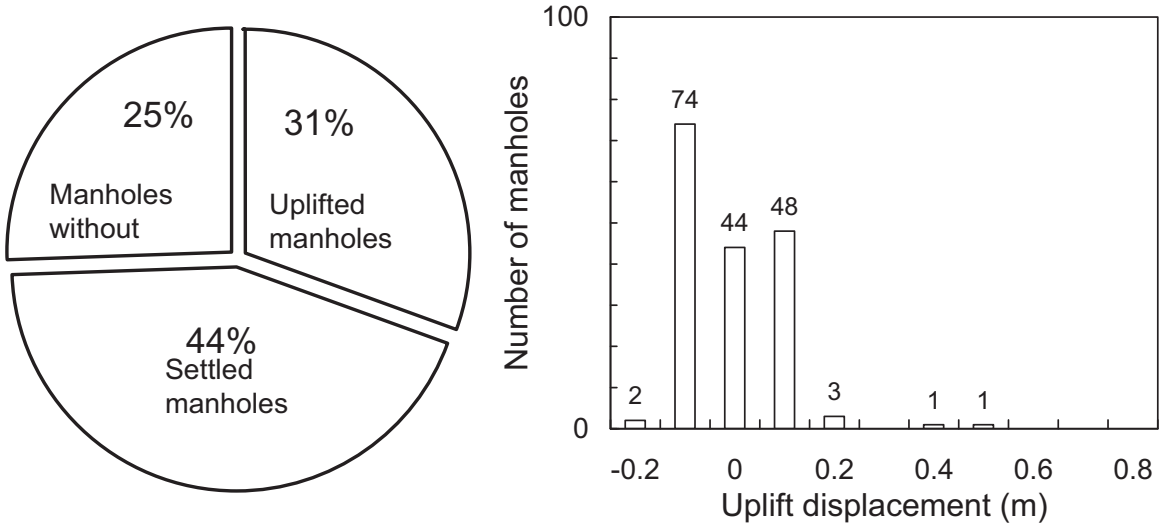

Fig. 5.7 Histogram of magnitude of manhole uplift in Zone 1.

Figure 5.8 shows a cross section of damaged manholes and pipelines in detail with a borehole log in affected areas which are described as a tetragon in Fig. 5.6. Length of the manholes is in the range of approximately 1.8 ~ 3 m. The maximum uplift was 0.432 m for the manhole and 0.478 m for the pipe. In this cross section, the surface ground consists of clay material and a clay layer with low permeability may affect the uplift displacement during liquefaction. Although the ground water depth on the southern part is shallow (0.36 m), the uplift of the manhole is small. The reasons may be that the backfill surrounding the manholes was compacted by a moving load of people and vehicles near the main road as shown in Fig. 5.8. The maximum uplift (0.432 m) of the manhole occurred at about 100m form the south. The uplift displacement of the manhole is small on the northern part because the ground water depth is deep and the manhole is short. Because an apparent unit weight of short manholes is larger than that of the long manholes, short manholes may be more difficult to uplift compared with long manholes.

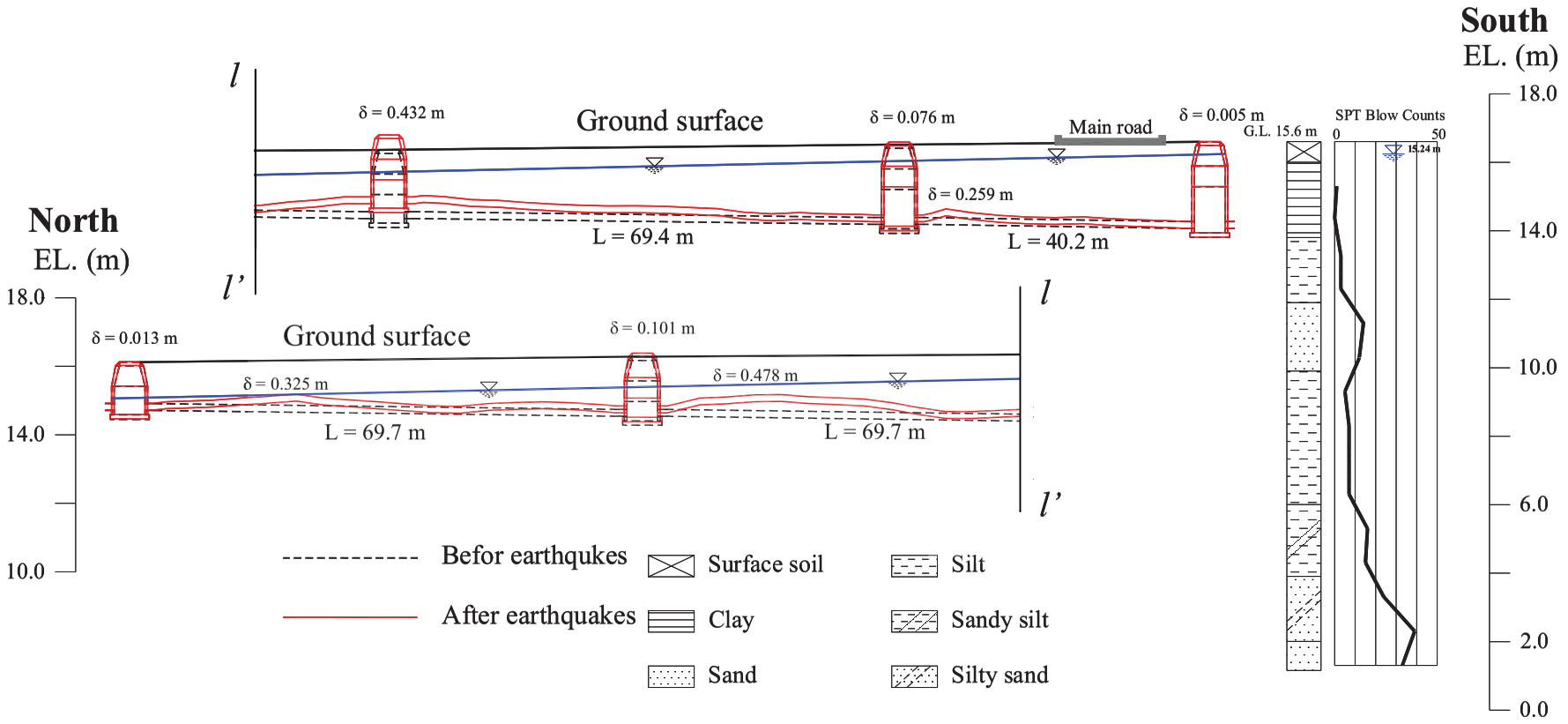

Fig. 5.8 Cross section of damaged manhole and pipelines shown in Zone 1.

Two types of uplift patterns for the pipes are found. First, the pipe attached to the manhole is uplifted by the pull of that uplifted manhole. The other is uplifted in the middle of two manholes by liquefaction of backfill regardless of the manhole uplift. Actually, the buried pipes are easier to uplift than manholes because the pipes are normally located deeper than the ground water table compared with manholes as shown in Fig. 5.8.

Foot of mountains (Zone 2)

The second site (Zone 2) shown in Fig. 5.4 which includes a total of 101 manholes (Table 5.2) is located at the foot of a mountain about 5 km east of Zone 1. Figure 5.9 shows a summary of the investigation in Zone 2. Red solid circles indicate uplifted manholes, yellow solid circles indicate settled manholes, blue solid circles indicate no damage to manhole and black solid triangles indicate locations of SPT borehole. Figure 5.10 shows a histogram of the magnitude of manhole uplift in Zone 2. In this figure, 43% of manholes are uplifted and the maximum uplift is about 0.528 m. 52% are settled and in 5% there is no damage. Comparing with plain field (Zone 1), manholes at the foot of the mountain were mainly settled and only 5% of manholes were not damaged.

Figure 5.11 shows a cross section of damaged manholes and pipelines in detail with borehole data which is described as a tetragon in Fig. 5.9. In this section, a clay layer is predominant and the clay layer near the ground surface is indicated as a thick black line. As shown in Fig. 5.11, the eastern side of the section is close to the mountain. The ground is inclined toward to west. On the western side, the surface ground consists of relatively stiff silt and clay material with a SPT blow count 1 to 7, and that of the eastern side consists of sandy clay/silt with a SPT blow count of 2 to 3. The ground water table is located at GL. -0.8 m in the west and GL -2.0 m in the east. The total length of the section is 289.5 m with 10

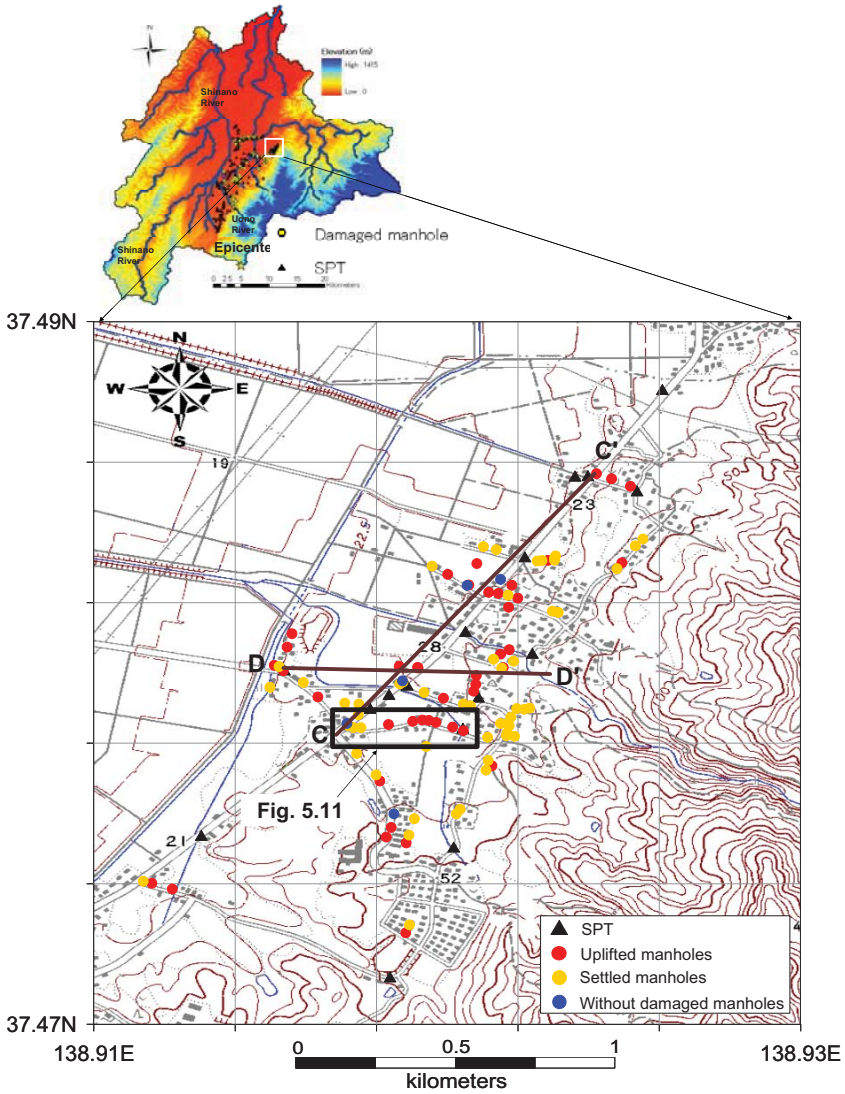

Fig. 5.9 Foot of the mountain (Zone 2) in Nagaoka.

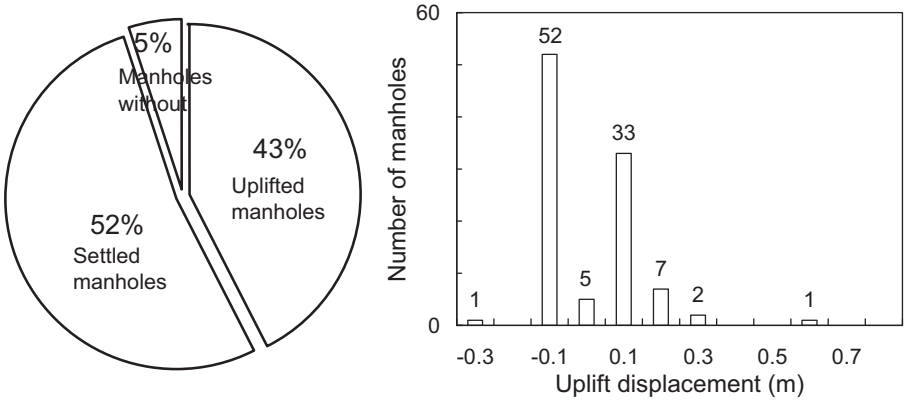

Fig. 5.10 Histogram of magnitude of manhole uplift in Zone 2.

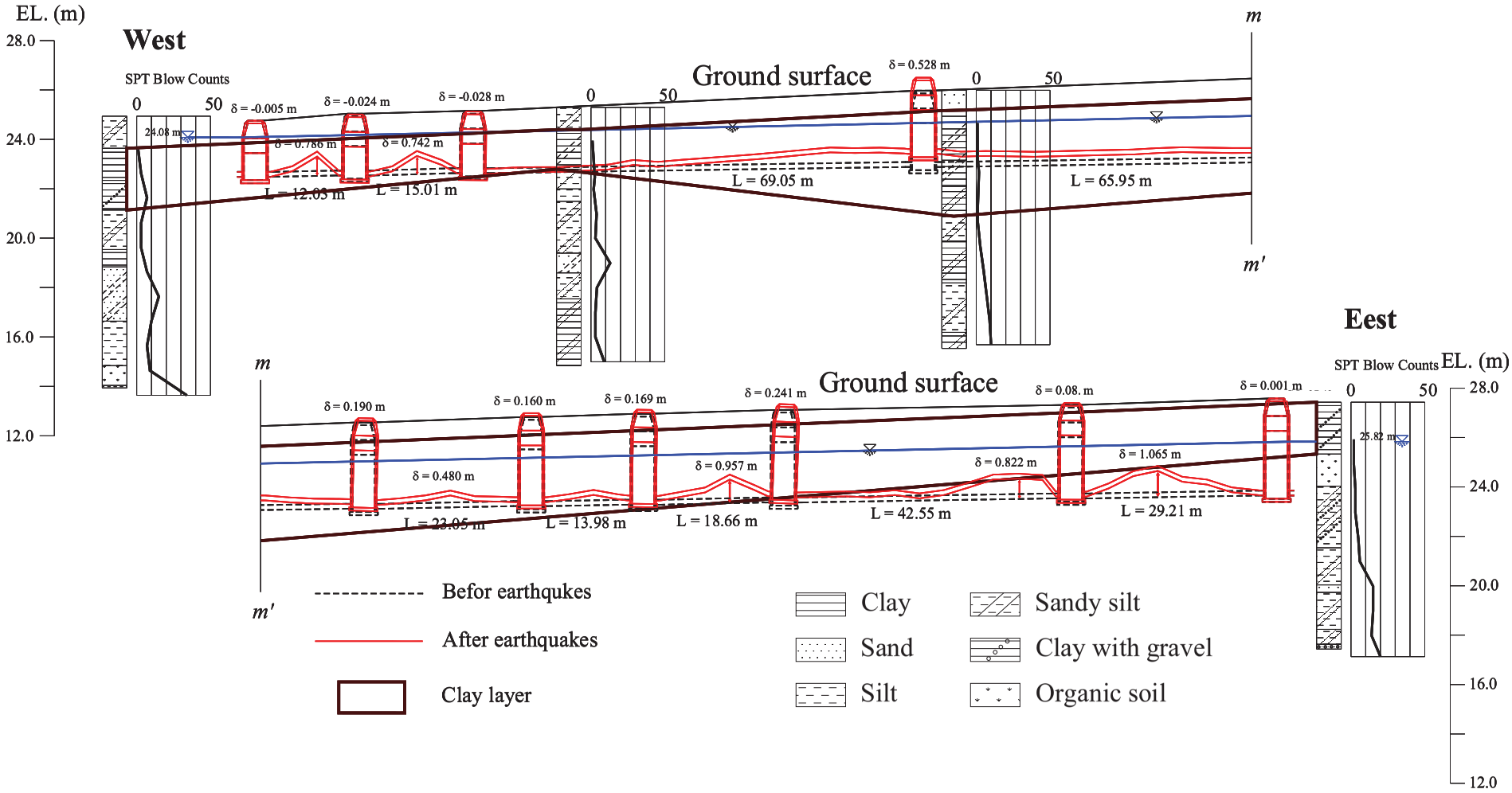

Fig. 5.11 Cross section of damaged manhole and pipelines shown in Zone 2.

manholes. Manhole length varies from 4 m (east side) to 3 m (west side) depending on the ground elevation and the required slope of pipelines for drainage. Maximum uplift amount, δ, is 0.528 m. Pipelines were also heavily damaged and the maximum upward movement is 1.065 m in the eastern side. As shown in Fig. 5.11, pipelines are typically moved upward in the middle of manholes with small uplifts. This trend is also found in Zone 1 (Fig. 5.8). Zone 2 is predominantly clay material compared with Zone 1. On the basis of these, the clay material with low permeability may affect the uplift displacement during liquefaction.

5.3 Amount of uplift of manholes vs. geotechnical parameters obtained from the SPT borehole logs

To investigate the detailed relationship between the uplift amount and ground water table as a primary factor, the uplift amount of the manholes is compared with geotechnical parameter obtained from the SPT borehole logs. In accordance with this, the relationship between the uplift amount of the manholes and the native subsoil material, which is a secondary factor near the ground surface, is also discussed.

5.3.1 Plain field (Zone 1)

In Zone 1, three cross sections (*A* to *C*) were selected to investigate the relationship between the vertical displacement of manholes and geotechnical parameters obtained from the SPT borehole logs. Section *A-A'* crossed from the eastern to western part and sections *B-B'* and *C-C'* were selected to investigate the effect of loose sand with a SPT blow count of 5 to 10 near the Shinano River. SPT boreholes were selected nearest the manholes.

Figure 5.12 shows the relationship between SPT borehole logs and uplift displacement at a

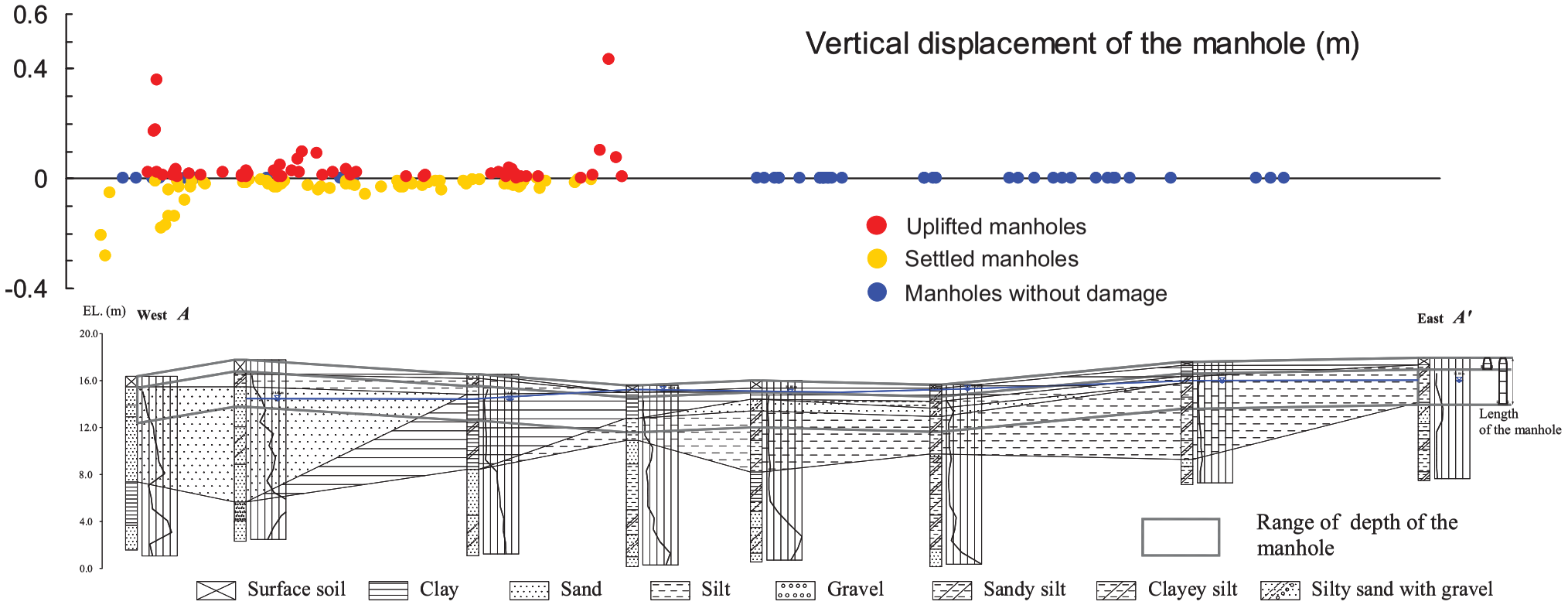

Fig. 5.12 Relationship between vertical displacement of the manhole and SPT borehole logs (*A-A'*).

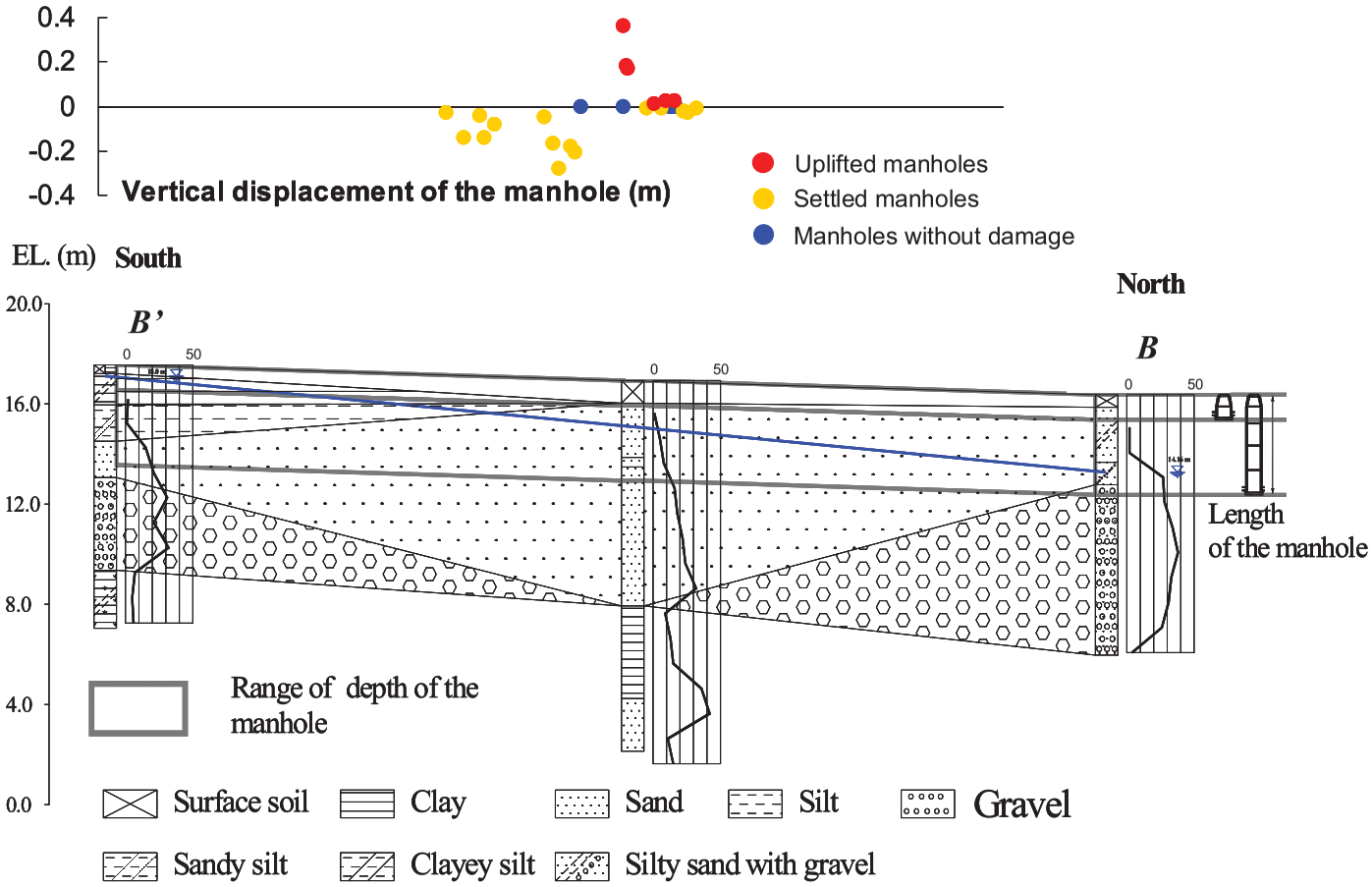

Fig. 5.13 Relationship between vertical displacement of the manhole and SPT borehole logs (*B-B'*).

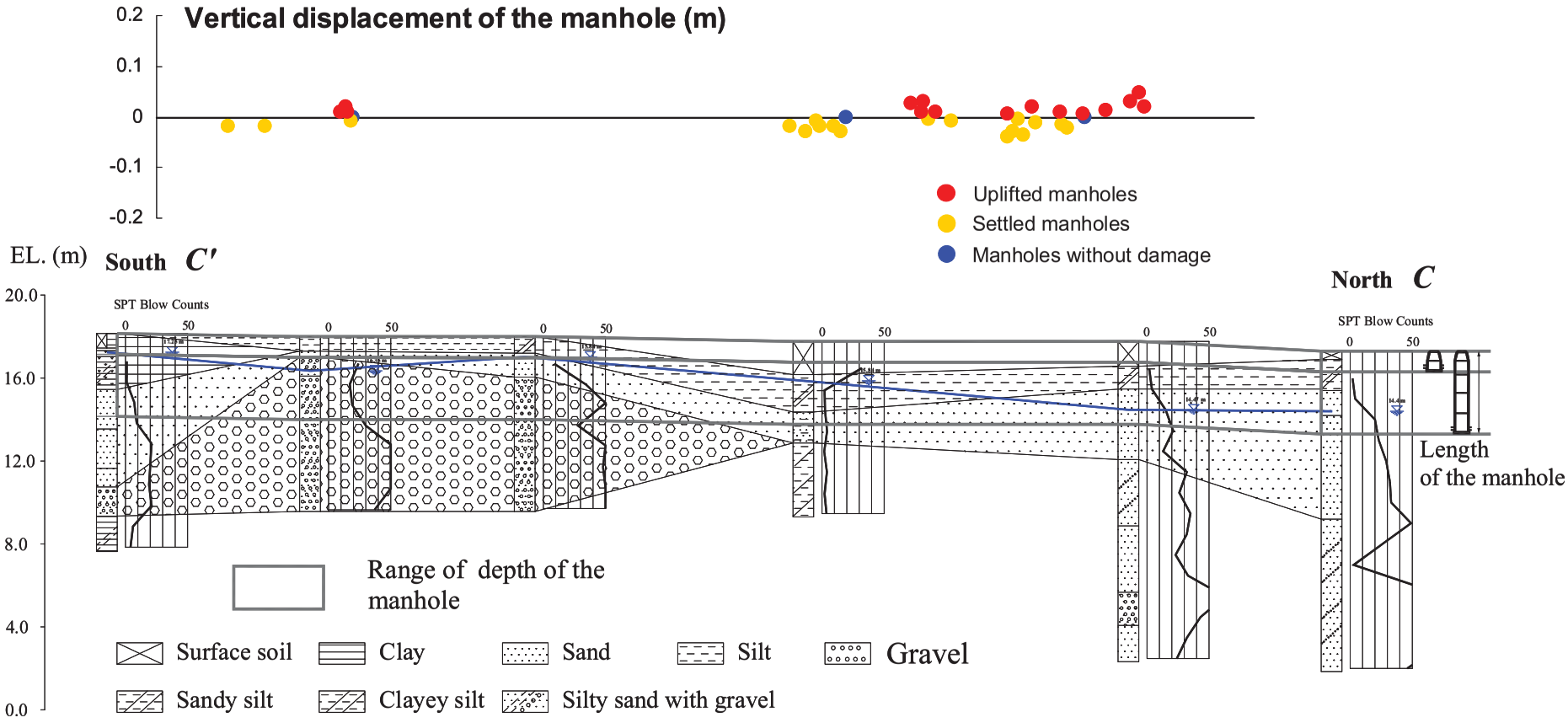

Fig. 5.14 Relationship between vertical displacement of the manhole and SPT borehole logs (*C-C'*).

cross section *A-A'* in Fig. 5.6. A thick gray line indicates the length of the manhole and it is in the range of 1 m ~ 4 m. A blue line indicates the depth of ground water table. The damage of the manhole was not observed on the eastern part where sandy silt is dominant in the native ground. Many manholes were uplifted and settled on the western part located at near the Shinano River. The maximum uplift was observed at the subsurface ground with a low ground water depth (0.36 m) and a thick clay layer with low permeability composite surrounding the manhole. Manholes were also uplifted by about 0.4 m and settled by about 0.3 m nearest the Shinano River in a sand layer with low SPT blow counts (less than 10).

Figure 5.13 shows a relationship between SPT borehole logs and uplift displacement at a cross section *B-B'* in Fig. 5.6. As shown in Fig. 5.13, many manholes were uplifted and settled in sand ground with a low SPT blow count. The uplift of manholes may be instigated by liquefaction of sandy ground with a low SPT blow count in the native ground. Namely, if the native ground was liquefied with the backfill, the manholes may be uplifted much more or the manhole may be sunken with the settlement of the native ground after earthquakes.

In Fig. 5.14, although the ground water table was deep on the northern part where the surface soil was deposited by embankments or reclamations, the uplift displacement is relatively large compared with that on the southern part at cross section *C-C'*. The uplift may be related to the thickness of surface soil (Fill thickness: embankment and reclamation) because the manhole is a shallow structure with the maximum length of about 4 m from the ground surface. The uplift displacement is also relatively small on the southern area because the gravel layer with a high permeability, which is difficult to liquefy (JGS, 1994), is subsisted at the cross section *C-C'*.

On the basis of these, the uplift displacement may be related to the depth of the ground water table, thickness of the clay layer, SPT blow counts and fill thickness in the native ground.

5.3.2 Foot of mountains (Zone 2)

Figure 5.15 shows the relationship between the SPT borehole logs and the uplift displacements of manholes at cross section *D-D'* in Fig. 5.9. The SPT boreholes were selected nearest one from manholes. The elevation varies from 22.57 m to 27.10 m, up and down. A thick gray line indicates the length of the manholes in the range of 1 m ~ 4 m. A blue line indicates the location of the ground water table. On the southern side in this section, the surface ground consists of clay and silt material and that of the northern side consists of clay and sand silt. The maximum uplift (0.528 m) was observed on the southern side where the ground water is located at the depth of 0.86 m from the ground surface and a thick clay layer with low permeability is dominant. The magnitude of uplift is about 0.1 m in the center of the section which consists of sandy silt and gravel.

Figure 5.16 shows a relationship in a cross section *E-E'* in Fig. 5.9. The eastern side of the section is close to the mountain. The ground is inclined toward west. Large magnitudes of the uplift were observed in the center of the section where the ground water depth coincides with a shallow location from the ground surface and a clay layer is dominant. A small magnitude of uplift is observed in the eastern and western sides. The reason for that may be that the surface ground consists of gravel with a high permeability on the eastern side, and the surface ground consists of relatively stiff sandy silt on the western side.

In Zone 2, the relationship between the uplift displacement and surface soil (fill thickness: embankment and reclamation) was not found because surface soil is not predominant in Zone 2. However, the uplift displacement may be related to the thickness of the clay layer, SPT blow count and the depth of the ground water table as shown in Zone 1.

Especially, the maximum uplift displacements are observed when the ground water table coincides with a shallow location from the ground surface in Zone 1 and Zone 2.

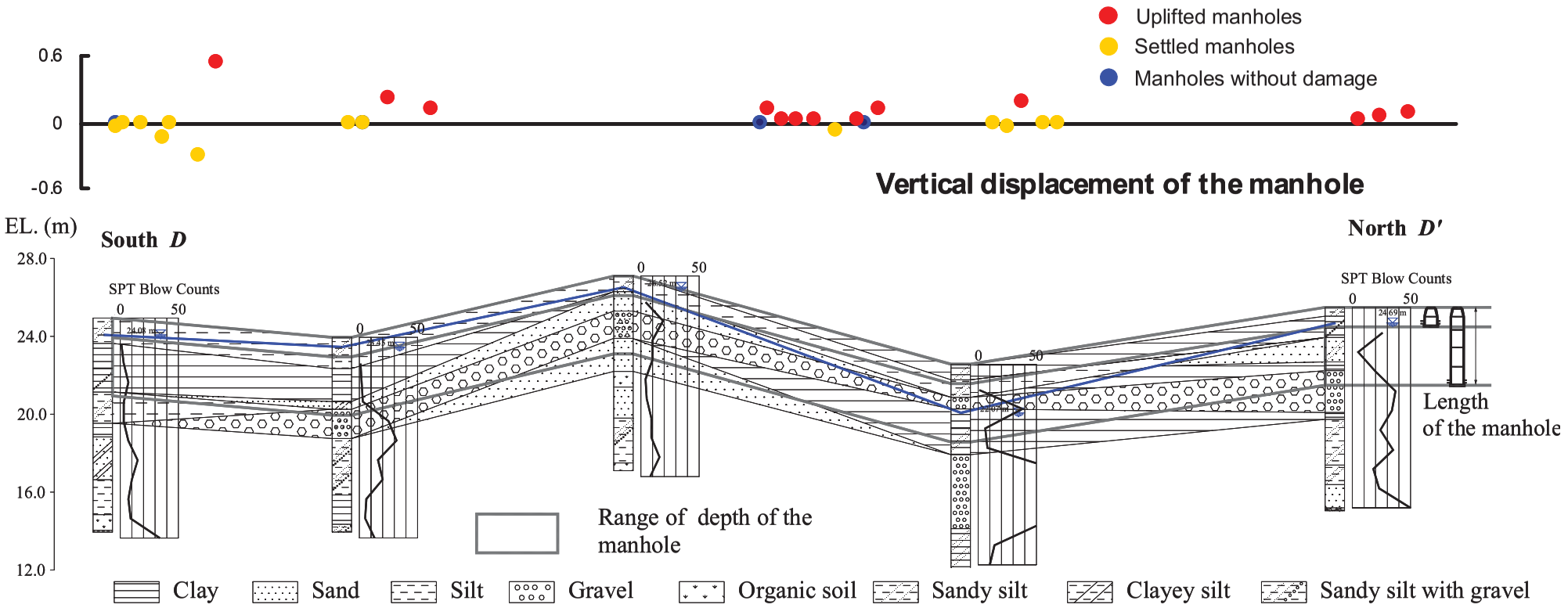

Fig. 5.15 Relationship between vertical displacement of the manhole and SPT borehole logs (*D-D'*).

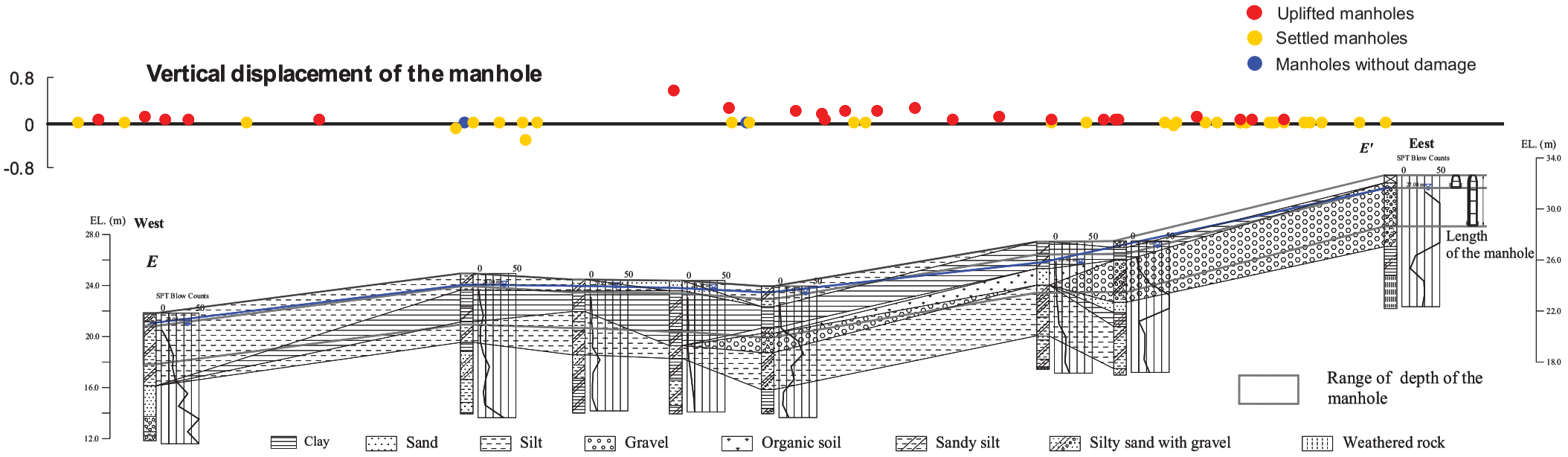

Fig. 5.16 Relationship between vertical displacement of the manhole and SPT borehole logs (*E-E'*).

5.4 Application of the simplified and detailed method to the case history in Nagaoka city

From the results of comparisons between damaged manholes and the SPT borehole logs, the ground water table had a large influence on the uplift displacement of the manholes as a primary factor. Using the relationship between the uplift of manholes and the ground water table, methods for estimation of uplift displacement proposed in this study are introduced to the case history in Nagaoka city and the application of the methods is verified. Data of manhole uplifts were obtained from the field investigation and the ground water table was obtained through the interpolation of the ground water table of the SPT borehole logs.

In order to verify the application of the simplified method, the method is applied to the case history in Nagaoka city during 2004 Niigata-ken Chuetsu, Japan, earthquake. Table 5.3 shows the parameters used as input data of the proposed method. Unit weight of the manhole is calculated targeting the standard No. 1 Manhole (JSWA 2001). Manhole length varies from 1 m to 4 m depending on the ground elevation and the required slope of pipelines for drainage. For comparison between the uplift displacement of manholes observed in Nagaoka city and predicted displacement, the following assumptions are made. (a) In general, the cross-sectional area of a trench is more or less in a limited range, a $\approx 2.0 \times d$ to minimize the working space in the trench for reducing construction costs. (2) Backfill was completely liquefied ($r_u = 1$). (3) Friction angle of a manhole and non-liquefiable backfill, δ, is 10 deg.. (4) Coefficient of lateral earth pressure, K, is 0.5.

Figure 5.17 shows uplift displacements predicted by the simplified method and those observed in Nagaoka city during the 2004 Niigata Chuetsu earthquake (Δf is the uplift displacement of the manhole, h is the manhole length, and h_w is the depth of ground water

table). To calculate the uplift displacement, some manholes whose length was unknown were excluded. Total number of manholes was 197 and the predicted uplift displacement was calculated for each observed manhole. As shown in Fig. 5.17, black circles indicate observed manhole uplifts and blue triangles indicate predicted ones. The observed uplift displacement is under the predicted ones. It indicates that the proposed method is reasonable to estimate the maximum uplift displacement considering that all the data are plotted within the predicted boundary of the maximum uplift.

In the simplified method, influences on uplift behavior by magnitude of earthquakes and the relative density of backfill could not be considered. However, they have large influence on the uplift behavior as well as liquefaction of the ground. In Chapter 2, the increase in excess pore water pressure ratio was small when the relative density of backfill is high and amplitude of the input acceleration is small. On basis of this, uplift displacements for a manhole of a 2 m length considering various excess pore water pressure ratios are plotted to consider their effects for uplift behavior as indicated by thick line (r_u = 1.0), dotted line (r_u = 0.7) and thin line (r_u = 0.5) in Fig. 5.17. Although, the predicted uplift displacement can not precisely reflect the effects for amplitude of the input acceleration or the relative density of backfill, tendency of the uplift displacement can be represented. As shown in Fig. 5.17, the predicted uplift displacements show a tendency to decrease with low excess pore water pressure ratio.

A detailed method by numerical analysis can not be carried out for the Nagaoka case history because the magnitude of manhole uplifts in Nagaoka was widely distributed and soil condition of backfill, which is a major cause for the uplift phenomenon of manholes, could not be investigated before the earthquakes. Thus, the results of Chapter 4 which were consistent with centrifuge test data are applied to Nagaoka case history. Also, the uplift displacements predicted by the numerical analysis when ground water table coincides with the ground surface

Table 5.3 Parameters for the backfill, manhole and trench used in Nagaoka case histories.

Max. void ratio	e_{max}	0.99	
Min. void ratio	e_{min}	0.59	
Density	G_s	2.67	
Unit weight of non-saturated backfill	γ_t	14.1	kN/m^3
Unit weight of saturated backfill	γ_{sat}	18.6	kN/m^3
Unit weight of reinfored concrete	γ_c	23.5	kN/m^3
Diameter of a manhole	d	1.05	m
Trench width	a	$d\times2$	m
Excess pore water pressure ratio	r_u	1	
Friction angle of a manhole and Non-liquefiable backfill	δ	10	deg.
Coefficient of lateral earth pressure	K	0.5	

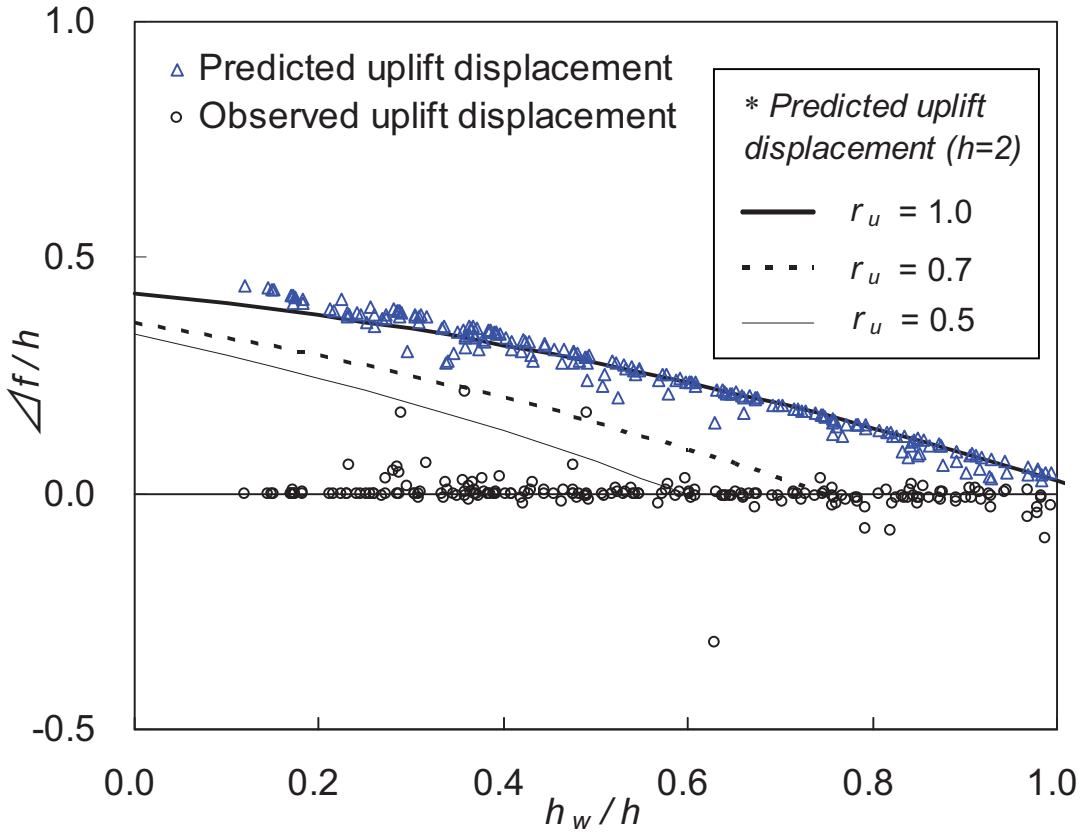

Fig. 5.17 Uplift displacements predicted by the simplified method and observed in Nagaoka city during the 2004 Niigata-ken Chuetsu, Japan, Earthquake.

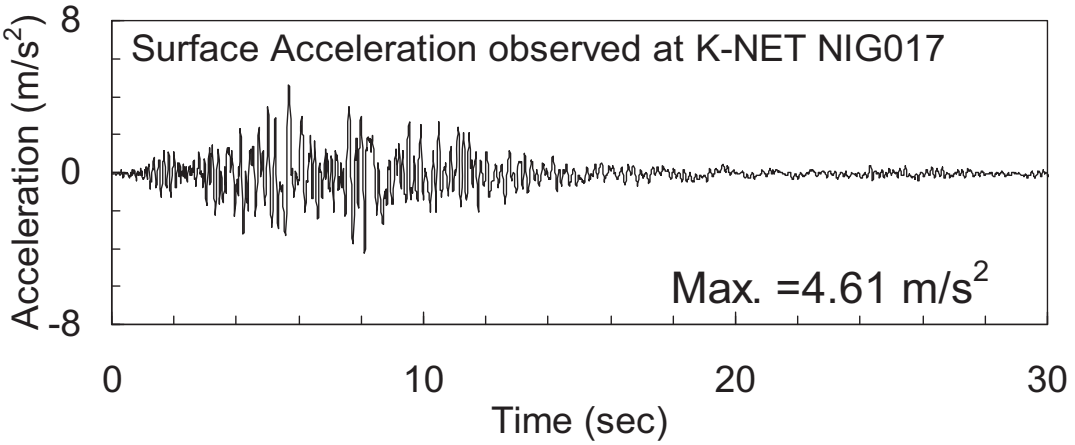

Fig. 5.18 Surface acceleration observed at the K-NET (NIG017) station in Nagaoka city.

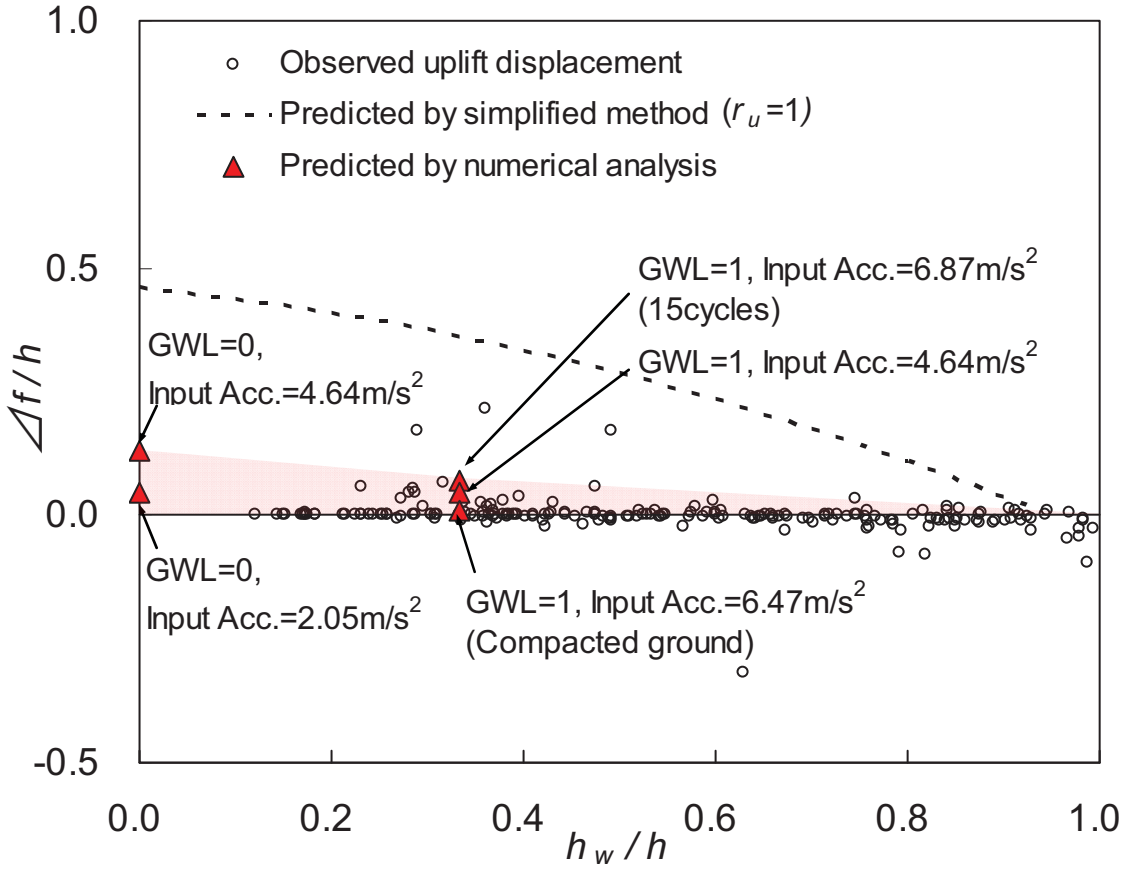

Fig. 5.19 Uplift displacements predicted by the numerical analysis as detailed method and observed in Nagaoka city during the 2004 Niigata-ken, Chuetsu, Japan, earthquake.

and amplitude of the input acceleration is 4.64 m/s^2 are added based on the surface acceleration (PGA=4.61 m/s^2) [Fig. 5.18] observed at the K-NET (NIG017) station in Nagaoka city. As shown in Fig. 5.19, the uplift displacements predicted by the numerical analysis are changing according to amplitude of input acceleration, number of load cycles, soil conditions of backfill and the depth of the ground water table. The relatively low magnitude of manhole uplift in Nagaoka is plotted in the range of the predicted boundary by numerical analysis. This fact suggests that the numerical analysis as detailed method can be applied to estimate for low magnitude of the manhole uplifts with the various soil/structure/shake conditions as well as the transient behaviors of the manholes during shaking. High magnitude manhole uplifts is plotted within the predicted boundary by the simplified method.

5.5 Amount of uplift of manholes vs. the native subsoil material as a secondary factor near the ground surface

5.5.1 Correlation study

To evaluate the spatial correlation with factors affecting the uplift behavior of manholes, correlation analysis is conducted. The correlation analysis is mainly conducted for secondary factors including the depth of the ground water table which are properties of the native subsoil near the ground surface such as SPT blow counts, thickness of clay layer, and thickness of surface soil (embankment and reclamation).

IDW (Inverse Distance Weighted) method was used for an interpolation. Total (cumulative) thickness of clay layers near the surface shallower than 5 m, and the average SPT blow counts of sand layers near the surface shallower than 5 m, and surface fill thickness are to be qualitatively investigated through the contour maps shown in Fig. 5.20. Figure 5.20(a) to (e) is

for Zone 1 and Fig. 5.20(f) to (j) is for Zone 2. Location of manholes is indicated by pin markers in Fig. 5.20(a) and (f), and that of the SPT boreholes is indicated by triangle markers in Fig. 5.20(b) to (e) and (g) to (j). The contour map in Fig. 5.20(a) and (f) is the normalized uplift of manholes relative to the manhole length for Zone 1 and Zone 2, respectively, to reduce the factor for which the length of the manholes is affecting the uplift.

The area with a relatively shallow ground water table is located at the place where the maximum uplift of manhole are observed as shown in Fig. 5.20(b) of Zone 1 and (g) of Zone 2. However, the ground water table is located at the depth of 2 m from the ground surface in a western side where a relatively large uplift (10% for manhole length) is observed as shown in Fig. 5.20(b). In Fig. 5.20(d) and (h), total thickness of clay layers located at a large magnitude of manhole uplift is about 1.5 m to 3 m. In Fig. 5.20(e) and (i), manholes are largely uplifted in the sandy layer with low SPT blow counts of less than 10 and are also largely uplifted in the native ground with fill thickness of 0.6 to 1 m in Fig. 5.20(e). However, a large magnitude of the uplift is observed in the native ground with fill thickness of 0.1 m in Fig. 5.20(j). In some parts, manholes surrounding the native ground with a shallow ground water table, thick clay layer, low SPT blow counts and thick fill layer are not sure to uplift. Since both manholes and boreholes are not distributed uniformly, correlation analysis may be erroneous in some part.

To investigate the relationship between the uplift displacement and soil properties of the native ground, clearly, factors affecting the uplift displacement are extracted from the contour map as shown in Fig. 5.20. Uplift displacements of manholes observed in Nagaoka are used. The relationships are compared as shown in Fig. 5.21. Many manholes suffered no damage, sinkage, or uplift, and the correlations between uplift displacement and factors affecting the uplift are not found in Fig. 5.21. In the case of the thickness of the clay layer, the maximum uplift was observed at the location with thickness of 0.8 m (ground water depth coincides with

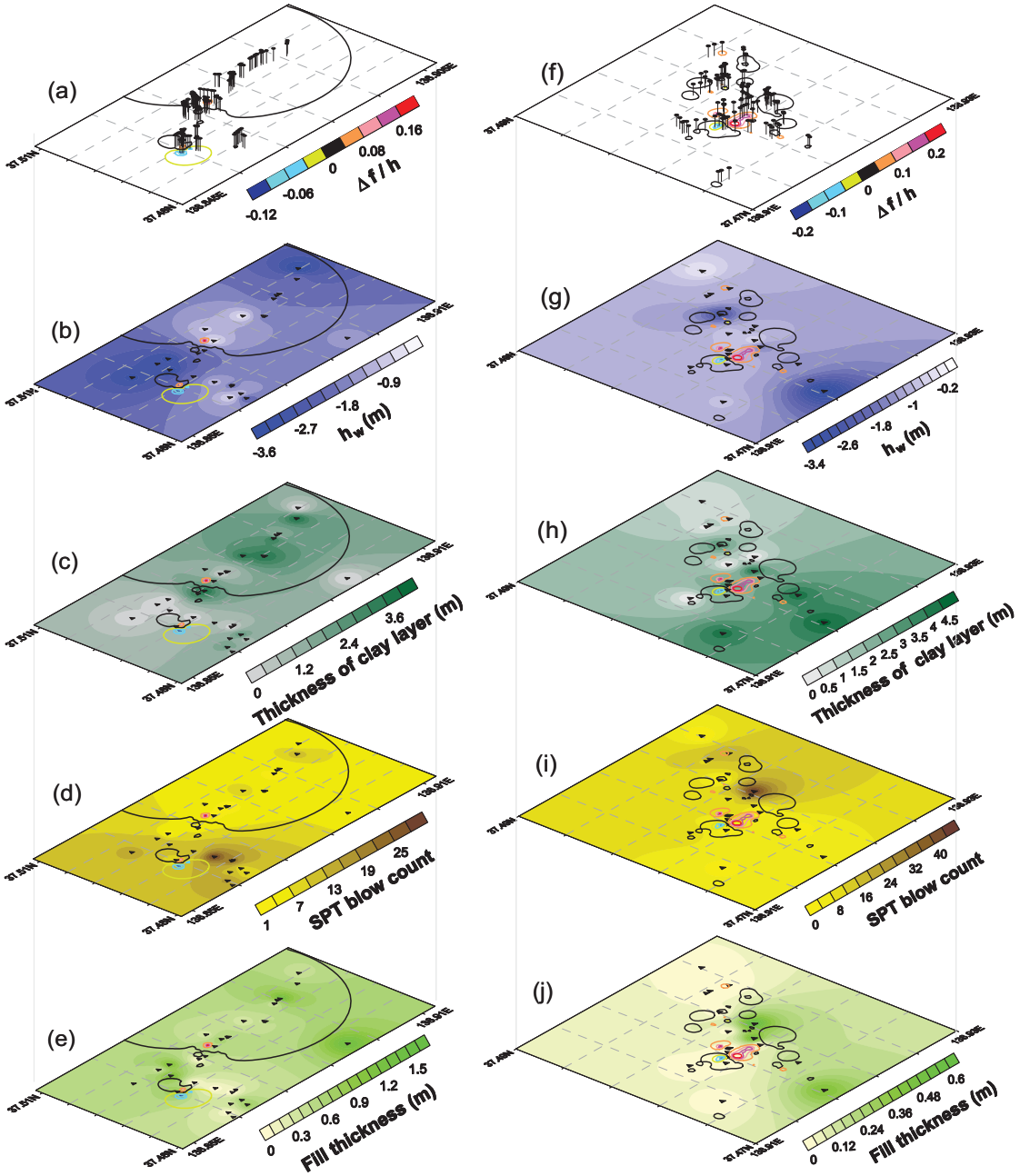

Fig. 5.20 Contour maps of manhole uplift (a) and (f), Ground water depth (b) and (g), Total thickness of clay layer shallower than 5 meters from the ground surface (c) and (h), SPT blow counts of sand layers shallower than 5 meters from the ground surface (d) and (i), and Fill thickness (e) and (j). Pin markers in (a) and (f) indicate manhole location, and triangle markers in (a) to (j) indicate borehole locations. (a)~(e) are for Zone 1 and (f)~(j) are for Zone2.

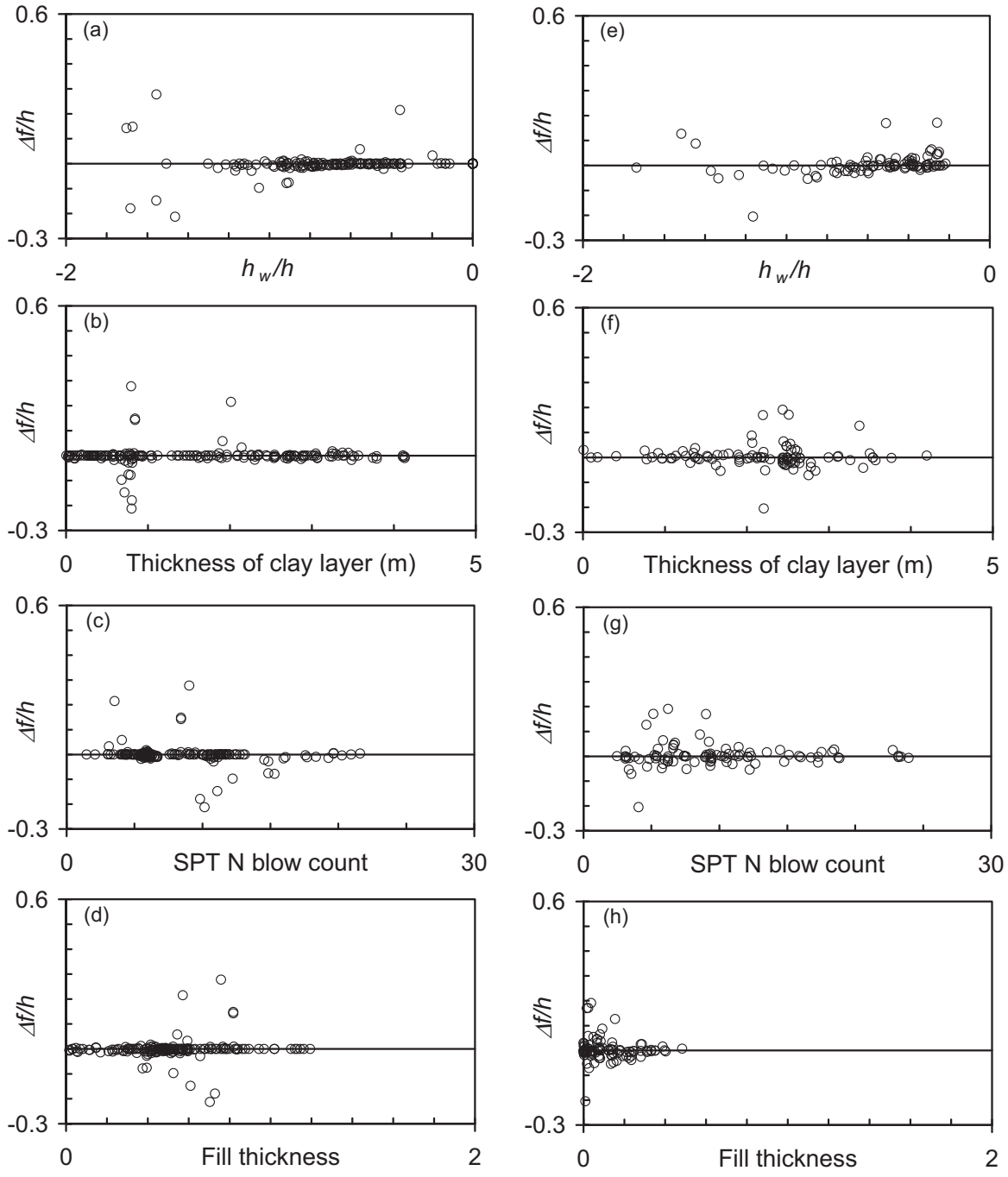

Fig. 5.21 Relationship between uplift displacement and factors of native ground extracted from contour map; Ground water depth (a) and (e), Total thickness of clay layer shallower than 5 meters from the ground surface (b) and (f), SPT blow counts of sand layers shallower than 5 meters from the ground surface (c) and (g), and Fill thickness (d) and (h). (a) ~ (d) are for Zone 1 and (e) ~ (h) are for Zone2.

the depth of 0.3 m from the ground surface) in Fig. 5.21(a). In the same uplift level, 20% of manholes were settled or was not uplift. Namely, the magnitude of uplift is changing in the same level for each factor as shown in Fig. 5.21. The reason is that the factors are related to the uplift displacement multiply. Therefore, regression analysis is required to estimate the correlation in combination with factors affecting the uplift.

Figure 5.22 shows the result of regression analysis. Vertical axis calculated uplift displacements by the regression analysis and horizontal axis by the observed ones. Discrepancies are still observed between the predicted and observed. For example, when the observed uplift displacement is 0.43m, corresponding predicted uplift is 0.14m in Zone 1. In Zone 2, when the observed uplift displacement is 0.53m, corresponding predicted uplift is 0.18m.

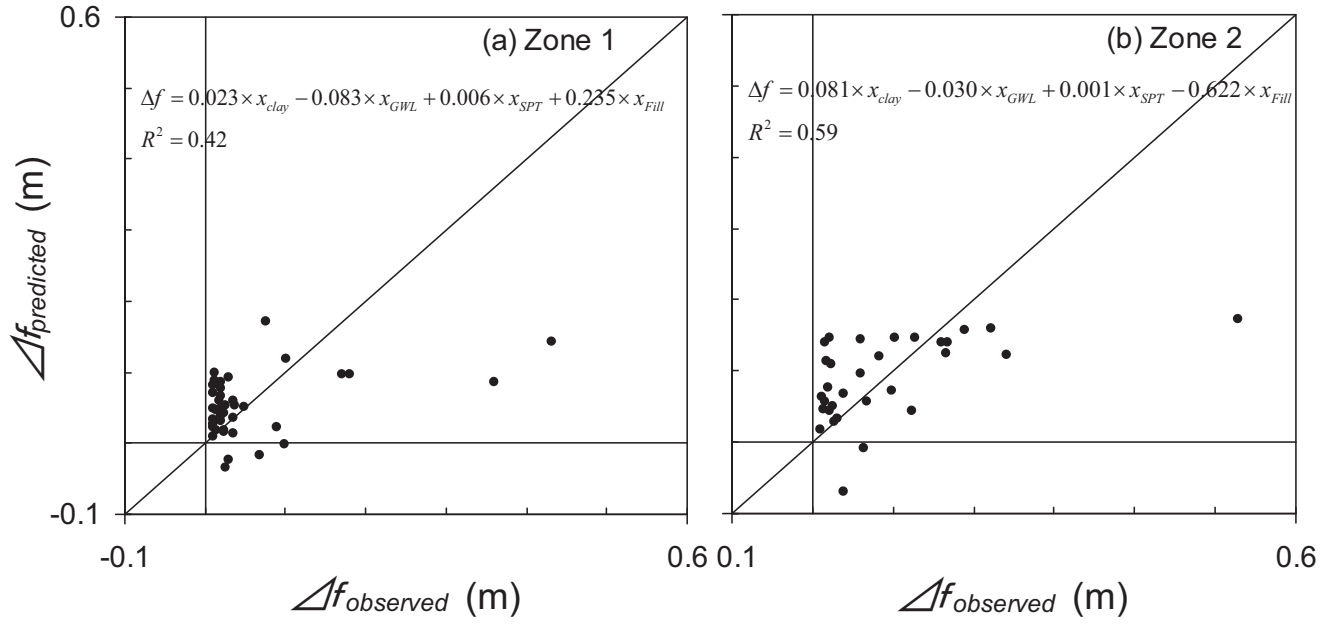

Fig. 5.22 Predicted uplift by regression analysis and observed uplift in study area; (a) Zone 1, (b) Zone 2.

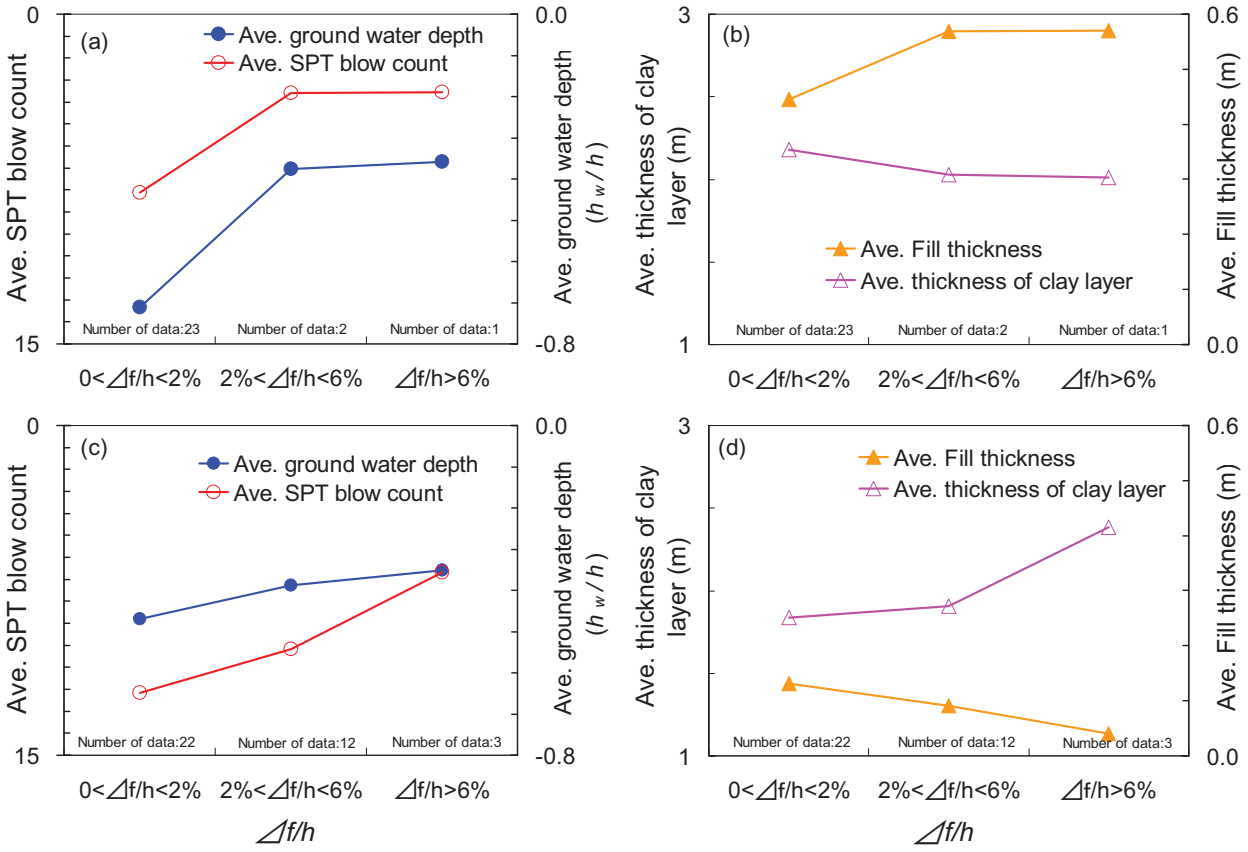

Fig. 5.23 Average value of each factor corresponding to the uplift displacement; (a) and (b) are in Zone 1. (c) and (d) are in Zone 2.

Figure 5.23 shows the average of each factor corresponding to the uplift displacement. Normalized uplift displacements were divided into $0<\triangle f/h<2\%$, $2<\triangle f/h<6\%$ and $6\%<\triangle f/h$. Number of data corresponding to the intervals is 23, 2 and 1 for Zone 1, and 22, 12, 3 for Zone 2. In Fig. 5.23, the uplift displacement shows a tendency to increase in the native ground with shallow ground water table and low SPT blow count for Zone 1 and Zone 2. The uplift displacement is increased in the native ground with a thick clay layer for Zone 2, however, does not change with thickness of the clay layer in Zone 1. In Zone 1, the relationship between the uplift displacement and thickness of the clay layer is not clearly derived because sandy

material is more dominant than clayey material. The relationships found between the uplift displacements and associated parameters (ground water table, SPT blow count and thickness of clay layer) agree with those found in the centrifuge model tests. The uplift displacement is increased in the native ground with the thick surface soil in Zone 1. However, a contrary trend is shown in Zone 2, because the surface soil is rarely subsisted in Zone 2.

5.6 Summary

To verify the application of the methods for estimation of uplift displacement of a manhole in liquefied ground, the case history in Nagaoka city during the 2004 Niigata-ken Chuetsu, Japan, earthquake was used. In accordance with this, relationships between the uplift displacements and some factors which may affect the uplift behavior of the manholes field survey were also investigated. Factors considered in the investigation are the depth of the ground water table as a primary factor and the native subsoil material near the ground surface such as SPT blow counts, thickness of clay layer, and thickness of surface soil (embankment and reclamation) as a secondary factor.

The study area is located about 20 km north of the epicenter. Length of manhole is in the range of 1 m ~ 4 m. Two areas were selected as the study area. One (Zone 1) is located near the Shinano River, which caused tremendous damage to many types of structures and the ground due to liquefaction in Niigata city in the 1964 Niigata earthquake. The other (Zone 2) is located at the foot of a mountain as far as 4 km east of Zone 1. The field investigation data shows pipeline damage as well as damage on manholes. From the field investigation data of damaged sewage pipes and manholes collected after the earthquake by the Nagaoka city government, the maximum uplift of the manhole was about 0.432 m and 0.528 m, and the pipe was about 0.478 m and 1.065 m in Zone 1 and 2, respectively. The maximum uplift occurred in the native

ground with a shallow ground water table as a primary factor, which has a large influence on manhole uplift behavior. The ground water table where the maximum uplifts were observed is located at the depth of 0.36 m and 0.86 m from the ground surface in Zone 1 and Zone 2, respectively.

Simplified and detailed methods for estimation of the uplift displacement of a manhole proposed in this study were applied to the relationship between the uplift of manholes and the depth of the ground water table and the application of the methods was verified. Data of manhole uplift were obtained from the field investigation and the depth of the ground water table was obtained through the interpolation of ground water table of the SPT borehole logs. First, to verify the application of the simplified method, the method was introduced to Nagaoka case history. The results show observed uplift displacement was plotted under a predicted boundary by the simplified method. It indicates that the simplified method is reasonable to estimate the maximum uplift displacement. Also, the increase in excess pore water pressure ratio was small when the relative density of backfill is high and amplitude of input acceleration is small as in Chapter 2. On the basis of this, uplift displacements for a manhole of 2 m length considering various excess pore water pressure ratios (r_u = 1.0, 0.7 and 0.5) were plotted to consider their effects on uplift behavior. The uplift displacements predicted by the simplified method show a tendency to decrease with low excess pore water pressure ratio.

Results of the numerical analysis as a detailed method in Chapter 4 were compared with the Nagaoka case history. Low magnitude of manhole uplift in Nagaoka was in the range of the predicted boundary by numerical analysis. This fact suggests that the numerical analysis as detailed method can be applied to predict for low magnitude of manhole uplift with the various soil/structure/shake conditions.

To evaluate the spatial correlation with factors, correlation analysis was conducted. The

correlation analysis was mainly conducted for secondary factors, which are SPT blow counts, thickness of clay layer, and thickness of surface soil, and also for ground water table as a primary factor. The relationships with the secondary factors were derived as follows:

(1) The uplift displacement showed a tendency to increase with low SPT blow count in Zone 1 and 2. Especially, the correlation with SPT blow count was excellent in Zone 1 which is located near the Shinano River.

(2) The uplift displacement was increased in the native ground with a thick clay layer for Zone 1 and Zone 2 in detailed cross sections of damaged sewerage pipe lines with a borehole log. However, the relationship of the uplift displacement and the thickness of the clay layer were not observed in Zone 1 through the results of the regression analysis. The reason is that sandy material was more dominant than clayey material in Zone 1. Especially, the correlation with the thickness of clay layer was excellent in Zone 2 which is located at the foot of a mountain.

(3) The uplift displacement was increased in the native ground with thick surface soil in Zone 1. However, a contrary trend was shown in Zone 2, because surface soil is subsisted rarely in Zone 2.

The uplift displacement was increased when the ground water, as a primary factor, coincided with a shallow location from the ground surface in Zone 1 and Zone 2.The relationships found between the uplift displacements and associated parameters (loose ground, clay material and the depth of ground water table) significantly agree with those found in the centrifuge model tests of Chapter 2.

6. Mitigation measures against uplift of buried geotechnical structures

6.1 Introduction

In previous chapters, the increase of excess pore water pressure in liquefied ground during earthquakes was revealed to be one of the important factors affecting the uplift behavior of a manhole through a series of centrifuge model tests. Also, the uplift displacement could be estimated by the simplified method considering the excess pore water pressure ratio as a component of uplift force acting on a manhole. On the basis of these, it is found that reduction of excess pore water pressure is the key to reduce the uplift displacement of a manhole. In this chapter, practical applications are discussed based on the results obtained in the present research.

First, mitigation measures against uplift behavior are discussed. Numbers of mitigation measures against manhole uplift for newly constructed ones have been proposed and already implemented practically (Ishinabe et al., 1999; Yasuda et al., 2001; Yasuda, 2003; Yoshida et al, 2006; Matsushima el at., 2007; Kiku et al., 2007) and those mitigation measures proved to be effective after the 2007 Niigata-ken Chuetsu-oki, Japan, earthquake (Morii and Nishino, 2008; JGS, 2009). However, development of mitigation measures against uplift for existing manholes is still remaining and challenging issue.

In this chapter, two mitigation methods are proposed targeting existing manholes as follows: (1) mitigation method which can reduce excess pore water pressure in liquefied ground (2) compaction of backfill which can control increase of excess pore water pressure. The effectiveness of the devices is investigated and validated through the centrifuge studies.

Finally, the performance-based design procedure with the simplified method is proposed as an application derived from this research activities.

6.2 Mitigation measures against uplift of a buried structure

6.2.1 Mitigation measure by reduction of excess pore water pressure

The mitigation measure which can dissipate the pressurized water caused by liquefaction into the manhole (Konishi et al. 2008) is proposed and the effectiveness is verified through centrifuge model tests. Figure 6.1 shows the schematic view of the mechanism for the mitigation measure. The mitigation device consists of a filtering net which is installed at the connection of a sewerage pipe and manhole, and a pipe is installed with the filtering net in the manhole as shown in Fig. 6.1 (Konishi et al., 2008). Before earthquakes, the water level in the pipe connected to the filtering net is the same with the ground water table around the manhole because the filtering net is connected to the pipe as shown in Fig. 6.1(a). However, during

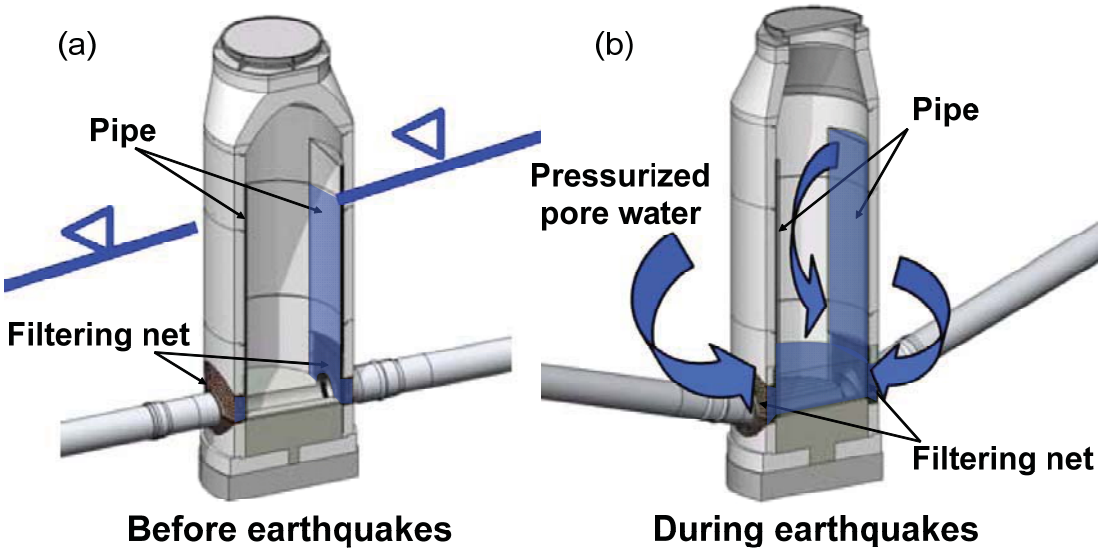

Fig. 6.1 Schematic view for a countermeasure (Konishi et al., 2008): (a) before earthquakes, (b) after earthquakes.

earthquakes, excess pore water pressure in the ground around the manhole gradually increases, and the pressurized pore water is guided into the manhole through the filtering net and pipe due to a pressure difference between the outside and inside of the manhole as shown in Fig. 6.1(b). Therefore, the uplift of the manhole is mitigated because of a decreasing buoyant force acting on the manhole by dissipating excess pore water pressure into the manhole and increasing weight by added water in the manhole.

The mitigation measure was used in the centrifuge model tests as Model No. 2 and Model No. 3. Model No. 2 [Fig. 6.2(a) and (c)] has the filtering net with a diameter of 10 mm, while Model No. 3 [Fig. 6.2(b) and (d)] has that of 15 mm in model scale. The length of the pipe connected with the filtering net in the manhole is 100 mm in model scale [Fig. 6.2(a), (b) and

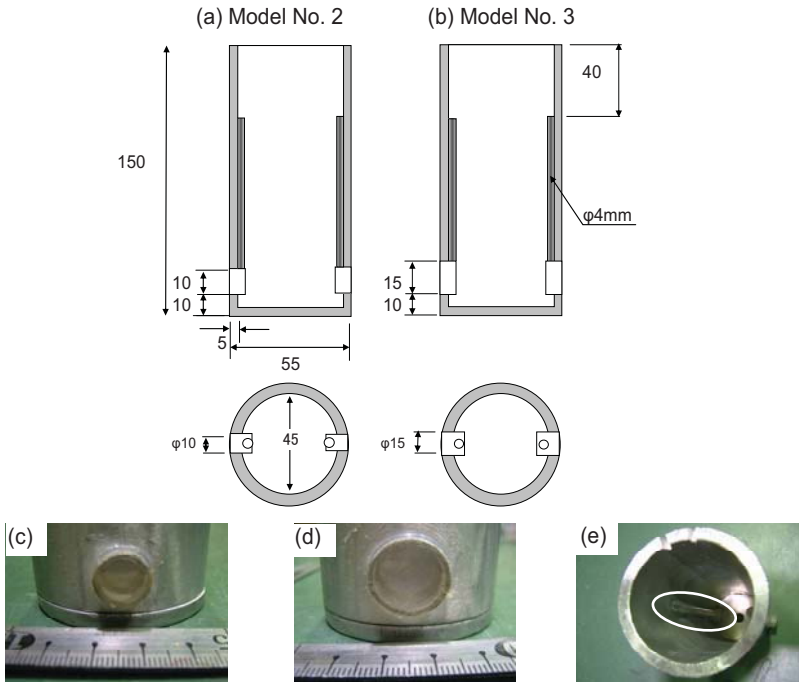

Fig. 6.2 Model manhole and mitigation measures used in the tests; Model No. 2 with filtering net of 10 mm (a), Model No. 3 with filtering net of 15 mm (b), filtering nets installed Manhole No. 2 (c) and Manhole No. 3 (d) and pipes attached to a device to guide pressurized pore water into the manhole during shaking (e).

(e)]. To verify the effects of the measure, the tests were conducted with a deeper ground water depth of 1 m so that the pore water does not flow into the manhole before shaking. A mesh (75 μm) which made from stainless was attached at the filtering net to prevent sandy soil incoming into the manhole as shown in Fig. 6.2(c) and (d).

The mitigation method has a fatal fault in that it is hard to dissipate the pressurized pore water into the manhole when the manhole starts to uplift because the pipe in the manhole is uplifted with the manhole. Therefore, another device is proposed to overcome this limitation. The device is installed between a manhole and the native ground by beam structure as shown in Fig. 6.3. The device can help accelerate the dissipation of the excess pore water pressure into the manhole during the manhole uplift by delaying manhole uplift due to the increase in the resistance force.

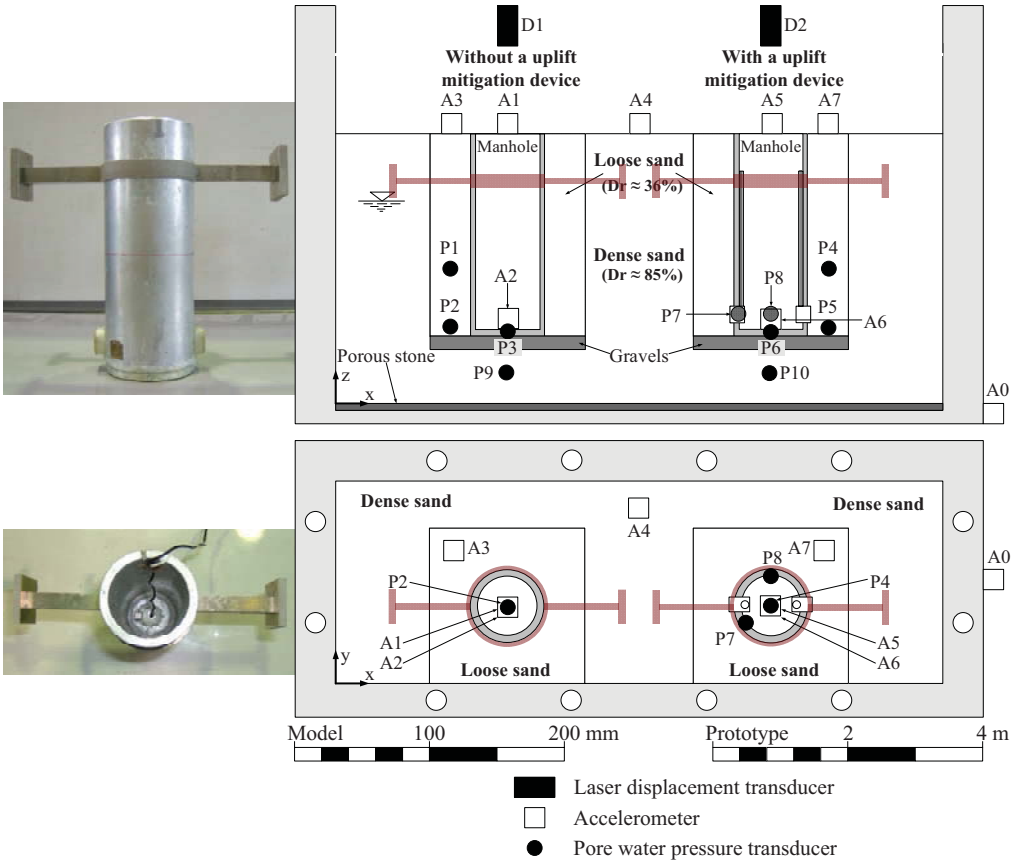

Fig. 6.3 Centrifuge model test set-up to increase the resistance force (CS22).

6.2.2 Mitigation measure by compaction of backfill

Compaction of backfill is the most effective mitigation measure against the uplift behavior of a manhole as well as liquefaction of the ground during earthquakes. However, the backfill in the trench for existing manholes is difficult to be compacted because pipes connected to the manhole may take some damages during soil compaction. A new method which can compact backfill without damaging connected pipes is also proposed as shown in Fig. 6.4.

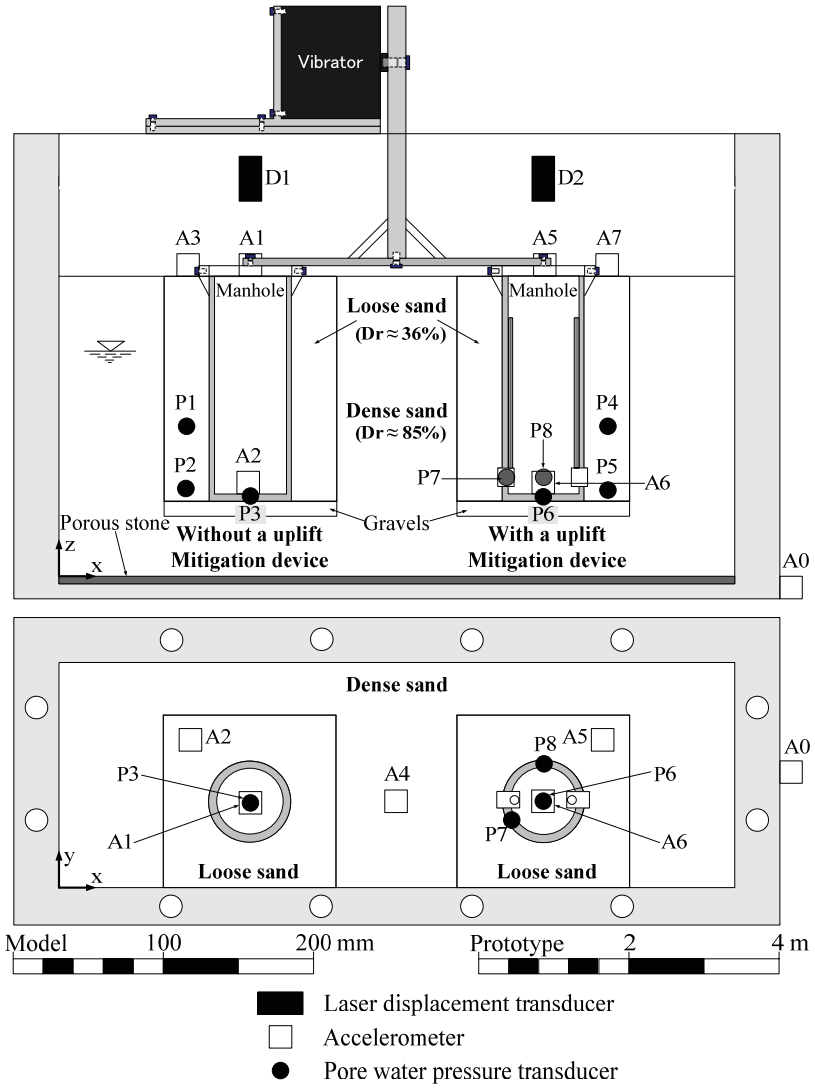

Fig. 6.4 Centrifuge model test set-up to compact backfill

Figure 6.4 shows the schematic view which can illustrate the mechanism for compaction of backfill. As shown Fig. 6.4, a vibrator is connected to the manholes by beam structures and the backfill is compacted by shaking the manholes. Figure 6.5 shows model manholes installed with the vibrator for compaction of backfill. If the uplift of the manhole could not be mitigated completely, the filtering net which is installed as a part of the connection of a sewerage pipe and manhole can be used together as a mitigation measure against uplift [Fig. 6.4: Right].

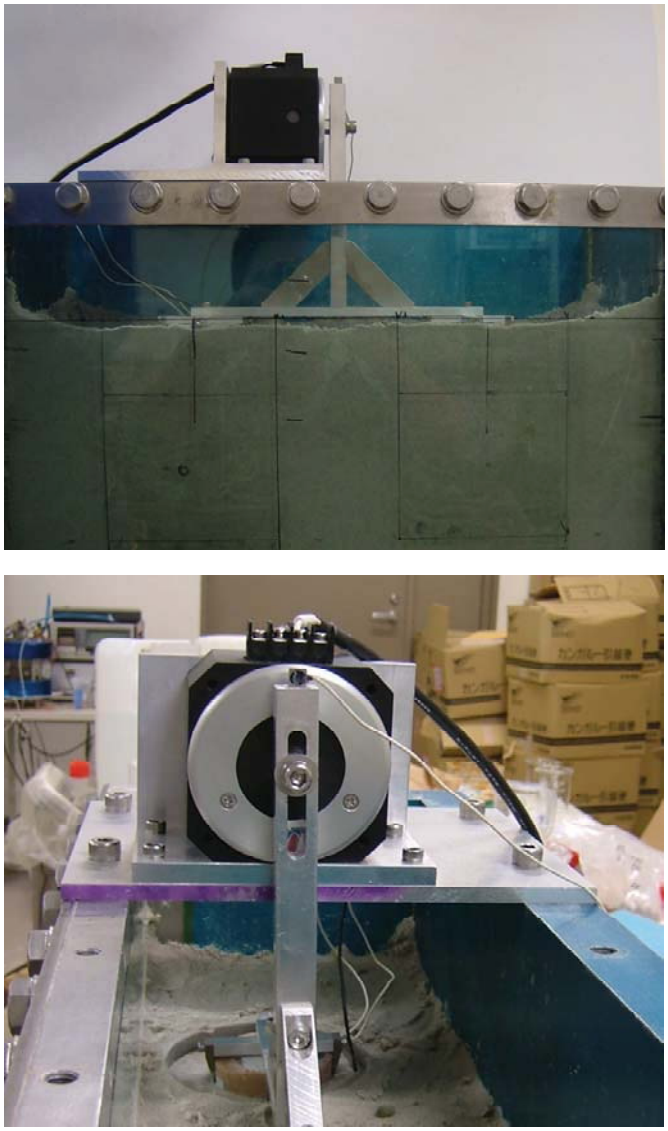

Fig. 6.5 Model manholes installed device for compaction of backfill

Figure 6.6 shows effects of the compaction by shaking the manhole. The relative density of backfill was recalculated through settled volume of the trench after shaking the manhole. Figure 6.6(a) indicates the relationship between the settlement of backfill and the relative density of backfill (Silica sand) used in centrifuge model tests. The relative density shows a tendency to increase with the settlement of backfill. The relative density is increased from 36% to 72% due to shaking the manhole for one minute in Fig. 6.6(b). The effectiveness of compacted model manhole and ground is verified through a centrifuge model test.

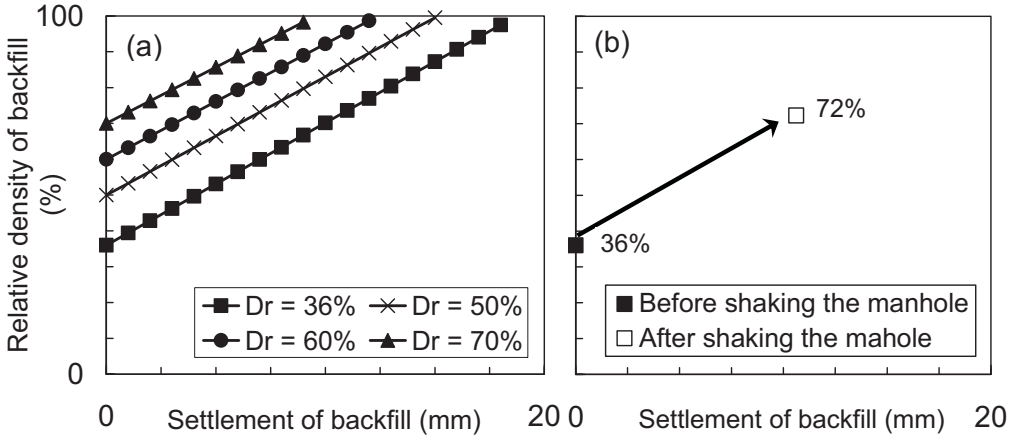

Fig. 6.6 Compaction of backfill by shaking the manhole

6.2.3 Results of the tests

The centrifuge model tests in Chapter 2 were conducted for model manholes with/without a mitigation measure against the uplift to verify the effectiveness of the mitigation methods against the uplift behavior of a manhole. Figure 6.7 shows the results of the centrifuge model tests. CS2 and CS3 are test results for comparison between Model No. 2 (CS2) and Model No. 3 (CS3). CS21 is test result for Model No. 1 and Model No. 3 introducing the mitigation measure as shown in Fig. 6.3. CS22 is test result for compacted backfill. The maximum input accelerations for selected tests are in the range of 6.62 ~ 7.25 m/s^2 (Table 2.3 of Chapter 2). For

convenience, effect for amplitude of input motion is neglected because amplitude of input acceleration for all tests is almost at the same level.

In CS2 and CS3 of Fig. 6.7, uplift displacements for Model No. 1 (no mitigation device) are in the same level (0.95 m). The uplift displacement for Model No. 2 of CS2 (0.92 m) is larger than that of Model No. 3 of CS3 (0.77 m). It indicates that mitigation effects of a filtering net with large size (30 cm) is larger than that of small size (20 cm). However, reduction level of uplift displacement is small because the pipe in the manhole is uplifted with the manhole. Namely, it is hard to dissipate the pressurized pore water into the manhole when manholes are uplifted rapidly. In CS21 of Fig. 6.7, the uplift displacement is about 0.25 m for Model No. 3 and is 0.70 m for Model No. 1(no mitigation device). This fact indicates that the device in Fig. 6.3 is effective at reducing the uplift displacement as well as accelerate the dissipation of the excess pore water pressure into the manhole (Model No. 3) during the manhole uplift. In CS22, the uplift displacement is about 0.13 m for with/without mitigation measure.

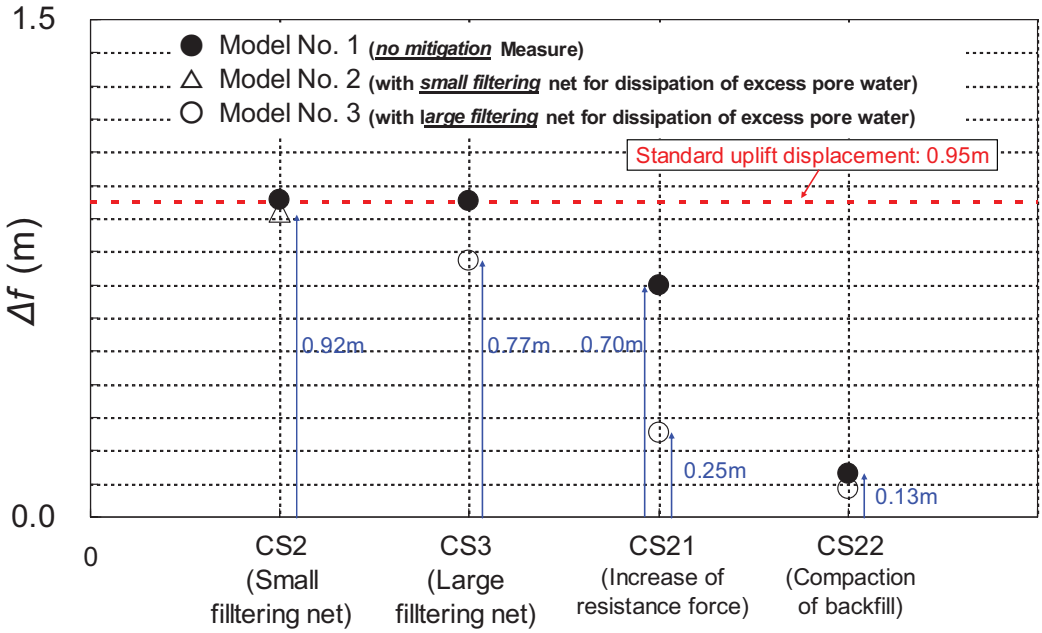

Fig. 6.7 Results of centrifuge model test for mitigation measures.

As shown in Figs. 6.3 and 6.4, P7 installed beside the filtering net could be compared with P8 installed perpendicular to the filtering net at the back of the manhole at the same depth to evaluate the effects of the mitigation device of Model No. 3. While the pore water pressure of P8 had a fluctuation under a spike, the spike was gone in P7 as shown in Fig. 6.8. The amplitude of P8 is also lager than that of P7. These inclinations might be effects by the filtering net during dissipating the pore water into the manhole.

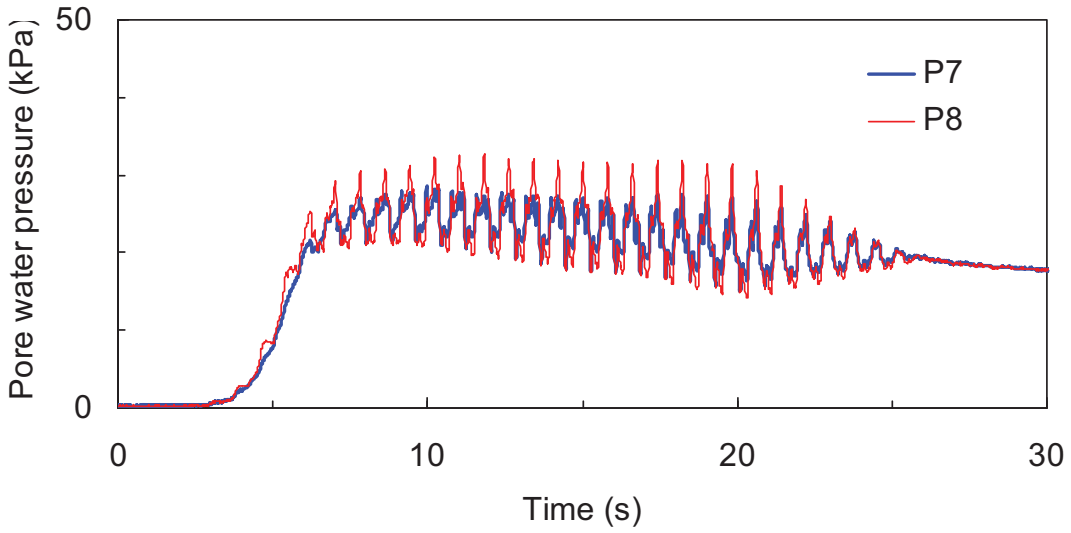

Fig. 6.8 Excess pore water pressure measured in CS21 to evaluate effectiveness of filtering net.

Figure 6.9 shows the dissipated pore water in the manhole after strong shaking. A lot of pore water (depth of 82 cm in proto scale) was guided into the manhole for CS21, in which the filtering net for dissipation of pore water was to be effective due to the increase in the resistance force by the beam structure connected to the manhole and native ground. On the other hand, a little of pore water (depth of 12 cm in proto scale) was guided in Model No. 3 of CS3 as shown in Fig. 6.9(a) and (c), in which the filtering net for dissipation of pore water was not to be effective due to the large magnitude of manhole uplift.

(a) (b) (c)

Fig. 6.9 Pore water dissipated in the manhole: (a) Model No. 3 for CS21, (a) Model No. 1 for CS21, (a) Model No. 3 for CS3

6.3 Application to the seismic design against uplift of a buried structure

Large magnitude of uplift displacement of the manhole is depending on the increase of excess pore water pressure in liquefied ground during earthquakes. The simplified method which can consider the increase of excess pore water pressure as term of r_u can be applied to the seismic design to predict of the uplift displacement of geotechnical buried structures. Also, it is difficult to judge whether a large magnitude of the manhole uplift is triggered or not through the safety factor (Koseki, 1997a) which has been recommended for use in present design practice (JRA, 1986). The liquefaction resistance ratio, F_L, is defined as the ratio between the cyclic shear stress required to cause liquefaction and the equivalent cyclic shear stress induced by earthquakes (Kramer, 1996). In practice, it has been widely used for evaluation of initiation of liquefaction. The relationship between the liquefaction resistance ratio and the excess pore pressure ratio is proposed as follows:

$$r_u = \begin{cases} F_L^{-p} & (F_L \geq 1) \\ 1 & (F_L < 1) \end{cases} \qquad (1)$$

where p is the parameter representing the characteristics of excess pore water pressure generation. The parameter p in Eq. (1) is assigned to be 7 in Design Manual for Common Utility Ducts (Japan Road Association, 1986) based on cyclic undrained triaxial tests on reconstituted samples of relatively clean sands. Fig. 6.10 illustrates the relationship expressed by Eq. (1). By substituting Eq. (1) in Eqs. (9) and (10) of Chapter 3, the estimated uplift displacement, settlement of backfill, and total displacement can be computed as a function of the liquefaction resistance ratio. Here, the ratio is assumed to be averaged over the depth of the trench. Estimated displacements are plotted against liquefaction resistance ratio in Fig. 6.11.

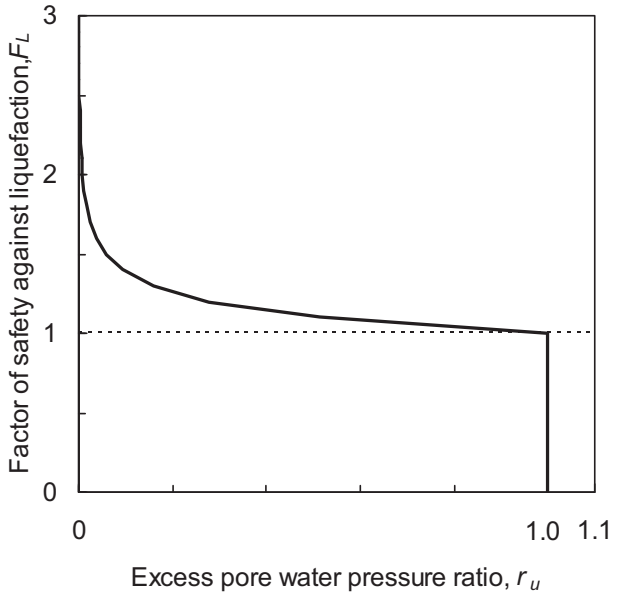

Fig. 6.10 Relationship of liquefaction resistance ratio (F_L) and excess pore pressure ratio (r_u) (JRA, 1986).

As shown in Fig. 6.11(a), increase in the liquefaction resistance ratio greatly reduces the uplift displacement. When the thickness of the non-liquefiable layer, h_w, is small, i.e., the ground water table is located close to the surface, the uplift displacement is large but the rate of reduction is much higher with an increase in the liquefaction resistance ratio [Fig. 6.11(a)]. The

tendency is showing for the settlement of backfill in Fig. 6.11(b).

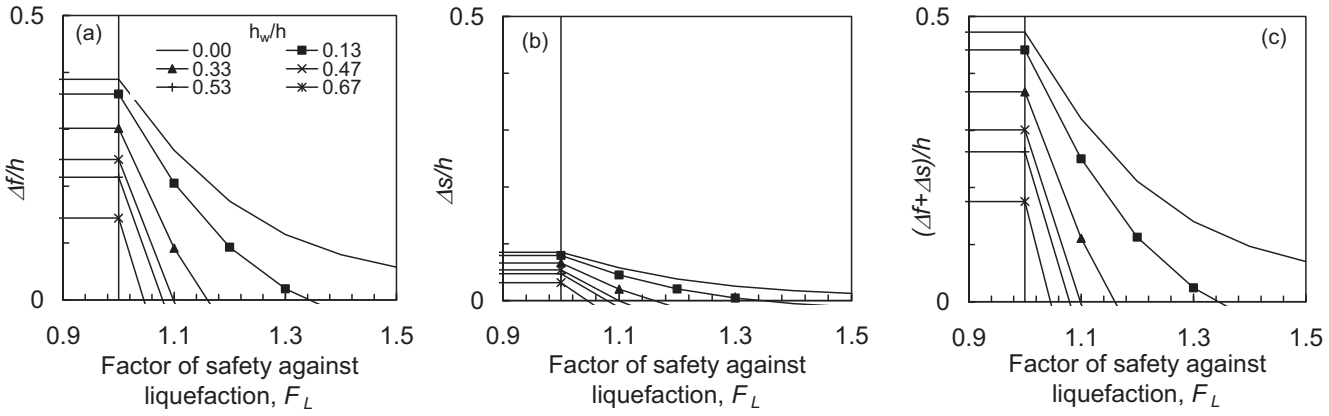

Fig. 6.11 Relationship between liquefaction resistance ratio (F_L) and normalized (a) uplift displacement , (b) settlement of backfill, and (c) total vertical displacement.

To apply to the seismic design for uplift for a buried structure, a flow diagram is proposed as shown in Fig. 6.12. The flow diagram includes judgement of liquefaction of backfill as well as estimated the uplift displacement proposed in this study. To judge liquefaction of backfill, a liquefaction resistance ratio F_L was used. The procedure of the flow diagram is as follows: First, the initial relative density of backfill is adequately chosen. The corrected SPT blow counts are estimated from the relative density, and R_L is then decided (Japan Road Association, 1990). Also, earthquake-induced cyclic shear stress ratio, L, is can be evaluated by using measured PGA (Peak Ground Acceleration) during earthquakes. Then, the liquefaction resistance ratio F_L can be calculated. Excess pore water ratio, r_u, is decided through Eq. (1). By substituting r_u in Eqs. (9) and (10) of Chapter 3, the estimated uplift displacement, settlement of backfill, and total displacement can be computed. The process is rotated until the uplift displacement becomes smaller than the limitation in performance design (for example Honda, et al. 2002).

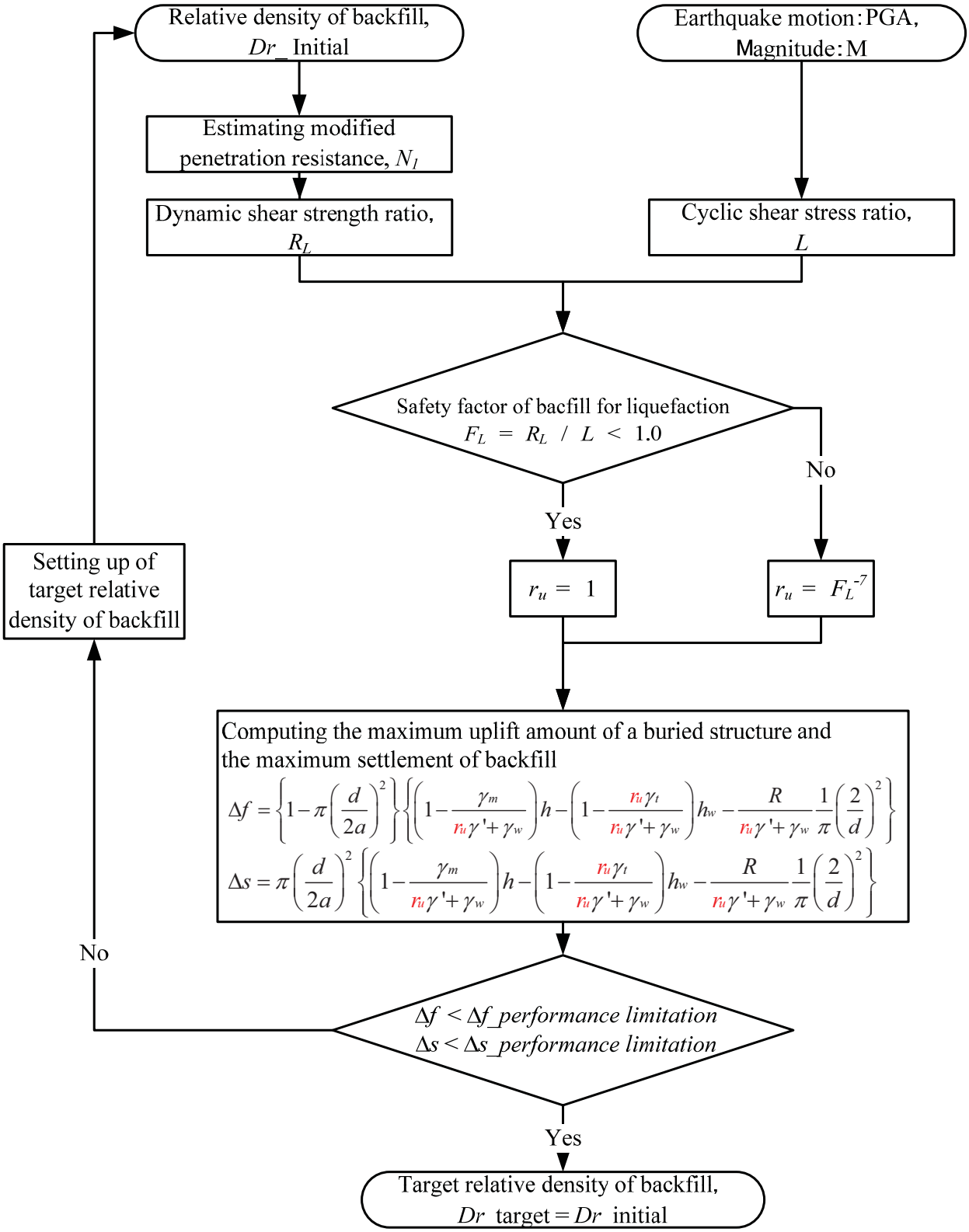

Fig. 6.12 Flow diagram of the seismic design for uplift of a buried structure.

6.4 Summary

Two mitigation methods against the uplift behavior of a buried structure were proposed targeting existing manholes based on results of previous chapters where excess pore water pressure is the key to reduce the uplift displacement of a manhole. One mitigation method can reduce excess pore water pressure. The other is compaction of backfill which can control the increase of excess pore water pressure.

The most prominent mitigation measure is to compact backfill. To see effectiveness of compacted ground against uplift behavior, backfill was compacted from Dr ≈ 36% to Dr ≈ 72% by shaking the manhole and the effectiveness was verified through the centrifuge model tests. For comparisons of compacted and loose backfill, a standard test case is as follows: ground water table is located at the depth of 1 m from the ground surface, length of model manhole is 3 m and the relative density of backfill and native ground is about 36% and 85%, respectively. Amplitude of input acceleration is 7.15 m/s^2. The uplift displacement (standard uplift displacement) in loose backfill (Dr ≈ 36%) was about 0.95 m, whereas the uplift displacement in compacted backfill (Dr ≈ 72%) is about 0.13 m under amplitude of input acceleration of 6.79 m/s^2. However, manholes in compacted backfill could be uplifted largely if a large amplitude of input acceleration is applied.

The uplift displacement for Model No. 2 with a small filtering net for dissipation of pore water was decreased by 0.92 m from the standard uplift displacement (0.95 m) and the uplift displacement for Model No. 3 with large filtering net was decreased by 0.77 m. This indicates that the mitigation measure by dissipating the excess pore water is effective. However, the reduction level of uplift displacement is relatively small because the pipe connected to the filtering net in the manhole uplifted with the uplifting of the manhole. Thus, another device was proposed to help accelerate the dissipation of pore water into the manhole during the

manhole uplift as shown in Fig. 6.3. Using the device, the uplift displacement was decreased by 0.25 m for Model No. 3 and 0.70 m for Model No. 1(no mitigation device) from the standard uplift displacement (0.95 m). This fact indicates that the device in Fig. 6.3 is effective at reducing the uplift displacement as well as accelerate the dissipation of pore water into the manhole (Model No. 3) during the manhole uplift.

From the test results for mitigation methods proposed in this research, which are compaction of backfill and dissipation of pore water, have to cooperate to mitigate the uplift amount of the manholes in the field.

A flow diagram was proposed to apply to the seismic design for uplift of a buried structure. The flow diagram includes liquefaction limit of backfill as well as estimated the maximum uplift displacement proposed in this study.

7. Conclusions

This thesis presents assessing uplift displacement of buried structures in liquefied ground during earthquakes. Considering the importance of lifeline facilities, the uplift behaviour of sewerage manholes was investigated in detail through centrifuge studies and case histories. A simplified method based on the equilibrium of vertical forces acting on a buried structure to predict the maximum uplift displacement of a manhole was developed and validated by comparison with centrifuge test data. The drawbacks of this simplified method which is gives only the maximum amount of uplift and is incapable of predicting transient behaviors during shaking were overcome through numerical analysis as a detailed method based on the mechanism of a continuum body. Furthermore, the methods for assessment of uplift displacement were verified by comparing the calculated results with the observed manhole uplifts during an earthquake. The main results of this thesis are summarized as follows:

In chapter 2, a series of centrifuge model tests was performed to study the uplift mechanism of buried structures in liquefied ground and to investigate the secondary factors affecting indirectly the uplift behavior as well as the primary factors affecting directly the uplift behavior. Condition for backfill in the trench, the depth of the ground water table and the amplitude of input acceleration are primary factors affecting directly the uplift amount by liquefaction. Condition of native ground is a secondary factor accelerating the uplift of the manhole by squeezing of liquefied native ground.

The manhole started to lift up when the EPWP (Excess Pore Water Pressure) in the middle of the backfill and that of the bottom of the manhole exceeded the initial effective vertical stress. The uplift of the manholes was related to primary factors as follows: The uplift

displacement of manholes tends to increase when the depth of the ground water table is shallow, the relative density of backfill is low, amplitude of the input acceleration is large or the number of load cycles is increased, the cross-sectional area of trench is wide, the length of the manhole is long, and the apparent unit weight of manholes is small. Effects of secondary factors against uplift behavior were as follows: The uplift displacement is largely increased when the native ground was loose ground (Dr ≈ 36%) and the uplift displacement is increased when the native soils under the manhole were liquefied.

The EPWPR (Excess Pore Water Pressure Ratio) was identified as one of the important factor affecting the uplift behavior based on the facts that the safety factor (Koseki et al., 1997b) using EPWPR measured in backfill as an input data could evaluate the triggering of manhole uplift and the uplift displacement was increased with a rapid build-up of the EPWPR. Among factors considered in the centrifuge studies, the most important factors affecting the increase in EPWPR were the depth of the ground water table, the relative density of backfill and the amplitude of the input acceleration, and they were also largely affecting the uplift amount of the manholes.

In chapter 3, a simplified method was proposed to estimate the maximum uplift displacement of a manhole in liquefied ground based on the equilibrium of vertical forces acting on a manhole under the assumption that the continuity of the volume in the trench during liquefaction in unchanged. Forces acting on the manhole are the dead weight of the manhole and the frictional force between the manhole and backfill above the ground water table as a downward force, and hydrostatic pressure and the uplift force acting on the bottom of the manhole due to liquefied backfill as upward forces. The validity of the simplified method including assumptions of no volume change or continuity in the trench was identified through

a simple model test by using the boiling method as a preliminary study. The maximum uplift displacements measured in the simple tests were plotted under a predicted boundary by the simplified method. Also, quantitative relationships between uplift displacement and the thickness of the non-liquefied layer above the ground water table, the unit weight of backfill and the size of the trench were derived from the proposed simplified method.

To verify validation or application of the simplified method, predicted uplift displacements were compared with centrifuge test data. The measured uplift displacements were plotted under the uplift displacements predicted by the simplified method in which EPWPR measured in the centrifuge model tests was used as a component to derive uplift force acting on the bottom of the manhole. However, the simplified method tended to overestimate the uplift displacement when the uplift displacement did not reach the maximum amount.

To overcome limitations of the simplified method, in chapter 4, two dimensional effective stress analyses based on multiple shear mechanism for soil were conducted on the uplift behavior of a buried structure. The effective stress analysis based on mechanics of a continuum body can estimate transient behaviors of manholes during shaking as well as the maximum uplift displacement. Also, it is possible to evaluate both failure modes and the extent of displacement/stress/ductility/strain subjected to the complex soil-structure interaction. The results of the numerical analysis were compared with centrifuge test data. The uplift displacements computed by the numerical analysis were fairly good with the centrifuge test data whose uplift displacements were overestimated by the simplified method. Also, the numerical analysis tended to underestimate the uplift displacement when a high magnitude of uplift displacement occurred such as a manhole uplift under large amplitude of input acceleration or in the saturated backfill whose ground water table coincides with the ground

surface. However, results in a series of numerical analysis for uplift behavior of the manholes show that the effective stress analysis can overcome the limitation of the simplified method.

In chapter 5, to verify the application of the methods, the methods were applied to the Nagaoka case history of the 2004 Niigata-ken Chuetsu, Japan, earthquake. Before performing this, the ground water table, as a primary factor, was identified as one of the important factors affecting the uplift amount of the manholes through the database collected by field investigation which contains uplift displacement of manholes, location of the manholes, the SPT borehole logs and their locations. Based on the relationship between observed manhole uplifts and the ground water table in Nagaoka, the methods for estimation of the uplift displacement proposed in this study were applied to Nagaoka case history and the application of the methods was verified. Observed uplift displacements were plotted under a predicted boundary by the simplified method and the simplified method could express effects of the relative density for backfill and magnitude of earthquakes by controlling EPWPR. It indicates that the proposed method is reasonable to estimate the maximum uplift displacement. Also, the low magnitude of manhole uplift in Nagaoka was in the range of the predicted boundary by the detailed method through the effective stress analysis. This fact suggests that numerical analysis can be applied to an estimation for low magnitude of manhole uplift with the various soil/structure/shake conditions. Finally, correlation analysis was conducted to evaluate the spatial correlation between the manhole uplift and secondary factors which are properties of native subsoil near the ground surface such as SPT blow counts, thickness of clay layer, and thickness of surface soil (embankment and reclamation). The uplift displacement tended to increase in the native ground with low SPT blow count, thickness of clay layer and thick surface soil. Also, relationships found between the uplift displacements and associated

parameters (loose ground, clay material and the depth of ground water table) significantly agree with those found in the centrifuge model tests.

In chapter 6, practical applications were discussed based on the results obtained in the present research. It is found that the EPWPR was an important factor affecting the uplift behavior of a manhole and EPWPR is then the key to reduce the uplift displacement of a manhole. On the basis of this, two mitigation methods against uplift behavior were proposed. One mitigation method can reduce EPWP. The other is compaction of backfill by shaking the manhole which can control an increase of EPWP. The effectiveness of the mitigation methods was validated through the centrifuge model tests. The most prominent mitigation measure was to compact backfill. The uplift displacement for loose backfill (Dr ≈ 36%) was about 0.95 m, whereas the uplift displacement for compacted backfill (Dr ≈ 72%) was about 0.13 m under the same test condition. However, manholes in compacted backfill can be uplifted largely if a large amplitude of the input acceleration was applied. Mitigation measure by dissipating pore water during strong shaking was also effective based on the fact that the uplift displacements were decreased by 0.25 m compared with results of no mitigation measure (0.95 m). From the test results for mitigation measures, the mitigation methods proposed in this research which are compaction of backfill and dissipation of excess pore water have to be cooperated to mitigate the uplift amount of the manholes in the field.

Lastly, a flow diagram was proposed to apply to the seismic design for uplift of a buried structure. The flow diagram included a liquefaction limit of backfill as well as estimated the maximum uplift displacement proposed in this study.

REFERENCES

ASCE. (1974). Earthquake damage evaluation and design considerations for underground structures, February, *American Society of Civil Engineers*, Los Angeles Section.

Bardet, J. P., Tobita, T., Mace, N. and Hu, J. (2002). Regional modeling of liquefaction-induced ground deformation, *Earthquake Spectra, Earthquake Engineering Research Institute*, Vol.18, No. 1, pp.19-46.

Bartlett, S. F. and Youd, T. L. (1995). Empirical prediction of lateral spread displacement, *Journal of Geotechnical Engineering, ASCE*, Vol.121, No. 4, pp.316-329.

Bransby, M. F., Newson, T. A., Brunning, P., and Davies, M. C. R. (2001). Numerical and centrifuge modeling of the upheaval resistance of buried pipelines, *Proc., 20th Int. Conf. on Offshore Mechanics and Arctic Engineering*, Rio de Janeiro, Brazil.

Cabinet Office. (2006). A collection of disaster data after the 1995 Hanshin/Awaji Earthquake, (http://www.bousai.go.jp/1info/kyoukun/hanshin_awaji/nenpyo/index.html) (in Japanese).

Chin, E. L., Craig, W. H., and Cruickshank, M. (2006). Uplift resistance of pipelines buried in cohesionless soil, *Proc., 6th Int. Conf. on Physical Modelling in Geotechnics*. Ng, Zhang, and Wang, eds., Vol. 1, Taylor & Francis Group, London, pp.723–728.

Cheuk, C. Y., White, D. J. and Bolton, M. D. (2008). Uplift mechanisms of pipes buried in sand, *Journal of Geotechnical and Geoenvironmental Engineering, ASCE*, Vol.134, No. 2, pp.154-163.

Dewoolkar, M.M., Ko, H.Y., Stadler, A.T. and Astaneh, S.M.F. (1999). A Substitute Pore Fluid for Seismic Centrifuge Modeling, *Geotechnical Testing Journal*, GTJODJ, Vol. 22, No. 3, pp.196-210.

Dowding, C.H. and Rozen, A. (1978). Damage to rock tunnels from earthquake shaking, *J. Geotech. Eng. Div.*, ASCE, Vol. 104, GT2, pp.175–191.

Duke, C.M. and Leeds, D.J. (1959). Effects of Earthquakes on Tunnels, *Paper Presented at the RAND Second Protective Construction Symposium*, March, pp.24–26.

Elgamal, A., Yang, Z., Parra, E. and Ragheb, A. (2003). Modeling of cyclic mobility in saturated cohesionless soils, *International Journal of Plasticity*, Vol.19, No. 6, pp.883-905.

Hamada, M. (1991). Report of damage reconnaissance for the 1990 Philipine, Luzon Earthquake, *Association for Development of Earthquake Prediction*, pp.89 (in Japanese).

Honda, A., Nakase, H., Yasuda, S. & Suehiro, T. (2002). Study on permissible uplift of buried structures, *Proceedings of Annual Conference of the Japan Society of Civil Engineers*, pp.1439-1440 (in Japanese).

Hall, W.J. and O'Rourke, T.D. (1991). Seismic behavior and vulnerability of pipelines, *Proc 3 US Conf Lifeline Earthquake*, pp.761–73.

Iai, S. and Matsunaga, Y. (1991). Mechanism of uplift of underground structures due to liquefaction, *International Symposium on Natural Disaster Reduction and Civil Engineering*, *JSCE*, Osaka, pp.297- 306.

Iai, S., Matsunaga, Y. and Kameoka, T. (1992a). Strain space plasticity model for cyclic mobility, *Soils and Foundations, Japanese Society of Soil Mechanics and Foundation Engineering*, Vol.32, No. 2, pp.1- 15.

Iai, S., Matsunaga, Y. and Kameoka, T. (1992b). Analysis of undrained cyclic behavior of sand under anisotropic consolidation, *Soils and Foundations, Japanese Society of Soil Mechanics and Foundation Engineering*, Vol.32, No. 2, pp.16- 20.

Iai, S. and Ozutsumi, O. (2005).Yield and cyclic behavior of a strain space multiple mechanism model for granular materials, *International Journal for Numerical and Analytical Methods in Geomechanics*, Vol.29, pp.417-442.

Iai, S., Tobita, T. and Imai, J. (2005). Centrifuge model tests of uplift behavior of manhole in liquefable deposit, *Proceedings 28th JSCE Earthquake Engineering Symposium*, paper No.04 (in Japanese, with English abstract).

Ichii, K., Seto, N. and Kidera, H. (2008). Characteristics of uplifting velocity of a buried pipe in liquefied ground, *Geotechnical Earthquake Engineering and Soil Dynamics IV*, *ASCE*, Sacramento, California, USA, GSP181.

Ishihara, K. (1993). Liquefaction and flow failure during earthquakes, *The 33rd Rankine lecture, Geotechnique*, Vol.43, No. 3, pp.351 - 415.

Ishihara, K. and Towhata, I. (1980). One-dimensional soil response analysis during earthquakes based on effective stress analysis, *Journal of the faculty of engineering, The University of Tokyo (B)*, Vol. XXXV, No. 4, pp.655-700.

Ishihara, K. and Yoshimine, M. (1992). Evaluation of settlements in sand deposits following liquefaction during earthquakes, *Soils and Foundations, Japanese Society of Soil Mechanics and Foundation Engineering*, Vol.32, No. 1, pp.173-188.

Ishinabe, H.,Yasuda, S., Murasawa, Y.,Takanami, K. and Kobayashi, T. (1999). A study on liquefacts strength cement deep mixing soil reinforced with fiber, *Proceeding of The 54th Annual Conference of the Japan Society of Civil Engineer*, pp. 498-499 (in Japanese, with English abstract).

Japan Road Association. (1986). Design manual for common utility ducts, pp.58-71 (in Japanese).

JGS. (1994). Reconnaissance report on the 1993 Kushiro-oki Earthquake and the Noto-hanto-oki Earthquake (in Japanese).

JGS. (1997). Reconnaissance report on the 1993 Hokkaid- -nansei-oki Earthquake (in Japanese).

JGS. (1998). Reconnaissance report on the 1994 Hokkaido- toho-oki Earthquake (in Japanese).

JGS. (1998). Uplift behavior and damage of underground structures caused by liquefaction, *Report to The 48th Geotechnical Engineering Symposium*, No., pp.48-51, 115.

JGS. (2003). Uplift behavior and damage of underground structures caused by liquefaction, *Report to The 48th Geotechnical Engineering Symposium*, No., pp.48-51, 115.

JGS. (2009). Reconnaissance report on the 2007 Niigata-ken Chuestu, Japan, Earthquke (in Japanese).

JSCE. (1988). Earthquake Resistant Design for Civil Engineering Structures in Japan, *Japanese Society of Civil Engineers*, Tokyo.

JSWA. (2001). A sewer facility design · A design guidance and interpretation, *Japan Sewage Works Association*.

JSWA. (2006). Seismic guidance for mitigation measures against damage to sewerage facilities, *Japan Sewage Works Association*.

JSWA. (2009). The coverage rate of sewerage treatment systems and The enforcement situation, *Japan Sewage Works Association,* (http://www.jswa.jp/05_arekore/07_fukyu/index.html).

Kaneshiro, J.Y., Power, M. and Rosidi, D. (2000). Empirical correlations of tunnel performance during earthquakes and aseismic aspects of tunnel design, *Proceedings of the Conference on Lessons Learned From Recent Earthquakes*, On Earthquakes in Turkey 1999, November 8–11.

Kiku, H., Yasuda, S., Tanaka, T. and Itou, T. (2004). Damage of sewerage systems in Toyokoro town during the 2003 Tokachi-oki, Japan, Earthquake, *The 59nd Japan National Conference on Civil Engineering*, Japan, pp.423-424 (in Japanese).

Kiku, H., Fukunaga, R., Kimura, M., Takahashi, M. and Matsumoto, M. (2007). Shaking table test on mechanism of uplift of manhole due to liquefaction, *The 42nd Japan National Conference on Geotechnical Engineering*, Nagoya, Japan, pp.1887-1888 (in Japanese).

Kobayashi, I., Tateishi, M., Yoshioka, T. & Shimazu, M. (1991). Geology of Nagaoka District, *Geological Survey of Japan*, Tsukuba, Japan (in Japanese, with English abstract).

Konishi, Y., Tobita, T., Takahashi, K. and Takeuchi, M. (2008). Estimation of uplift displacement and evaluation of countermeasure against uplift of a sewage manhole, *Journal of Japan Sewage Works Association*, Vol.45, No. 553, pp.99-111 (in Japanese).

Koseki, J., Matsuo, O. and Koga, Y. (1997a). Uplift behavior of underground structures caused by liquefaction of surrounding soil during earthquake, *Soils and Foundations, Japanese Geotechnical Society*, Vol.37, No. 1, pp.97-108.

Koseki, J., Matsuo, O., Ninomiya, Y. and Yoshida, T. (1997b). Uplift of sewer manhole during the 1993 Kushiro-Oki earthquake, *Soils and Foundations, Japanese Geotechnical Society*, Vol.37, No. 1, pp.109-121.

Koseki, J., Matsuo, O., and Tanaka, S. (1998). Uplift of sewer pipes caused by earthquake-induced liquefaction of surrounding soil, *Soils and Foundations, Japanese Geotechnical Society*, Vol.38, No. 3, pp.75-87.

Lee, K. L. and Albaisa, A. (1974). Earthquake induced settlements in saturated sands, *Journal of Geotechnical Engineering Division, ASCE*, Vol.100, No. 4, pp.387-406.

Ling, H.I., Mohri, Y.,Kawabata, T., Liu, H., Burke, C. and Sun, L. (2003). Centrifugal modeling of seismic behavior of large-diameter pipe in liquefiable soil, *J Geotech Geoenviron Eng*, *ASCE*, Vol. 129, No. 12, pp.1092–1101.

Matsushima, O., Meguro, R., Matsuda, K., Nakata, U. and Matsuo, M. (2007). Research on Countermeasures to Prevent Uplift of Sewage Manholes (WIDE Safety Pipe method), *Annuals of Japan Institute of Wastewater Engineering Technology,* (in Japanese).

Martin, G. R., Finn, W. D. L. and Seed, H. B. (1975). Fundamentals of liquefaction under cyclic loading, *Journal of Geotechnical Engineering, ASCE*, Vol.101, No. 5, pp.423-438.

Metolose Brochure, Shin-Etsu Chemical Co., Ltd., 1997, Cellulose Dept., 6―1, Ohtemachi 2-chome, *Chiyoda-ku*, Tokyo, Japan.

Mohri,Y., Kawabata,T., Ling, H. I., and Sun, L. (2000). Model Tests of Uplift Resistance on Buried Pipe, *Transaction of JSIDRE*, Vol. 205, pp.25-33 (in Japanese with English Abstract) .

Morii, T. and Nishino, N. (2008). Effective Soil Improvement against Liquefaction Examined in the Niigataken Chuetsu-oki Earthquake in 2007, *Bull.Facul.Agric.Niigata Univ.*, Faculty of Agriculture, Niigata University (in Japanese with English abstract).

Nagase, H. and Ishihara, K. (1988). Liquefaction-induced compaction and settlement of sand during earthquake, *Soils and Foundations, Japanese Geotechnical Society*, Vol.28, No. 14, pp.66-76.

National Astronomical Observatory of Japan (2003). Chronological scientific tables, *Maruzen Co., Ltd.*, Japan. (in Japanese)

Ng, C. W. W., and Springman, S. M. (1994). Uplift resistance of buried pipelines in granular materials, *Centrifuge 94*, Leung, Lee, and Tan, eds., pp.753–758.

Nishio, N. (1994). Mechanism of projection of sewerage manholes above ground due to soil liquefaction, *Structural engineering /earthquake engineering, Japan Sociaty of Civil Engineering,* Vol. 11, No. 3, pp.51-54.

Oka, F., Yashima, A., Tateishi, Y., Taguchi, Y. and Yamashita, S. (1999). A cyclic elasto-plastic constitutive model for sand considering a plastic-strain dependence of the shear modulus, *Geotechnique*, Vol.49, No. 5, pp.661-680.

Okamoto, S. (1984). Introduction to earthquake engineering, second edition, *University of Tokyo Press*, pp.88.

Orense, R.P., Morimoto, I., Yamamoto, Y., Yumiyama, T., Yamamoto, H. and Sugawara K. (2003). Study on wall-type gravel drains as liquefaction countermeasure for underground structures, *Soil Dyn Earthquake Eng*, Vol. 23, No. 1, pp.19–39.

O'Rourke, T.D. and Hamada, M. (1992). Case studies of liquefaction and lifeline performance during past earthquakes, Technical Report NCEER-92-0002, *National Center for Earthquake Engineering Research, State University of New York, Buffalo*, Vol. 2.

O'Rourke, T.D., Goh, S.H., Menkiti, C.O. and Mair, R.J. (2001). Highway tunnel performance during the 1999 Duzce earthquake, *Proc 15th Int Conf Soil Mech Geotech Eng.*

O'Rourke, T.D., Gowdy, T.E., Stewart, H.E. and Pease, J.W. (1991). Lifeline and geotechnical aspects of the 1989 Loma Prieta Earthquake, *Proc of the 2nd international conference on recent advances in geotechnical earthquake engineering and soil dynamics.* Rolla (MO), Univ. of Missouri-Rolla, pp.1601–1612.

Owen, G.N. and Scholl, R.E. (1981). Earthquake engineering of large underground structures, *Federal Highway Administration and National Science Foundation*, Report no. FHWA/RD-80/195

Ozutsumi, O., Sawada, S., Iai, S., Takeshima, Y., Sugiyama, W. and Shimasu, T. (2002). Effective Stress Analyses of Liquefaction-Induced Deformation in River Dikes, *Journal of Soil Dynamics and Earthquake Engineering*, Vol.22, pp.1075-1082.

Ozutsumi, O., Yamamoto, Y., Adachi, M., Sekiya, C., Kawanaka, M., Eitade, K., Tsuchiya, C., Shimazu, T., Iai, S. and Tagawa, S. (2003). Examination of the uplift mechanism of underground pipe by experimental analysis based on the effective stress method, *The 48th Geotechnical Engineering Symposium, Japan*.

Power, M., Rosidi, D. and Kaneshiro, J. (1998). Seismic vulnerability of tunnels-revisited, In: Ozedimir, L., (Ed.), *Proceedings of the North American Tunneling Conference*, *Elsevier*, Long Beach, CA, USA.

Rathje, E., M., Kelson, K., Ashford, S., A., Kawamata, Y., Towhata, I., Kokusho, T. and Bardet, J. P. (2006). Geotech-nical aspects of the 2004 Niigata Ken Chuetsu, Japan, earthquake, *Earthquake Spectra, Earthquake Engineering Research Institute* 22(S1): S23-S46.

Sasaki, T. and Tamura, K. (2002). Simplified method to predict liquefaction-induced uplift displacement of underground structures, *the 11th Japan Earthquake Engineering Symposium*, pp.1068-1070.

Sawada, S., Ozutsumi, O. and Iai, S. (2000). Analysis of liquefaction induced residual deformation for two types of quay walls: analysis by "FLIP", *Proceedings of the 12th World Conference on Earthquake Engineering* (Auckland), No.2486.

Schmidt, B., Hashash, Y., Stimac, T. (1998). US immersed tube retrofit, *Tunnels Tunneling Int*. 30 (11), pp.22-24.

Scawthorn, C., Miyajima, M., Ono, Y., Kiyono, J. and Hamada, M. (2006). Lifeline aspects of the 2004 Niigata ken Chu-etsu, Japan, earthquake, *Earthquake Spectra, Earthquake Engineering Research Institute* 22(S1): S89-S110.

Seed, H. B. and Idriss, I. M. (1971). Simplified procedure for evaluating soil liquefaction potential, *Journal of the Soil Mechanics and Foundation Division, ASCE*, Vol.97, No. 9, pp.1249-1274.

Sharma, S. and Judd, W.R. (1991). Underground opening damage from earthquakes, *Eng. Geol.,* Vol. 30,pp.263–276.

Stevens, P.R. (1977). A review of the effects of earthquakes on underground mines, *United States Geological Survey Open File Report*, US Energy Research and Development Administration, Reston, pp.77–313.

Tajimi, M. (1996). Damage done by the great earthquake disaster of the Hanshin-Awaji district to the Kobe Municipal Subway System and restoration works of the damage, *Jpn Railway Eng,* 137, pp.19–23.

Taniguchi, E. and Morishita, T. (1985). Uplift failure of under ground structures during the 1983 Nihonkai-Chubu Earthquake, *Research Report of Public Works Research Institute*, No. 2235 (in Japanese).

Tateishi, A., Oka, F. and Kotani, Y and Asai, R. (2009). Numerical analysis of uplift behavior of an underground structure due to liquefaction using an effective stress analysis method, *Performance-Based Design in Earthquake Geotechnical Engineering, Taylor & Fransis Group, London,* pp.1071-1079

Tatsuoka, F., Sasaki, T. and Yamada, S. (1984). Settlements in saturated sand induced by cyclic undrained simple shear, *Proceeding of the Eighth World Conference on Earthquake Engineering, San Francisco*, Vol. 111, pp.95-102.

Technical Committee on the Sewer Earthquake Countermeasures. (2005). Report of the Technical Committed on the Sewer Earthquake Countermeasures, Ministry of Land Infrastructure and Transport (in Japanese).

Tohda, J. (1996). Photographs of pipeline damage in Kobe, *Soils and Foundations*, Special Issue on Geotechnical Aspects of the January 17 1995 Hyogoken-Nambu Earthquake, Japanese Geotechnical Society.

Tokimatsu, K., Suzuki, Y. and Tamura, S. (1994). Preliminary report on geotechnical aspects of Hokkaido-Nansei-Oki Earthquake, *Research Report of Public Works Research Institute*, No. 2235 (in Japanese).

Tokimatsu, K. and Seed, H. B. (1987). Evaluation of settlements in sand due to earthquake shaking, *Journal of Geotechnical Engineering Division, ASCE*, Vol.113, CT8, pp.861-878.

Towata, I. and Ishihara, K. (1985). Modeling soil behaviour under principal stress axes rotation, *Proceeding of the Fifth International Conference on Numerical Method in Geomechanics*, Vol. 1, pp.523-530.

Trautmann, C. H., O'Rourke, T. D., and Kulhawy, F. H. (1985). Uplift force-displacement response of buried pipe, *J. Geotech. Engrg.*, Vol. 111, No. 9, pp.1061–1076.

Uno, H., Oka, F., Tanizaki, S. and Tateishi, A. (2009). Centrifuge model tests on the uplift behavior of an under ground structure during liquefaction and its numerical modeling, *Performance-Based Design in Earthquake Geotechnical Engineering, Taylor & Fransis Group, London,* pp.1041-1049.

Yanagisawa, Y., Kobayashi, I., Takeuchi, K., Tateishi, M., Chihara, K. & Kato, H. (1986). Geology of Ojiya District, *Geological Survey of Japan*, Tsukuba, Japan, (in Japanese, with English abstract).

Yasuda, S. (2003). Relationship between SPT N value and liquefaction by an earthquake, *Foundation Practice*, Vol. 31, No. 2, pp.50-53 (in Japanese).

Yasuda, S., Ishinabe, H. and Murasawa, Y. (2001). Static and dynamic strength of cement mixed soil reinforced by fibers, *Proc. of the International Symposium on Earth Reinforcement (IS Kyushu 2001)*, pp.171 ～176.

Yasuda, S., Nagase, H., Itafuji, S., Sawada, H. and Mine, K. (1995). A study on the mechanism of the floatation of buried pipes due to liquefaction, *Soil Dynamics and Earthquake, Transactions on the Built Environment*, WIT Press, Vol.14, pp.125-132.

Yasuda, S. (2005). Allowable displacement of the ground at the aspect of traffic flow after the 2004 Niigata-ken Chuetsu-ken, Japan, Earthquake, *The Japan National Conference on Earthquake Engineering*, pp.146-147.

Yasuda, S. and Kiku, H. (2006). Uplift of sewage manholes and pipes during the 2004 Niigataken-Chuetsu earthquake, *Soils and Foundations, Japanese Geotechnical Society*, Vol.46, No. 6, pp.885-894.

Yasuda, S., Yoshida, N., Adachi, K., Kiku, H. and Gose, S. (1999). A simplified analysis of liquefaction-induced residual deformation, *Proceedings of the 2nd International Conference on Earthquake Geotechnical Engineering*, pp.555-560.

Yasuda, S. and Tanaka, T. (2002). Liquefaction-induced damage of dense sands and silty sands under very strong shaking, *The eleventh Proceedings of the Japan Earthquake Engineering Symposium*, pp.885-890.

Yasuda, S., Tanaka, T. and Kiku, H. (2009). Uplift of sewage man-hole during 1993 Kushiro-oki EQ., 2003 Tokachi-oki EQ. and 2004 Niigataken Chuetsu EQ, *Earthquake geotechnical case histories for performance-based design, Taylor&Francis Group*, *London*, pp.95-108.

Yoshida, M., Tonoo, M., Miyajima, M. and Kitaura, M. (2006). Experimental study on Countermeasure against Liquefaction-Induced Floatation of Manhole using Recycled Materials Pecked in Sandbag, *The 42nd Japan National Conference on Geotechnical Engineering*, Nagoya, Japan, pp.1945-1956 (in Japanese).

Vanden Berghe, J. F., Cathie, D., and Ballard, J. C. (2005). Pipeline uplift mechanisms using finite element analysis, *Proc., 16th Int. Conf. of Soil Mechanics and Foundation Engineering*, Osaka, Japan, pp.1801–1804.

Wang, L.R.L., Shim, J.S., Ishibashi, I. and Wang, Y. (1990). Dynamic responses of buried pipelines during a liquefaction process, *Soil Dyn Earthquake Eng*, Vol.9. No. 1, pp.44–50.

Wang, W.L., Wang, T.T., Su, J.J., Lin, C.H., Seng, C.R. and Huang, T.H. (2001). Assessment of damage in mountain tunnels due to the Taiwan Chi-Chi Earthquake, *Tunnel Underground Space Technol*, 16(3), pp.133–50.

Wang, J.M. (1985). Distribution of earthquake damage to underground facilities during the 1976 Tang-shan earthquake, *Earthquake Spectra,* Vol. 1, No. 4, pp.741–57.

White, D. J., Barefoot, A. J., and Bolton, M. D. (2001). Centrifuge modeling of upheaval buckling in sand, *Int. J. Physical Modeling in Geotechnics*, Vol. 2, No. 1, pp.19–28.

Zienkiewicz, O. C. and Bettess, P. (1982). Soils and other saturated media under transient, dynamic conditions, *Soil mechanics-Transient and Cyclic Loads (Pande and Zienkiewicz eds.)*, John Wily and Sons, pp.1-16.

APPENDIX A

CS1

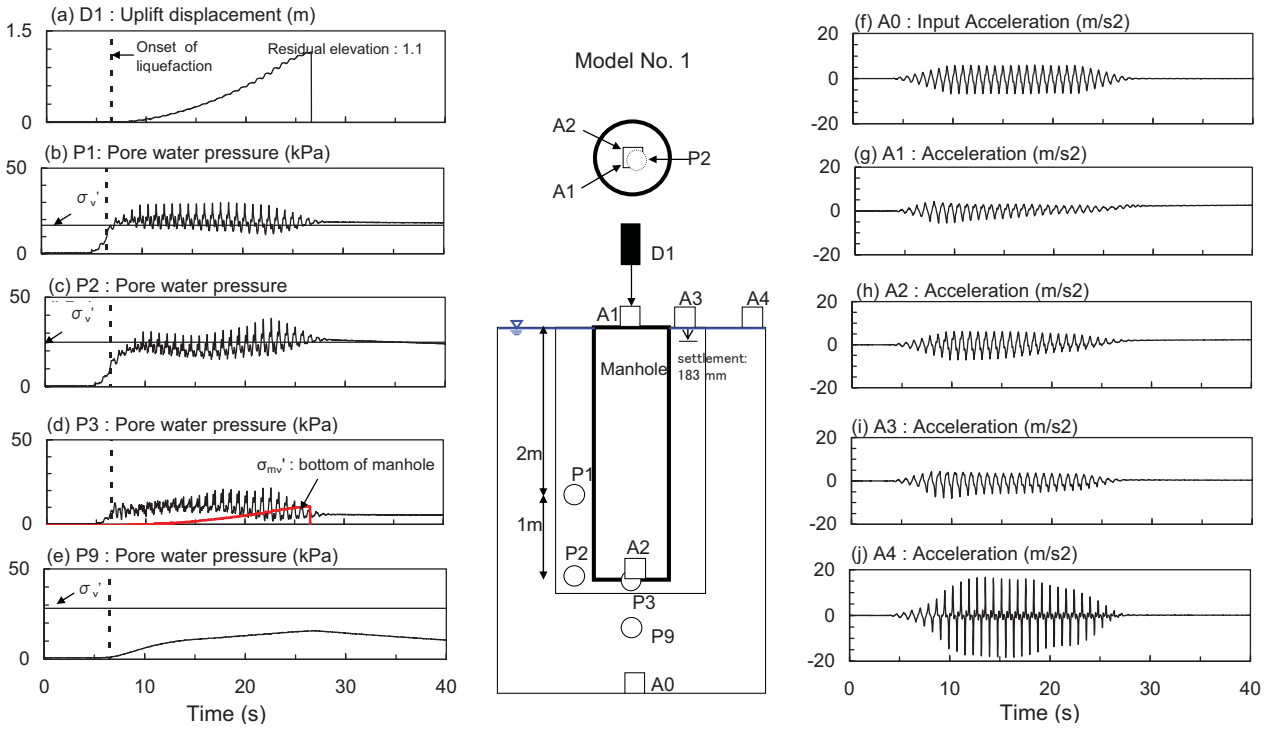

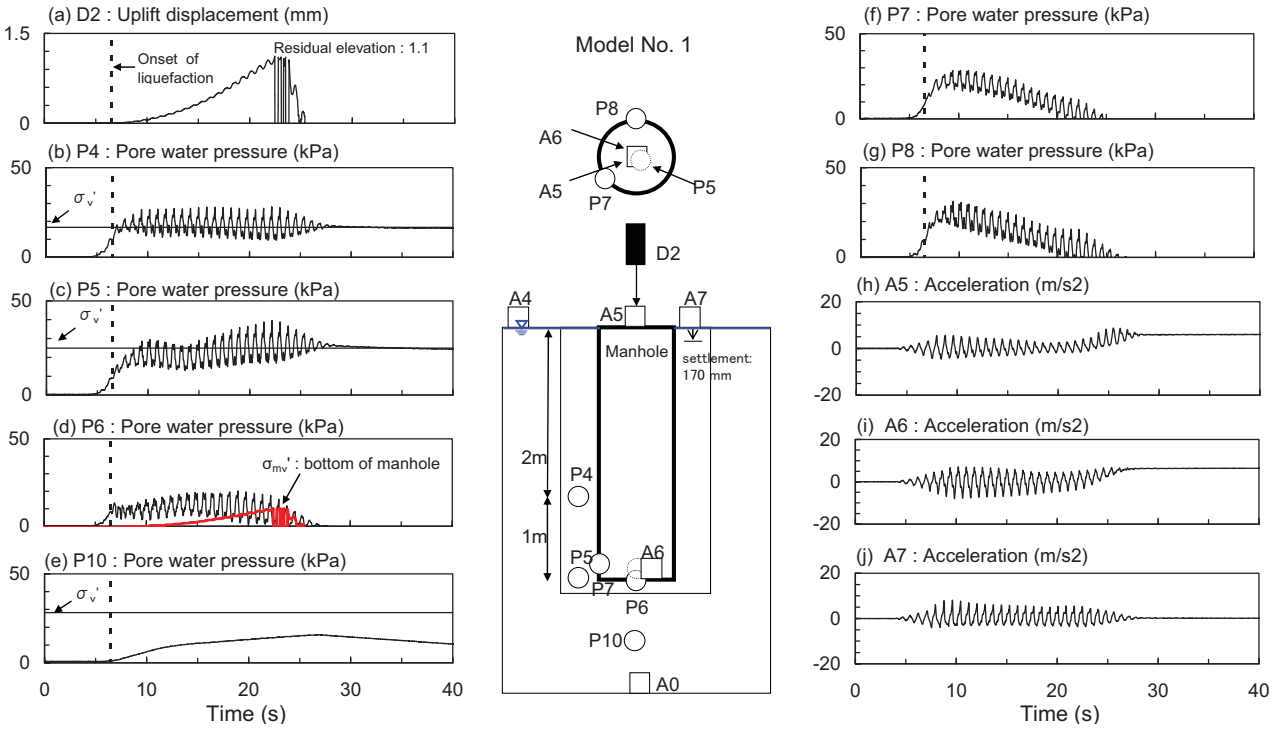

CS2

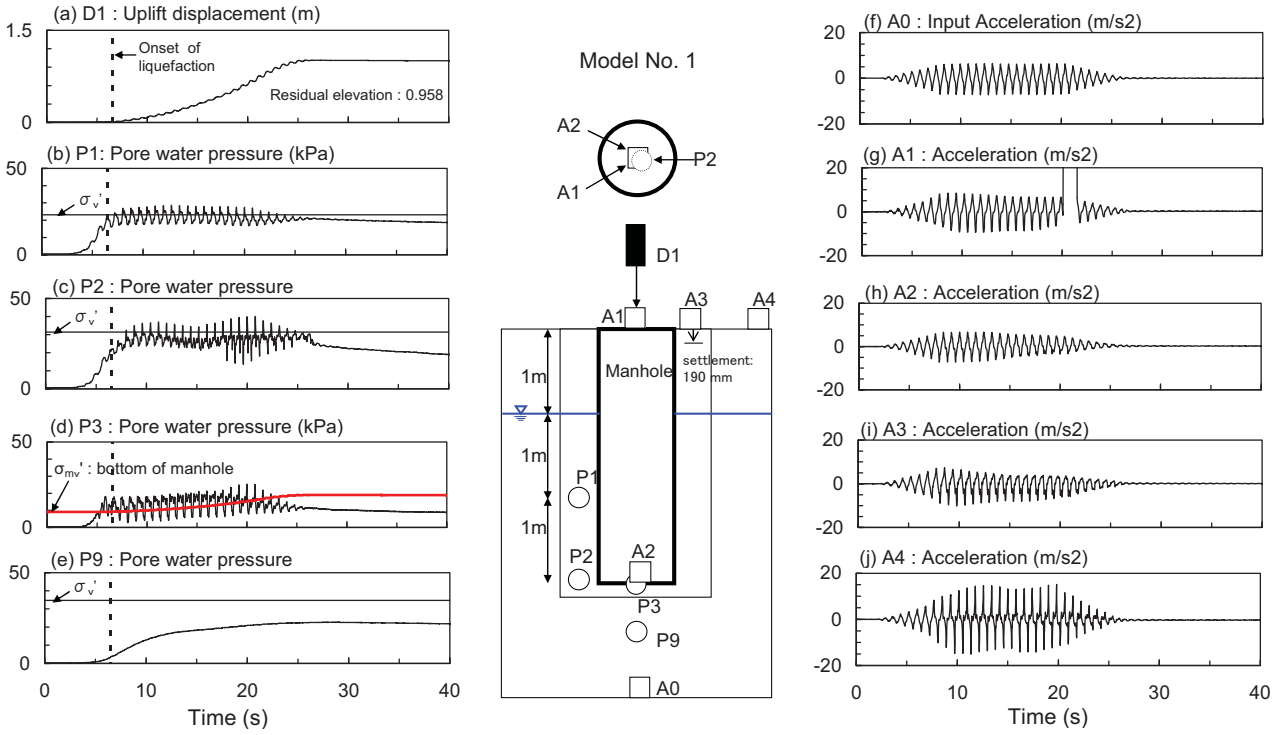
(a) D1 : Uplift displacement (m)
Onset of liquefaction
Residual elevation : 0.958
(b) P1: Pore water pressure (kPa)
(c) P2 : Pore water pressure
(d) P3 : Pore water pressure (kPa)
σmv' : bottom of manhole
(e) P9 : Pore water pressure
Time (s)
Model No. 1
A2
P2
A1
D1
A3
A4
Manhole
settlement: 190 mm
1m
P1
P2
A2
P3
P9
A0
(f) A0 : Input Acceleration (m/s2)
(g) A1 : Acceleration (m/s2)
(h) A2 : Acceleration (m/s2)
(i) A3 : Acceleration (m/s2)
(j) A4 : Acceleration (m/s2)
Time (s)

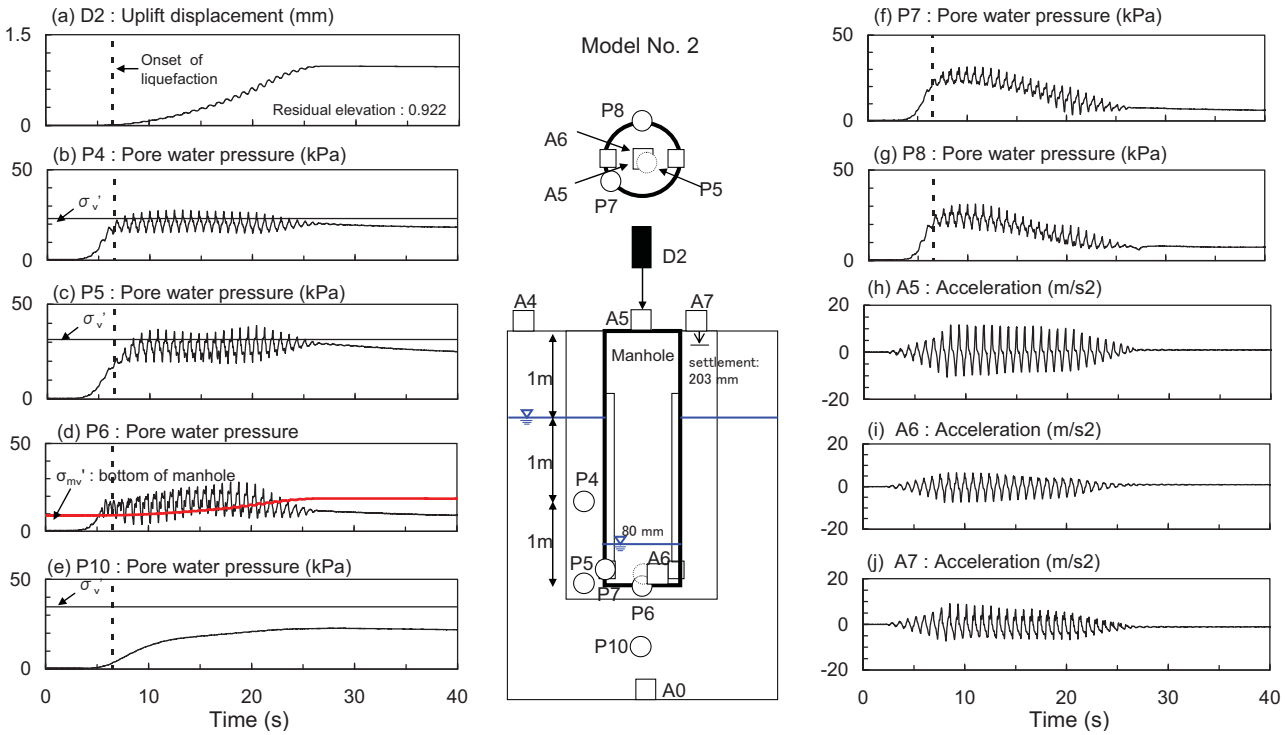
(a) D2 : Uplift displacement (mm)
Onset of liquefaction
Residual elevation : 0.922
(b) P4 : Pore water pressure (kPa)
(c) P5 : Pore water pressure (kPa)
(d) P6 : Pore water pressure
σmv' : bottom of manhole
(e) P10 : Pore water pressure (kPa)
Time (s)
Model No. 2
P8
A6
A5
P7
P5
D2
A4
A5
A7
Manhole
settlement: 203 mm
1m
P4
80 mm
P5
A6
P7
P6
P10
A0
(f) P7 : Pore water pressure (kPa)
(g) P8 : Pore water pressure (kPa)
(h) A5 : Acceleration (m/s2)
(i) A6 : Acceleration (m/s2)
(j) A7 : Acceleration (m/s2)
Time (s)

CS3

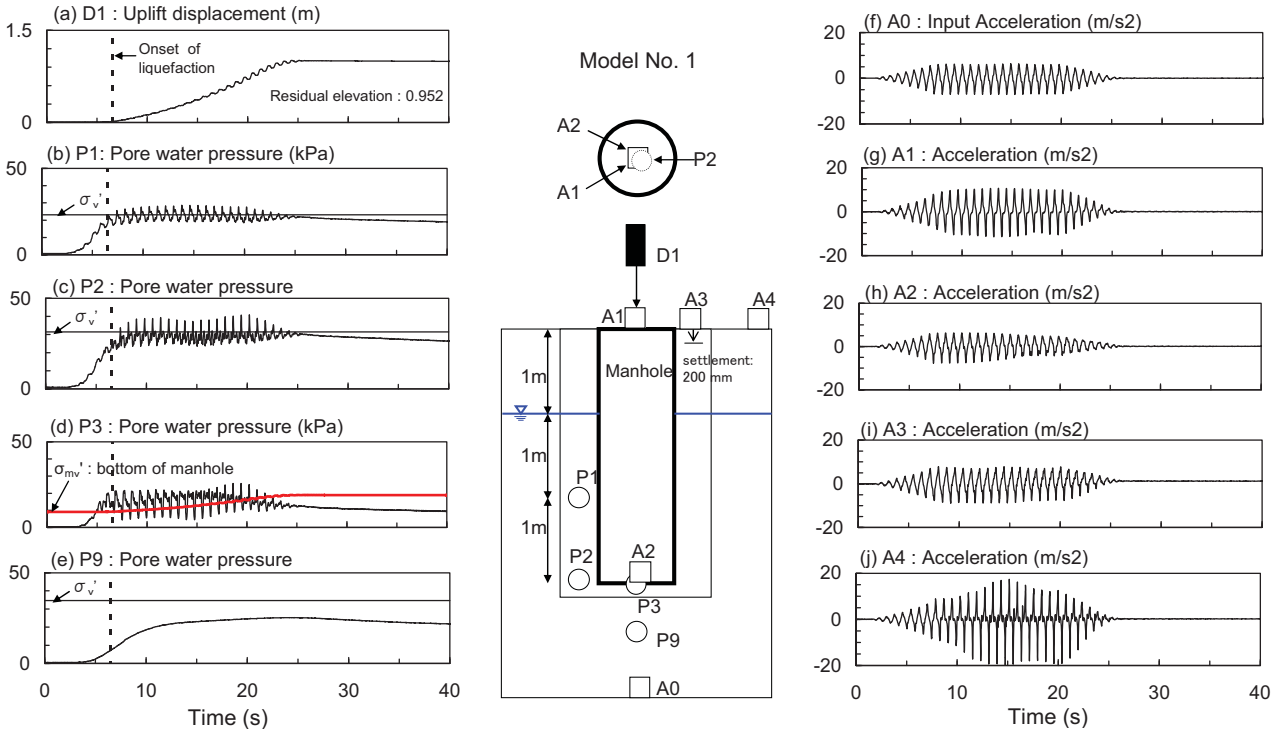
(a) D1 : Uplift displacement (m)
Onset of liquefaction
Residual elevation : 0.952
(b) P1: Pore water pressure (kPa)
(c) P2 : Pore water pressure
(d) P3 : Pore water pressure (kPa)
σmv' : bottom of manhole
(e) P9 : Pore water pressure
Time (s)
Model No. 1
A2
P2
A1
D1
A3
A4
Manhole
settlement: 200 mm
1m
P1
P2
A2
P3
P9
A0
(f) A0 : Input Acceleration (m/s2)
(g) A1 : Acceleration (m/s2)
(h) A2 : Acceleration (m/s2)
(i) A3 : Acceleration (m/s2)
(j) A4 : Acceleration (m/s2)
Time (s)

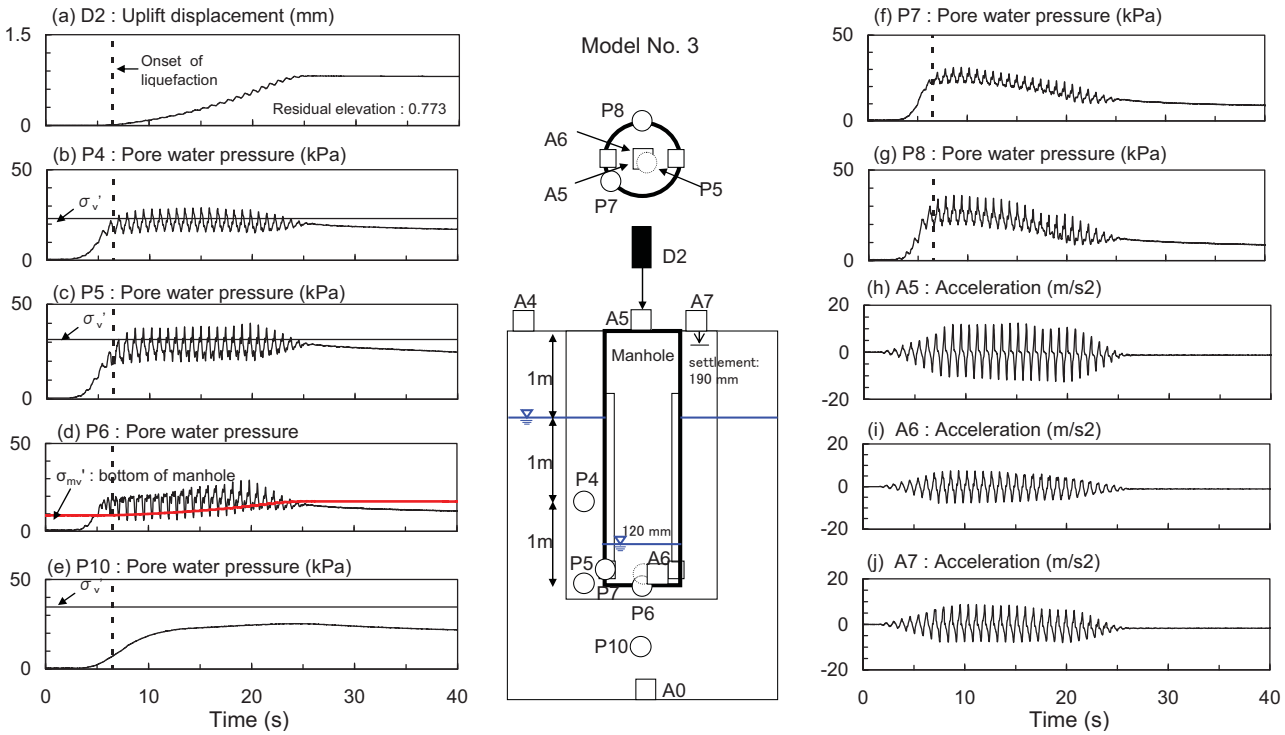
(a) D2 : Uplift displacement (mm)
Onset of liquefaction
Residual elevation : 0.773
(b) P4 : Pore water pressure (kPa)
(c) P5 : Pore water pressure (kPa)
(d) P6 : Pore water pressure
σmv' : bottom of manhole
(e) P10 : Pore water pressure (kPa)
Time (s)
Model No. 3
P8
A6
A5
P7
P5
D2
A4
A5
A7
Manhole
settlement: 190 mm
1m
P4
120 mm
P5
A6
P7
P6
P10
A0
(f) P7 : Pore water pressure (kPa)
(g) P8 : Pore water pressure (kPa)
(h) A5 : Acceleration (m/s2)
(i) A6 : Acceleration (m/s2)
(j) A7 : Acceleration (m/s2)
Time (s)

CS4

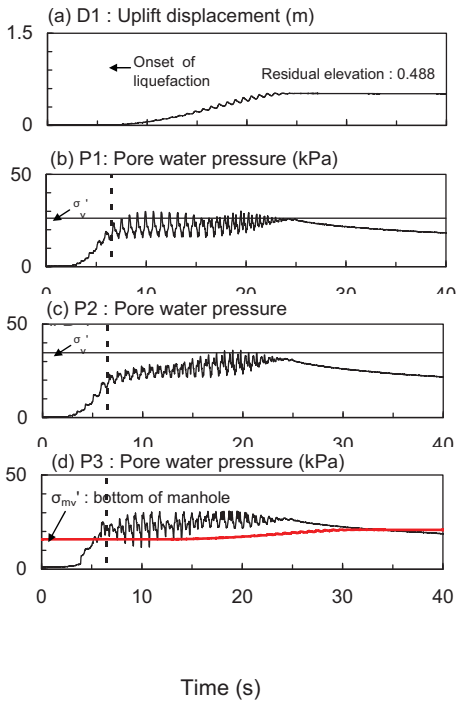
(a) D1 : Uplift displacement (m)
Onset of liquefaction
Residual elevation : 0.488
(b) P1: Pore water pressure (kPa)
(c) P2 : Pore water pressure
(d) P3 : Pore water pressure (kPa)
σmv' : bottom of manhole
Time (s)

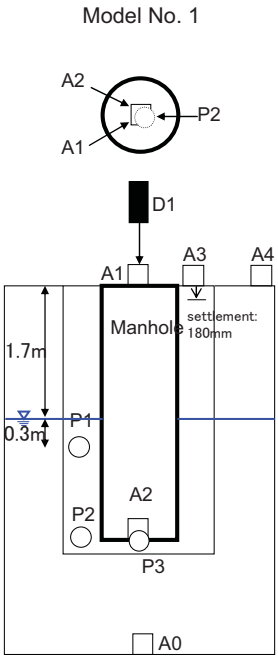
Model No. 1
A2
P2
A1
D1
A3
A4
settlement: 180mm
Manhole
1.7m
0.3m
P1
A2
P2
P3
A0

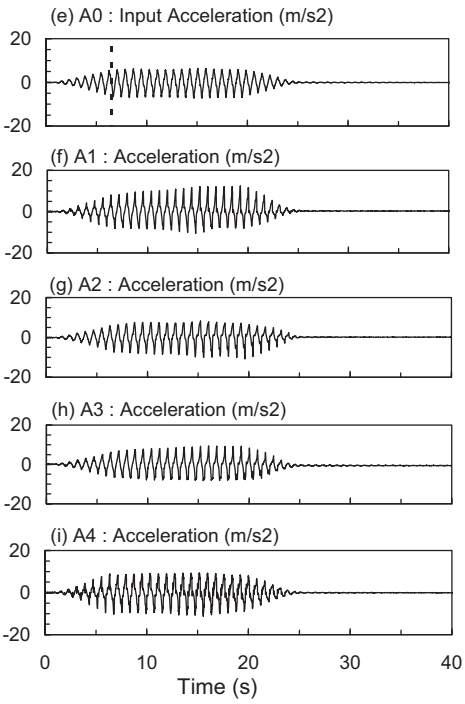
(e) A0 : Input Acceleration (m/s2)
(f) A1 : Acceleration (m/s2)
(g) A2 : Acceleration (m/s2)
(h) A3 : Acceleration (m/s2)
(i) A4 : Acceleration (m/s2)
Time (s)

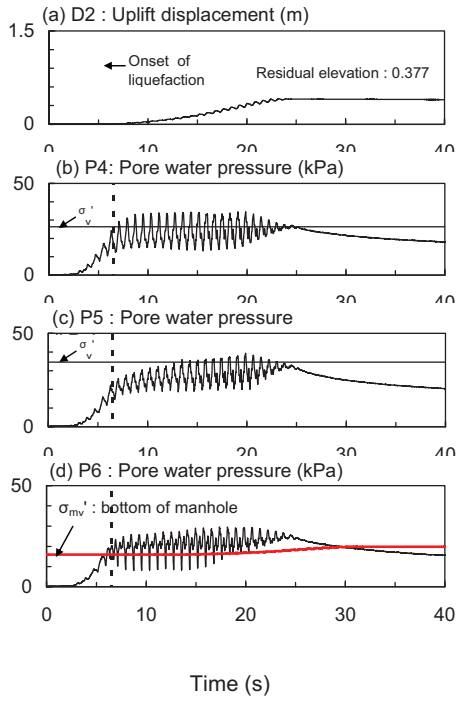
(a) D2 : Uplift displacement (m)
Onset of liquefaction
Residual elevation : 0.377
(b) P4: Pore water pressure (kPa)
(c) P5 : Pore water pressure
(d) P6 : Pore water pressure (kPa)
σmv' : bottom of manhole
Time (s)

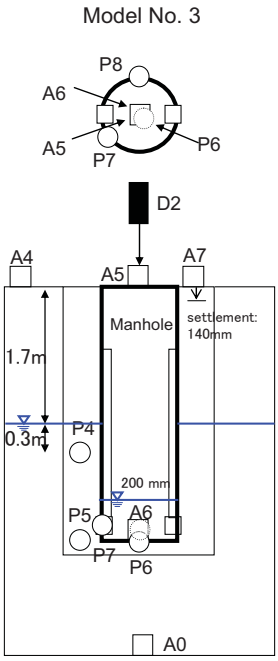
Model No. 3
P8
A6
A5
P7
P6
D2
A4
A5
A7
settlement: 140mm
Manhole
1.7m
0.3m
P4
200 mm
P5
A6
P7
P6
A0

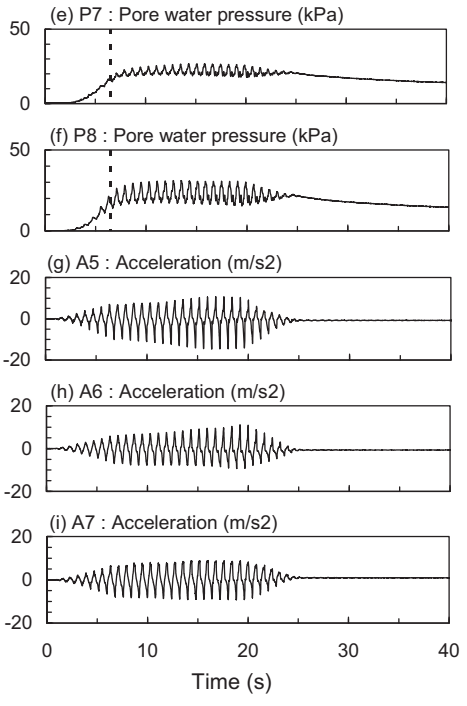
(e) P7 : Pore water pressure (kPa)
(f) P8 : Pore water pressure (kPa)
(g) A5 : Acceleration (m/s2)
(h) A6 : Acceleration (m/s2)
(i) A7 : Acceleration (m/s2)
Time (s)

CS6

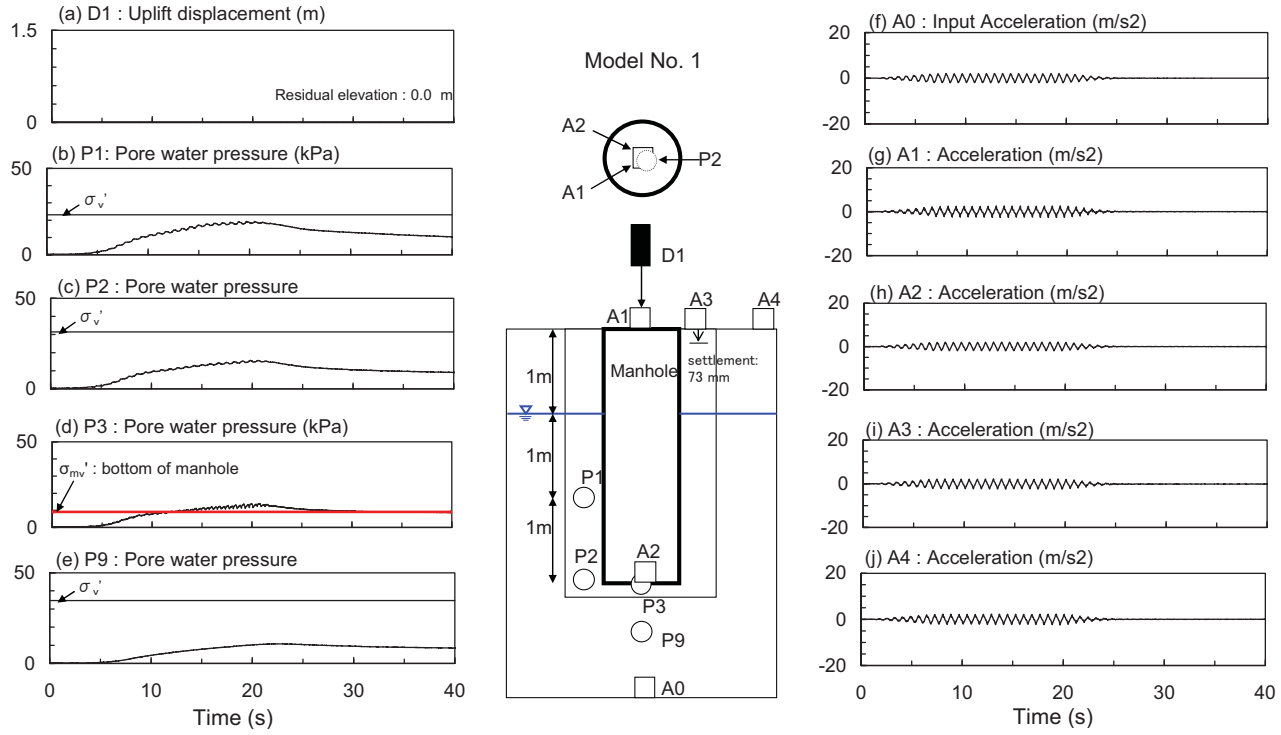
(a) D1 : Uplift displacement (m)
Residual elevation : 0.0 m
(b) P1: Pore water pressure (kPa)
(c) P2 : Pore water pressure
(d) P3 : Pore water pressure (kPa)
σmv' : bottom of manhole
(e) P9 : Pore water pressure
Time (s)
Model No. 1
A2
P2
A1
D1
A3
A4
Manhole
settlement: 73 mm
1m
P1
P2
A2
P3
P9
A0
(f) A0 : Input Acceleration (m/s2)
(g) A1 : Acceleration (m/s2)
(h) A2 : Acceleration (m/s2)
(i) A3 : Acceleration (m/s2)
(j) A4 : Acceleration (m/s2)
Time (s)

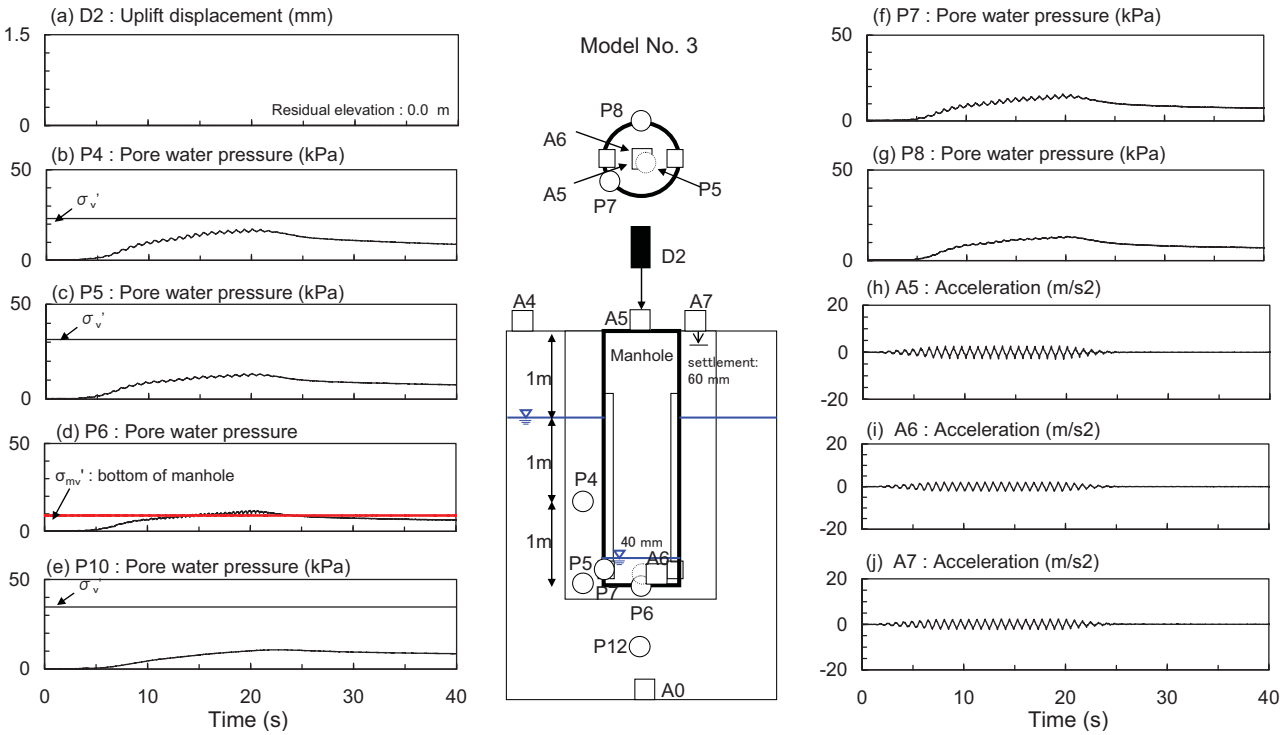
(a) D2 : Uplift displacement (mm)
Residual elevation : 0.0 m
(b) P4 : Pore water pressure (kPa)
(c) P5 : Pore water pressure (kPa)
(d) P6 : Pore water pressure
σmv' : bottom of manhole
(e) P10 : Pore water pressure (kPa)
Time (s)
Model No. 3
P8
A6
A5
P7
P5
D2
A4
A5
A7
Manhole
settlement: 60 mm
1m
P4
40 mm
P5
A6
P7
P6
P12
A0
(f) P7 : Pore water pressure (kPa)
(g) P8 : Pore water pressure (kPa)
(h) A5 : Acceleration (m/s2)
(i) A6 : Acceleration (m/s2)
(j) A7 : Acceleration (m/s2)
Time (s)

CS7

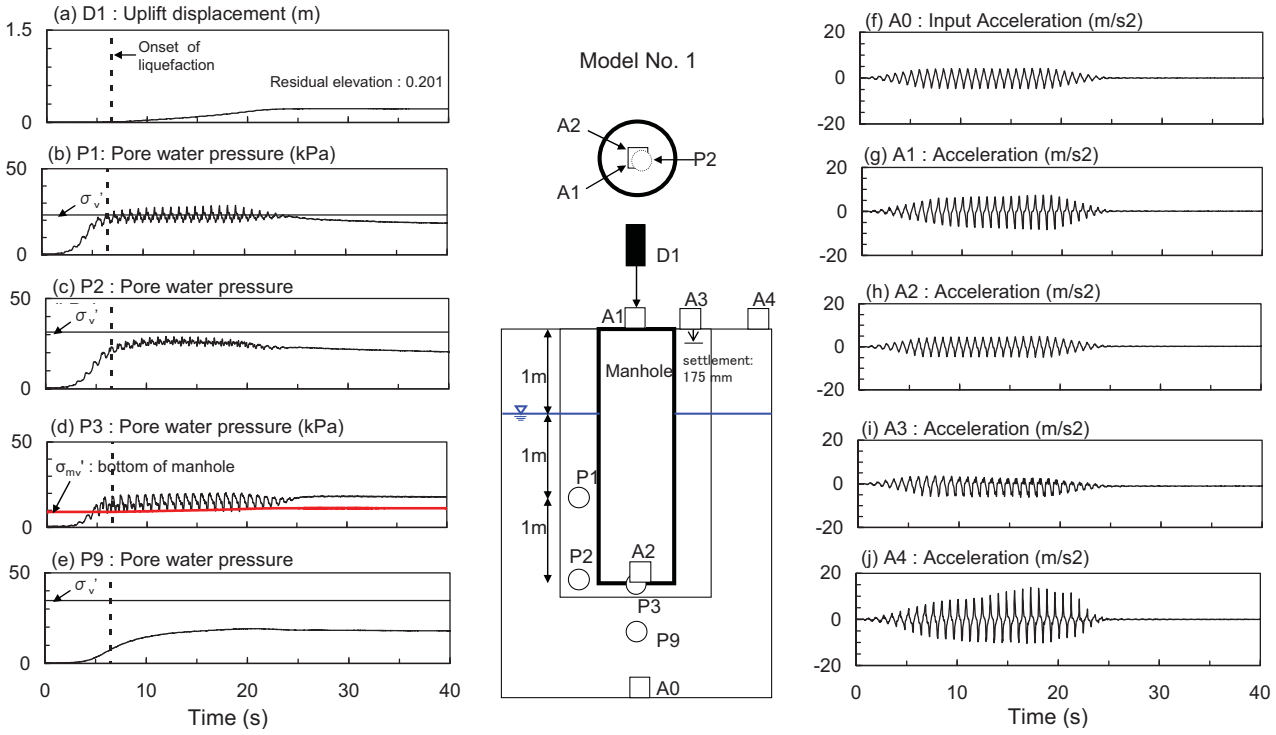
(a) D1 : Uplift displacement (m)
Onset of liquefaction
Residual elevation : 0.201
(b) P1: Pore water pressure (kPa)
(c) P2 : Pore water pressure
(d) P3 : Pore water pressure (kPa)
σmv' : bottom of manhole
(e) P9 : Pore water pressure
Time (s)
Model No. 1
A2
P2
A1
D1
A3
A4
Manhole
settlement: 175 mm
1m
1m
1m
P1
P2
A2
P3
P9
A0
(f) A0 : Input Acceleration (m/s2)
(g) A1 : Acceleration (m/s2)
(h) A2 : Acceleration (m/s2)
(i) A3 : Acceleration (m/s2)
(j) A4 : Acceleration (m/s2)
Time (s)

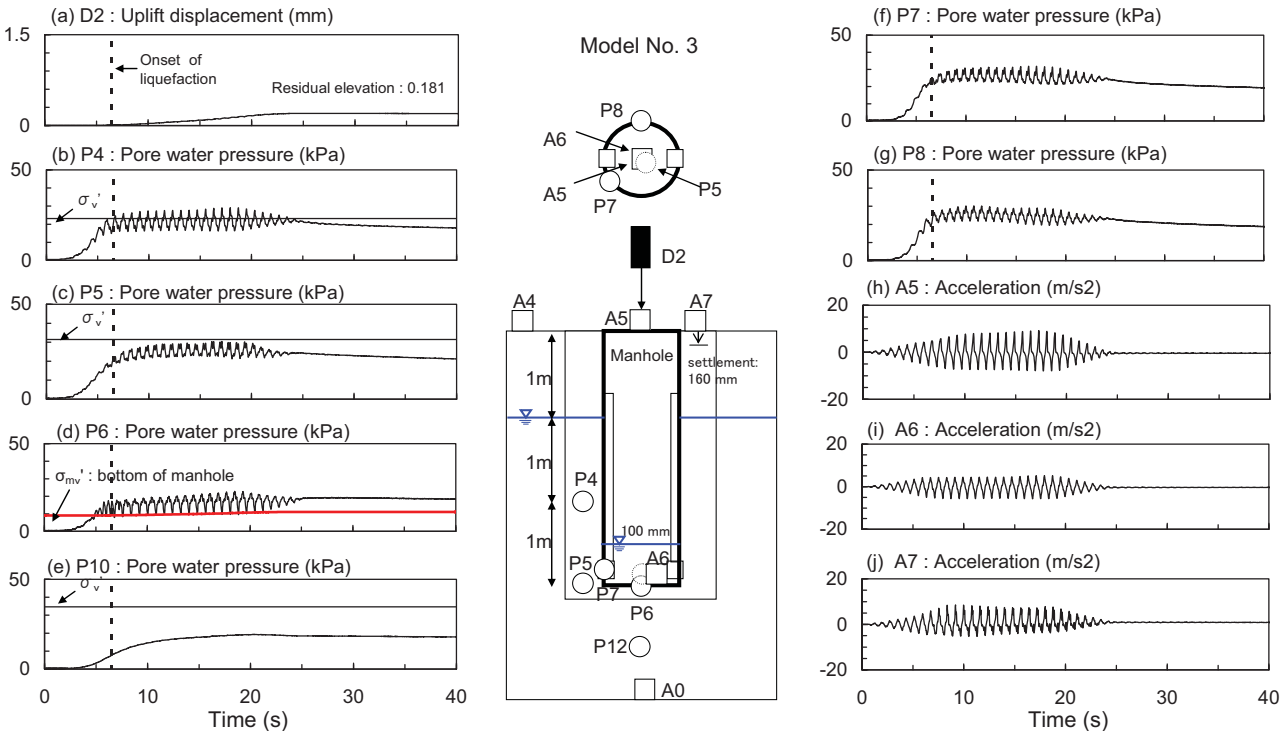
(a) D2 : Uplift displacement (mm)
Onset of liquefaction
Residual elevation : 0.181
(b) P4 : Pore water pressure (kPa)
(c) P5 : Pore water pressure (kPa)
(d) P6 : Pore water pressure (kPa)
σmv' : bottom of manhole
(e) P10 : Pore water pressure (kPa)
Time (s)
Model No. 3
P8
A6
A5
P7
P5
D2
A4
A5
A7
Manhole
settlement: 160 mm
1m
1m
1m
P4
100 mm
P5
A6
P7
P6
P12
A0
(f) P7 : Pore water pressure (kPa)
(g) P8 : Pore water pressure (kPa)
(h) A5 : Acceleration (m/s2)
(i) A6 : Acceleration (m/s2)
(j) A7 : Acceleration (m/s2)
Time (s)

CS8

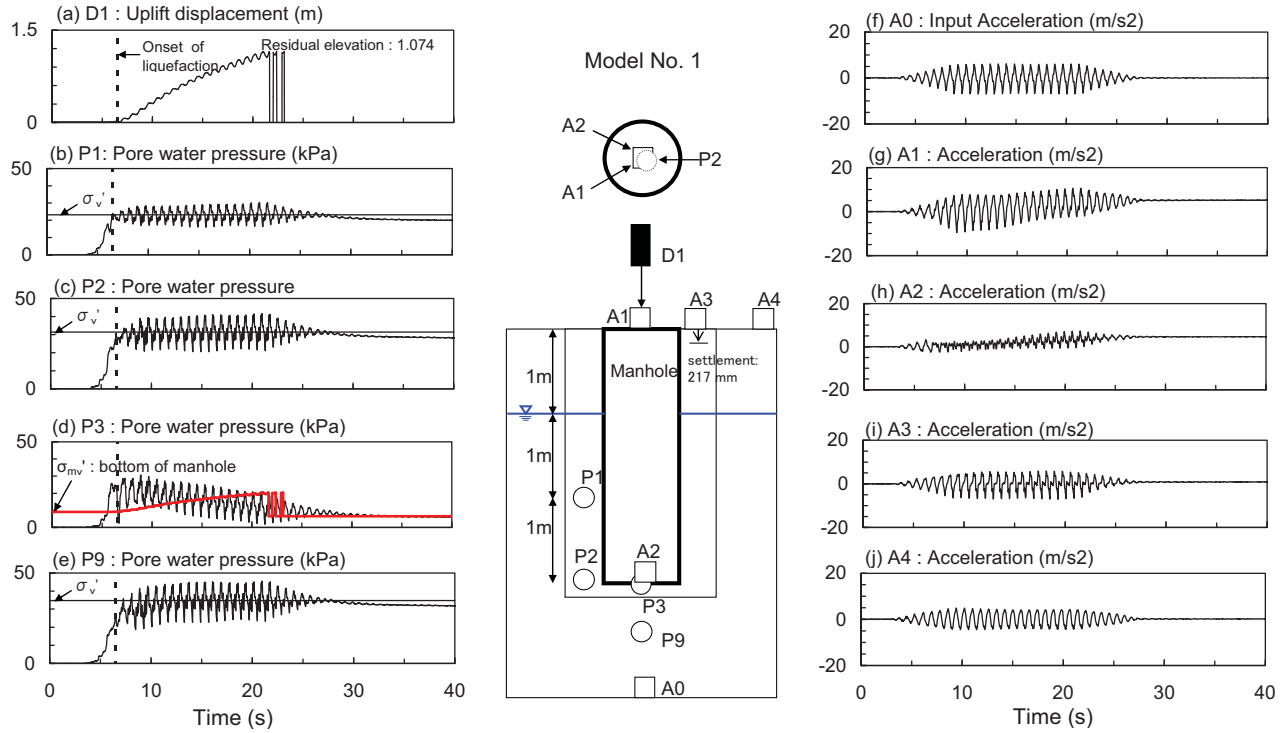
(a) D1 : Uplift displacement (m)
Onset of liquefaction
Residual elevation : 1.074
(b) P1: Pore water pressure (kPa)
(c) P2 : Pore water pressure
(d) P3 : Pore water pressure (kPa)
σmv' : bottom of manhole
(e) P9 : Pore water pressure (kPa)
Time (s)
Model No. 1
A2
P2
A1
D1
A3
A4
Manhole
settlement: 217 mm
1m
1m
1m
P1
P2
A2
P3
P9
A0
(f) A0 : Input Acceleration (m/s2)
(g) A1 : Acceleration (m/s2)
(h) A2 : Acceleration (m/s2)
(i) A3 : Acceleration (m/s2)
(j) A4 : Acceleration (m/s2)
Time (s)

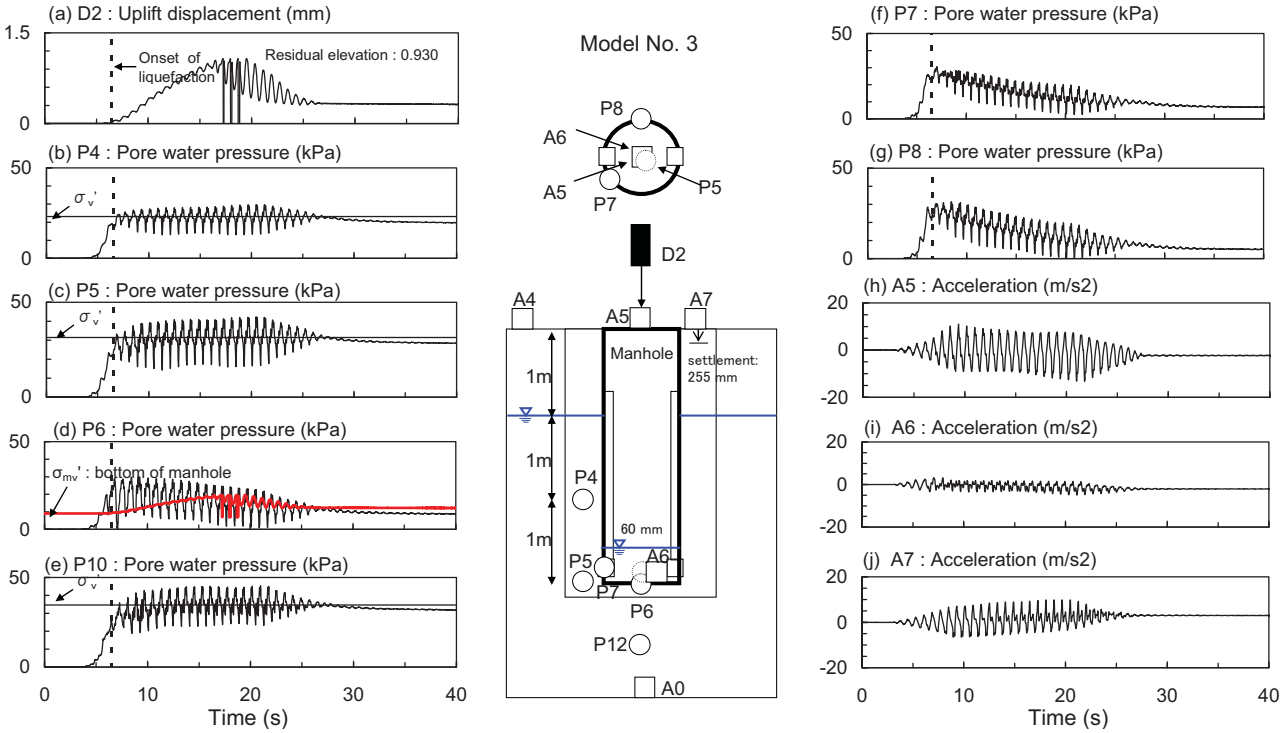
(a) D2 : Uplift displacement (mm)
Onset of liquefaction
Residual elevation : 0.930
(b) P4 : Pore water pressure (kPa)
(c) P5 : Pore water pressure (kPa)
(d) P6 : Pore water pressure (kPa)
σmv' : bottom of manhole
(e) P10 : Pore water pressure (kPa)
Time (s)
Model No. 3
P8
A6
A5
P7
P5
D2
A4
A5
A7
Manhole
settlement: 255 mm
1m
1m
1m
P4
60 mm
P5
A6
P7
P6
P12
A0
(f) P7 : Pore water pressure (kPa)
(g) P8 : Pore water pressure (kPa)
(h) A5 : Acceleration (m/s2)
(i) A6 : Acceleration (m/s2)
(j) A7 : Acceleration (m/s2)
Time (s)

CS9

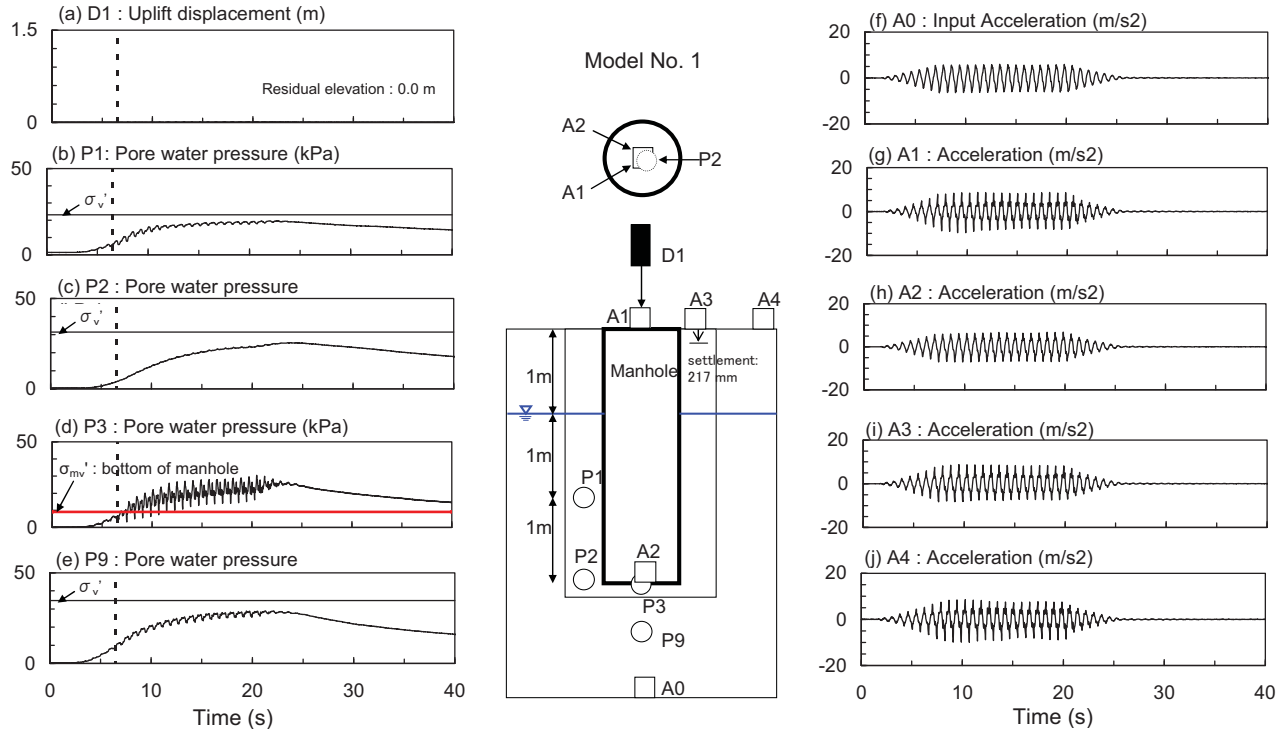
(a) D1 : Uplift displacement (m)
Residual elevation : 0.0 m
(b) P1: Pore water pressure (kPa)
(c) P2 : Pore water pressure
(d) P3 : Pore water pressure (kPa)
σmv' : bottom of manhole
(e) P9 : Pore water pressure
Time (s)
Model No. 1
A2
P2
A1
D1
A3
A4
Manhole
settlement:
217 mm
1m
P1
P2
A2
P3
P9
A0
(f) A0 : Input Acceleration (m/s2)
(g) A1 : Acceleration (m/s2)
(h) A2 : Acceleration (m/s2)
(i) A3 : Acceleration (m/s2)
(j) A4 : Acceleration (m/s2)
Time (s)

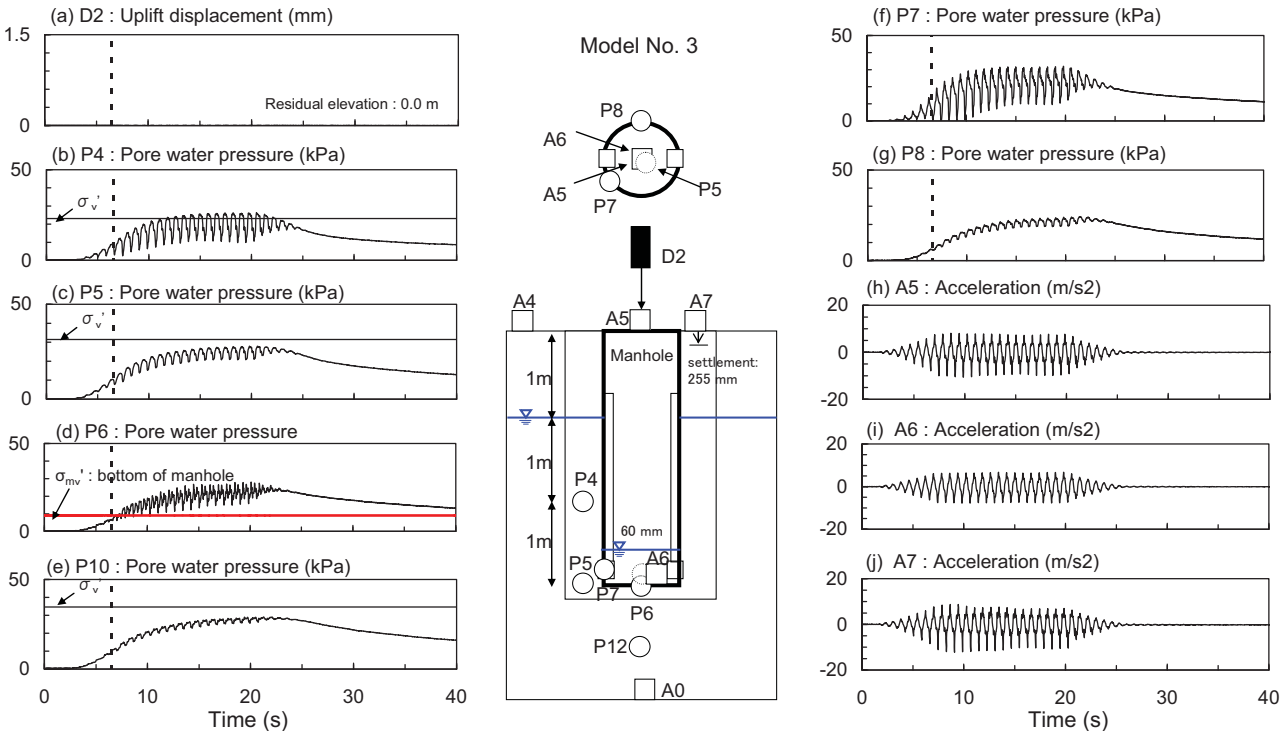
(a) D2 : Uplift displacement (mm)
Residual elevation : 0.0 m
(b) P4 : Pore water pressure (kPa)
(c) P5 : Pore water pressure (kPa)
(d) P6 : Pore water pressure
σmv' : bottom of manhole
(e) P10 : Pore water pressure (kPa)
Time (s)
Model No. 3
P8
A6
A5
P7
P5
D2
A4
A5
A7
Manhole
settlement:
255 mm
1m
P4
60 mm
P5
A6
P7
P6
P12
A0
(f) P7 : Pore water pressure (kPa)
(g) P8 : Pore water pressure (kPa)
(h) A5 : Acceleration (m/s2)
(i) A6 : Acceleration (m/s2)
(j) A7 : Acceleration (m/s2)
Time (s)

CS10

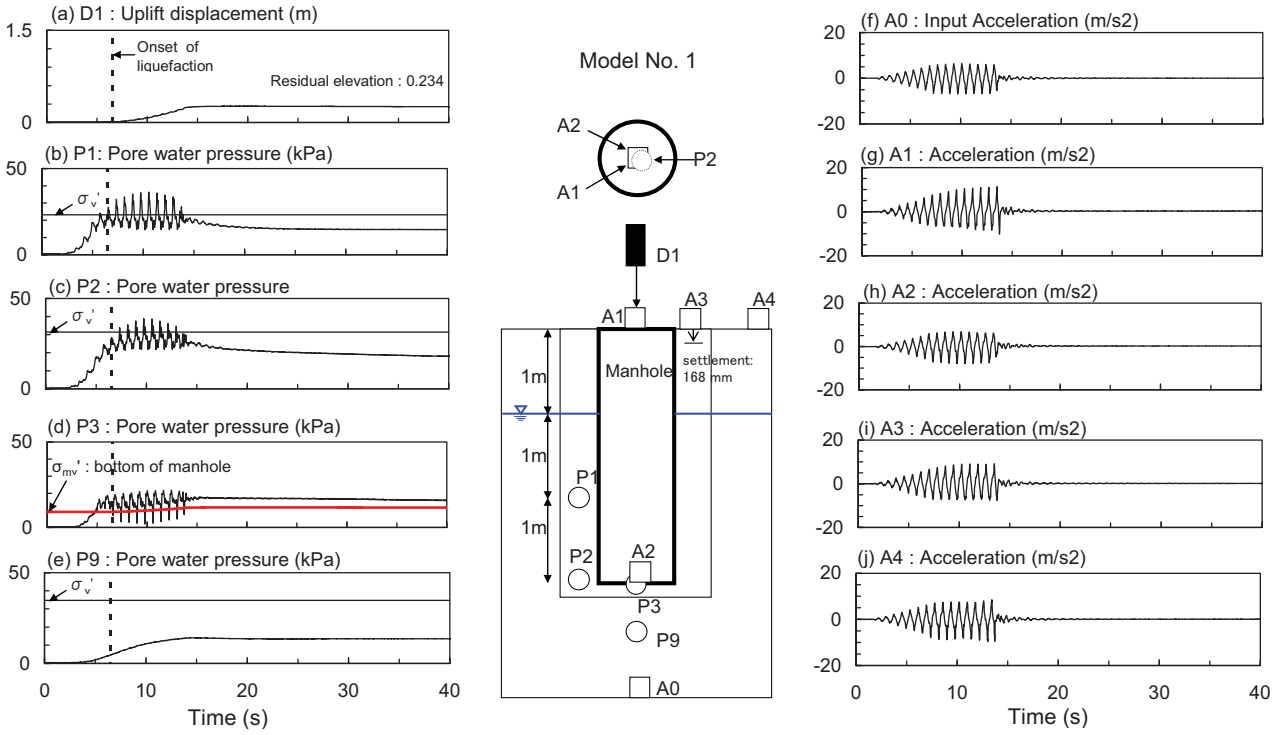
(a) D1 : Uplift displacement (m)
Onset of liquefaction
Residual elevation : 0.234
(b) P1: Pore water pressure (kPa)
(c) P2 : Pore water pressure
(d) P3 : Pore water pressure (kPa)
σmv' : bottom of manhole
(e) P9 : Pore water pressure (kPa)
Time (s)
Model No. 1
A2
P2
A1
D1
A3
A4
Manhole
settlement: 168 mm
1m
1m
1m
P1
P2
A2
P3
P9
A0
(f) A0 : Input Acceleration (m/s2)
(g) A1 : Acceleration (m/s2)
(h) A2 : Acceleration (m/s2)
(i) A3 : Acceleration (m/s2)
(j) A4 : Acceleration (m/s2)
Time (s)

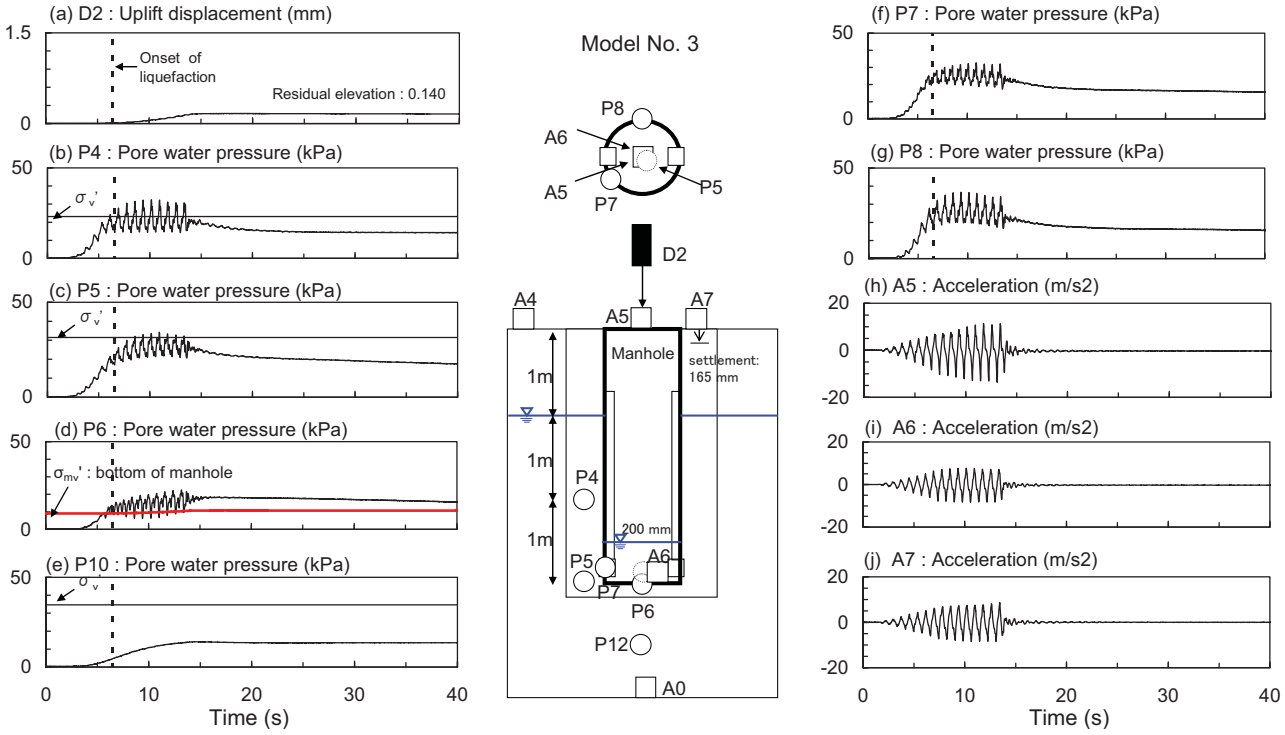
(a) D2 : Uplift displacement (mm)
Onset of liquefaction
Residual elevation : 0.140
(b) P4 : Pore water pressure (kPa)
(c) P5 : Pore water pressure (kPa)
(d) P6 : Pore water pressure (kPa)
σmv' : bottom of manhole
(e) P10 : Pore water pressure (kPa)
Time (s)
Model No. 3
P8
A6
A5
P7
P5
D2
A4
A5
A7
Manhole
settlement: 165 mm
1m
1m
1m
P4
200 mm
P5
A6
P7
P6
P12
A0
(f) P7 : Pore water pressure (kPa)
(g) P8 : Pore water pressure (kPa)
(h) A5 : Acceleration (m/s2)
(i) A6 : Acceleration (m/s2)
(j) A7 : Acceleration (m/s2)
Time (s)

CS11

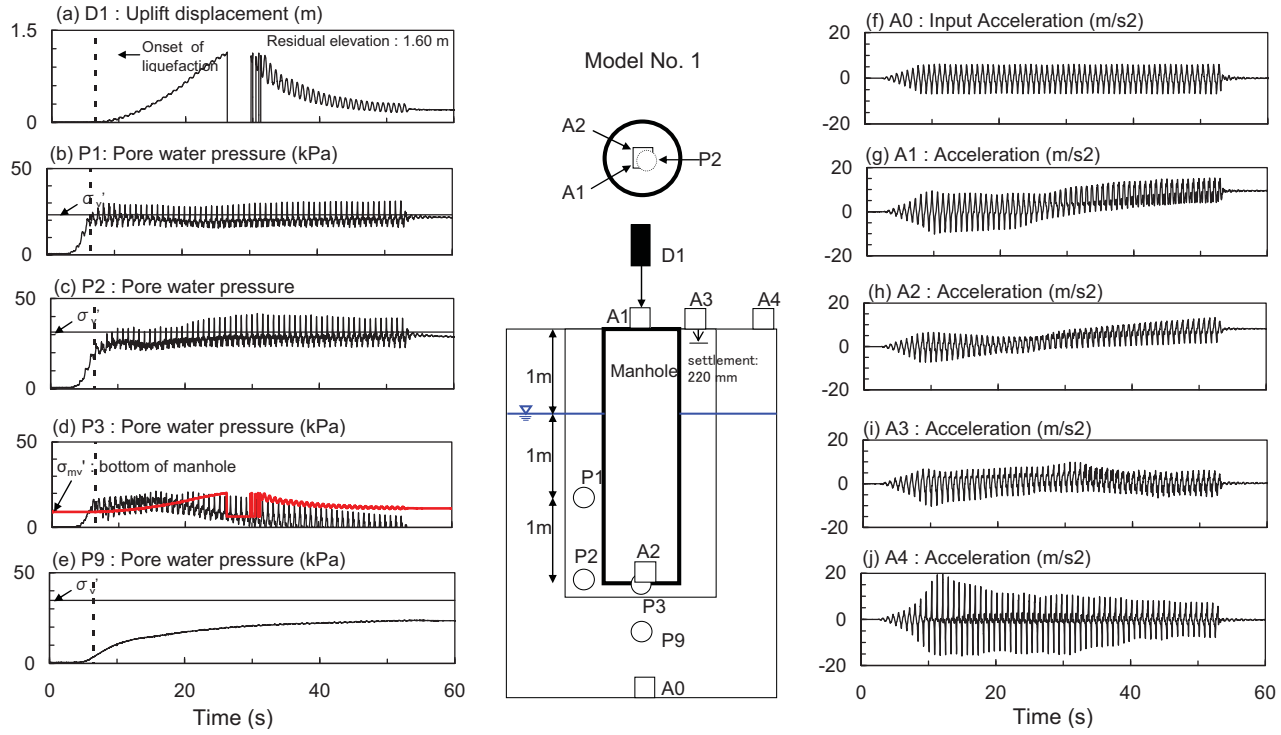
(a) D1 : Uplift displacement (m)
Onset of liquefaction
Residual elevation : 1.60 m
(b) P1: Pore water pressure (kPa)
(c) P2 : Pore water pressure
(d) P3 : Pore water pressure (kPa)
σmv' : bottom of manhole
(e) P9 : Pore water pressure (kPa)
Time (s)
Model No. 1
A2
P2
A1
D1
A3
A4
Manhole
settlement: 220 mm
1m
1m
1m
P1
P2
A2
P3
P9
A0
(f) A0 : Input Acceleration (m/s2)
(g) A1 : Acceleration (m/s2)
(h) A2 : Acceleration (m/s2)
(i) A3 : Acceleration (m/s2)
(j) A4 : Acceleration (m/s2)
Time (s)

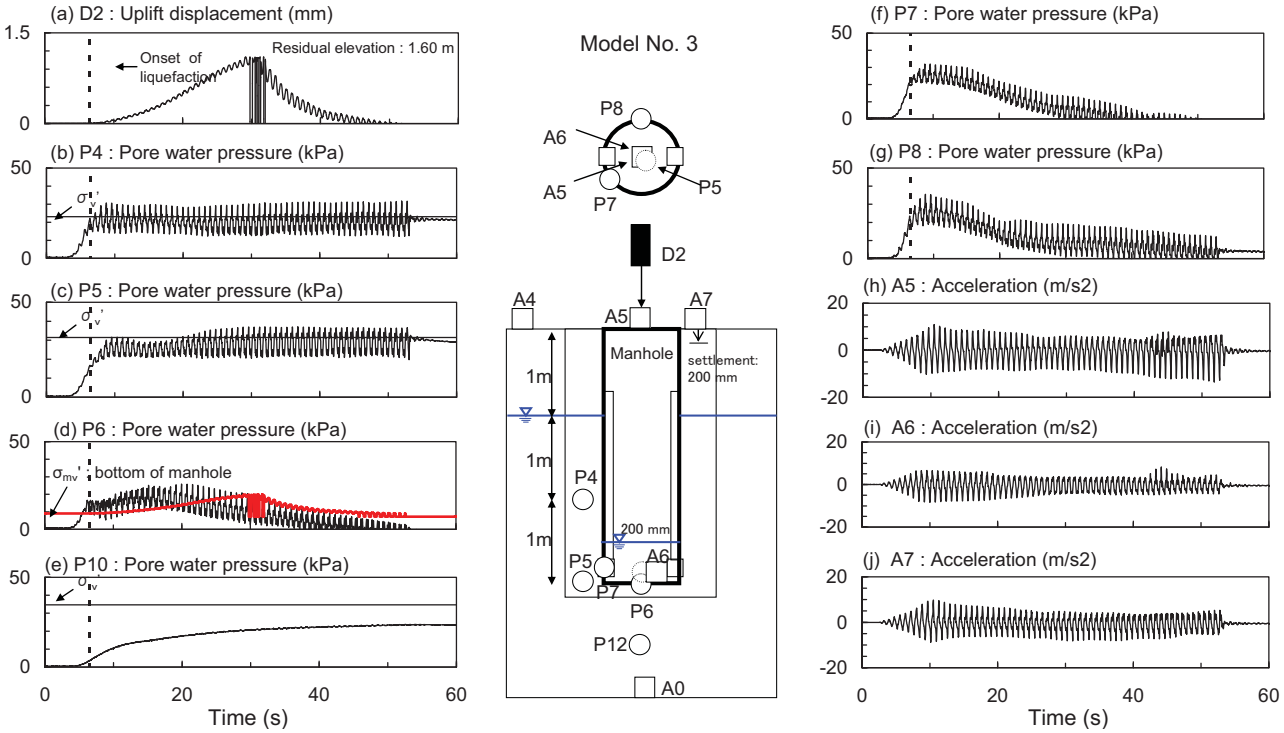
(a) D2 : Uplift displacement (mm)
Onset of liquefaction
Residual elevation : 1.60 m
(b) P4 : Pore water pressure (kPa)
(c) P5 : Pore water pressure (kPa)
(d) P6 : Pore water pressure (kPa)
σmv' : bottom of manhole
(e) P10 : Pore water pressure (kPa)
Time (s)
Model No. 3
P8
A6
A5
P7
P5
D2
A4
A5
A7
Manhole
settlement: 200 mm
1m
1m
1m
P4
200 mm
P5
A6
P7
P6
P12
A0
(f) P7 : Pore water pressure (kPa)
(g) P8 : Pore water pressure (kPa)
(h) A5 : Acceleration (m/s2)
(i) A6 : Acceleration (m/s2)
(j) A7 : Acceleration (m/s2)
Time (s)

CS12

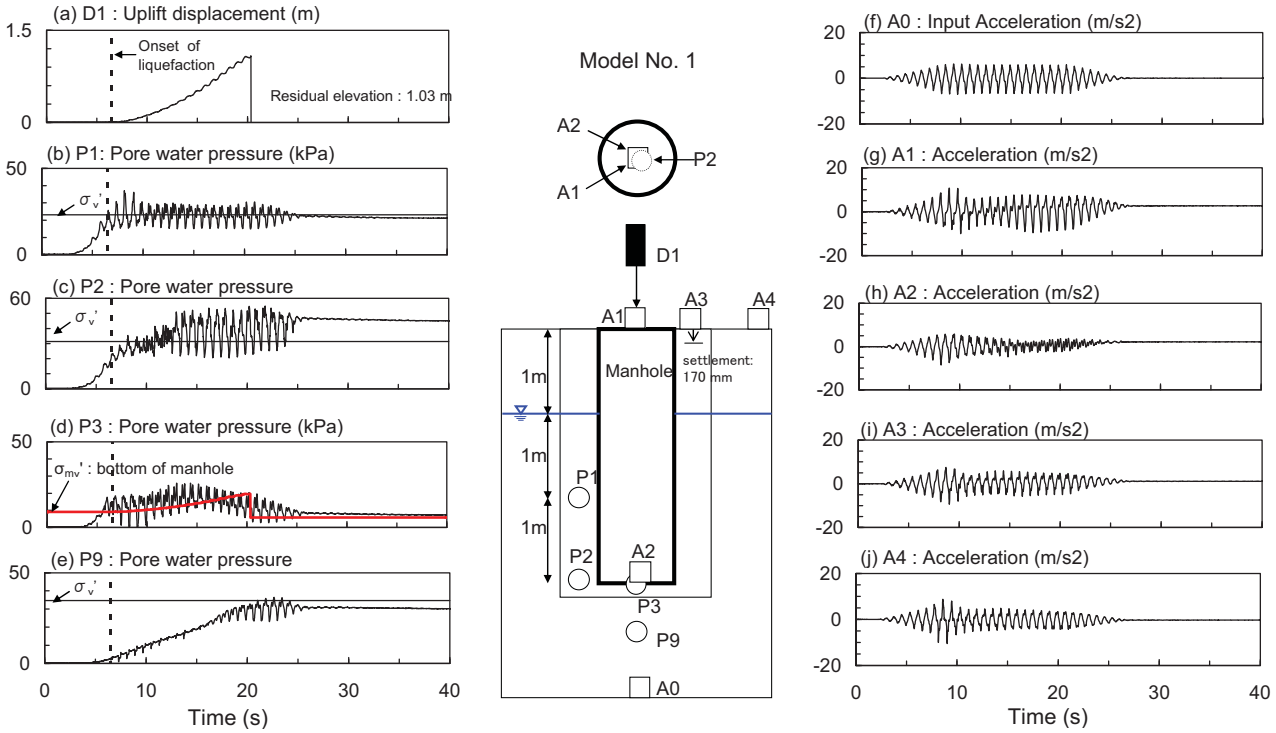
(a) D1 : Uplift displacement (m)
Onset of liquefaction
Residual elevation : 1.03 m
(b) P1: Pore water pressure (kPa)
(c) P2 : Pore water pressure
(d) P3 : Pore water pressure (kPa)
σmv' : bottom of manhole
(e) P9 : Pore water pressure
Time (s)
Model No. 1
A2
P2
A1
D1
A3
A4
Manhole
settlement: 170 mm
1m
P1
P2
A2
P3
P9
A0
(f) A0 : Input Acceleration (m/s2)
(g) A1 : Acceleration (m/s2)
(h) A2 : Acceleration (m/s2)
(i) A3 : Acceleration (m/s2)
(j) A4 : Acceleration (m/s2)
Time (s)

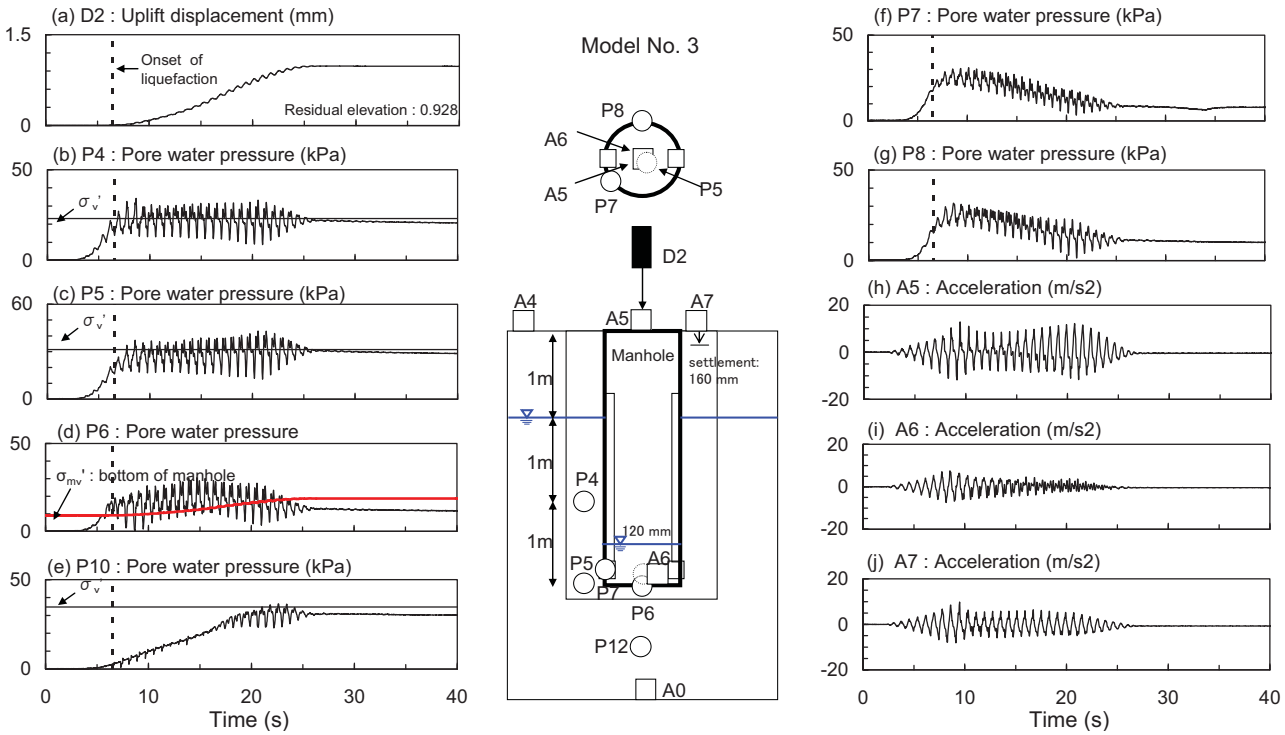
(a) D2 : Uplift displacement (mm)
Onset of liquefaction
Residual elevation : 0.928
(b) P4 : Pore water pressure (kPa)
(c) P5 : Pore water pressure (kPa)
(d) P6 : Pore water pressure
σmv' : bottom of manhole
(e) P10 : Pore water pressure (kPa)
Time (s)
Model No. 3
P8
A6
A5
P7
P5
D2
A4
A5
A7
Manhole
settlement: 160 mm
1m
P4
120 mm
P5
A6
P7
P6
P12
A0
(f) P7 : Pore water pressure (kPa)
(g) P8 : Pore water pressure (kPa)
(h) A5 : Acceleration (m/s2)
(i) A6 : Acceleration (m/s2)
(j) A7 : Acceleration (m/s2)
Time (s)

CS13

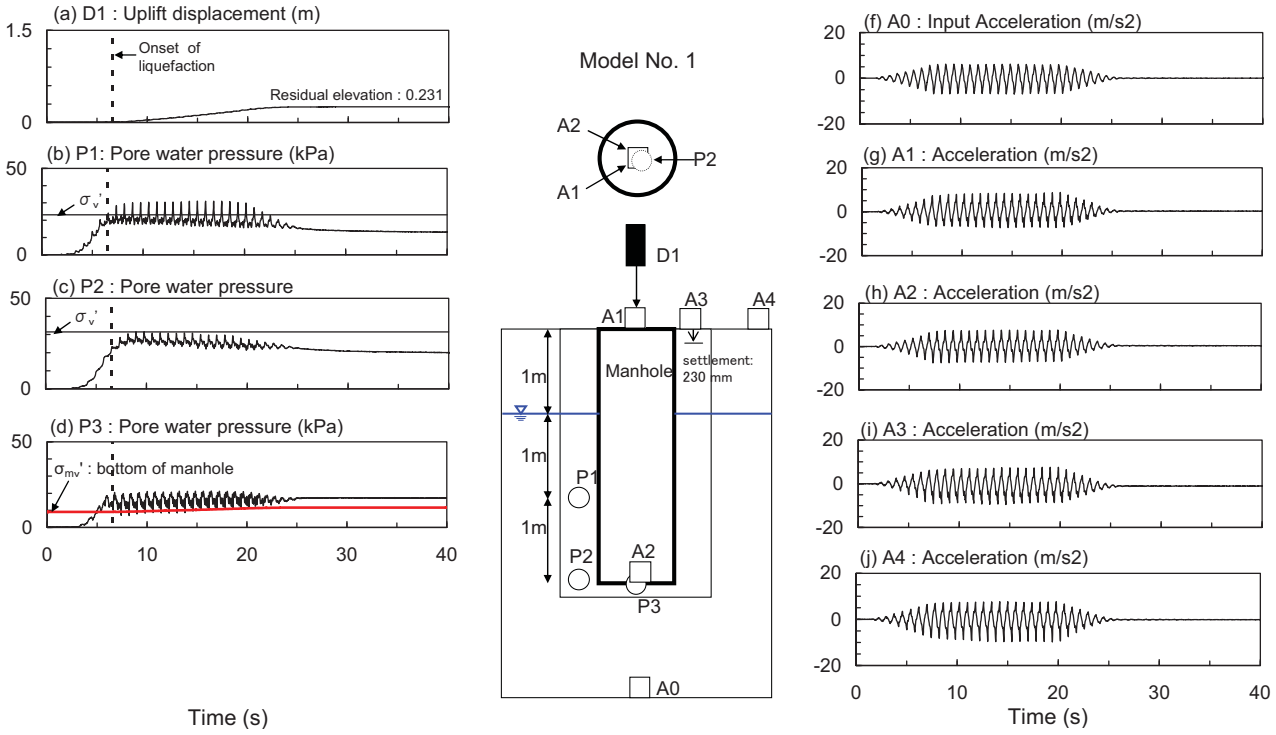
(a) D1 : Uplift displacement (m)
Onset of liquefaction
Residual elevation : 0.231
(b) P1: Pore water pressure (kPa)
(c) P2 : Pore water pressure
(d) P3 : Pore water pressure (kPa)
σmv' : bottom of manhole
Time (s)
Model No. 1
A2
P2
A1
D1
A3
A4
Manhole
settlement: 230 mm
1m
1m
1m
P1
P2
A2
P3
A0
(f) A0 : Input Acceleration (m/s2)
(g) A1 : Acceleration (m/s2)
(h) A2 : Acceleration (m/s2)
(i) A3 : Acceleration (m/s2)
(j) A4 : Acceleration (m/s2)
Time (s)

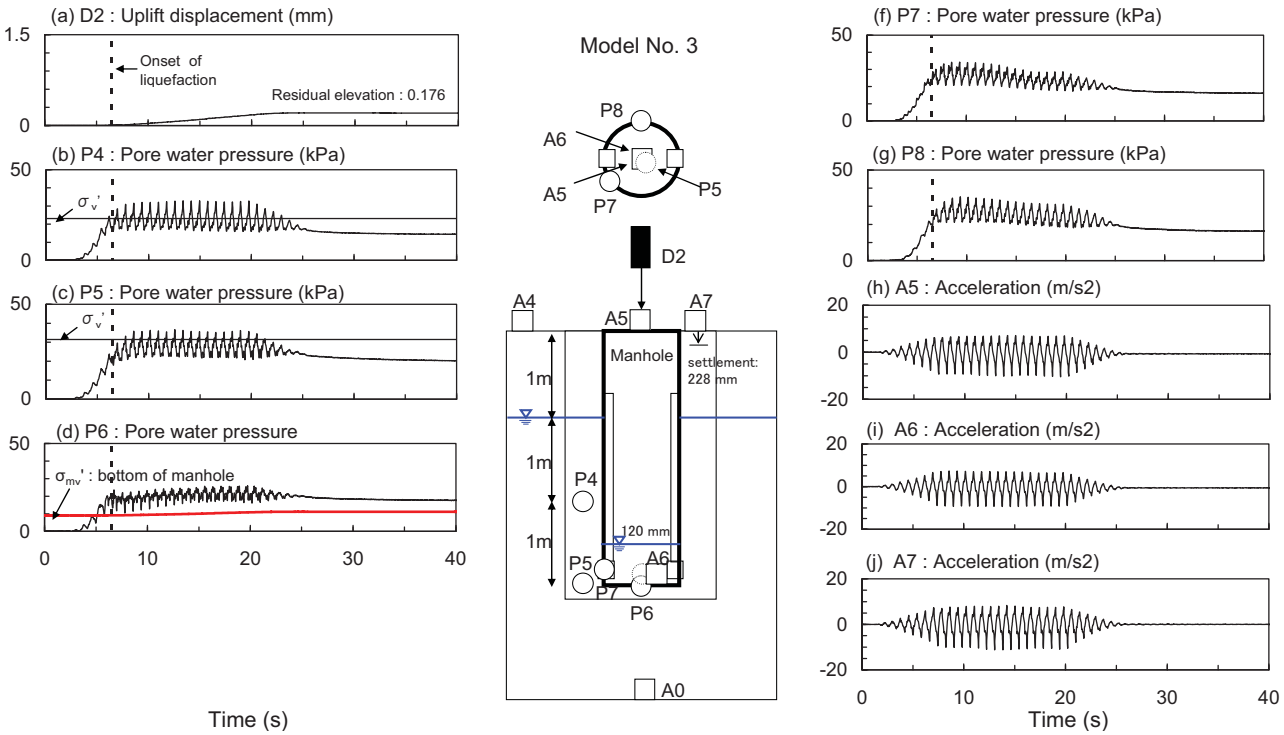
(a) D2 : Uplift displacement (mm)
Onset of liquefaction
Residual elevation : 0.176
(b) P4 : Pore water pressure (kPa)
(c) P5 : Pore water pressure (kPa)
(d) P6 : Pore water pressure
σmv' : bottom of manhole
Time (s)
Model No. 3
P8
A6
A5
P7
P5
D2
A4
A5
A7
Manhole
settlement: 228 mm
1m
1m
1m
P4
120 mm
P5
A6
P7
P6
A0
(f) P7 : Pore water pressure (kPa)
(g) P8 : Pore water pressure (kPa)
(h) A5 : Acceleration (m/s2)
(i) A6 : Acceleration (m/s2)
(j) A7 : Acceleration (m/s2)
Time (s)

CS14

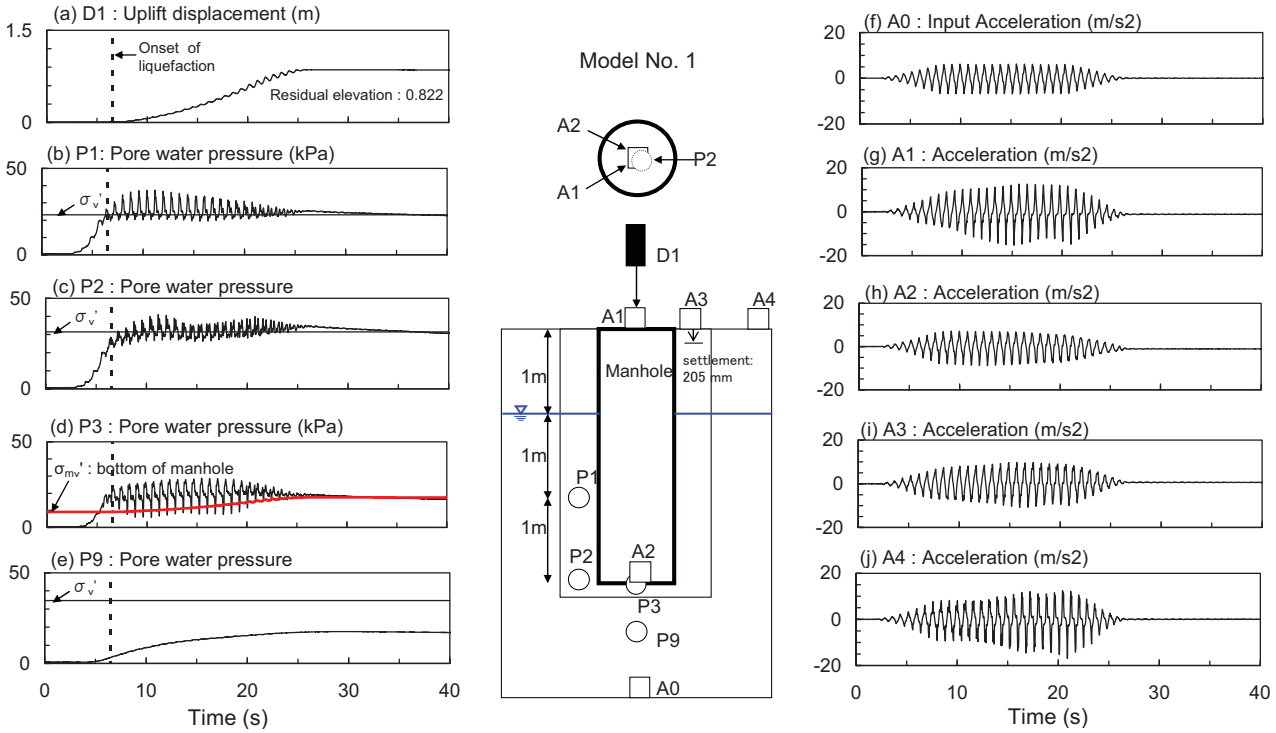
(a) D1 : Uplift displacement (m)
Onset of liquefaction
Residual elevation : 0.822
(b) P1: Pore water pressure (kPa)
(c) P2 : Pore water pressure
(d) P3 : Pore water pressure (kPa)
σmv' : bottom of manhole
(e) P9 : Pore water pressure
Time (s)
Model No. 1
A2
P2
A1
D1
A3
A4
Manhole
settlement: 205 mm
1m
P1
P2
A2
P3
P9
A0
(f) A0 : Input Acceleration (m/s2)
(g) A1 : Acceleration (m/s2)
(h) A2 : Acceleration (m/s2)
(i) A3 : Acceleration (m/s2)
(j) A4 : Acceleration (m/s2)
Time (s)

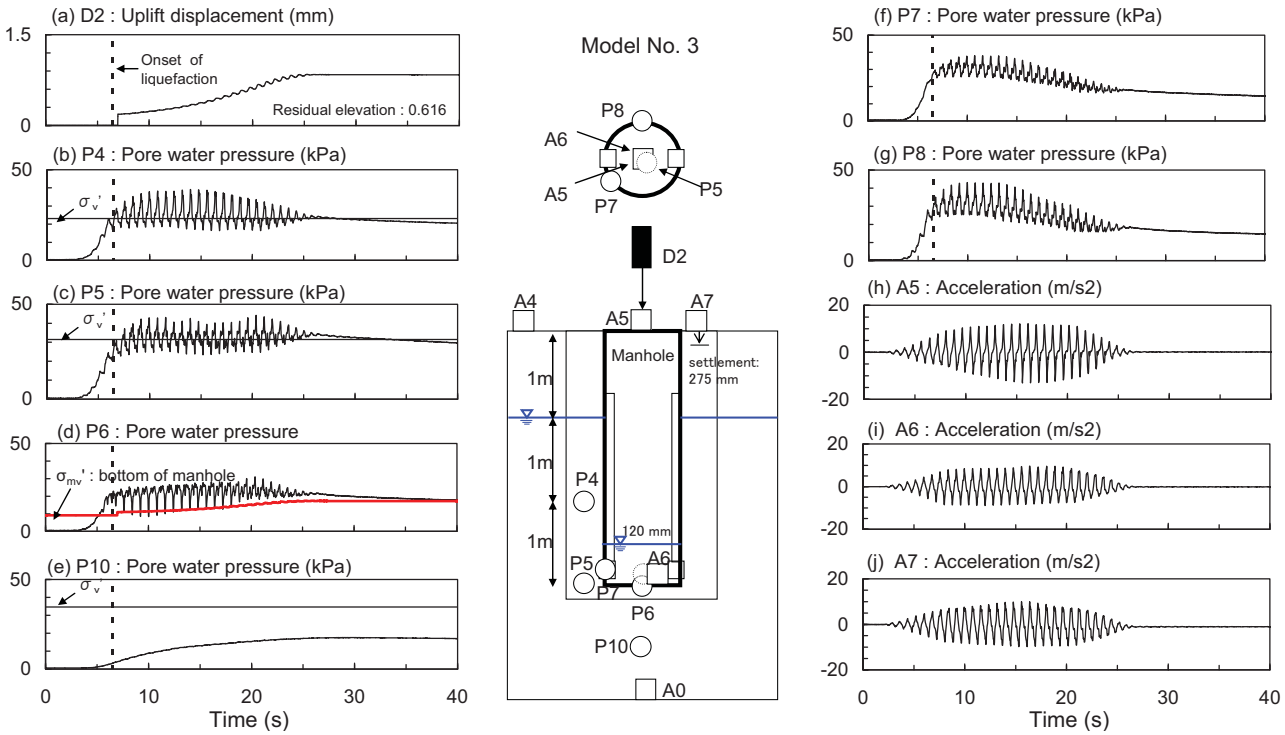
(a) D2 : Uplift displacement (mm)
Onset of liquefaction
Residual elevation : 0.616
(b) P4 : Pore water pressure (kPa)
(c) P5 : Pore water pressure (kPa)
(d) P6 : Pore water pressure
σmv' : bottom of manhole
(e) P10 : Pore water pressure (kPa)
Time (s)
Model No. 3
P8
A6
A5
P7
P5
D2
A4
A5
A7
Manhole
settlement: 275 mm
1m
P4
120 mm
P5
A6
P7
P6
P10
A0
(f) P7 : Pore water pressure (kPa)
(g) P8 : Pore water pressure (kPa)
(h) A5 : Acceleration (m/s2)
(i) A6 : Acceleration (m/s2)
(j) A7 : Acceleration (m/s2)
Time (s)

CS15

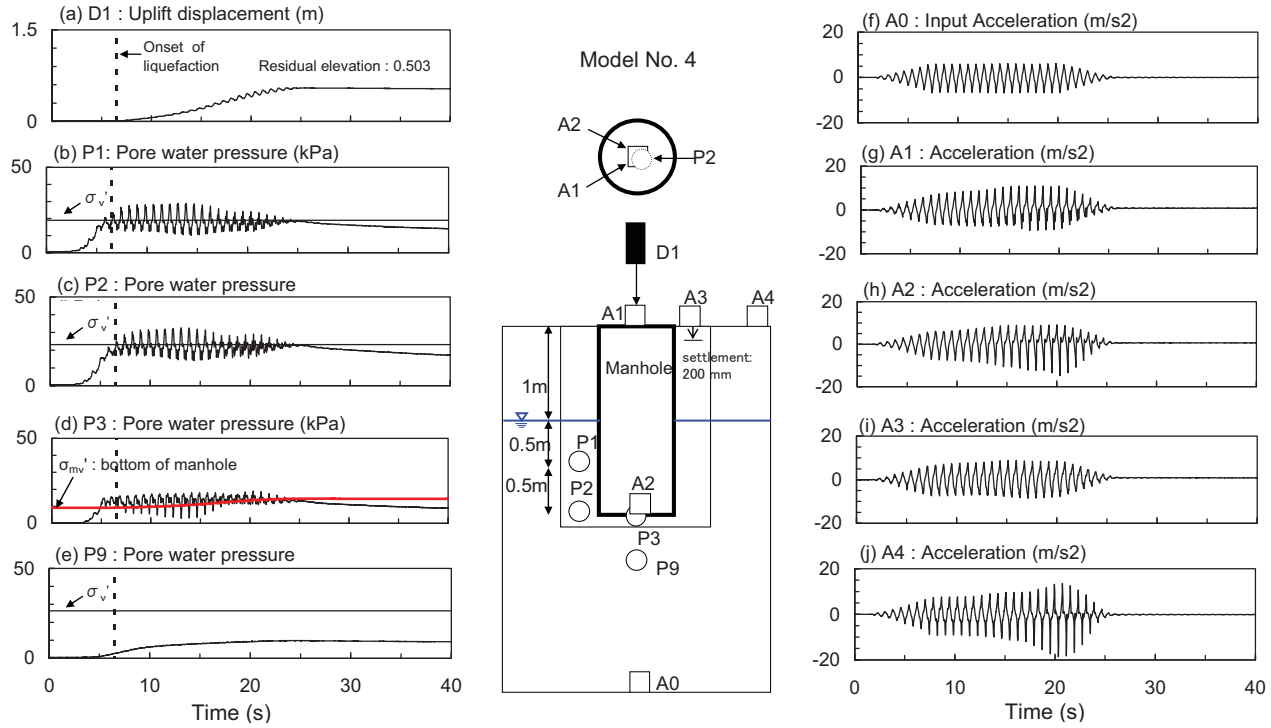
(a) D1 : Uplift displacement (m)
Onset of liquefaction
Residual elevation : 0.503
(b) P1: Pore water pressure (kPa)
(c) P2 : Pore water pressure
(d) P3 : Pore water pressure (kPa)
σmv' : bottom of manhole
(e) P9 : Pore water pressure
Time (s)
Model No. 4
A2
P2
A1
D1
A3
A4
Manhole
settlement: 200 mm
1m
0.5m
P1
0.5m
P2
A2
P3
P9
A0
(f) A0 : Input Acceleration (m/s2)
(g) A1 : Acceleration (m/s2)
(h) A2 : Acceleration (m/s2)
(i) A3 : Acceleration (m/s2)
(j) A4 : Acceleration (m/s2)
Time (s)

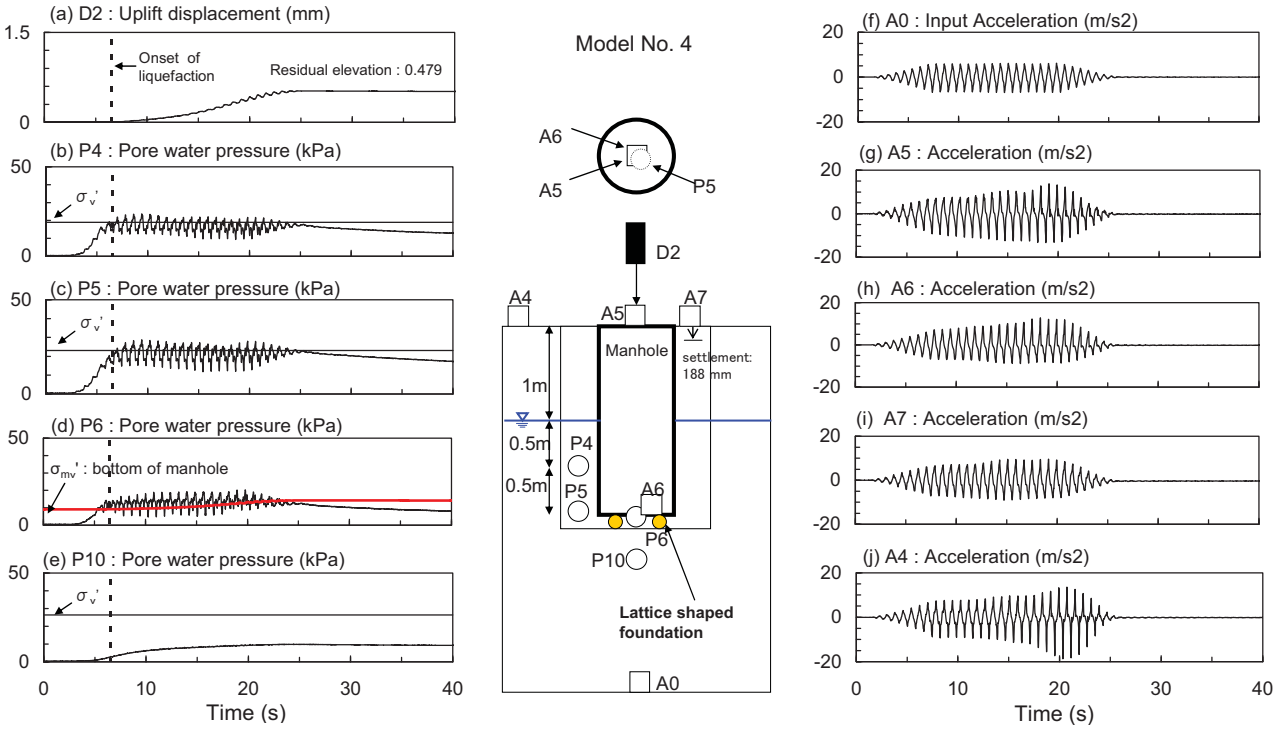
(a) D2 : Uplift displacement (mm)
Onset of liquefaction
Residual elevation : 0.479
(b) P4 : Pore water pressure (kPa)
(c) P5 : Pore water pressure (kPa)
(d) P6 : Pore water pressure (kPa)
σmv' : bottom of manhole
(e) P10 : Pore water pressure (kPa)
Time (s)
Model No. 4
A6
A5
P5
D2
A4
A5
A7
Manhole
settlement: 188 mm
1m
0.5m
P4
0.5m
P5
A6
P6
P10
Lattice shaped foundation
A0
(f) A0 : Input Acceleration (m/s2)
(g) A5 : Acceleration (m/s2)
(h) A6 : Acceleration (m/s2)
(i) A7 : Acceleration (m/s2)
(j) A4 : Acceleration (m/s2)
Time (s)

CS16

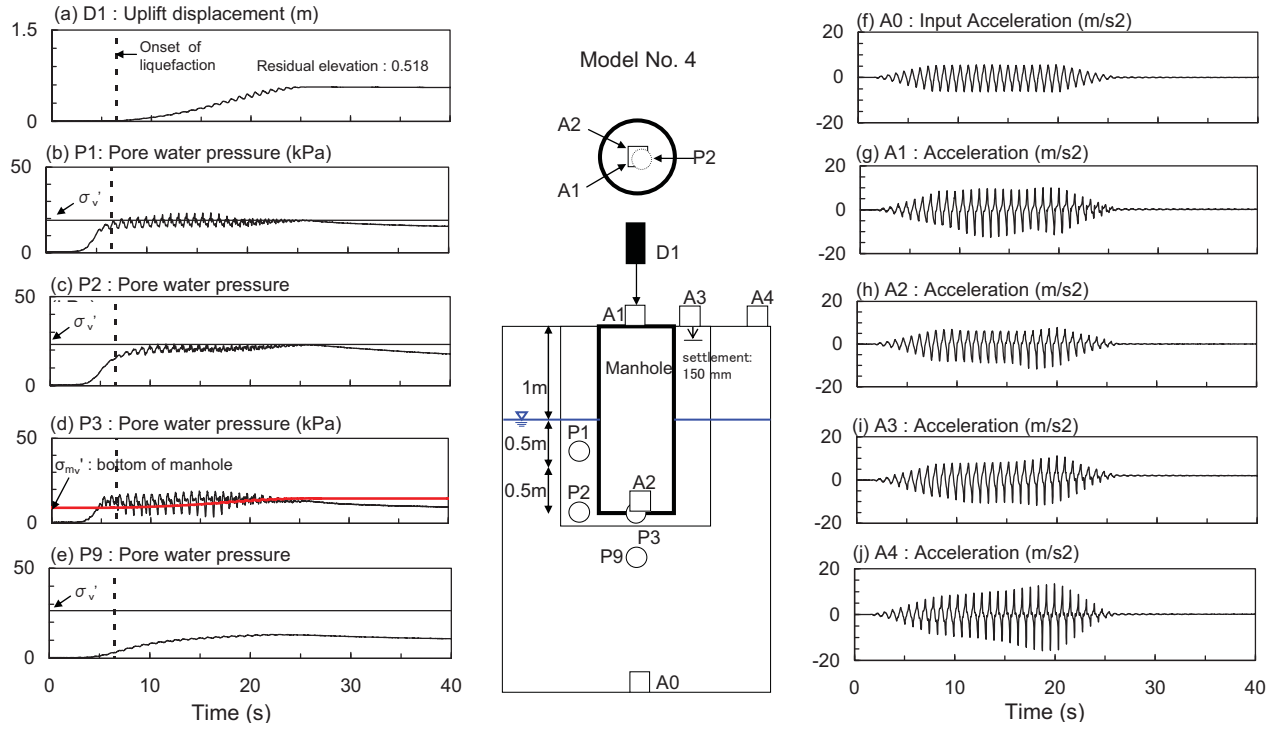
(a) D1 : Uplift displacement (m)
Onset of liquefaction
Residual elevation : 0.518
(b) P1: Pore water pressure (kPa)
(c) P2 : Pore water pressure
(d) P3 : Pore water pressure (kPa)
σmv' : bottom of manhole
(e) P9 : Pore water pressure
Time (s)
Model No. 4
A2
P2
A1
D1
A3
A4
Manhole
settlement: 150 mm
1m
0.5m
P1
0.5m
P2
A2
P3
P9
A0
(f) A0 : Input Acceleration (m/s2)
(g) A1 : Acceleration (m/s2)
(h) A2 : Acceleration (m/s2)
(i) A3 : Acceleration (m/s2)
(j) A4 : Acceleration (m/s2)
Time (s)

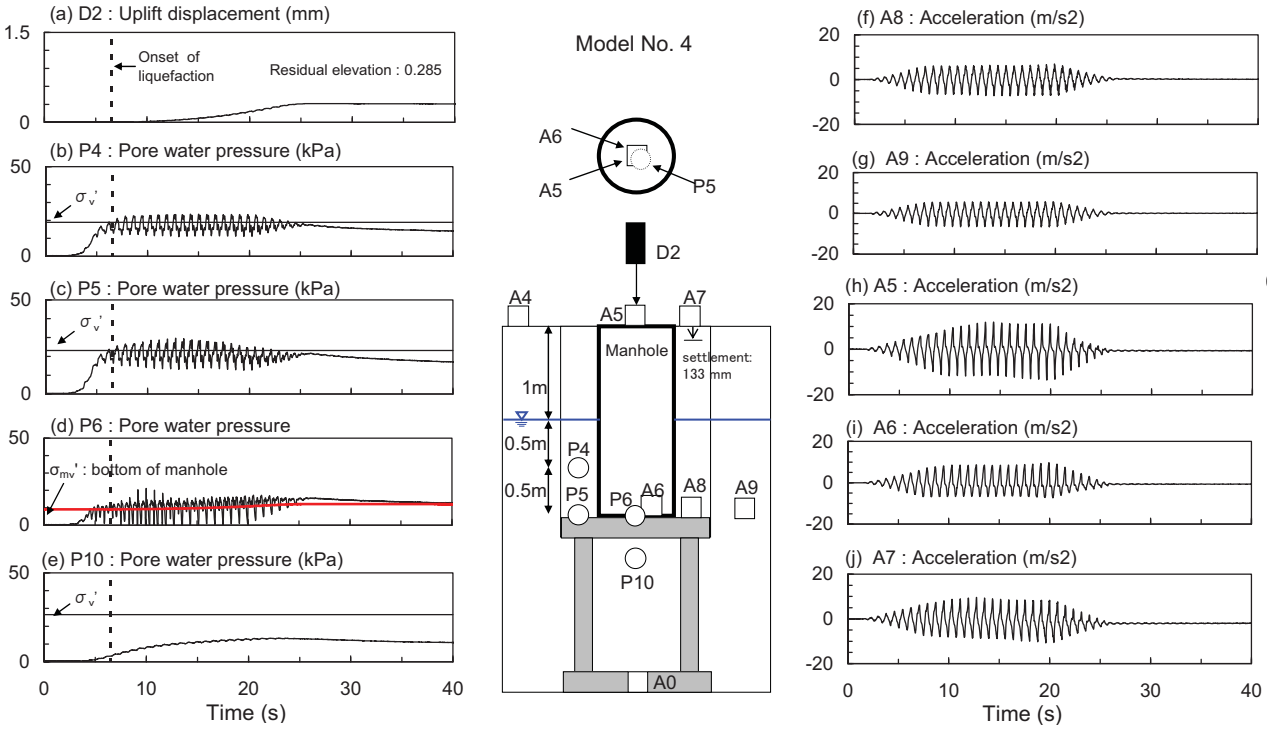
(a) D2 : Uplift displacement (mm)
Onset of liquefaction
Residual elevation : 0.285
(b) P4 : Pore water pressure (kPa)
(c) P5 : Pore water pressure (kPa)
(d) P6 : Pore water pressure
σmv' : bottom of manhole
(e) P10 : Pore water pressure (kPa)
Time (s)
Model No. 4
A6
A5
P5
D2
A4
A5
A7
Manhole
settlement: 133 mm
1m
0.5m
P4
0.5m
P5
P6
A6
A8
A9
P10
A0
(f) A8 : Acceleration (m/s2)
(g) A9 : Acceleration (m/s2)
(h) A5 : Acceleration (m/s2)
(i) A6 : Acceleration (m/s2)
(j) A7 : Acceleration (m/s2)
Time (s)

CS17

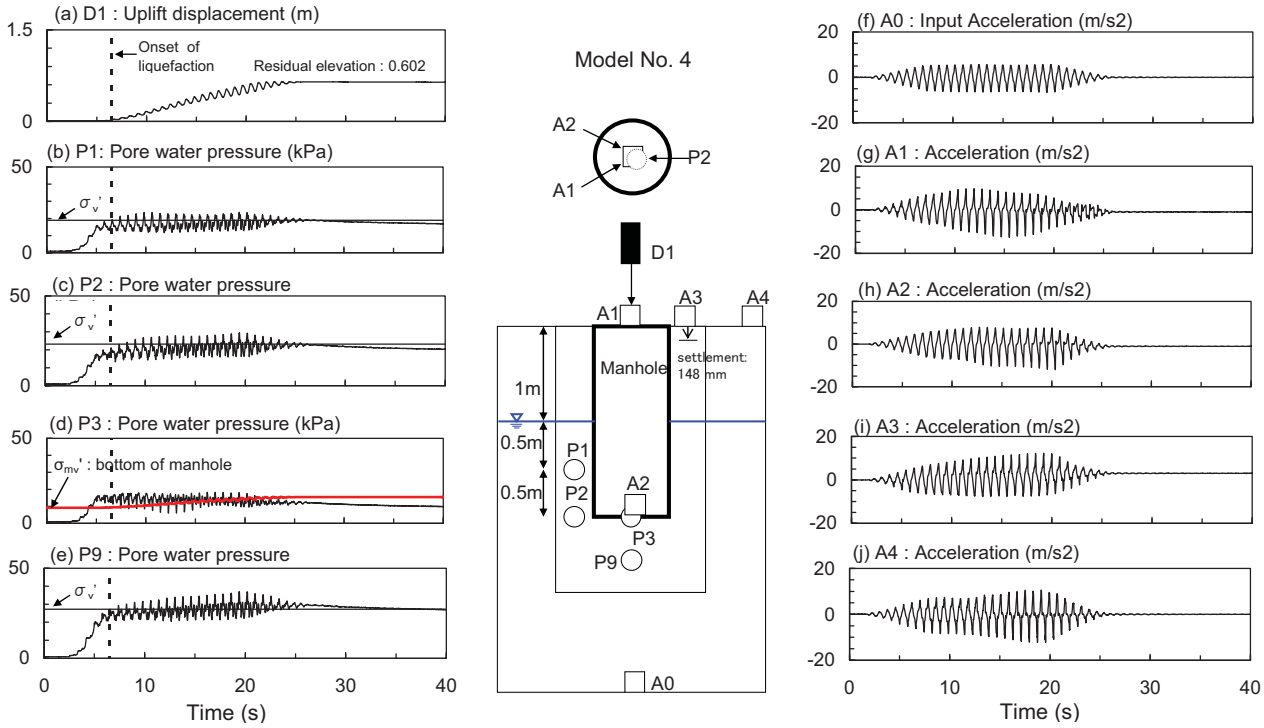
(a) D1 : Uplift displacement (m)
Onset of liquefaction
Residual elevation : 0.602
(b) P1: Pore water pressure (kPa)
(c) P2 : Pore water pressure
(d) P3 : Pore water pressure (kPa)
σmv' : bottom of manhole
(e) P9 : Pore water pressure
Time (s)
Model No. 4
A2
P2
A1
D1
A3
A4
Manhole
settlement: 148 mm
1m
0.5m
0.5m
P1
P2
A2
P3
P9
A0
(f) A0 : Input Acceleration (m/s2)
(g) A1 : Acceleration (m/s2)
(h) A2 : Acceleration (m/s2)
(i) A3 : Acceleration (m/s2)
(j) A4 : Acceleration (m/s2)
Time (s)

CS18

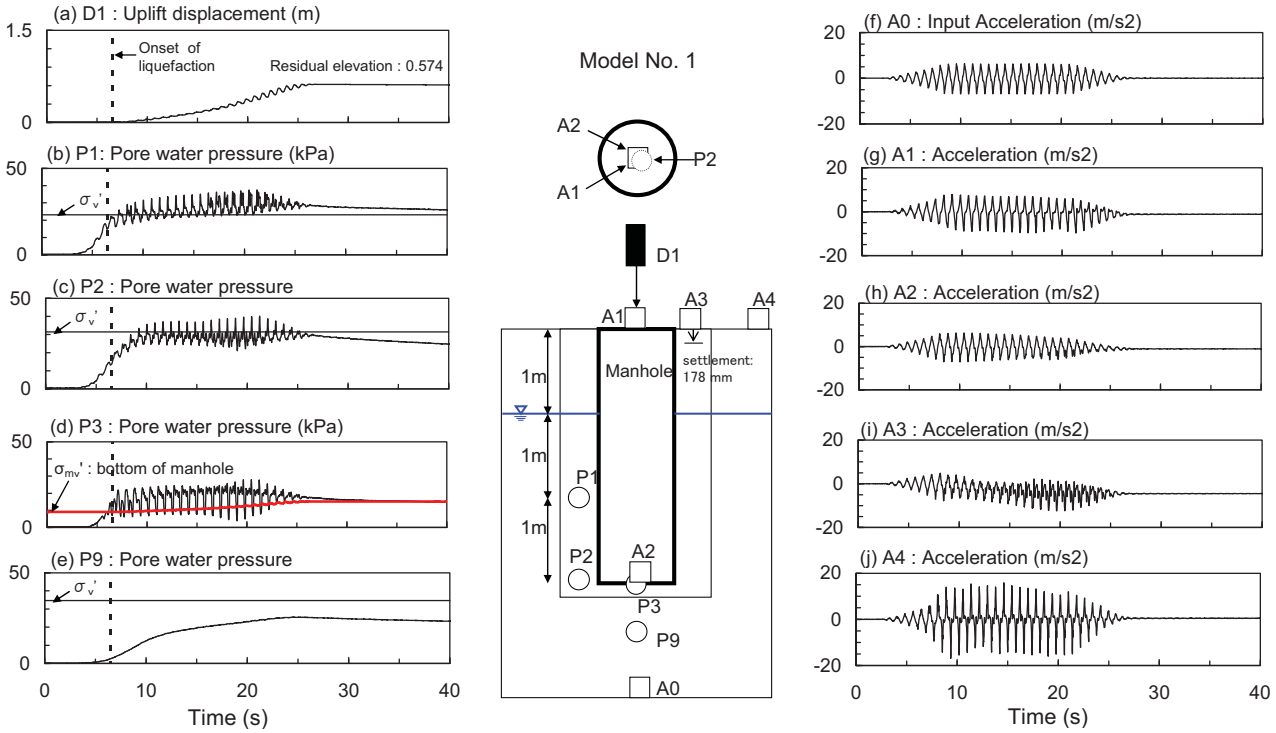
(a) D1 : Uplift displacement (m)
Onset of liquefaction
Residual elevation : 0.574
(b) P1: Pore water pressure (kPa)
(c) P2 : Pore water pressure
(d) P3 : Pore water pressure (kPa)
σmv' : bottom of manhole
(e) P9 : Pore water pressure
Time (s)
Model No. 1
A2
P2
A1
D1
A3
A4
Manhole
settlement: 178 mm
1m
1m
1m
P1
P2
A2
P3
P9
A0
(f) A0 : Input Acceleration (m/s2)
(g) A1 : Acceleration (m/s2)
(h) A2 : Acceleration (m/s2)
(i) A3 : Acceleration (m/s2)
(j) A4 : Acceleration (m/s2)
Time (s)

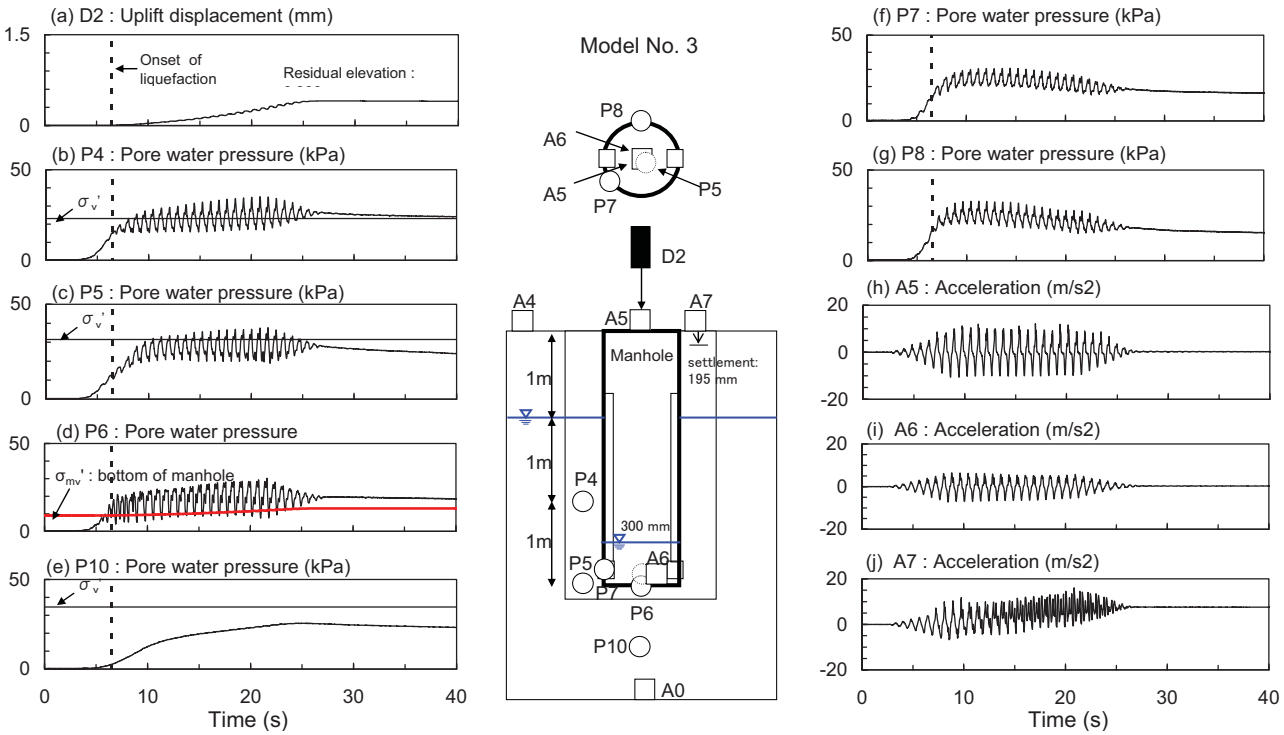
(a) D2 : Uplift displacement (mm)
Onset of liquefaction
Residual elevation :
(b) P4 : Pore water pressure (kPa)
(c) P5 : Pore water pressure (kPa)
(d) P6 : Pore water pressure
σmv' : bottom of manhole
(e) P10 : Pore water pressure (kPa)
Time (s)
Model No. 3
P8
A6
A5
P7
P5
D2
A4
A5
A7
Manhole
settlement: 195 mm
1m
1m
1m
P4
300 mm
P5
A6
P7
P6
P10
A0
(f) P7 : Pore water pressure (kPa)
(g) P8 : Pore water pressure (kPa)
(h) A5 : Acceleration (m/s2)
(i) A6 : Acceleration (m/s2)
(j) A7 : Acceleration (m/s2)
Time (s)

CS19

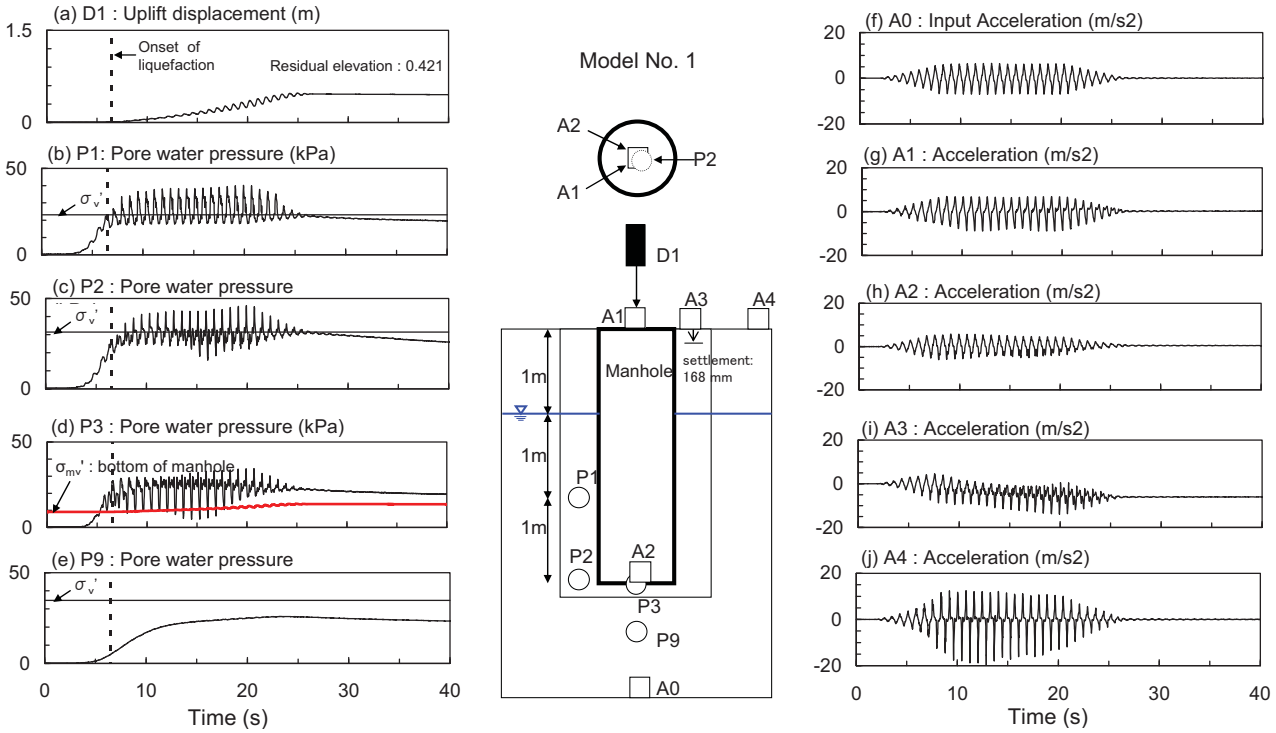
(a) D1 : Uplift displacement (m)
Onset of liquefaction
Residual elevation : 0.421
(b) P1: Pore water pressure (kPa)
(c) P2 : Pore water pressure
(d) P3 : Pore water pressure (kPa)
σmv' : bottom of manhole
(e) P9 : Pore water pressure
Time (s)
Model No. 1
A2
P2
A1
D1
A3
A4
Manhole
settlement: 168 mm
1m
P1
P2
A2
P3
P9
A0
(f) A0 : Input Acceleration (m/s2)
(g) A1 : Acceleration (m/s2)
(h) A2 : Acceleration (m/s2)
(i) A3 : Acceleration (m/s2)
(j) A4 : Acceleration (m/s2)
Time (s)

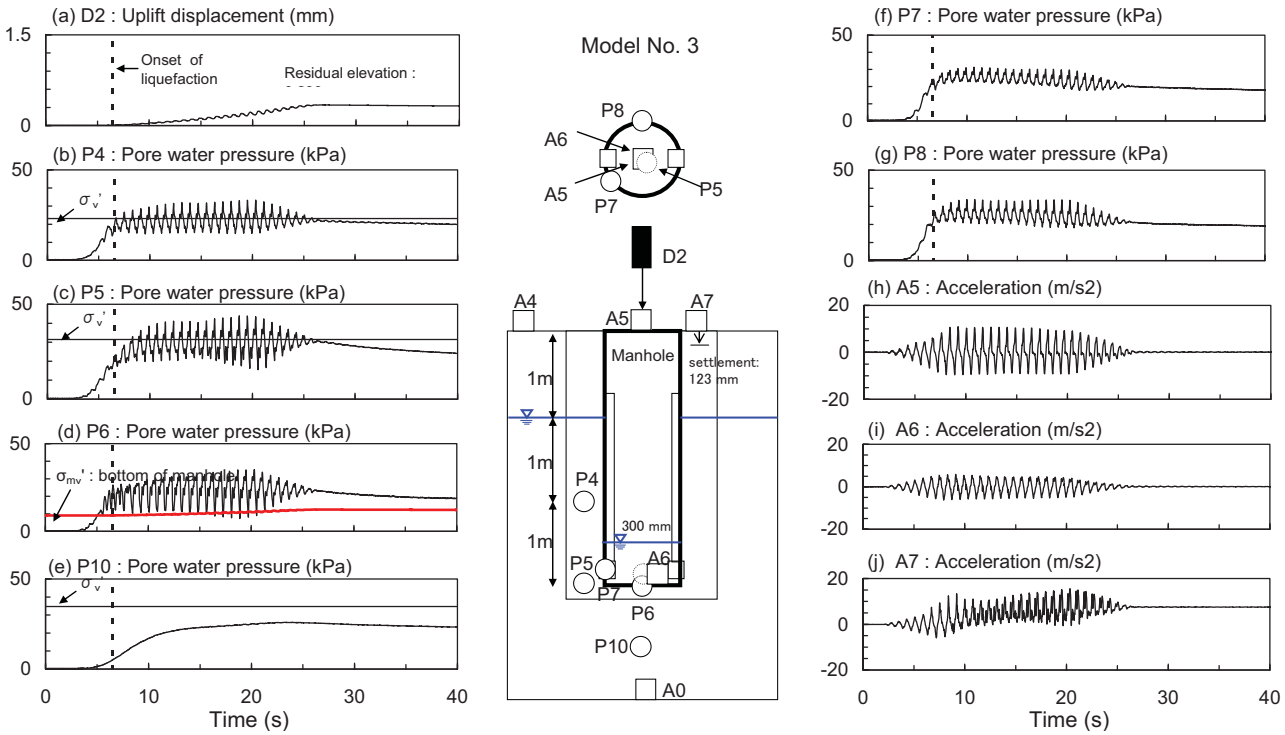
(a) D2 : Uplift displacement (mm)
Onset of liquefaction
Residual elevation :
(b) P4 : Pore water pressure (kPa)
(c) P5 : Pore water pressure (kPa)
(d) P6 : Pore water pressure (kPa)
σmv' : bottom of manhole
(e) P10 : Pore water pressure (kPa)
Time (s)
Model No. 3
P8
A6
A5
P7
P5
D2
A4
A5
A7
Manhole
settlement: 123 mm
1m
P4
300 mm
P5
A6
P7
P6
P10
A0
(f) P7 : Pore water pressure (kPa)
(g) P8 : Pore water pressure (kPa)
(h) A5 : Acceleration (m/s2)
(i) A6 : Acceleration (m/s2)
(j) A7 : Acceleration (m/s2)
Time (s)

CS20

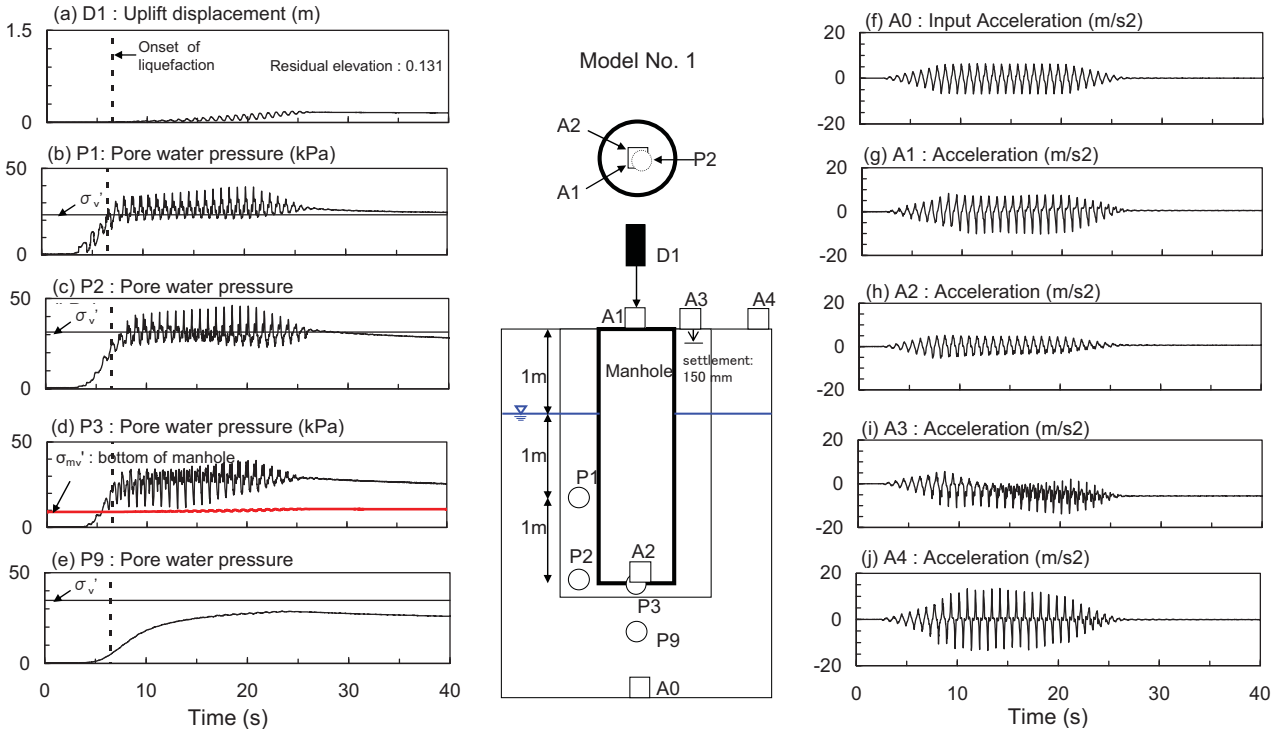
(a) D1 : Uplift displacement (m)
Onset of liquefaction
Residual elevation : 0.131
(b) P1: Pore water pressure (kPa)
(c) P2 : Pore water pressure
(d) P3 : Pore water pressure (kPa)
σmv' : bottom of manhole
(e) P9 : Pore water pressure
Time (s)
Model No. 1
A2
P2
A1
D1
A3
A4
Manhole
settlement: 150 mm
1m
P1
P2
A2
P3
P9
A0
(f) A0 : Input Acceleration (m/s2)
(g) A1 : Acceleration (m/s2)
(h) A2 : Acceleration (m/s2)
(i) A3 : Acceleration (m/s2)
(j) A4 : Acceleration (m/s2)
Time (s)

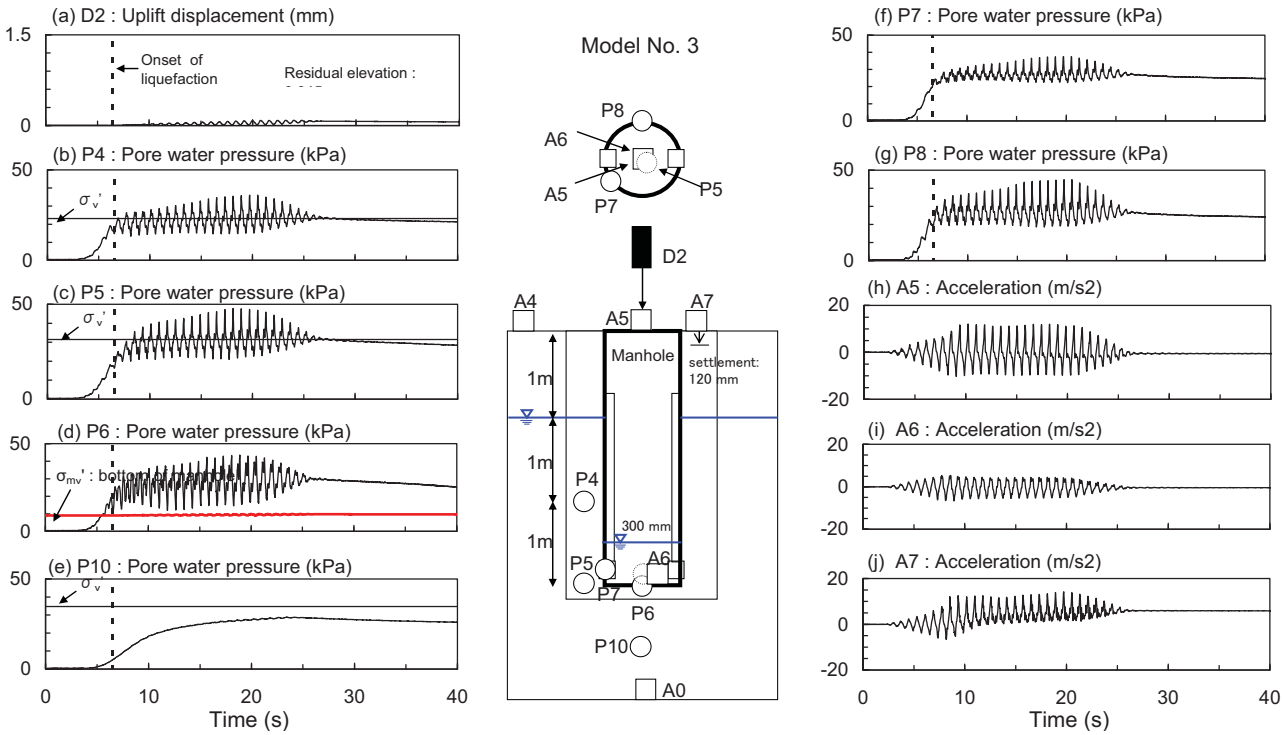
(a) D2 : Uplift displacement (mm)
Onset of liquefaction
Residual elevation :
(b) P4 : Pore water pressure (kPa)
(c) P5 : Pore water pressure (kPa)
(d) P6 : Pore water pressure (kPa)
σmv' : bottom of manhole
(e) P10 : Pore water pressure (kPa)
Time (s)
Model No. 3
P8
A6
A5
P7
P5
D2
A4
A5
A7
Manhole
settlement: 120 mm
1m
P4
300 mm
P5
A6
P7
P6
P10
A0
(f) P7 : Pore water pressure (kPa)
(g) P8 : Pore water pressure (kPa)
(h) A5 : Acceleration (m/s2)
(i) A6 : Acceleration (m/s2)
(j) A7 : Acceleration (m/s2)
Time (s)

CS21

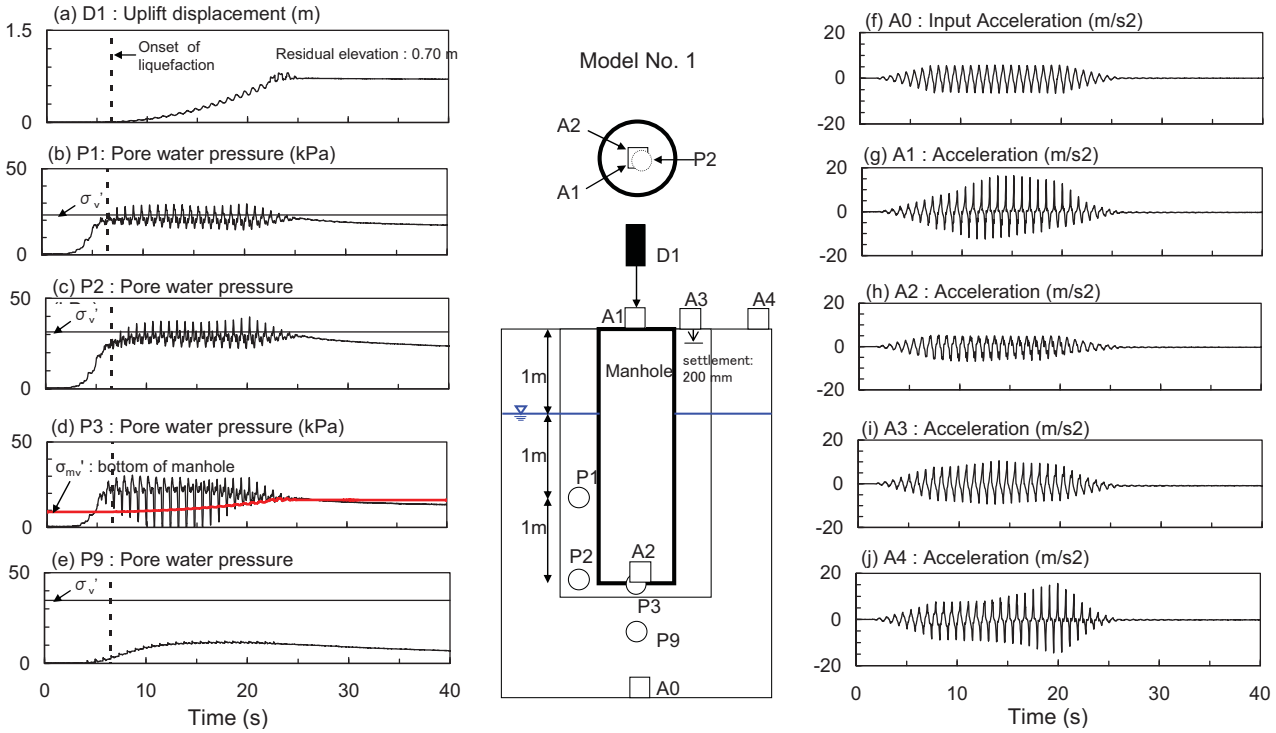
(a) D1 : Uplift displacement (m)
Onset of liquefaction
Residual elevation : 0.70 m
(b) P1: Pore water pressure (kPa)
(c) P2 : Pore water pressure
(d) P3 : Pore water pressure (kPa)
σmv' : bottom of manhole
(e) P9 : Pore water pressure
Time (s)
Model No. 1
A2
P2
A1
D1
A3
A4
Manhole
settlement: 200 mm
1m
P1
P2
A2
P3
P9
A0
(f) A0 : Input Acceleration (m/s2)
(g) A1 : Acceleration (m/s2)
(h) A2 : Acceleration (m/s2)
(i) A3 : Acceleration (m/s2)
(j) A4 : Acceleration (m/s2)
Time (s)

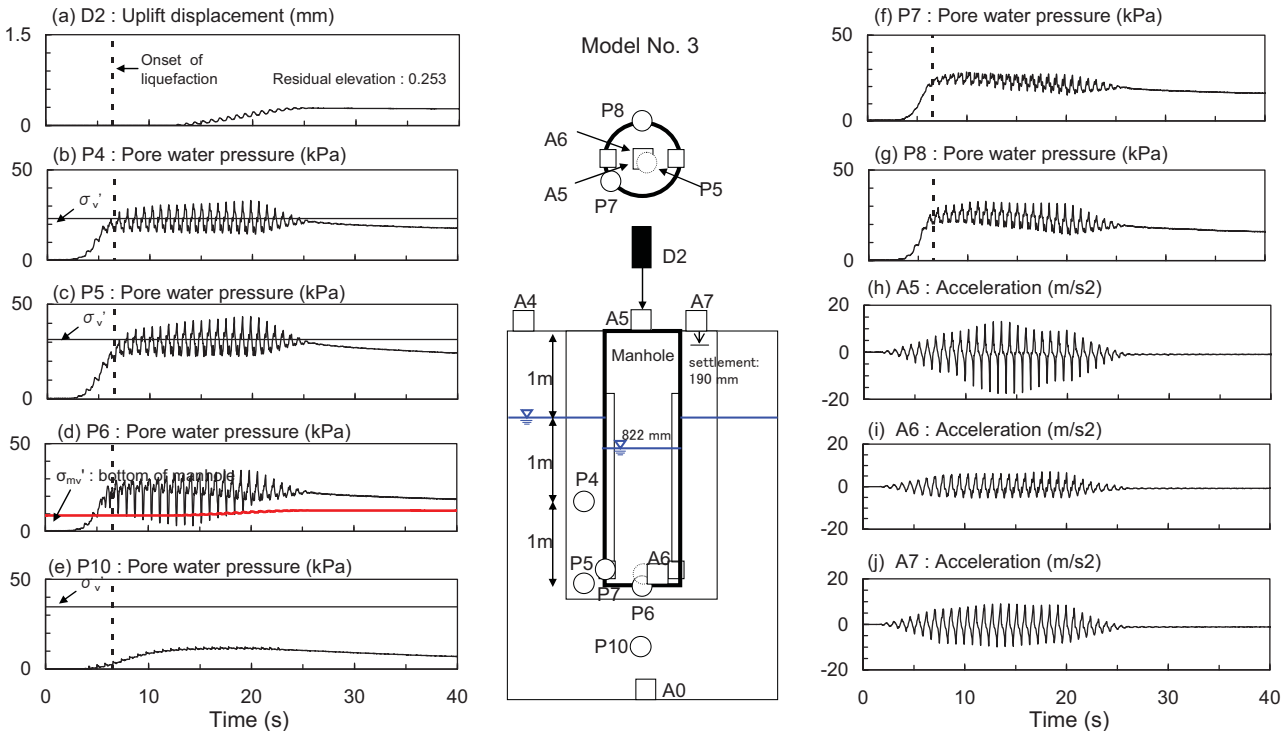
(a) D2 : Uplift displacement (mm)
Onset of liquefaction
Residual elevation : 0.253
(b) P4 : Pore water pressure (kPa)
(c) P5 : Pore water pressure (kPa)
(d) P6 : Pore water pressure (kPa)
σmv' : bottom of manhole
(e) P10 : Pore water pressure (kPa)
Time (s)
Model No. 3
P8
A6
A5
P7
P5
D2
A4
A5
A7
Manhole
settlement: 190 mm
822 mm
1m
P4
P5
A6
P7
P6
P10
A0
(f) P7 : Pore water pressure (kPa)
(g) P8 : Pore water pressure (kPa)
(h) A5 : Acceleration (m/s2)
(i) A6 : Acceleration (m/s2)
(j) A7 : Acceleration (m/s2)
Time (s)

CS22

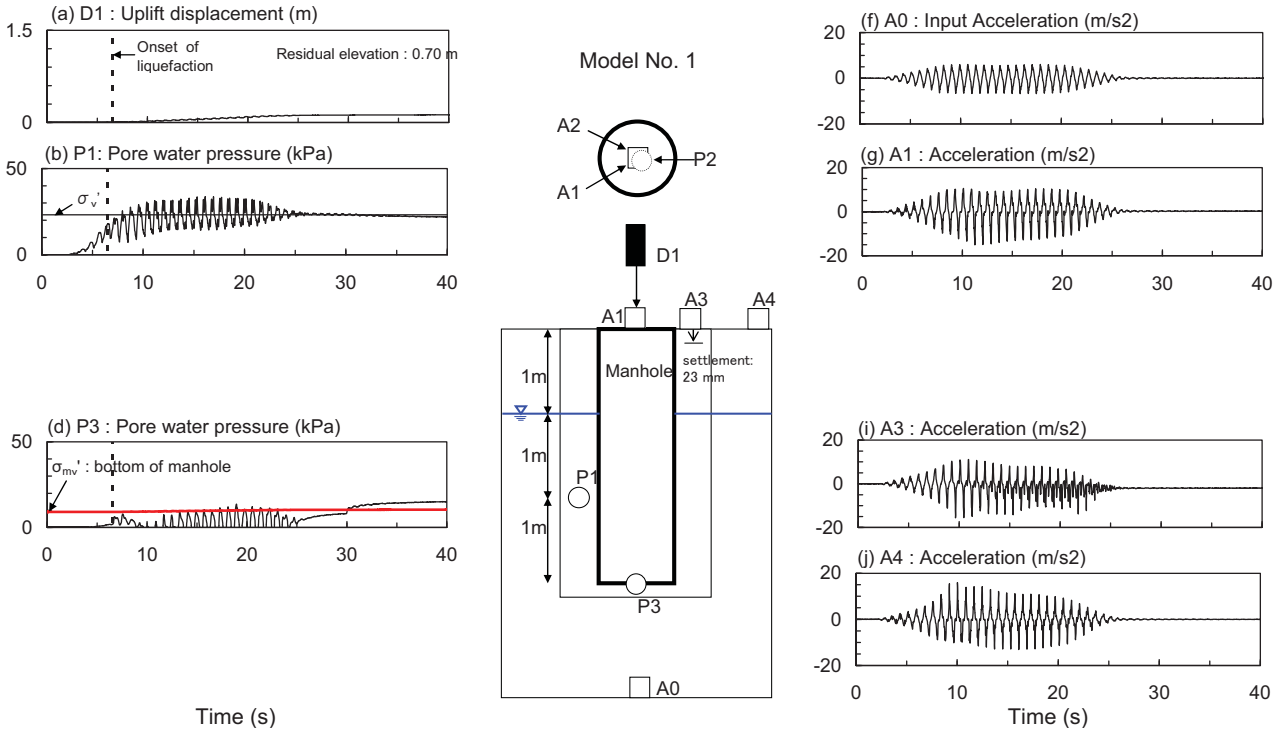
(a) D1 : Uplift displacement (m)
Onset of liquefaction
Residual elevation : 0.70 m
(b) P1: Pore water pressure (kPa)
(d) P3 : Pore water pressure (kPa)
σmv' : bottom of manhole
Time (s)
Model No. 1
A2
P2
A1
D1
A3
A4
Manhole
settlement: 23 mm
1m
P1
P3
A0
(f) A0 : Input Acceleration (m/s2)
(g) A1 : Acceleration (m/s2)
(i) A3 : Acceleration (m/s2)
(j) A4 : Acceleration (m/s2)
Time (s)

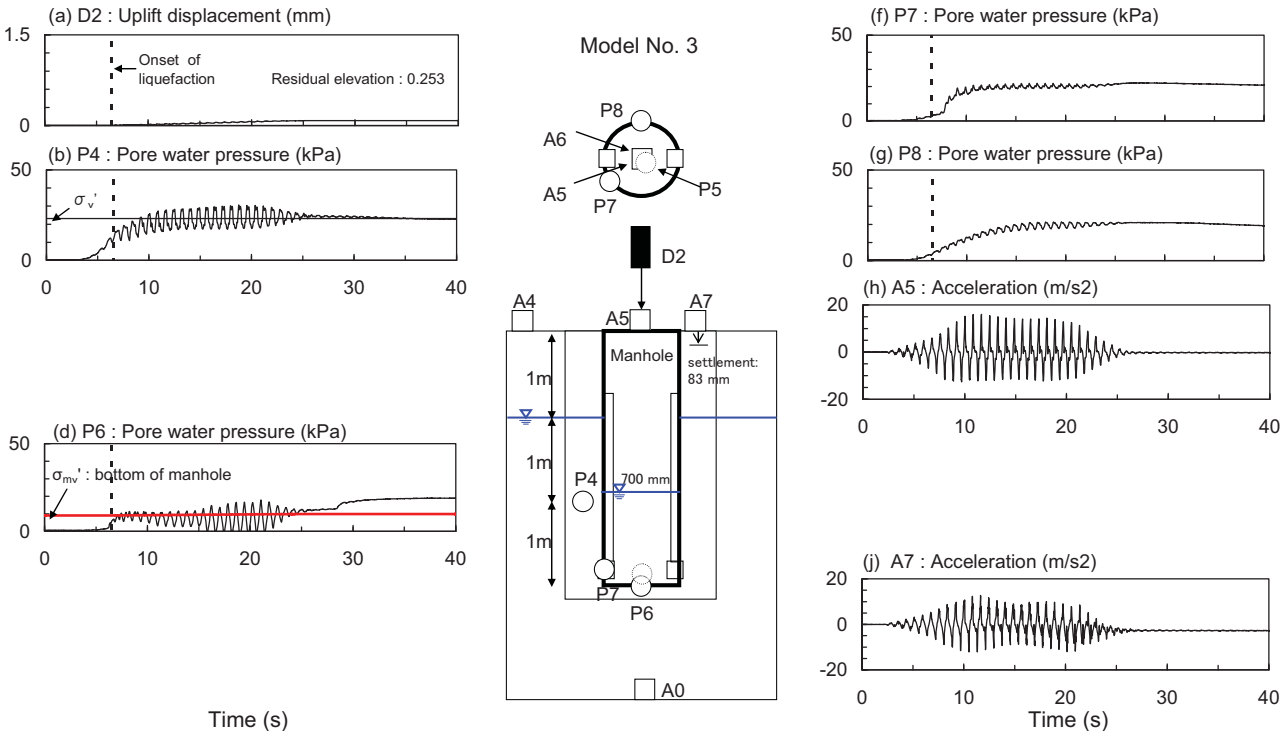
(a) D2 : Uplift displacement (mm)
Onset of liquefaction
Residual elevation : 0.253
(b) P4 : Pore water pressure (kPa)
(d) P6 : Pore water pressure (kPa)
σmv' : bottom of manhole
Time (s)
Model No. 3
P8
A6
A5
P7
P5
D2
A4
A5
A7
Manhole
settlement: 83 mm
1m
P4
700 mm
P7
P6
A0
(f) P7 : Pore water pressure (kPa)
(g) P8 : Pore water pressure (kPa)
(h) A5 : Acceleration (m/s2)
(j) A7 : Acceleration (m/s2)
Time (s)

APPENDIX B

CS1

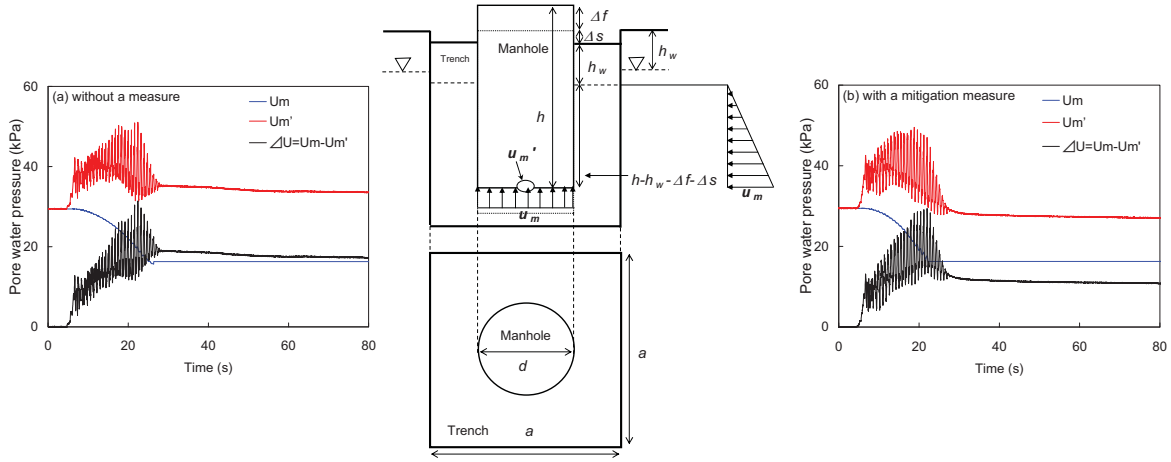

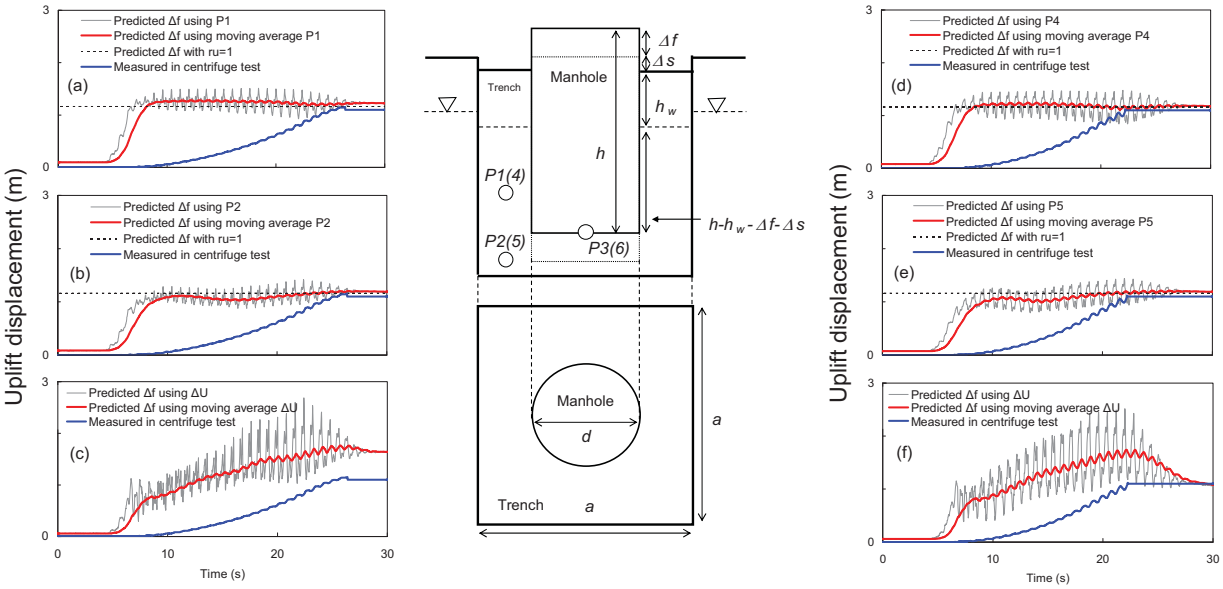

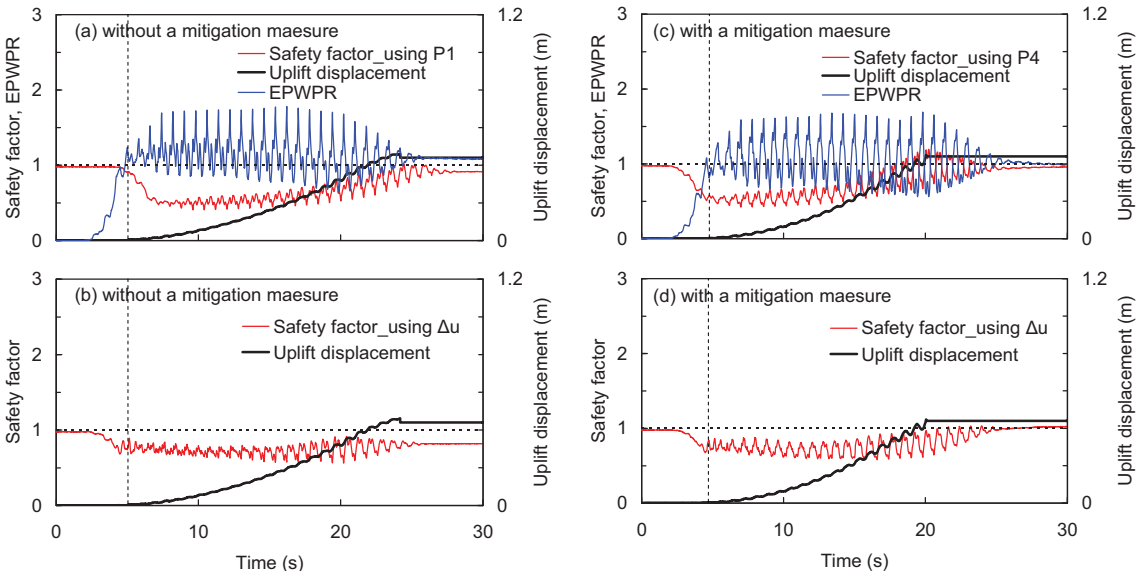

CS2

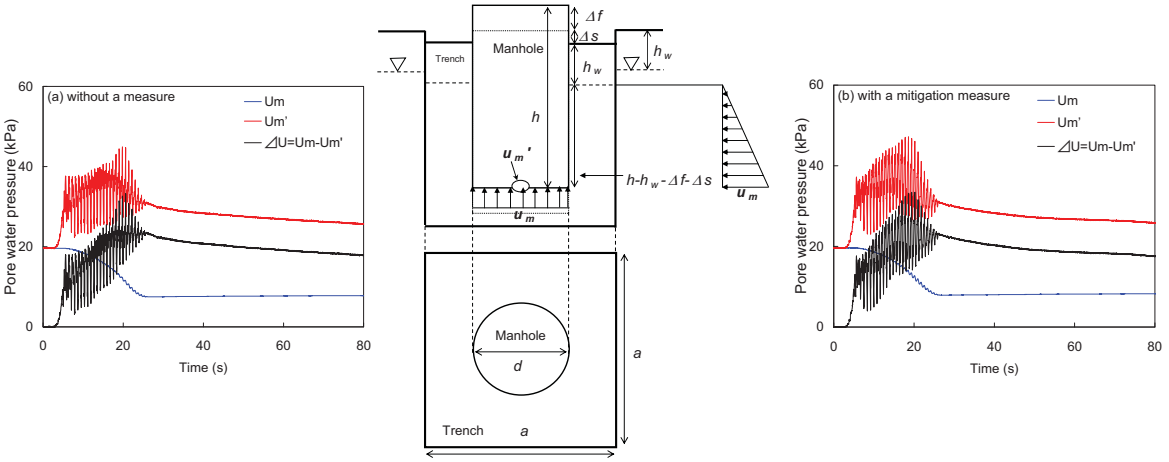
(a) without a measure
Um
Um'
⊿U=Um-Um'
Pore water pressure (kPa)
Time (s)
Trench
Manhole
Δf
Δs
h_w
h
u_m'
u_m
h-h_w-Δf-Δs
Manhole
d
a
Trench
a
(b) with a mitigation measure
Um
Um'
⊿U=Um-Um'
Pore water pressure (kPa)
Time (s)

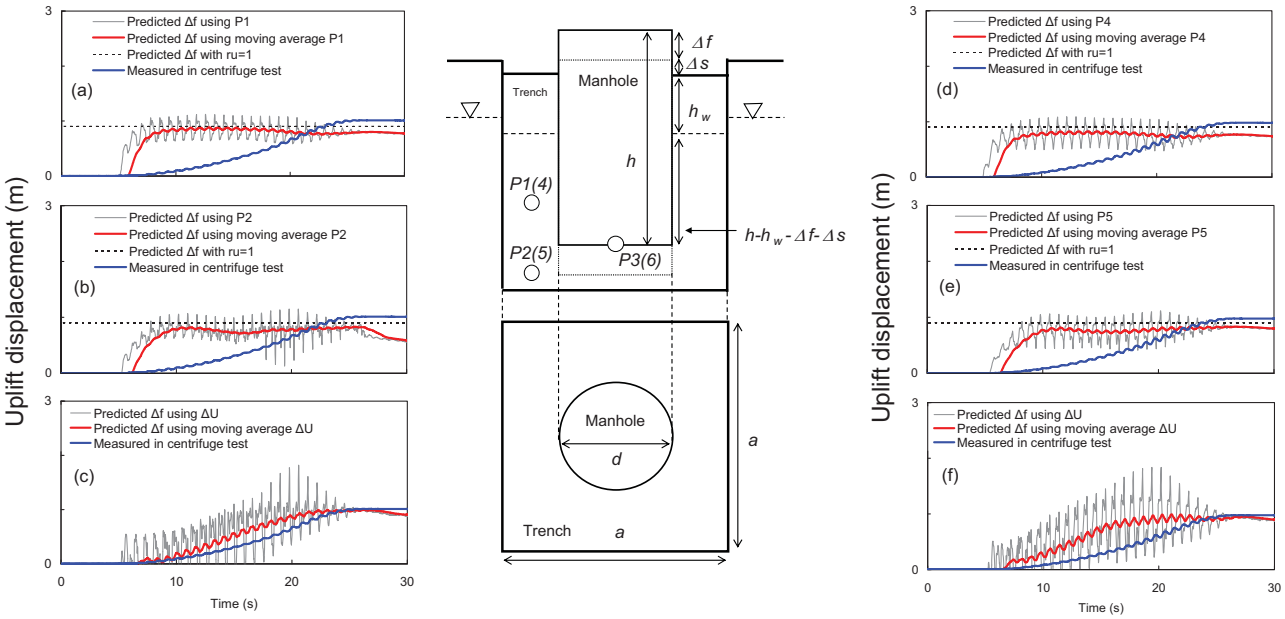
Predicted Δf using P1
Predicted Δf using moving average P1
Predicted Δf with ru=1
Measured in centrifuge test
(a)
Predicted Δf using P2
Predicted Δf using moving average P2
Predicted Δf with ru=1
Measured in centrifuge test
(b)
Predicted Δf using ΔU
Predicted Δf using moving average ΔU
Measured in centrifuge test
(c)
Uplift displacement (m)
Time (s)
Trench
Manhole
Δf
Δs
h_w
h
P1(4)
P2(5)
P3(6)
h-h_w-Δf-Δs
Manhole
d
a
Trench
a
Predicted Δf using P4
Predicted Δf using moving average P4
Predicted Δf with ru=1
Measured in centrifuge test
(d)
Predicted Δf using P5
Predicted Δf using moving average P5
Predicted Δf with ru=1
Measured in centrifuge test
(e)
Predicted Δf using ΔU
Predicted Δf using moving average ΔU
Measured in centrifuge test
(f)
Uplift displacement (m)
Time (s)

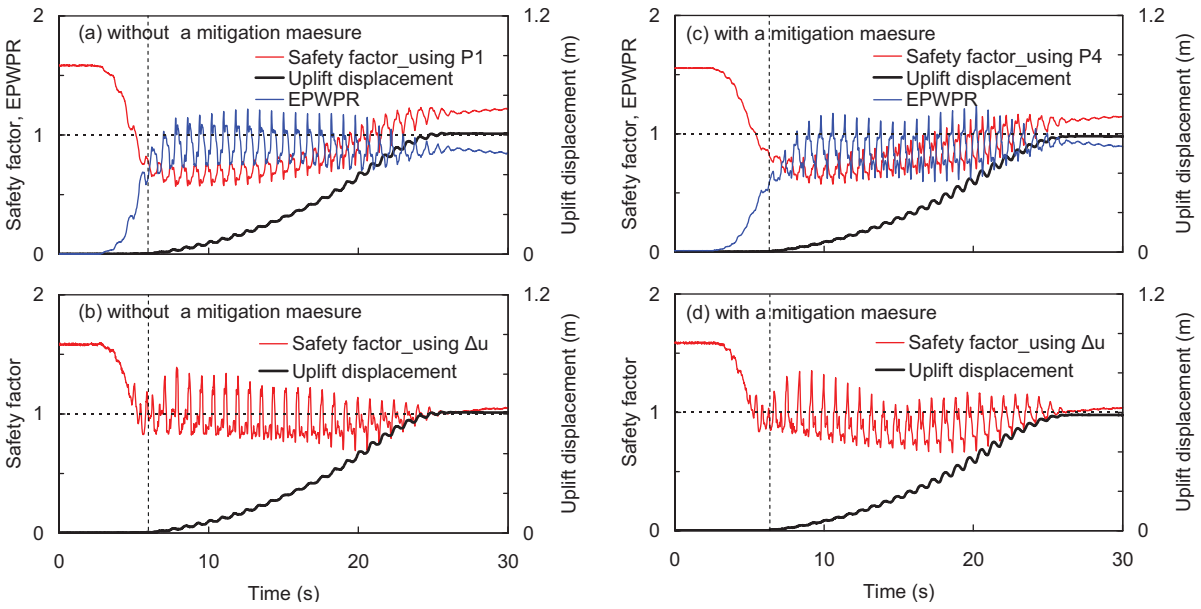
(a) without a mitigation maesure
Safety factor_using P1
Uplift displacement
EPWPR
Safety factor, EPWPR
Uplift displacement (m)
(c) with a mitigation maesure
Safety factor_using P4
Uplift displacement
EPWPR
Safety factor, EPWPR
Uplift displacement (m)
(b) without a mitigation maesure
Safety factor_using Δu
Uplift displacement
Safety factor
Uplift displacement (m)
Time (s)
(d) with a mitigation maesure
Safety factor_using Δu
Uplift displacement
Safety factor
Uplift displacement (m)
Time (s)

CS3

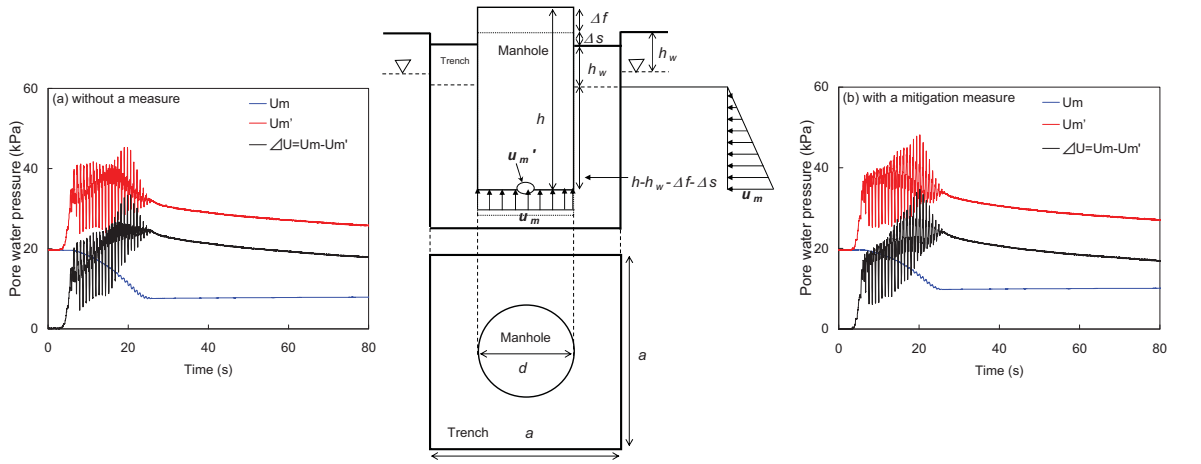
(a) without a measure
Um
Um'
⊿U=Um-Um'
Pore water pressure (kPa)
Time (s)
Trench
Manhole
h
h_w
Δf
Δs
u_m'
u_m
h-h_w-Δf-Δs
d
a
(b) with a mitigation measure

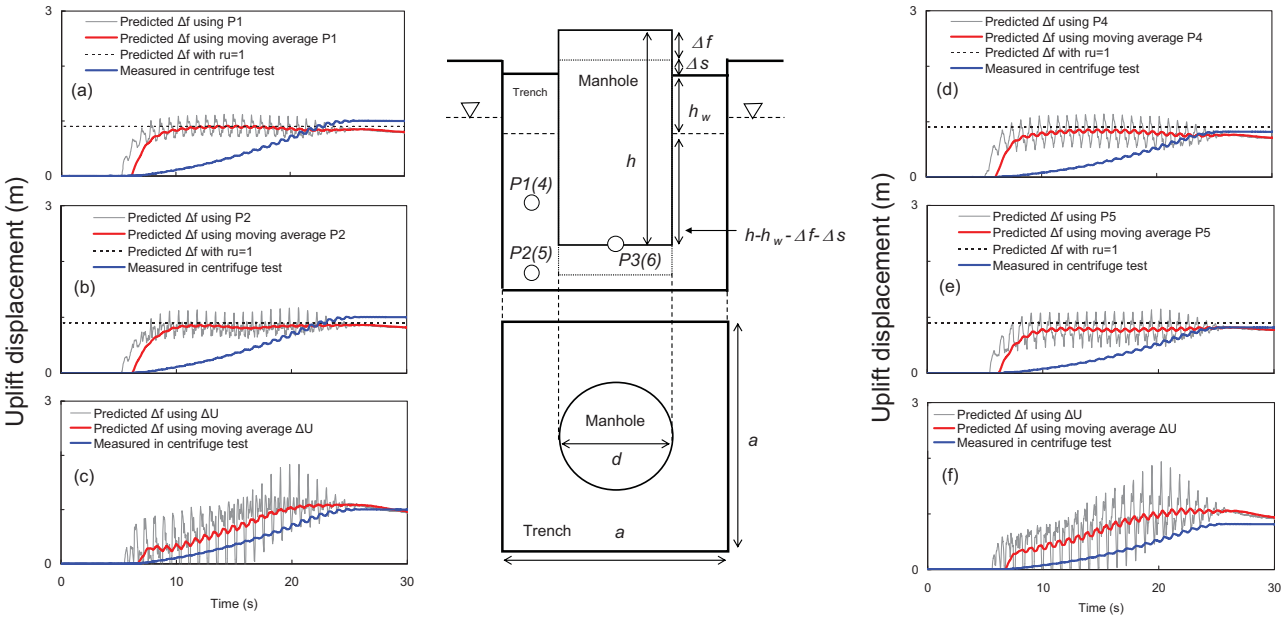
Predicted Δf using P1
Predicted Δf using moving average P1
Predicted Δf with ru=1
Measured in centrifuge test
(a)
Predicted Δf using P2
Predicted Δf using moving average P2
(b)
Predicted Δf using ΔU
Predicted Δf using moving average ΔU
(c)
Uplift displacement (m)
Time (s)
Trench
Manhole
h
h_w
Δf
Δs
P1(4)
P2(5)
P3(6)
h-h_w-Δf-Δs
d
a
Predicted Δf using P4
Predicted Δf using moving average P4
(d)
Predicted Δf using P5
Predicted Δf using moving average P5
(e)
(f)

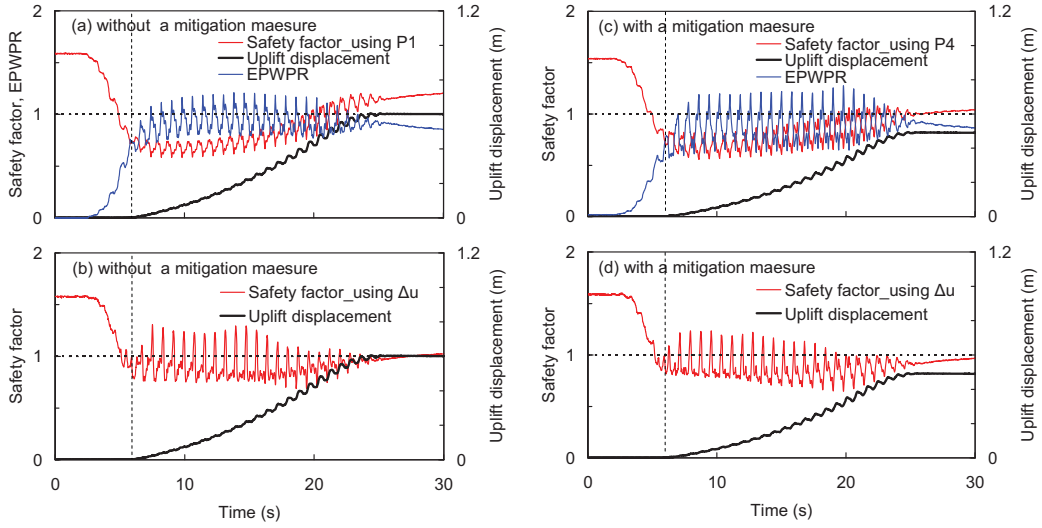
(a) without a mitigation maesure
Safety factor_using P1
Uplift displacement
EPWPR
Safety factor, EPWPR
Uplift displacement (m)
(b) without a mitigation maesure
Safety factor_using Δu
Safety factor
(c) with a mitigation maesure
Safety factor_using P4
(d) with a mitigation maesure
Time (s)

CS4

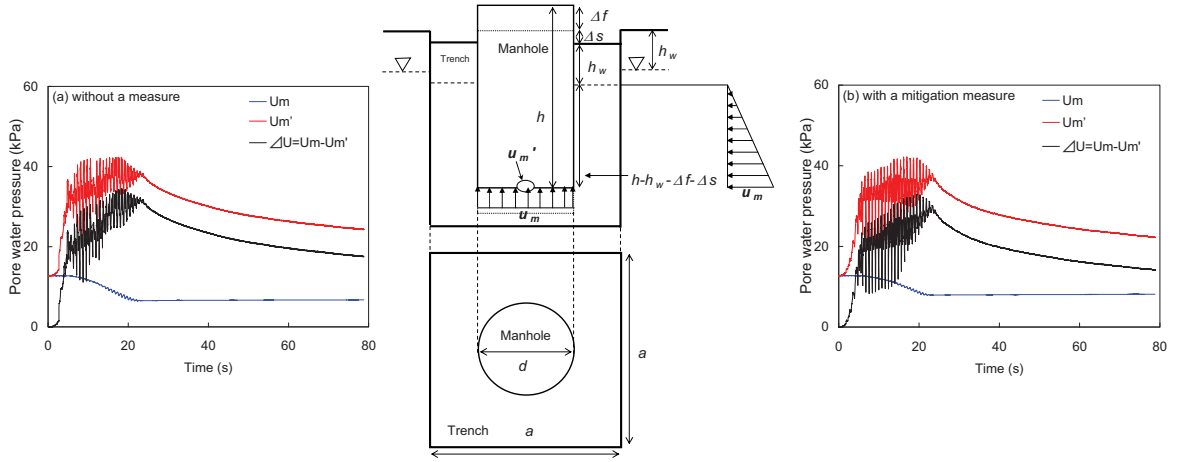
(a) without a measure
Um
Um'
⊿U=Um-Um'
Pore water pressure (kPa)
Time (s)
Trench
Manhole
Δf
Δs
h
h_w
u_m'
u_m
h-h_w-Δf-Δs
d
a
(b) with a mitigation measure

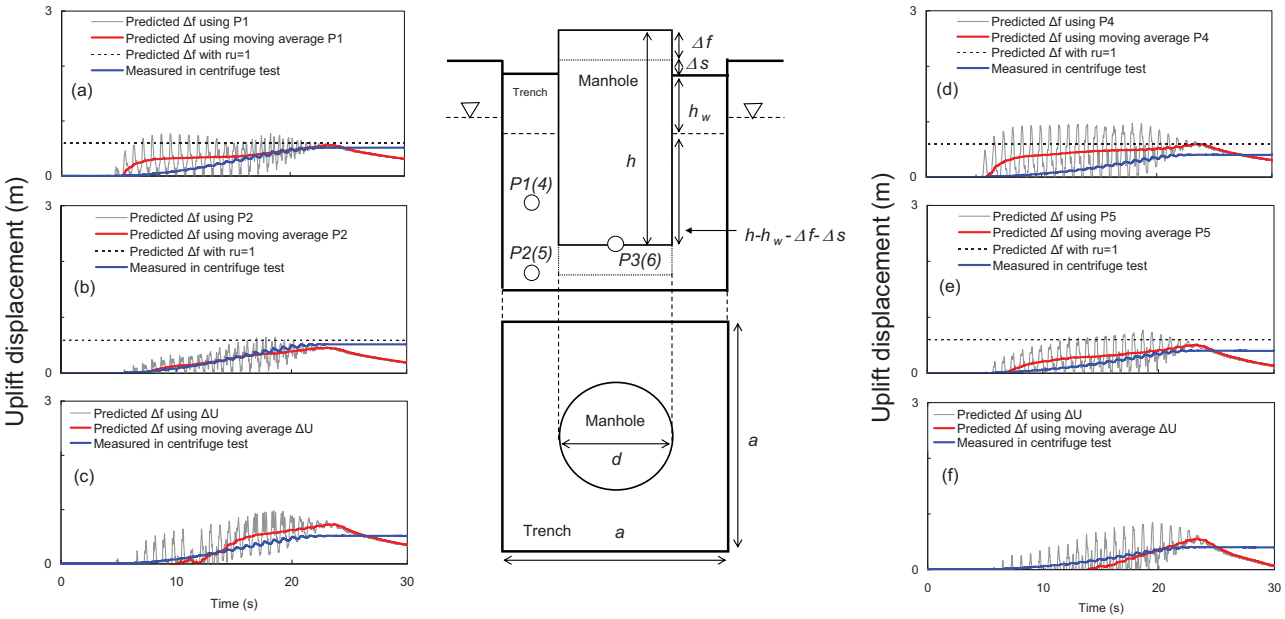
Predicted Δf using P1
Predicted Δf using moving average P1
Predicted Δf with ru=1
Measured in centrifuge test
(a)
Predicted Δf using P2
Predicted Δf using moving average P2
(b)
Predicted Δf using ΔU
Predicted Δf using moving average ΔU
(c)
Uplift displacement (m)
Time (s)
P1(4)
P2(5)
P3(6)
Predicted Δf using P4
Predicted Δf using moving average P4
(d)
Predicted Δf using P5
Predicted Δf using moving average P5
(e)
(f)

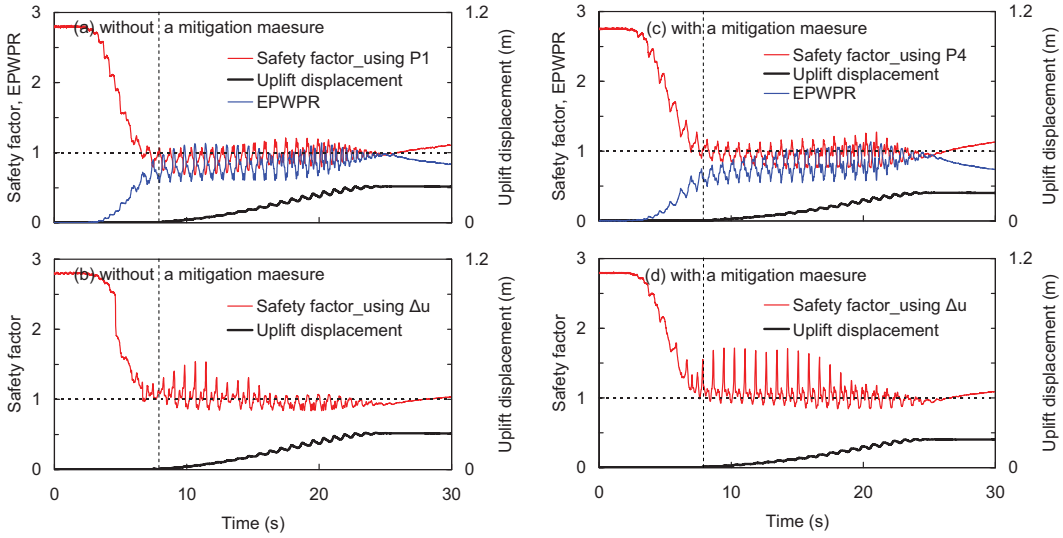
(a) without a mitigation maesure
Safety factor_using P1
Uplift displacement
EPWPR
Safety factor, EPWPR
Uplift displacement (m)
(c) with a mitigation maesure
Safety factor_using P4
(b) without a mitigation maesure
Safety factor_using Δu
Safety factor
(d) with a mitigation maesure
Time (s)

CS6

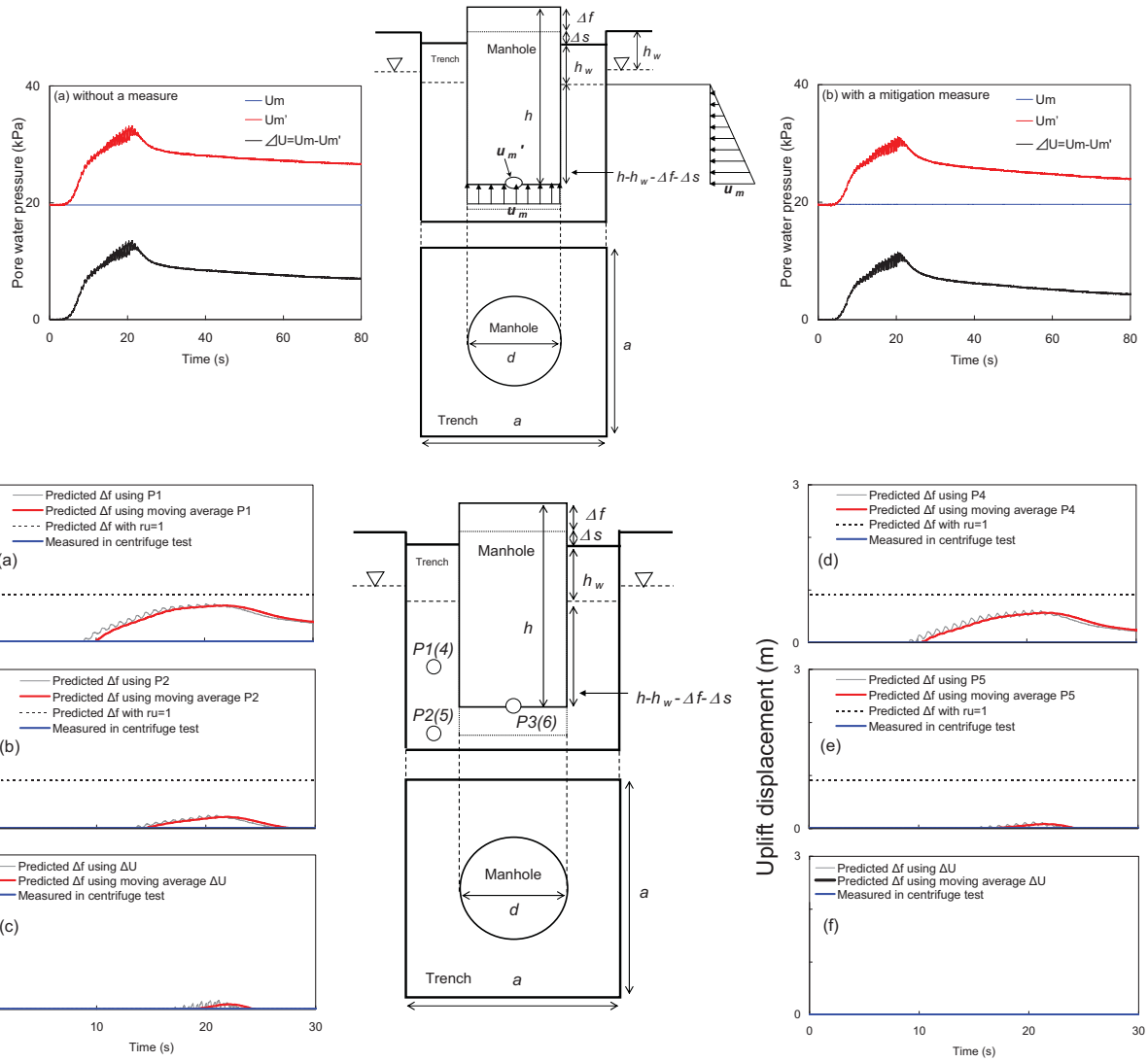
(a) without a measure
Um
Um'
⊿U=Um-Um'
Pore water pressure (kPa)
Time (s)
(b) with a mitigation measure
Trench
Manhole
h
h_w
Δf
Δs
u_m'
u_m
h-h_w-Δf-Δs
d
a

Predicted Δf using P1
Predicted Δf using moving average P1
Predicted Δf with ru=1
Measured in centrifuge test
(a)
Predicted Δf using P2
Predicted Δf using moving average P2
(b)
Predicted Δf using ΔU
Predicted Δf using moving average ΔU
(c)
Uplift displacement (m)
Time (s)
P1(4)
P2(5)
P3(6)
Predicted Δf using P4
Predicted Δf using moving average P4
(d)
Predicted Δf using P5
Predicted Δf using moving average P5
(e)
(f)

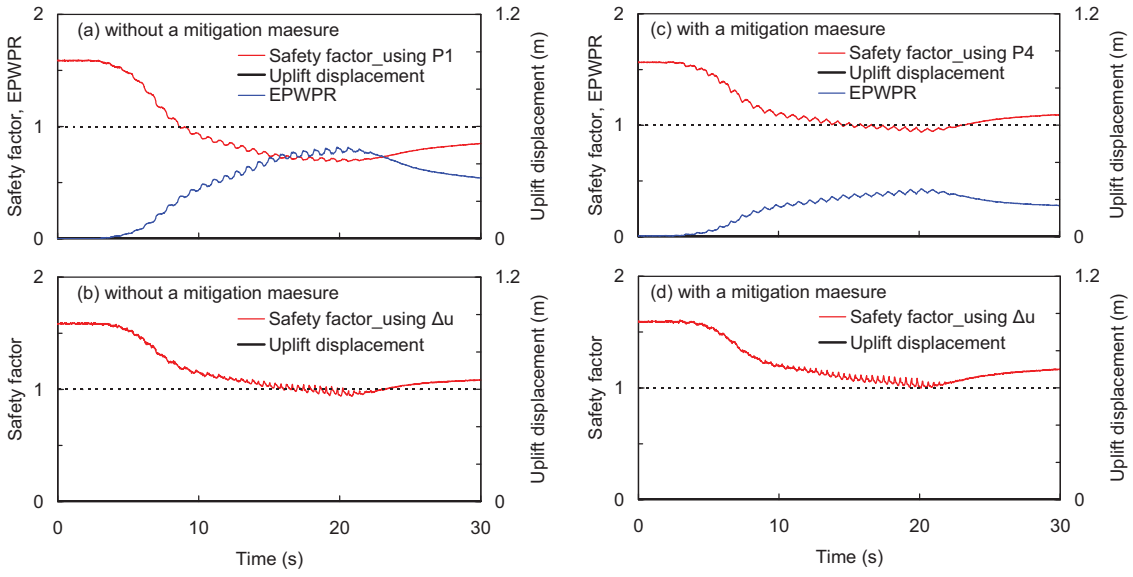
(a) without a mitigation maesure
Safety factor_using P1
Uplift displacement
EPWPR
Safety factor, EPWPR
Uplift displacement (m)
(c) with a mitigation maesure
Safety factor_using P4
(b) without a mitigation maesure
Safety factor_using Δu
Safety factor
(d) with a mitigation maesure
Time (s)

CS7

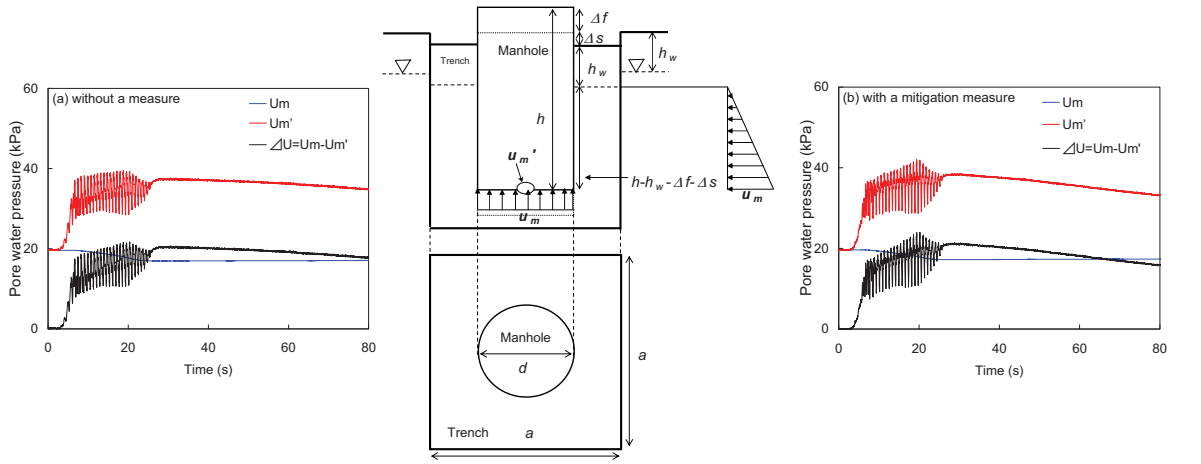
(a) without a measure
Um
Um'
⊿U=Um-Um'
Pore water pressure (kPa)
Time (s)
Trench
Manhole
h
h_w
Δf
Δs
u_m'
u_m
$h-h_w-\Delta f-\Delta s$
d
a
(b) with a mitigation measure

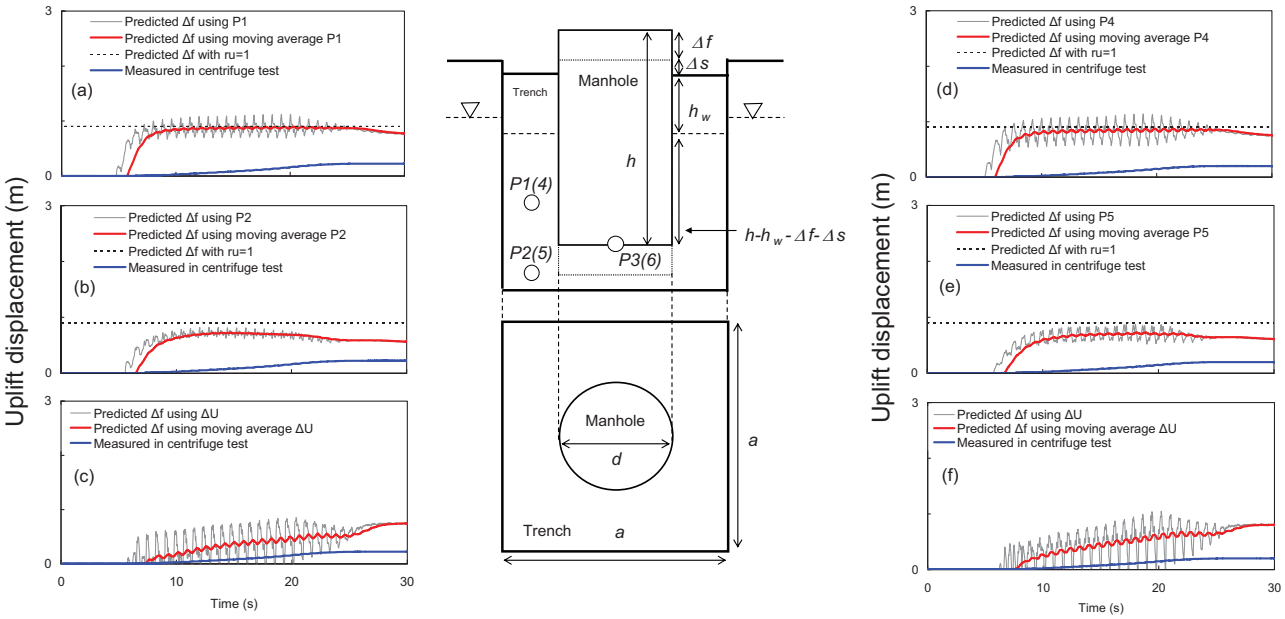
Predicted Δf using P1
Predicted Δf using moving average P1
Predicted Δf with ru=1
Measured in centrifuge test
(a)
Predicted Δf using P2
Predicted Δf using moving average P2
(b)
Predicted Δf using ΔU
Predicted Δf using moving average ΔU
(c)
Uplift displacement (m)
Time (s)
P1(4)
P2(5)
P3(6)
Predicted Δf using P4
Predicted Δf using moving average P4
(d)
Predicted Δf using P5
Predicted Δf using moving average P5
(e)
(f)

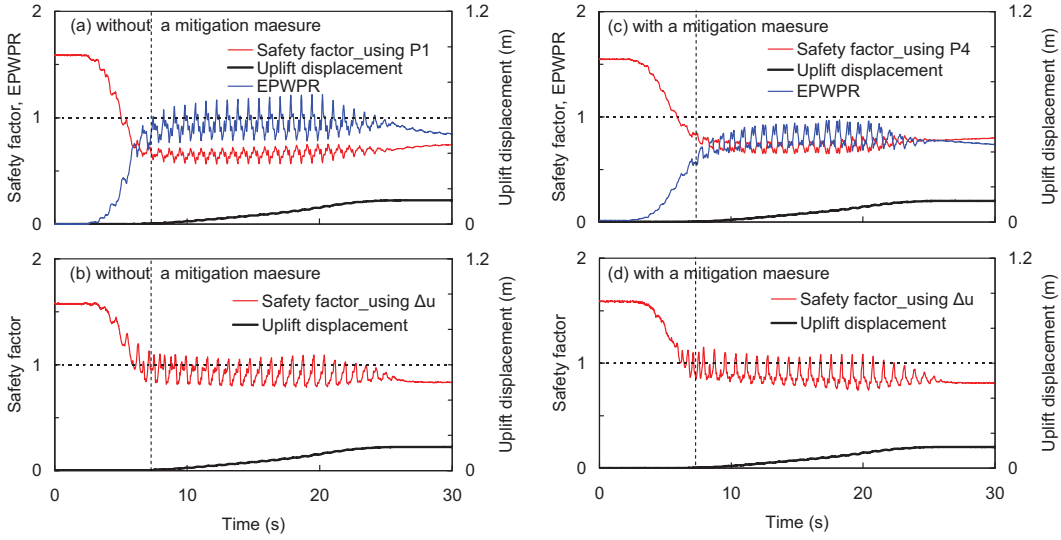
(a) without a mitigation maesure
Safety factor_using P1
Uplift displacement
EPWPR
Safety factor, EPWPR
Uplift displacement (m)
(c) with a mitigation maesure
Safety factor_using P4
(b) without a mitigation maesure
Safety factor_using Δu
Safety factor
(d) with a mitigation maesure
Time (s)

CS8

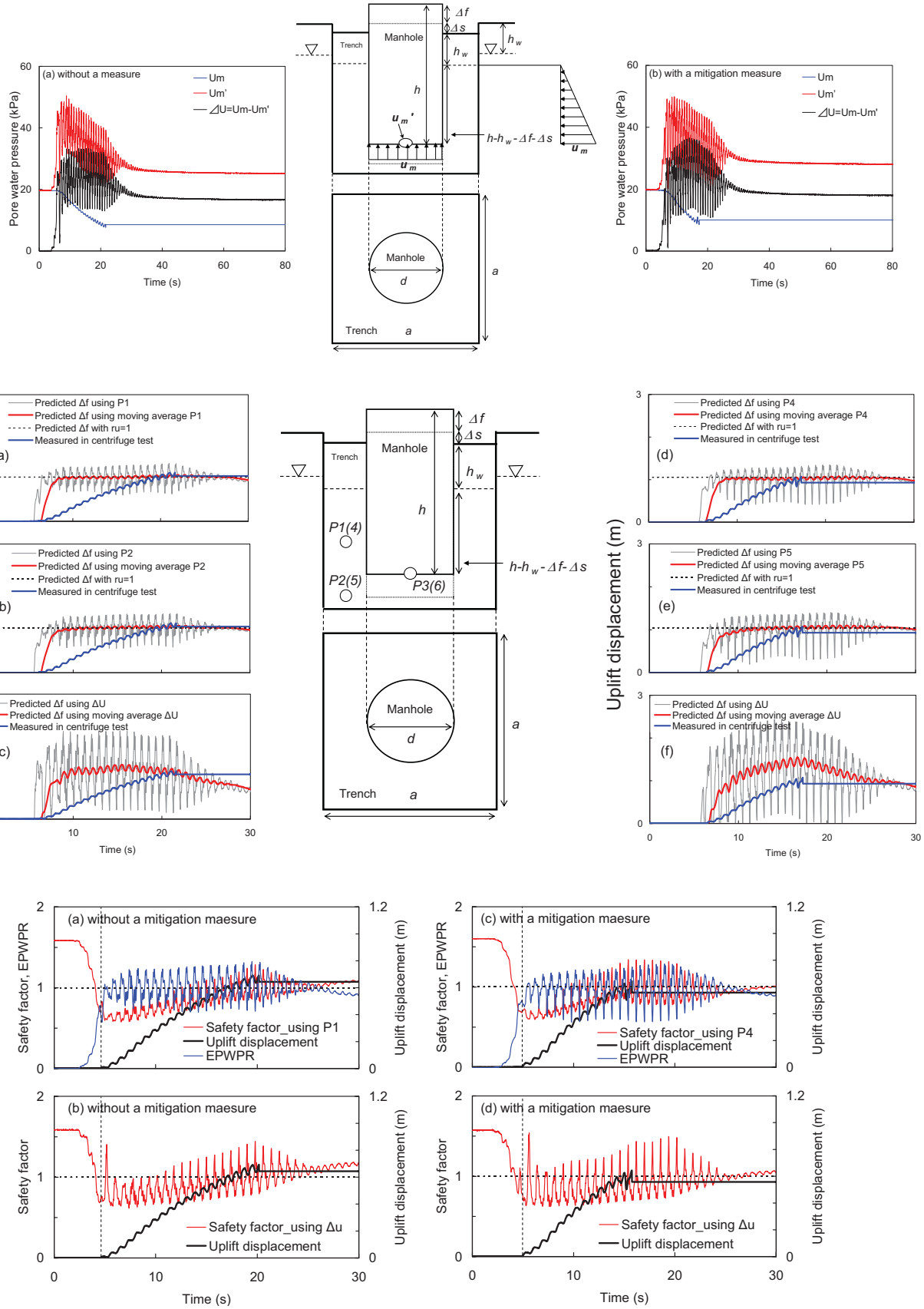
(a) without a measure
Um
Um'
⊿U=Um-Um'
Pore water pressure (kPa)
Time (s)
(b) with a mitigation measure
Trench
Manhole
Δf
Δs
h_w
h
u_m'
u_m
h-h_w-Δf-Δs
d
a
Predicted Δf using P1
Predicted Δf using moving average P1
Predicted Δf with ru=1
Measured in centrifuge test
(a)
Predicted Δf using P2
Predicted Δf using moving average P2
(b)
Predicted Δf using ΔU
Predicted Δf using moving average ΔU
(c)
Uplift displacement (m)
P1(4)
P2(5)
P3(6)
Predicted Δf using P4
Predicted Δf using moving average P4
(d)
Predicted Δf using P5
Predicted Δf using moving average P5
(e)
(f)
(a) without a mitigation maesure
Safety factor_using P1
Uplift displacement
EPWPR
(c) with a mitigation maesure
Safety factor_using P4
(b) without a mitigation maesure
Safety factor_using Δu
(d) with a mitigation maesure
Safety factor, EPWPR
Safety factor
Uplift displacement (m)

CS9

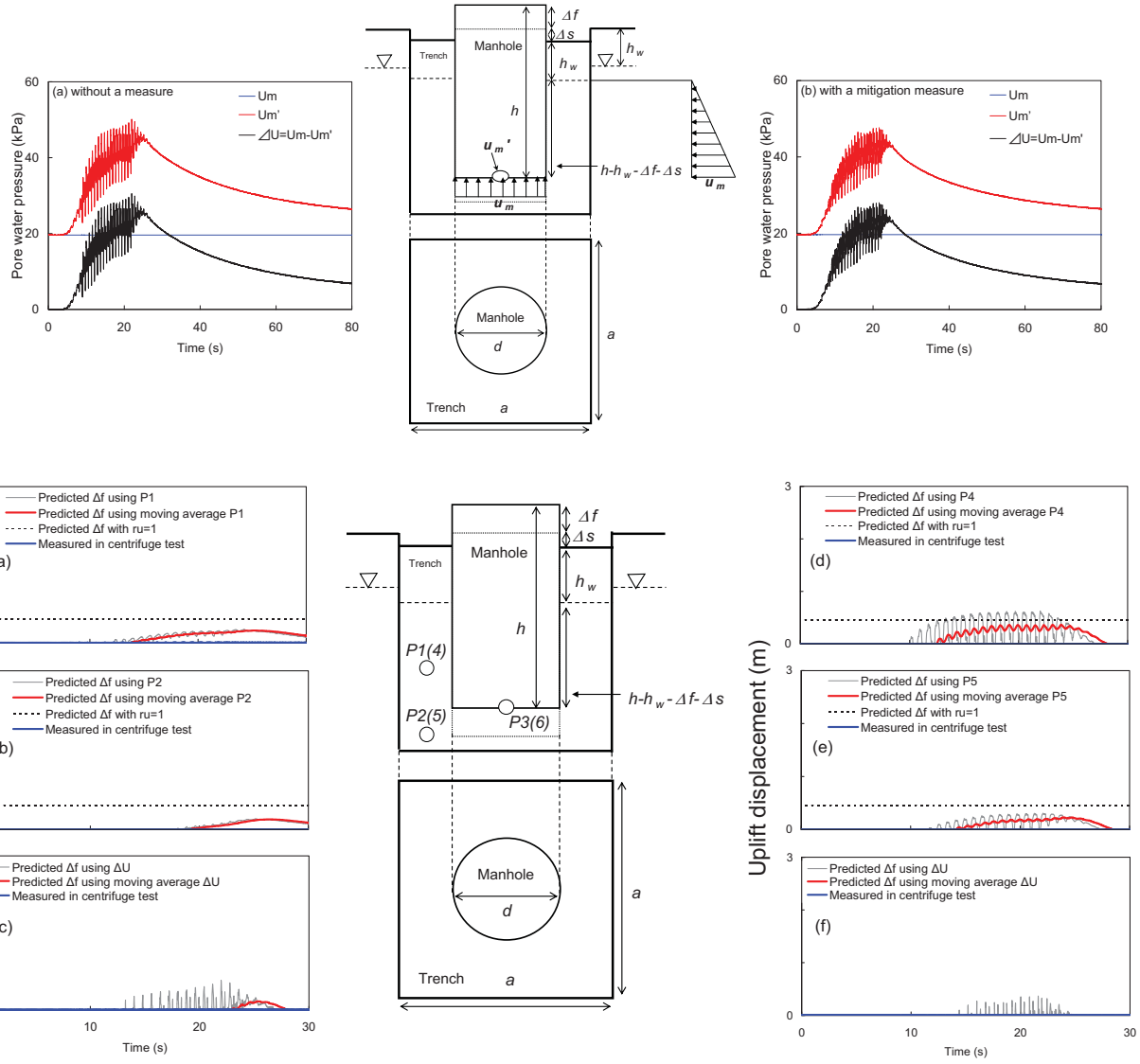
(a) without a measure
Um
Um'
⊿U=Um-Um'
Pore water pressure (kPa)
Time (s)
Trench
Manhole
h
h_w
Δf
Δs
u_m'
u_m
h-h_w-Δf-Δs
d
a
(b) with a mitigation measure
Predicted Δf using P1
Predicted Δf using moving average P1
Predicted Δf with ru=1
Measured in centrifuge test
(a)
Predicted Δf using P2
Predicted Δf using moving average P2
(b)
Predicted Δf using ΔU
Predicted Δf using moving average ΔU
(c)
Uplift displacement (m)
P1(4)
P2(5)
P3(6)
Predicted Δf using P4
Predicted Δf using moving average P4
(d)
Predicted Δf using P5
Predicted Δf using moving average P5
(e)
(f)

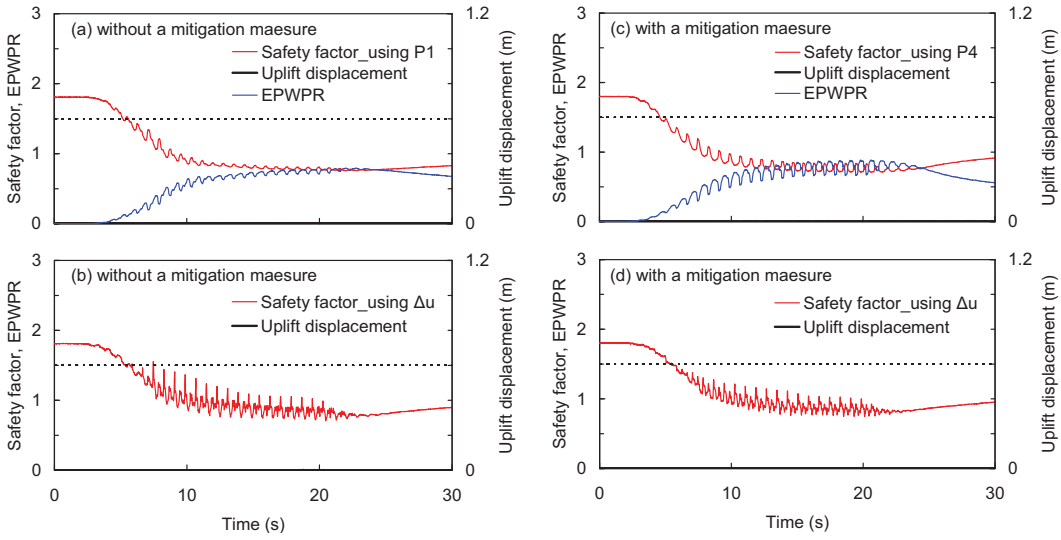
(a) without a mitigation maesure
Safety factor_using P1
Uplift displacement
EPWPR
(c) with a mitigation maesure
Safety factor_using P4
(b) without a mitigation maesure
Safety factor_using Δu
(d) with a mitigation maesure
Safety factor, EPWPR
Uplift displacement (m)
Time (s)

CS10

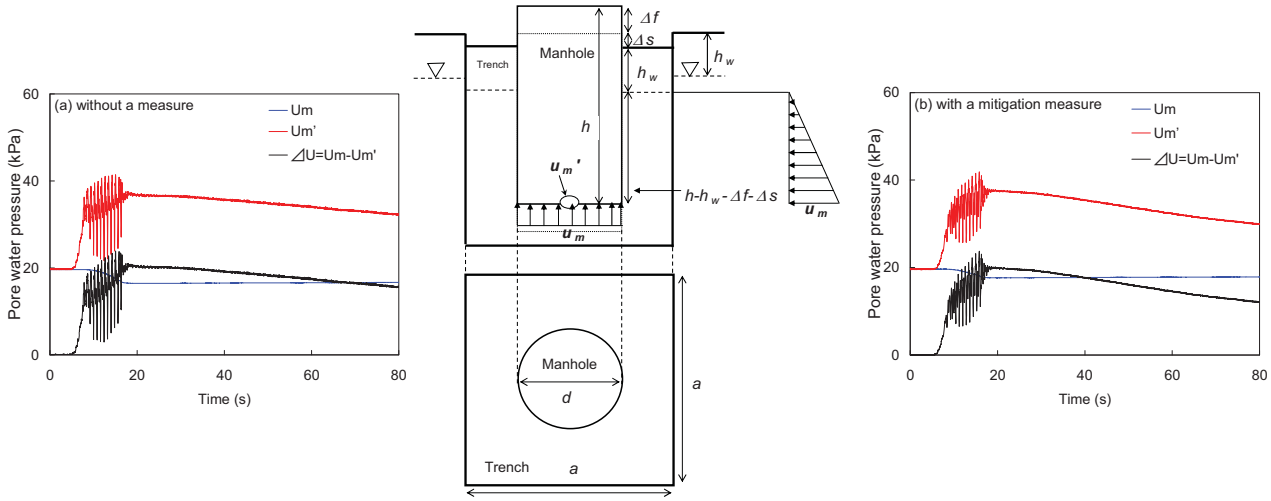
(a) without a measure
Um
Um'
⊿U=Um-Um'
Pore water pressure (kPa)
Time (s)
Trench
Manhole
Δf
Δs
h
h w
u m'
u m
h-h w-Δf-Δs
d
a
(b) with a mitigation measure

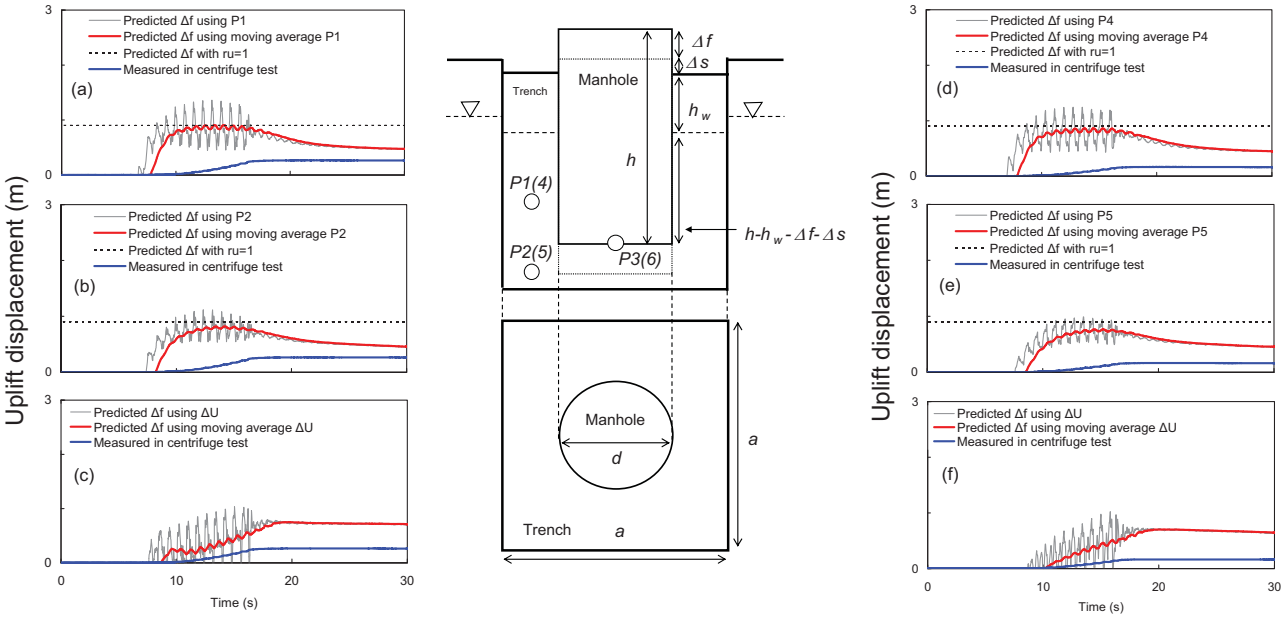
Predicted Δf using P1
Predicted Δf using moving average P1
Predicted Δf with ru=1
Measured in centrifuge test
(a)
Predicted Δf using P2
Predicted Δf using moving average P2
(b)
Predicted Δf using ΔU
Predicted Δf using moving average ΔU
(c)
Uplift displacement (m)
Time (s)
Trench
Manhole
P1(4)
P2(5)
P3(6)
h-h w-Δf-Δs
d
a
Predicted Δf using P4
Predicted Δf using moving average P4
(d)
Predicted Δf using P5
Predicted Δf using moving average P5
(e)
(f)

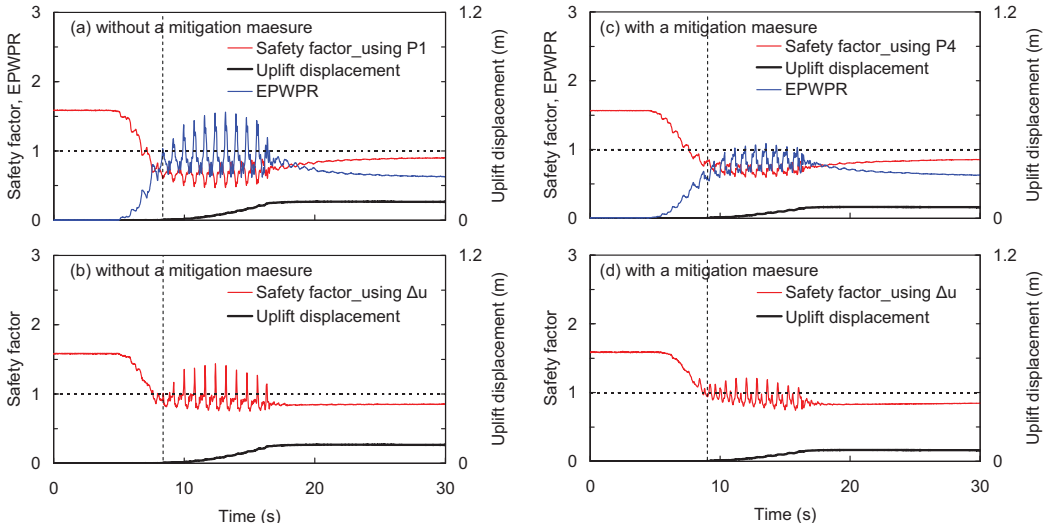
(a) without a mitigation maesure
Safety factor_using P1
Uplift displacement
EPWPR
Safety factor, EPWPR
Uplift displacement (m)
(c) with a mitigation maesure
Safety factor_using P4
(b) without a mitigation maesure
Safety factor_using Δu
Safety factor
(d) with a mitigation maesure
Time (s)

CS11

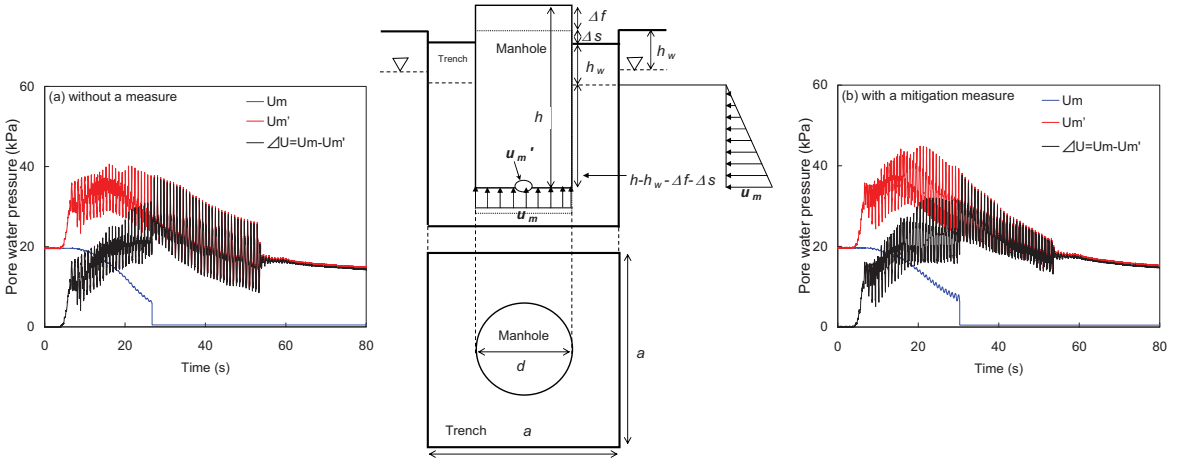
(a) without a measure
Um
Um'
⊿U=Um-Um'
Pore water pressure (kPa)
Time (s)
Trench
Manhole
Δf
Δs
h_w
h
u_m'
u_m
h-h_w-Δf-Δs
d
a
(b) with a mitigation measure

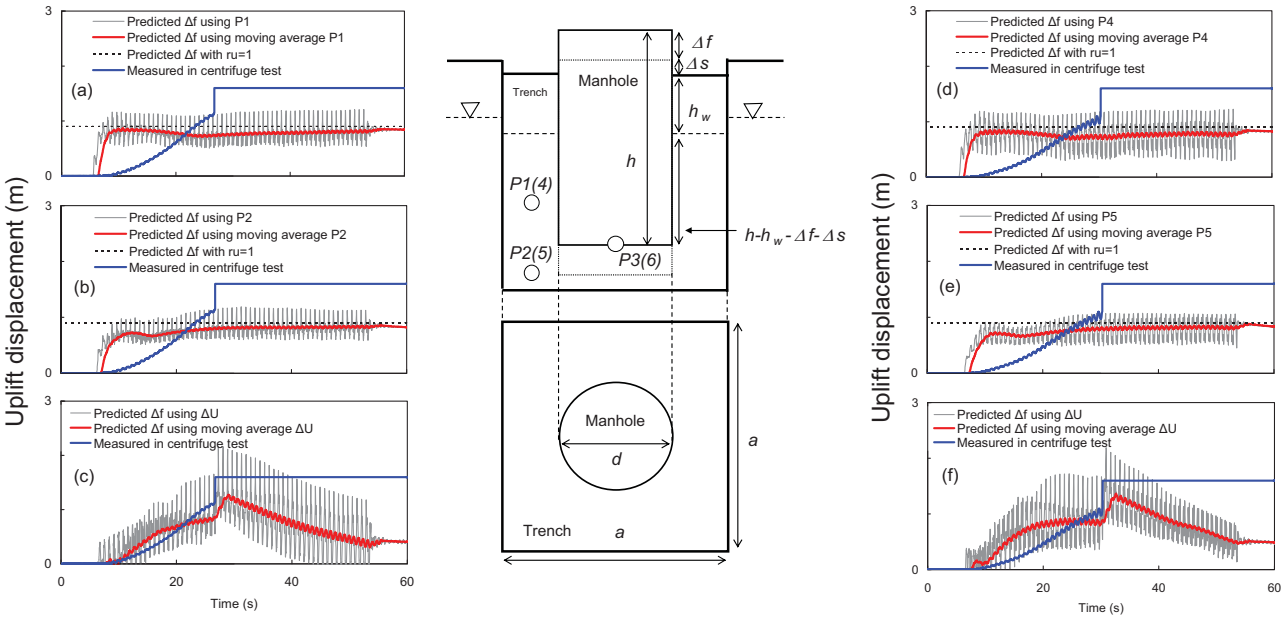
Predicted Δf using P1
Predicted Δf using moving average P1
Predicted Δf with ru=1
Measured in centrifuge test
(a)
Predicted Δf using P2
Predicted Δf using moving average P2
(b)
Predicted Δf using ΔU
Predicted Δf using moving average ΔU
(c)
Uplift displacement (m)
Time (s)
Trench
Manhole
P1(4)
P2(5)
P3(6)
Predicted Δf using P4
Predicted Δf using moving average P4
(d)
Predicted Δf using P5
Predicted Δf using moving average P5
(e)
(f)

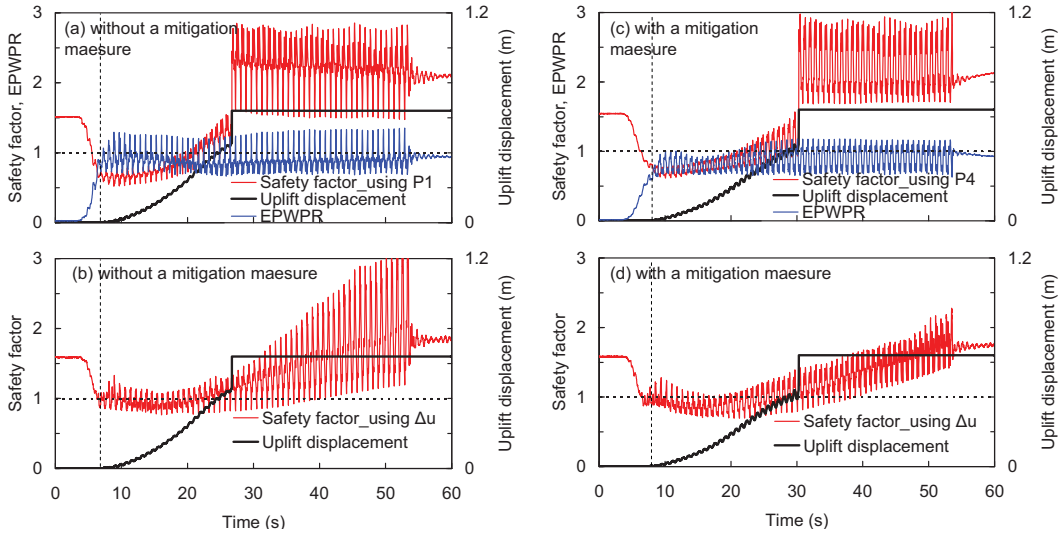
(a) without a mitigation maesure
Safety factor, EPWPR
Uplift displacement (m)
Safety factor_using P1
Uplift displacement
EPWPR
(c) with a mitigation maesure
Safety factor_using P4
(b) without a mitigation maesure
Safety factor
Safety factor_using Δu
(d) with a mitigation maesure
Time (s)

CS12

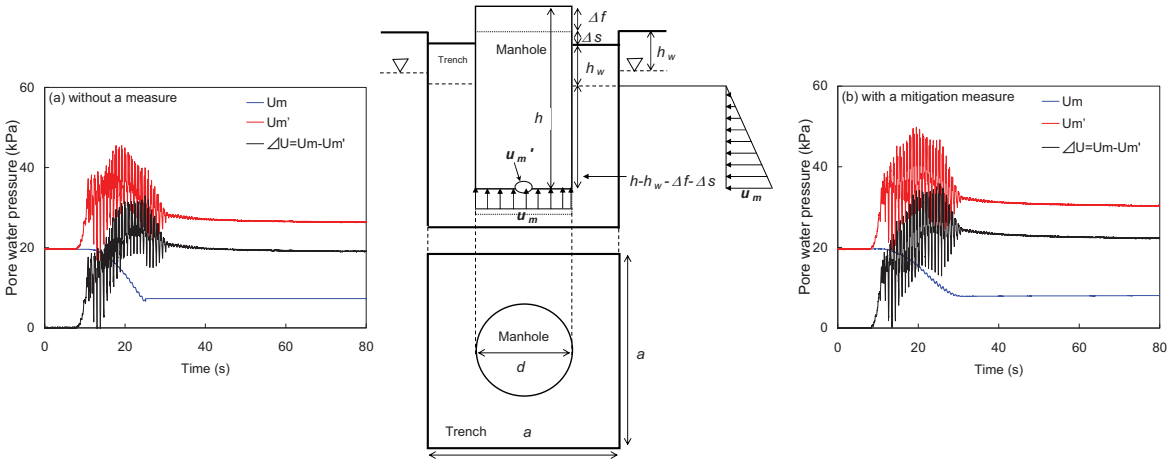
(a) without a measure
Um
Um'
⊿U=Um-Um'
Pore water pressure (kPa)
Time (s)
Trench
Manhole
Δf
Δs
h
h_w
u_m'
u_m
h-h_w-Δf-Δs
d
a
(b) with a mitigation measure

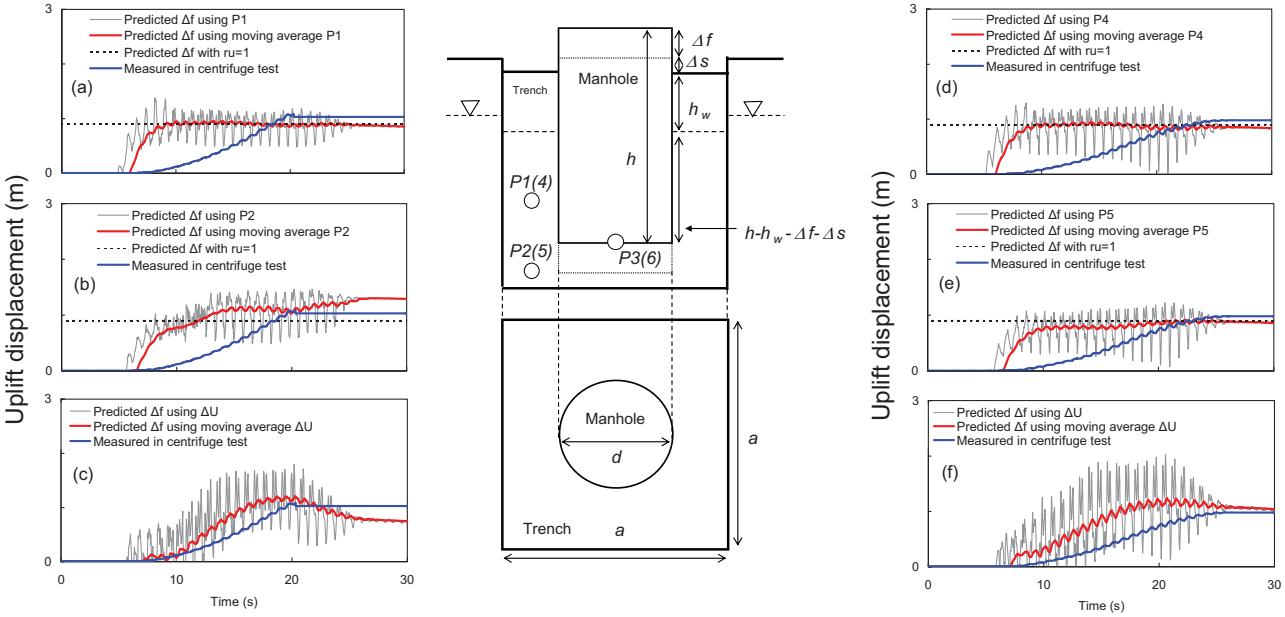
Predicted Δf using P1
Predicted Δf using moving average P1
Predicted Δf with ru=1
Measured in centrifuge test
(a)
Predicted Δf using P2
Predicted Δf using moving average P2
(b)
Predicted Δf using ΔU
Predicted Δf using moving average ΔU
(c)
Uplift displacement (m)
Time (s)
Trench
Manhole
P1(4)
P2(5)
P3(6)
Predicted Δf using P4
Predicted Δf using moving average P4
(d)
Predicted Δf using P5
Predicted Δf using moving average P5
(e)
(f)

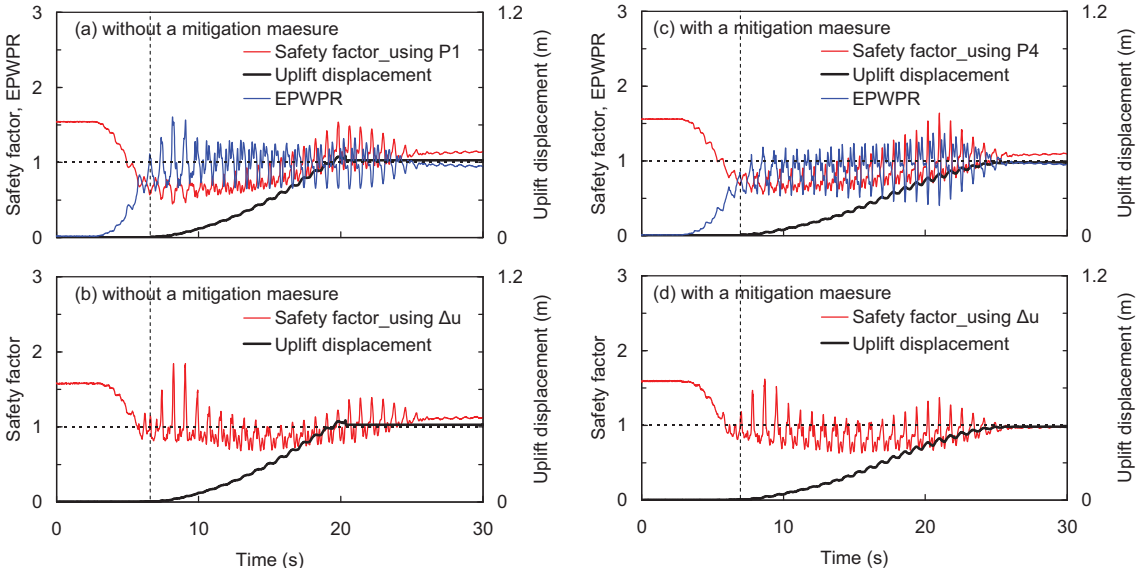
(a) without a mitigation maesure
Safety factor_using P1
Uplift displacement
EPWPR
Safety factor, EPWPR
Uplift displacement (m)
(c) with a mitigation maesure
Safety factor_using P4
(b) without a mitigation maesure
Safety factor_using Δu
Safety factor
(d) with a mitigation maesure
Time (s)

CS13

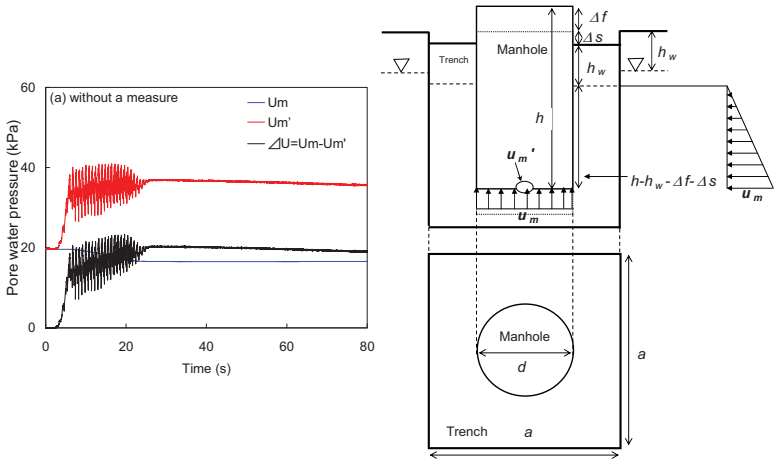
(a) without a measure
Um
Um'
⊿U=Um-Um'
Pore water pressure (kPa)
Time (s)
Trench
Manhole
h
h_w
Δf
Δs
u_m'
u_m
h-h_w-Δf-Δs
d
a
(b) with a mitigation measure

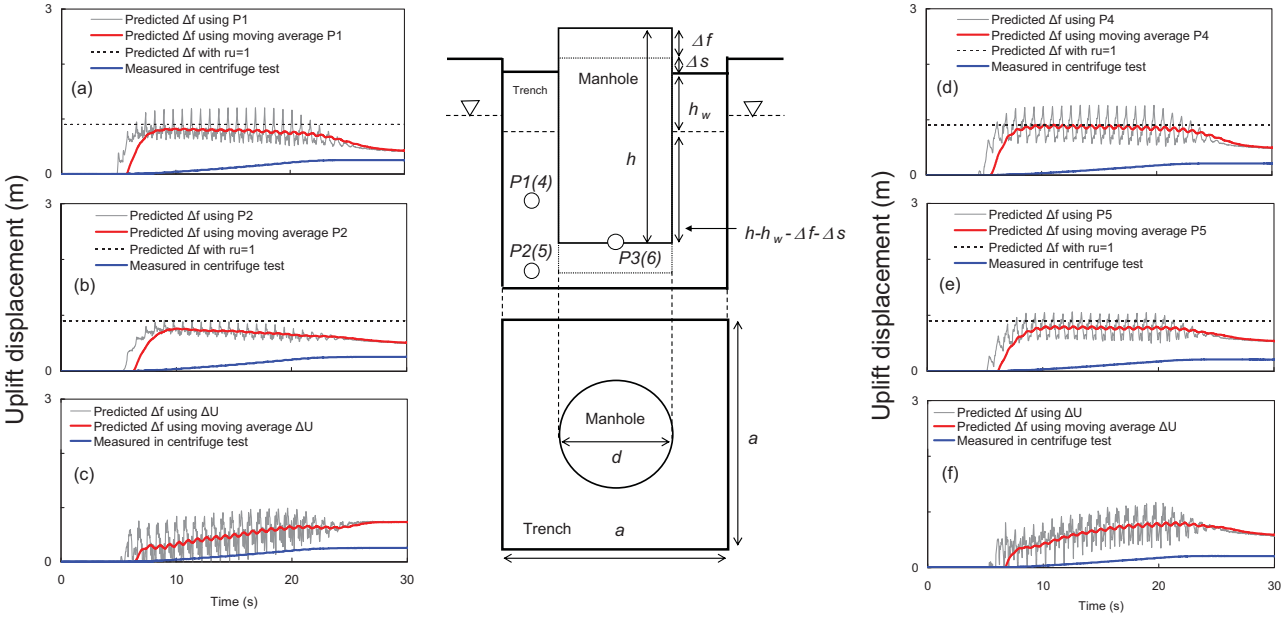
Predicted Δf using P1
Predicted Δf using moving average P1
Predicted Δf with ru=1
Measured in centrifuge test
(a)
Predicted Δf using P2
Predicted Δf using moving average P2
(b)
Predicted Δf using ΔU
Predicted Δf using moving average ΔU
(c)
Uplift displacement (m)
Time (s)
Trench
Manhole
P1(4)
P2(5)
P3(6)
h
h_w
Δf
Δs
h-h_w-Δf-Δs
d
a
Predicted Δf using P4
Predicted Δf using moving average P4
(d)
Predicted Δf using P5
Predicted Δf using moving average P5
(e)
Predicted Δf using ΔU
Predicted Δf using moving average ΔU
(f)

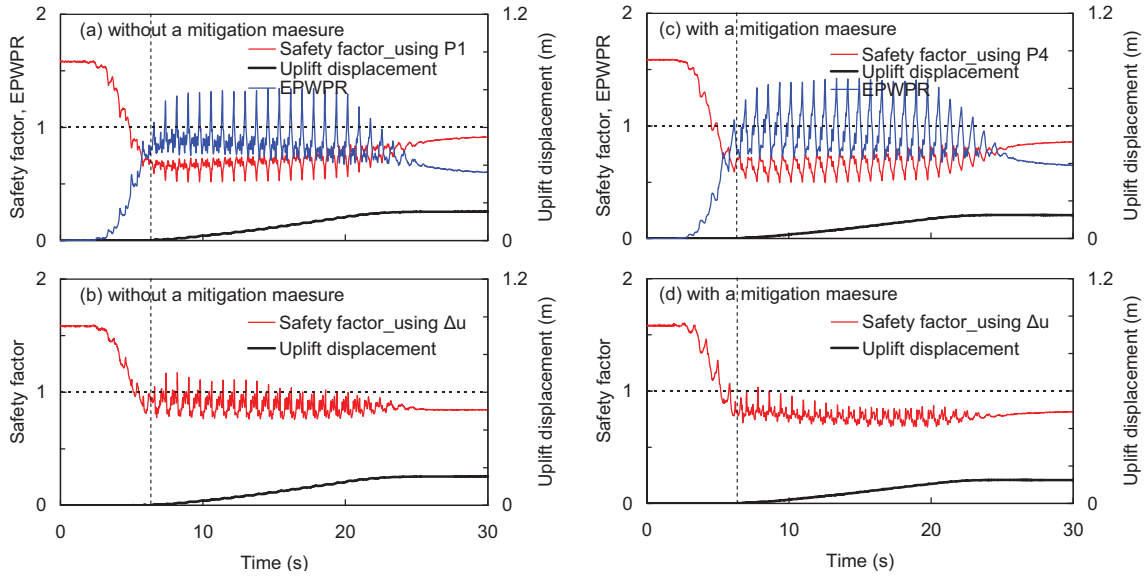
(a) without a mitigation maesure
Safety factor_using P1
Uplift displacement
EPWPR
(b) without a mitigation maesure
Safety factor_using Δu
(c) with a mitigation maesure
Safety factor_using P4
(d) with a mitigation maesure
Safety factor, EPWPR
Safety factor
Uplift displacement (m)
Time (s)

CS14

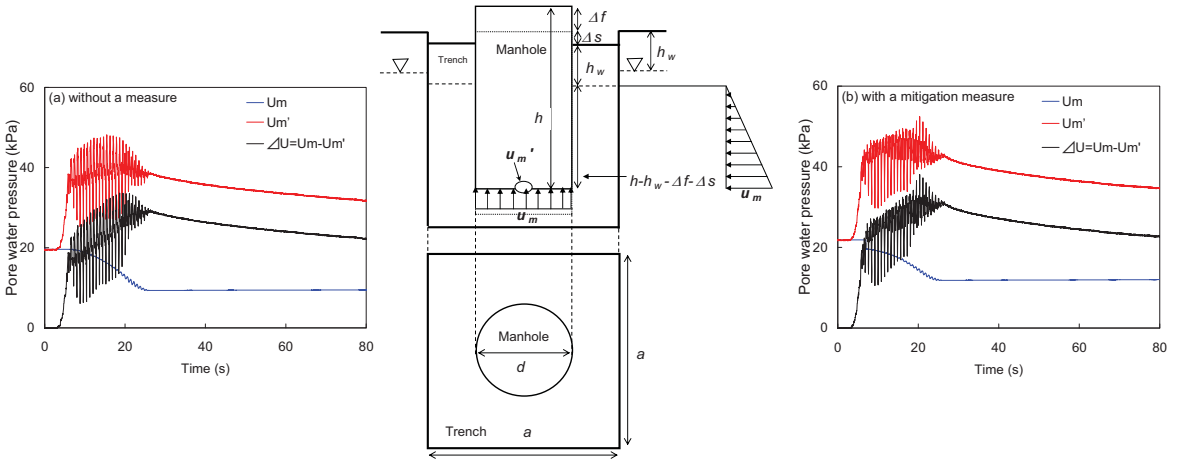
(a) without a measure
Um
Um'
⊿U=Um-Um'
Pore water pressure (kPa)
Time (s)
(b) with a mitigation measure
Manhole
Trench
Δf
Δs
h
h_w
u_m'
u_m
h-h_w-Δf-Δs
d
a

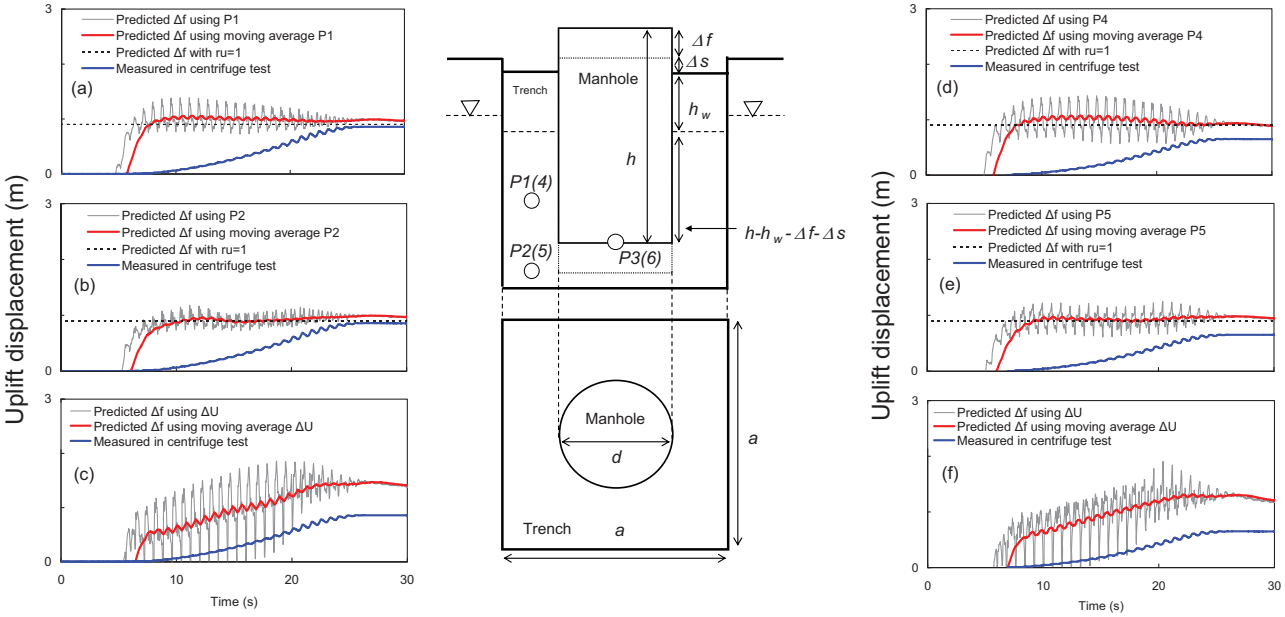
Predicted Δf using P1
Predicted Δf using moving average P1
Predicted Δf with ru=1
Measured in centrifuge test
(a)
Predicted Δf using P2
Predicted Δf using moving average P2
(b)
Predicted Δf using ΔU
Predicted Δf using moving average ΔU
(c)
Uplift displacement (m)
Time (s)
P1(4)
P2(5)
P3(6)
Predicted Δf using P4
Predicted Δf using moving average P4
(d)
Predicted Δf using P5
Predicted Δf using moving average P5
(e)
(f)

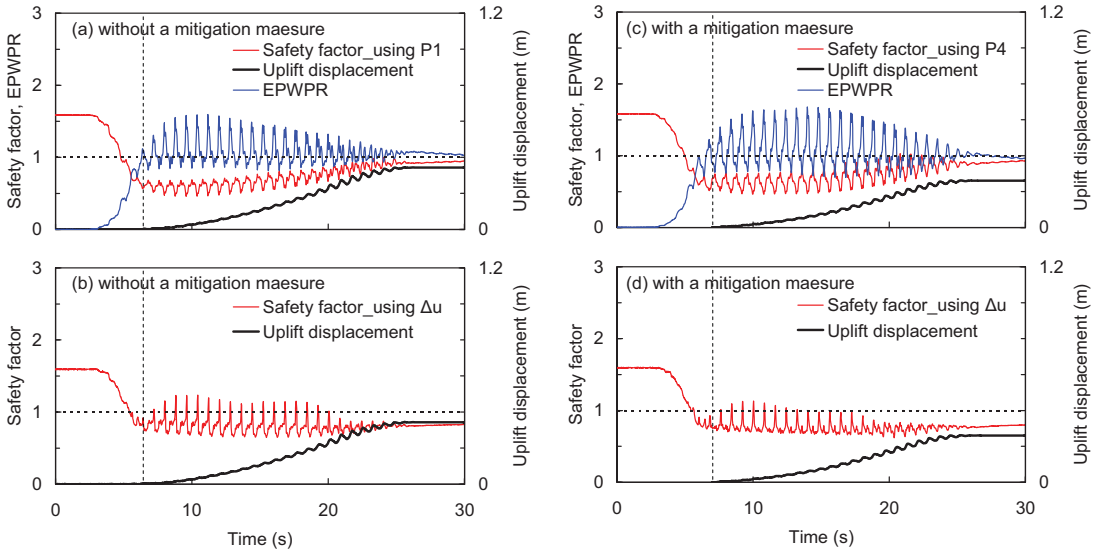
(a) without a mitigation maesure
Safety factor_using P1
Uplift displacement
EPWPR
Safety factor, EPWPR
Uplift displacement (m)
(c) with a mitigation maesure
Safety factor_using P4
(b) without a mitigation maesure
Safety factor_using Δu
Safety factor
(d) with a mitigation maesure
Time (s)

CS15

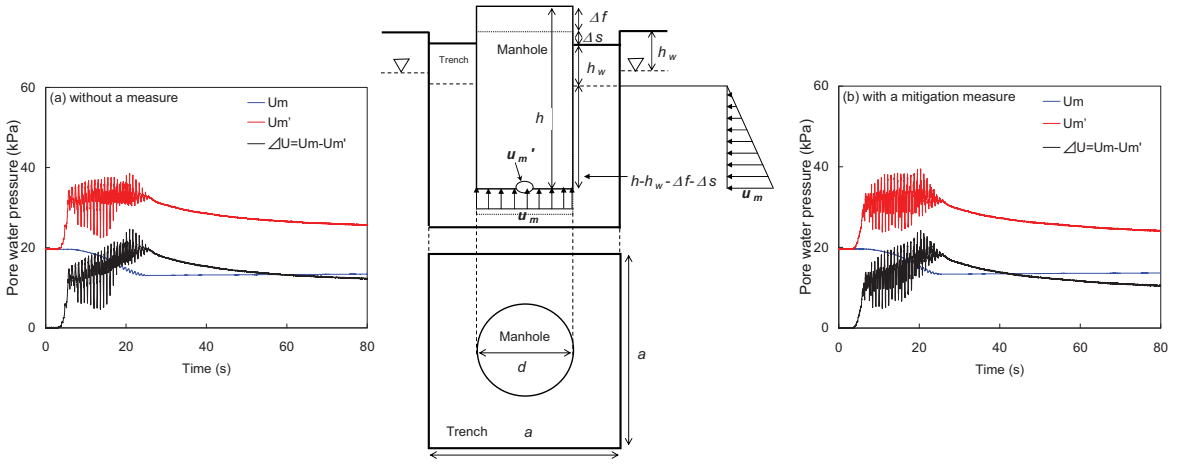
(a) without a measure
Um
Um'
⊿U=Um-Um'
Pore water pressure (kPa)
Time (s)
Trench
Manhole
Δf
Δs
h
h_w
u_m'
u_m
h-h_w-Δf-Δs
d
a
(b) with a mitigation measure

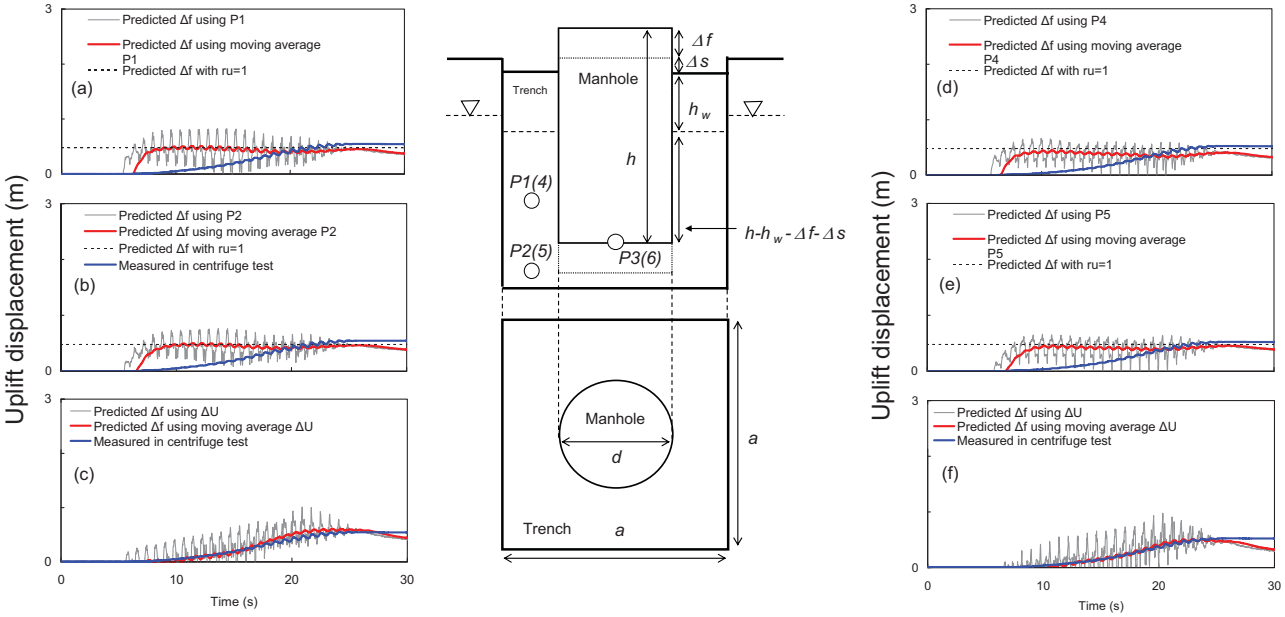
Predicted Δf using P1
Predicted Δf using moving average P1
Predicted Δf with ru=1
(a)
Predicted Δf using P2
Predicted Δf using moving average P2
Measured in centrifuge test
(b)
Predicted Δf using ΔU
Predicted Δf using moving average ΔU
(c)
Uplift displacement (m)
Time (s)
Trench
Manhole
P1(4)
P2(5)
P3(6)
Predicted Δf using P4
Predicted Δf using moving average P4
(d)
Predicted Δf using P5
Predicted Δf using moving average P5
(e)
(f)

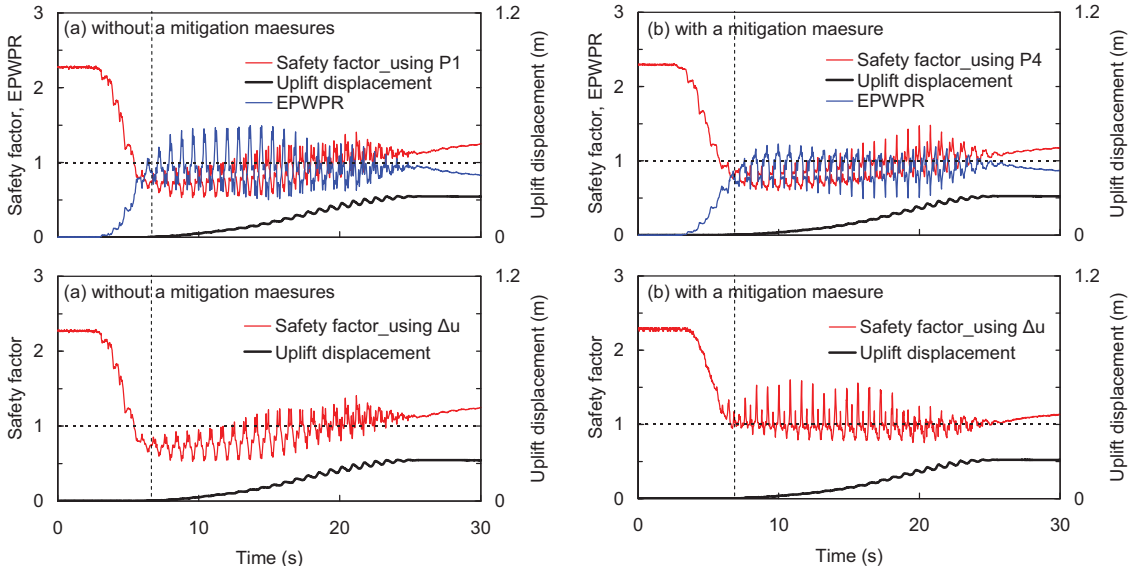
(a) without a mitigation maesures
Safety factor_using P1
Uplift displacement
EPWPR
Safety factor, EPWPR
Uplift displacement (m)
(b) with a mitigation maesure
Safety factor_using P4
Safety factor_using Δu
Safety factor
Time (s)

CS16

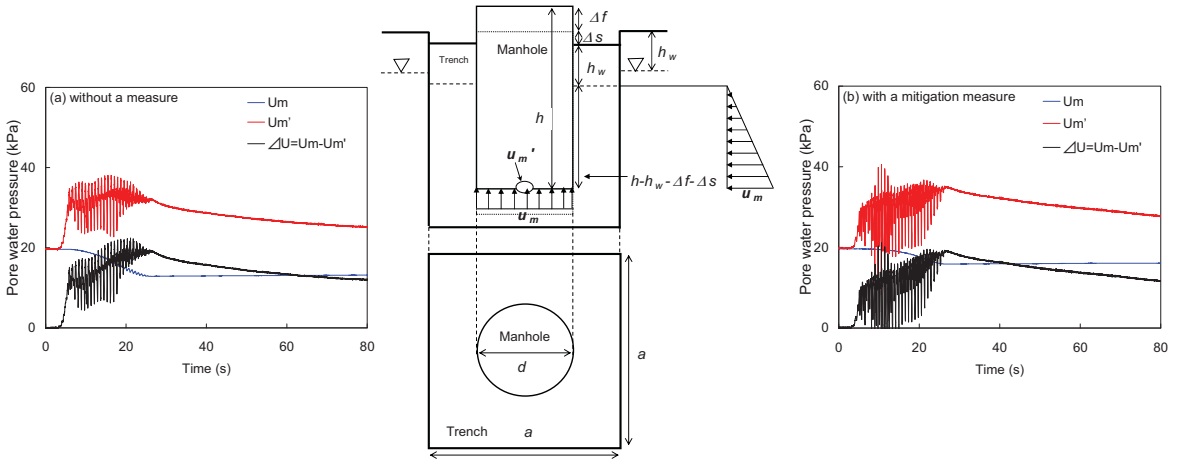
(a) without a measure
Um
Um'
⊿U=Um-Um'
Pore water pressure (kPa)
Time (s)
(b) with a mitigation measure
Manhole
Trench
h
h_w
Δf
Δs
u_m'
u_m
h-h_w-Δf-Δs
d
a

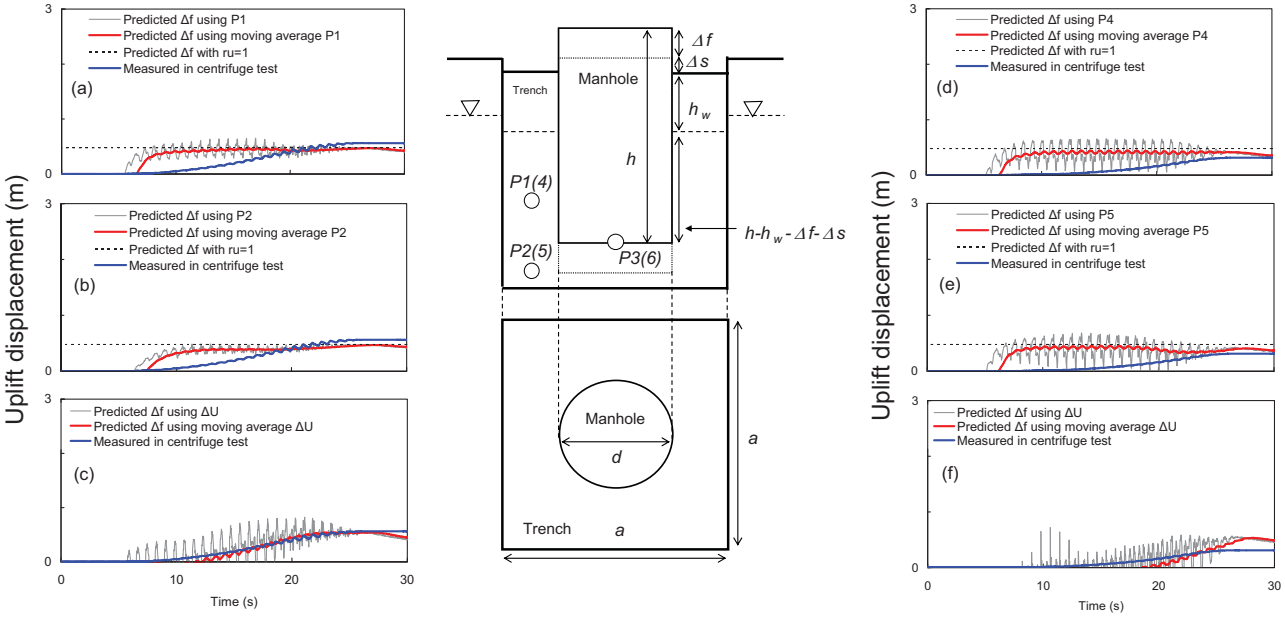
Predicted Δf using P1
Predicted Δf using moving average P1
Predicted Δf with ru=1
Measured in centrifuge test
(a)
Predicted Δf using P2
Predicted Δf using moving average P2
(b)
Predicted Δf using ΔU
Predicted Δf using moving average ΔU
(c)
Uplift displacement (m)
Time (s)
P1(4)
P2(5)
P3(6)
Predicted Δf using P4
Predicted Δf using moving average P4
(d)
Predicted Δf using P5
Predicted Δf using moving average P5
(e)
(f)

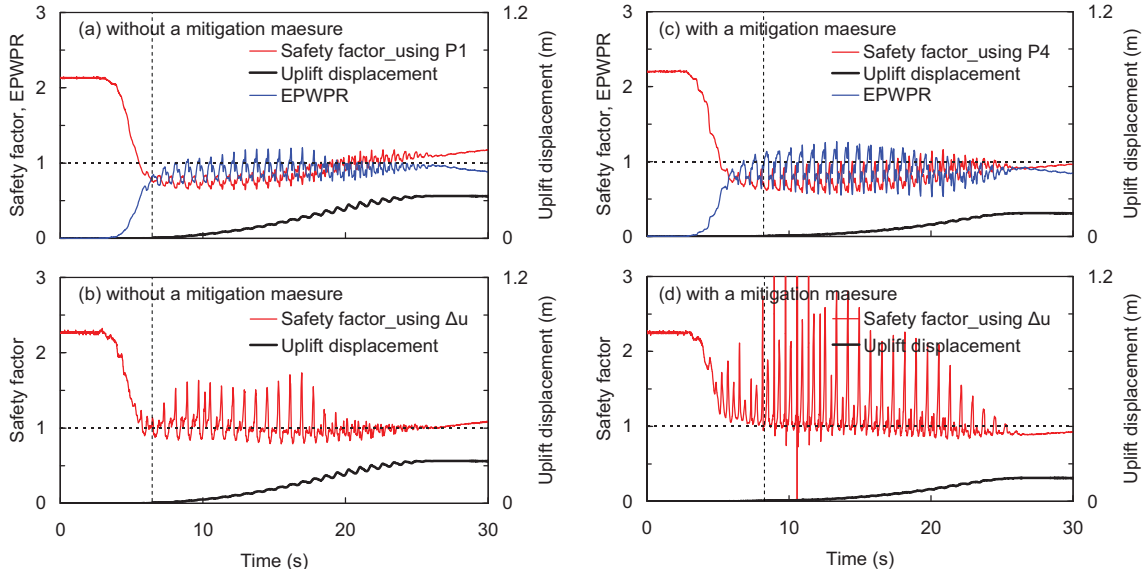
(a) without a mitigation maesure
Safety factor_using P1
Uplift displacement
EPWPR
(c) with a mitigation maesure
Safety factor_using P4
(b) without a mitigation maesure
Safety factor_using Δu
(d) with a mitigation maesure
Safety factor, EPWPR
Safety factor
Uplift displacement (m)
Time (s)

CS17

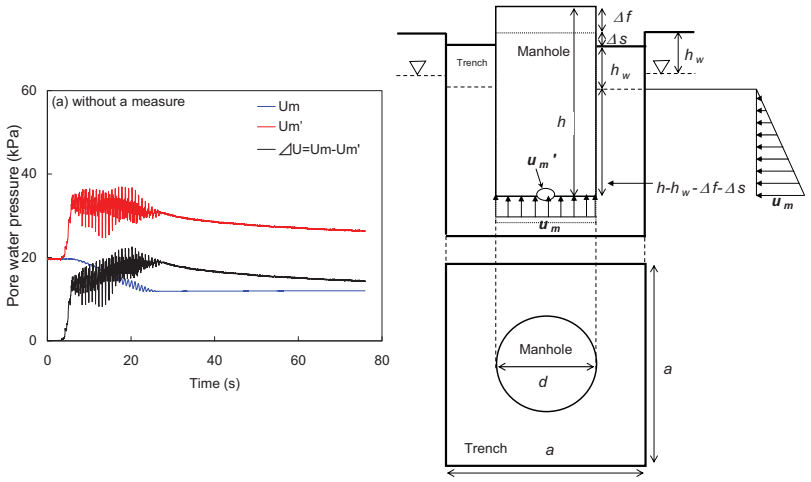
(a) without a measure
Um
Um'
⊿U=Um-Um'
Pore water pressure (kPa)
Time (s)
Trench
Manhole
Δf
Δs
h
h_w
u_m'
u_m
h-h_w-Δf-Δs
d
a

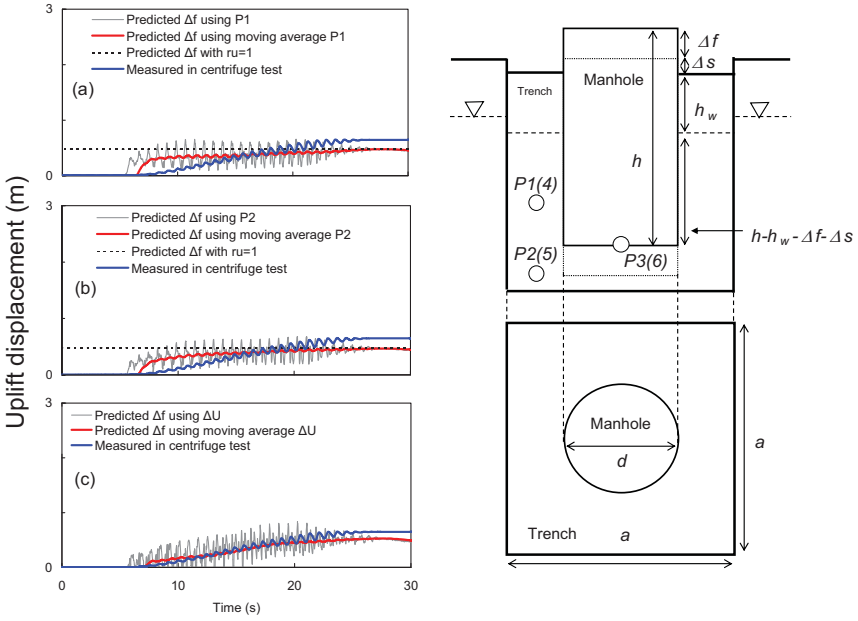
Predicted Δf using P1
Predicted Δf using moving average P1
Predicted Δf with ru=1
Measured in centrifuge test
(a)
Predicted Δf using P2
Predicted Δf using moving average P2
Predicted Δf with ru=1
Measured in centrifuge test
(b)
Predicted Δf using ΔU
Predicted Δf using moving average ΔU
Measured in centrifuge test
(c)
Uplift displacement (m)
Time (s)
Trench
Manhole
Δf
Δs
h
h_w
P1(4)
P2(5)
P3(6)
h-h_w-Δf-Δs
d
a

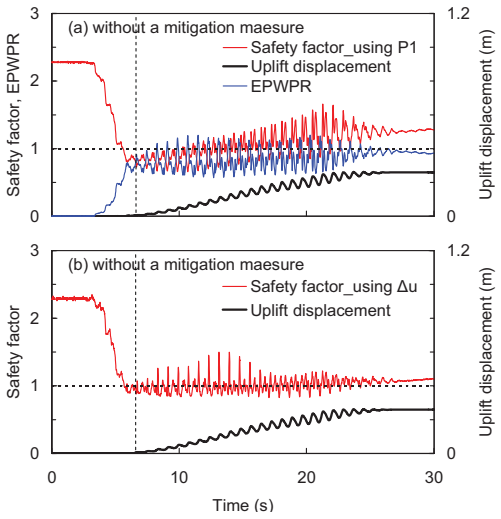
(a) without a mitigation maesure
Safety factor_using P1
Uplift displacement
EPWPR
Safety factor, EPWPR
Uplift displacement (m)
(b) without a mitigation maesure
Safety factor_using Δu
Uplift displacement
Safety factor
Time (s)

CS18

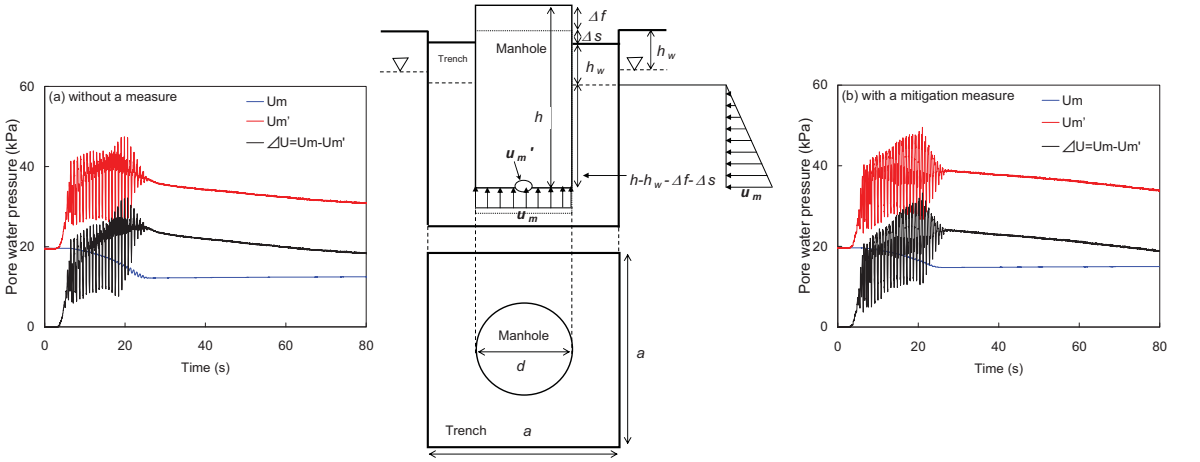
(a) without a measure
Um
Um'
⊿U=Um-Um'
Pore water pressure (kPa)
Time (s)
Trench
Manhole
Δf
Δs
h_w
h
u_m'
u_m
h-h_w-Δf-Δs
d
a
(b) with a mitigation measure

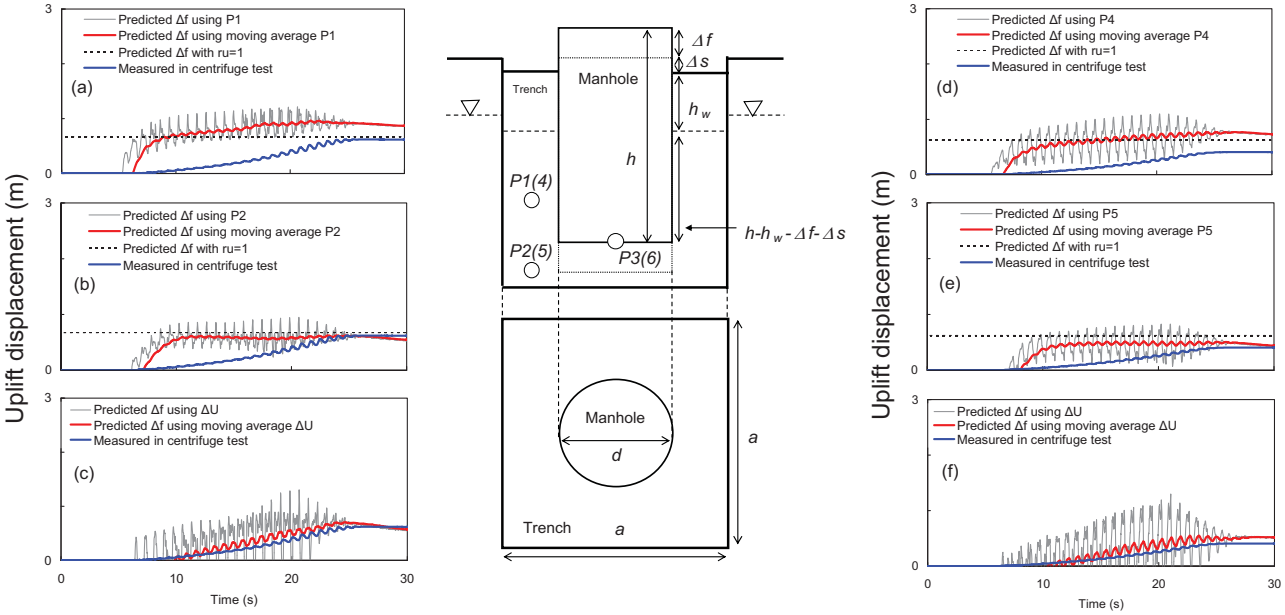
Predicted Δf using P1
Predicted Δf using moving average P1
Predicted Δf with ru=1
Measured in centrifuge test
(a)
Predicted Δf using P2
Predicted Δf using moving average P2
(b)
Predicted Δf using ΔU
Predicted Δf using moving average ΔU
(c)
Uplift displacement (m)
Time (s)
P1(4)
P2(5)
P3(6)
Predicted Δf using P4
Predicted Δf using moving average P4
(d)
Predicted Δf using P5
Predicted Δf using moving average P5
(e)
(f)

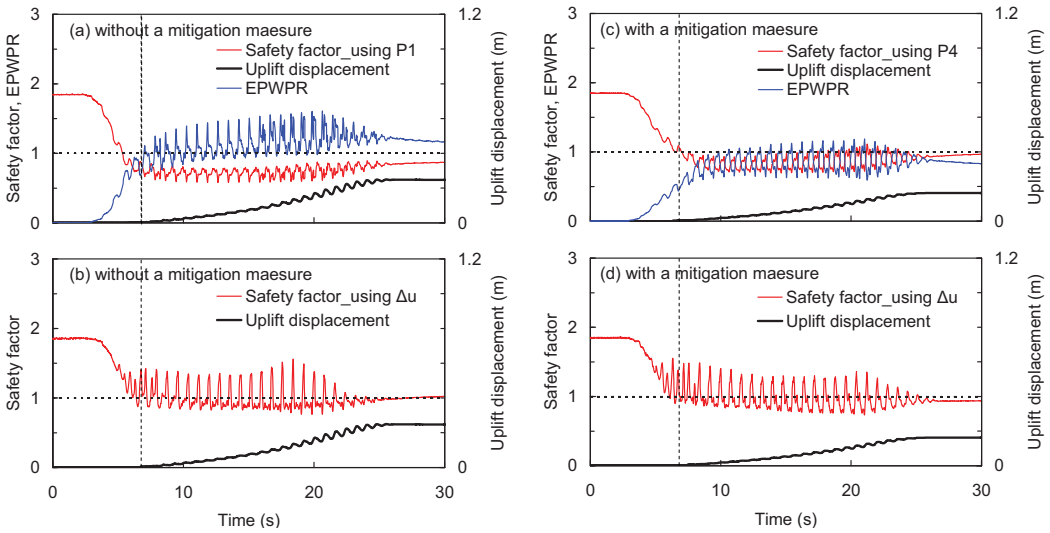
(a) without a mitigation maesure
Safety factor_using P1
Uplift displacement
EPWPR
Safety factor, EPWPR
Uplift displacement (m)
(c) with a mitigation maesure
Safety factor_using P4
(b) without a mitigation maesure
Safety factor_using Δu
Safety factor
(d) with a mitigation maesure
Time (s)

CS19

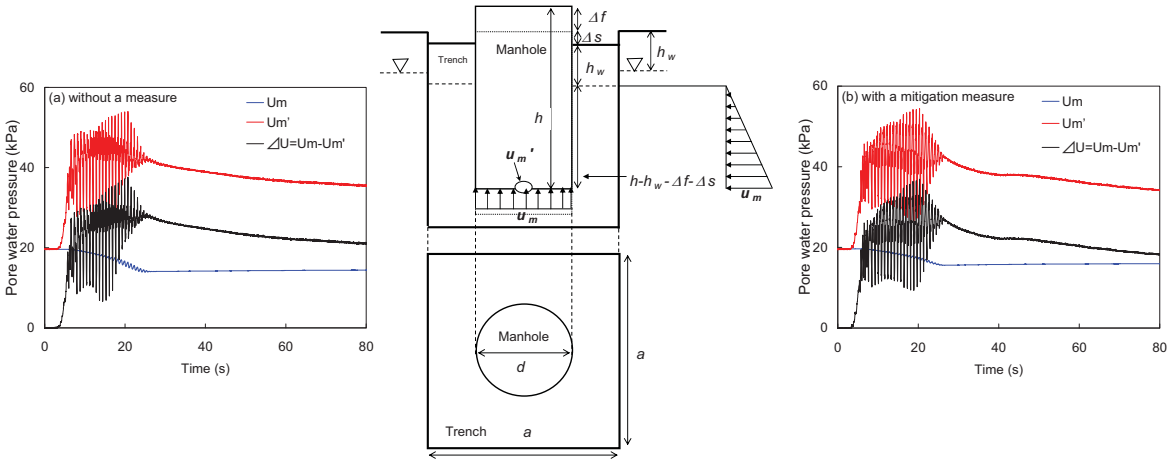
(a) without a measure
Um
Um'
⊿U=Um-Um'
Pore water pressure (kPa)
Time (s)
Trench
Manhole
Δf
Δs
h
h_w
u_m'
u_m
h-h_w-Δf-Δs
d
a
(b) with a mitigation measure

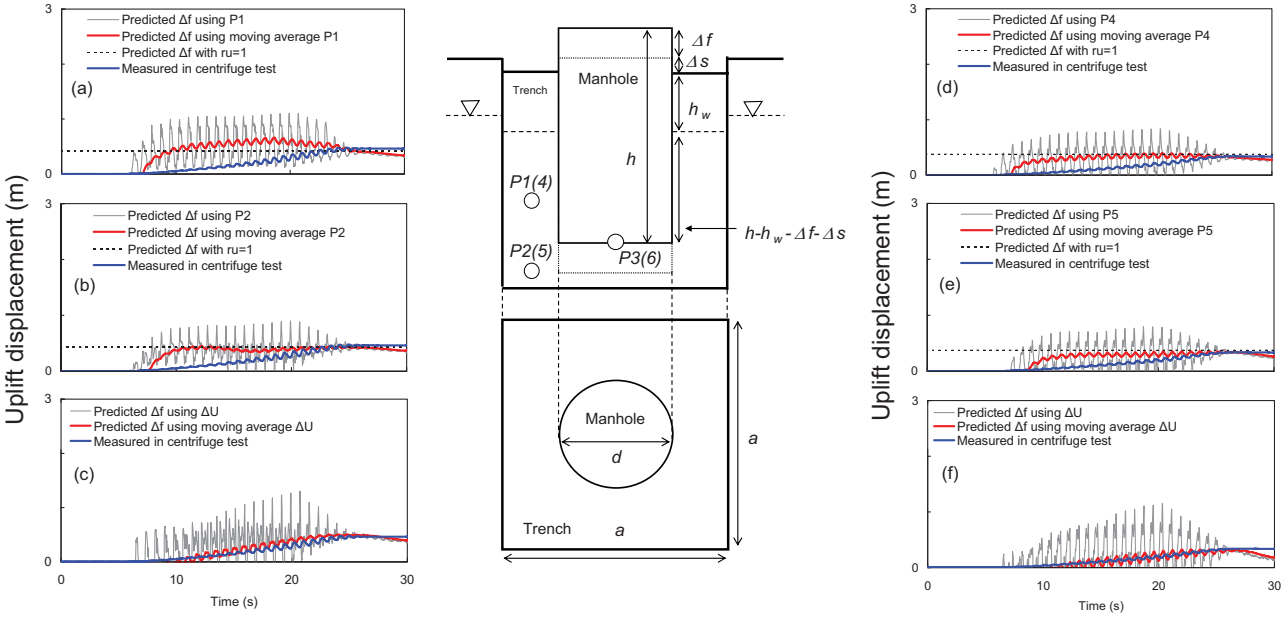
Predicted Δf using P1
Predicted Δf using moving average P1
Predicted Δf with ru=1
Measured in centrifuge test
(a)
Predicted Δf using P2
(b)
Predicted Δf using ΔU
Predicted Δf using moving average ΔU
(c)
Uplift displacement (m)
Time (s)
Trench
Manhole
P1(4)
P2(5)
P3(6)
Predicted Δf using P4
(d)
Predicted Δf using P5
(e)
(f)

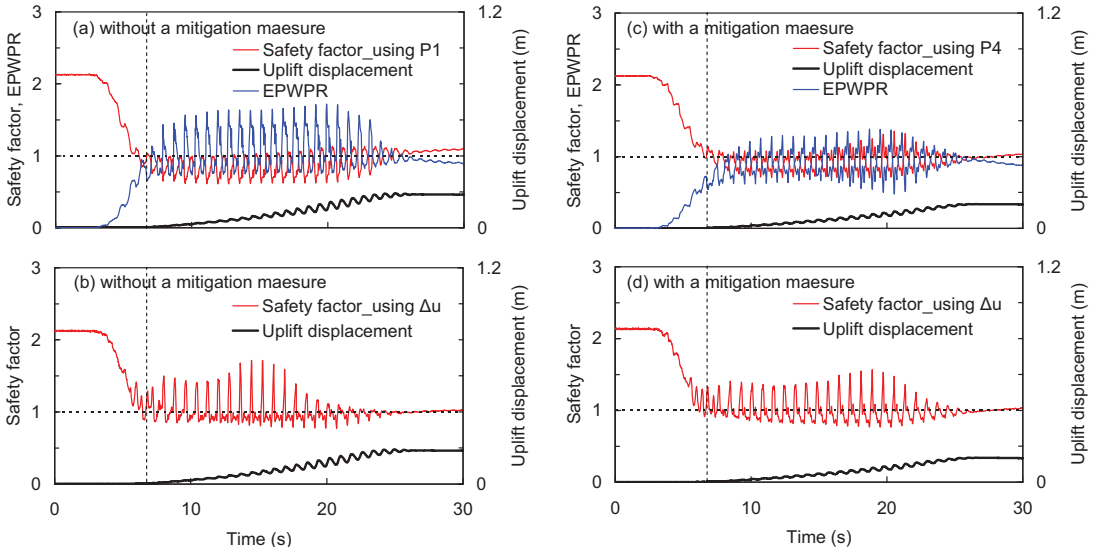
(a) without a mitigation maesure
Safety factor_using P1
Uplift displacement
EPWPR
Safety factor, EPWPR
Uplift displacement (m)
(c) with a mitigation maesure
Safety factor_using P4
(b) without a mitigation maesure
Safety factor_using Δu
Safety factor
(d) with a mitigation maesure
Time (s)

CS20

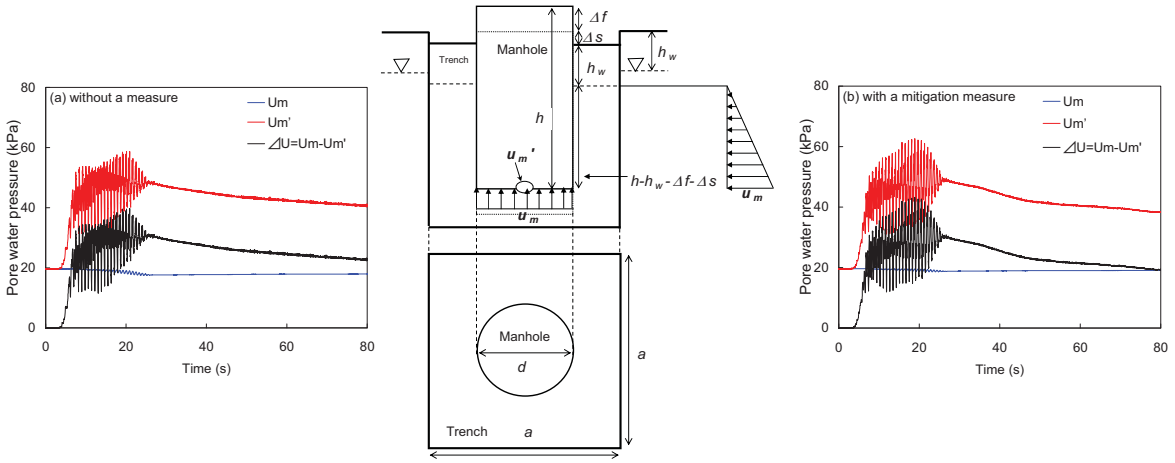
(a) without a measure
Um
Um'
⊿U=Um-Um'
Pore water pressure (kPa)
Time (s)
Trench
Manhole
Δf
Δs
h
h_w
u_m'
u_m
h-h_w-Δf-Δs
d
a
(b) with a mitigation measure

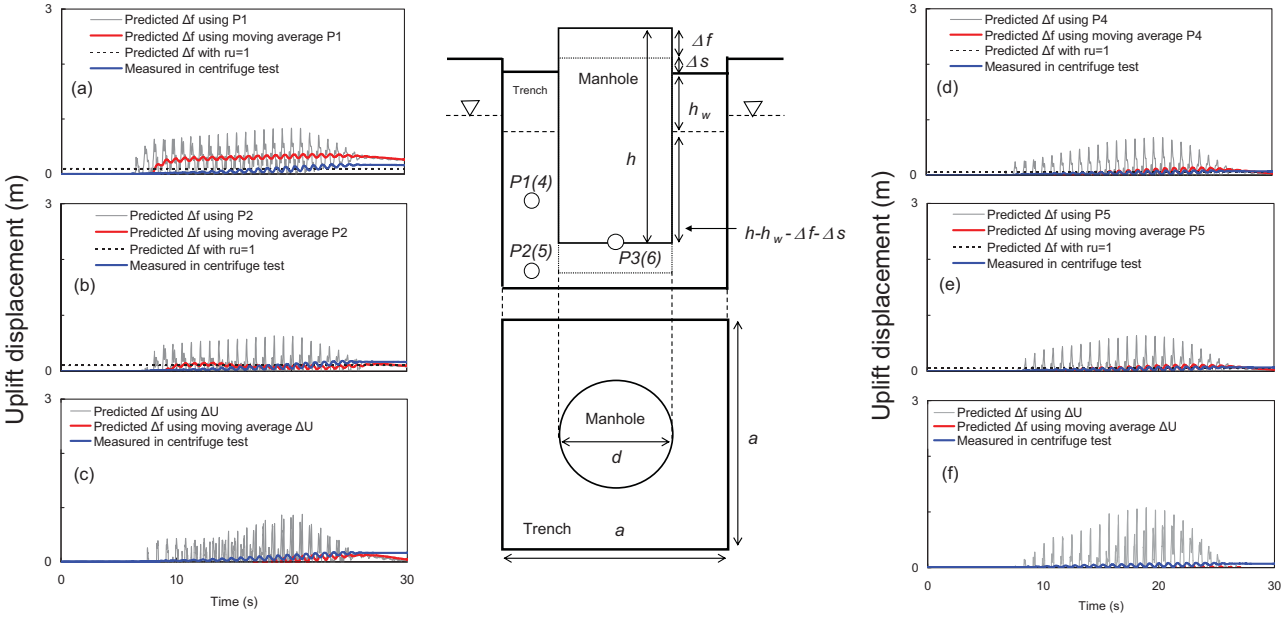
Predicted Δf using P1
Predicted Δf using moving average P1
Predicted Δf with ru=1
Measured in centrifuge test
(a)
Predicted Δf using P2
Predicted Δf using moving average P2
(b)
Predicted Δf using ΔU
Predicted Δf using moving average ΔU
(c)
Uplift displacement (m)
Time (s)
Trench
Manhole
P1(4)
P2(5)
P3(6)
Predicted Δf using P4
Predicted Δf using moving average P4
(d)
Predicted Δf using P5
Predicted Δf using moving average P5
(e)
(f)

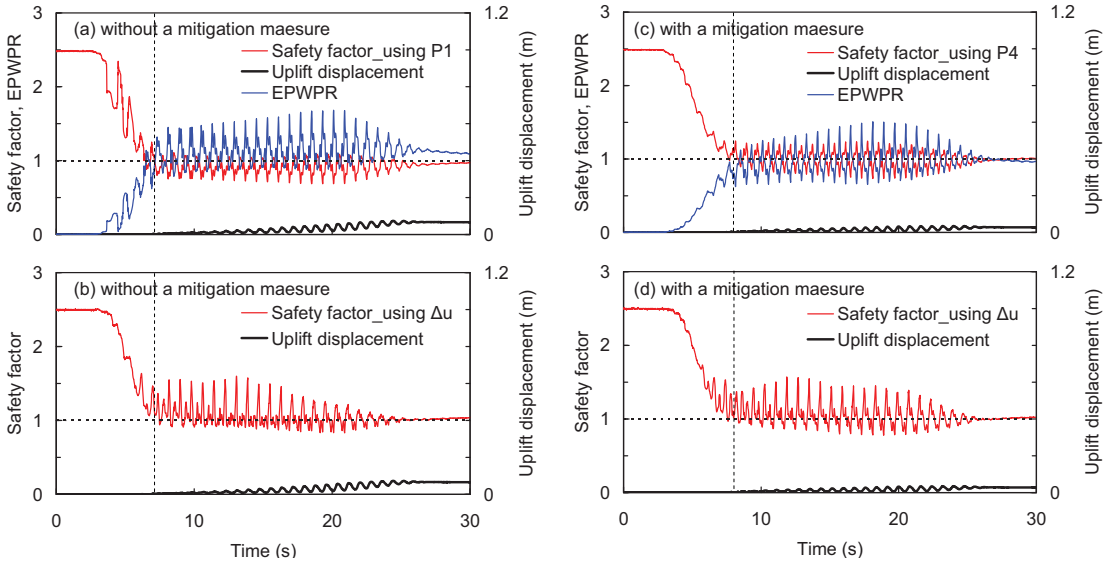
(a) without a mitigation maesure
Safety factor_using P1
Uplift displacement
EPWPR
(b) without a mitigation maesure
Safety factor_using Δu
(c) with a mitigation maesure
Safety factor_using P4
(d) with a mitigation maesure
Safety factor, EPWPR
Safety factor
Uplift displacement (m)
Time (s)

CS21

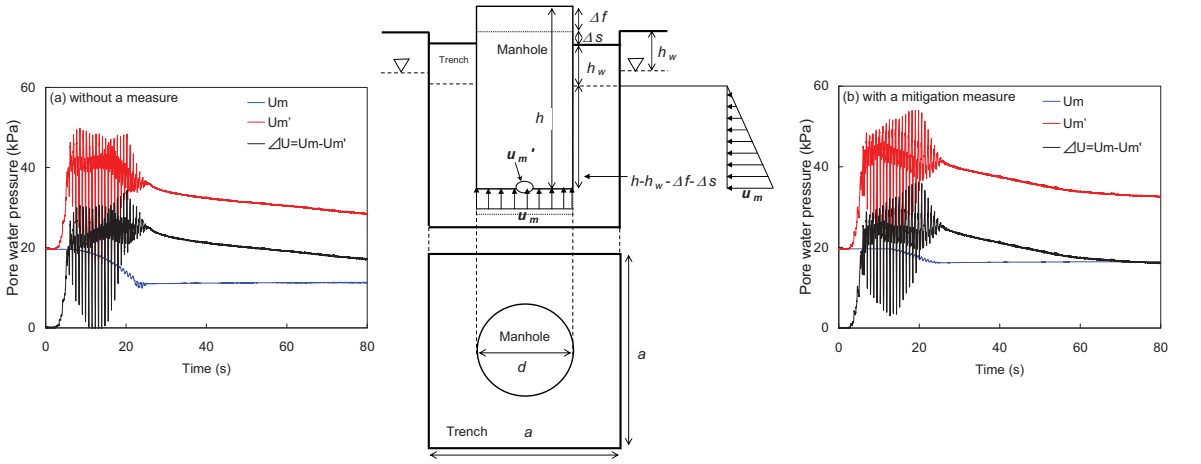
(a) without a measure
Um
Um'
⊿U=Um-Um'
Pore water pressure (kPa)
Time (s)
Trench
Manhole
Δf
Δs
h
h_w
u_m'
u_m
h-h_w-Δf-Δs
d
a
(b) with a mitigation measure

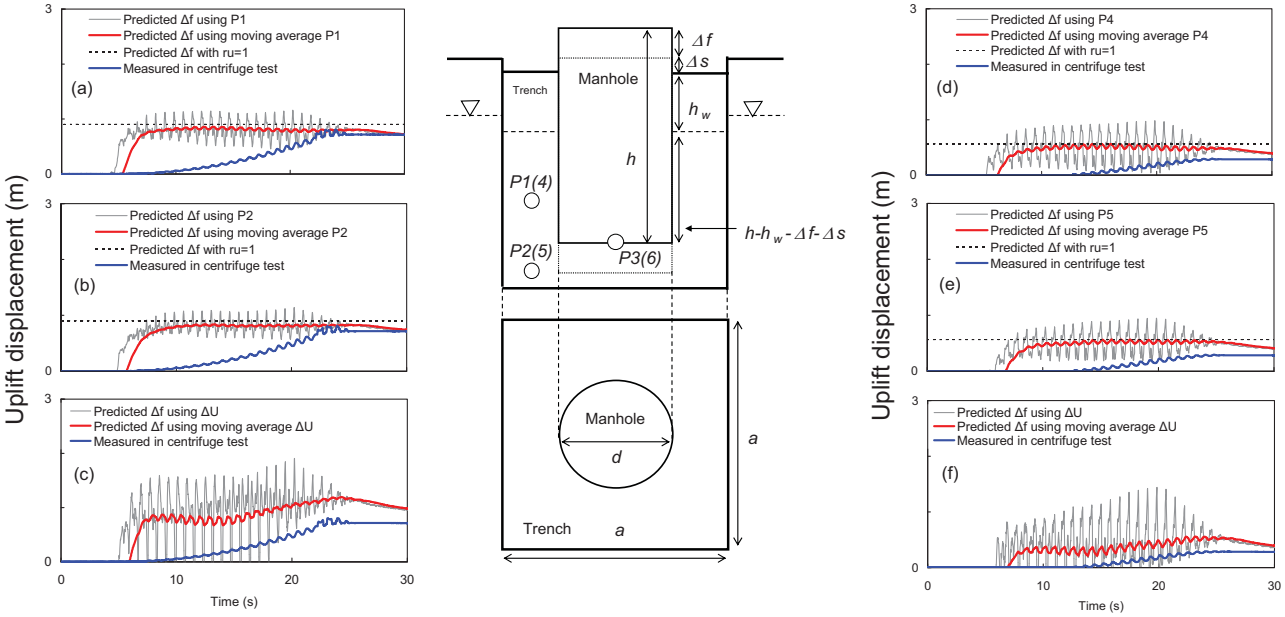
Predicted Δf using P1
Predicted Δf using moving average P1
Predicted Δf with ru=1
Measured in centrifuge test
(a)
Predicted Δf using P2
Predicted Δf using moving average P2
(b)
Predicted Δf using ΔU
Predicted Δf using moving average ΔU
(c)
Uplift displacement (m)
Time (s)
Trench
Manhole
P1(4)
P2(5)
P3(6)
Predicted Δf using P4
Predicted Δf using moving average P4
(d)
Predicted Δf using P5
Predicted Δf using moving average P5
(e)
(f)

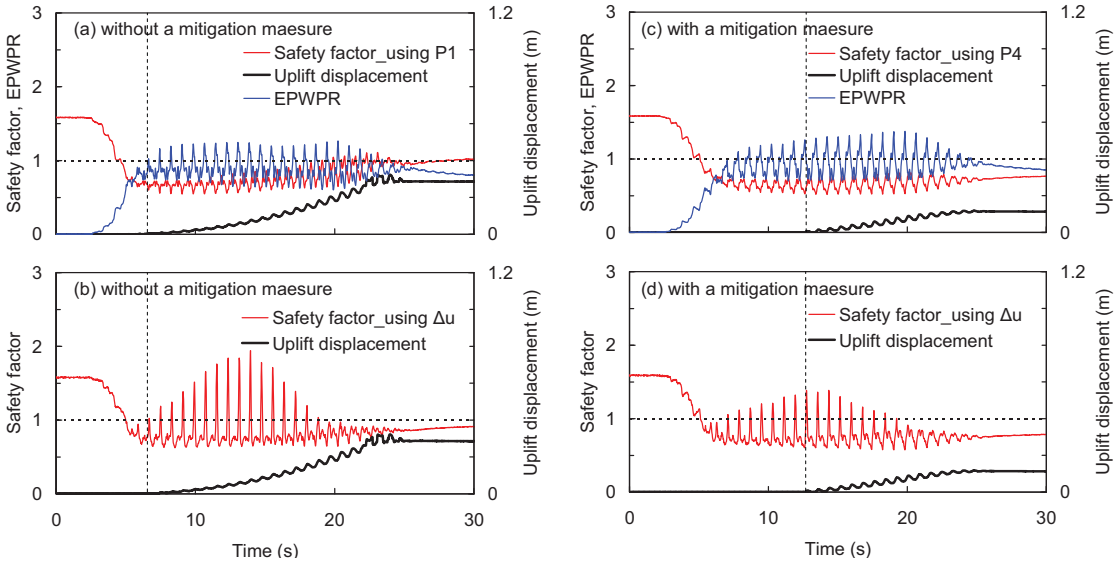
(a) without a mitigation maesure
Safety factor_using P1
Uplift displacement
EPWPR
(c) with a mitigation maesure
Safety factor_using P4
(b) without a mitigation maesure
Safety factor_using Δu
(d) with a mitigation maesure
Safety factor, EPWPR
Safety factor
Uplift displacement (m)
Time (s)

CS22

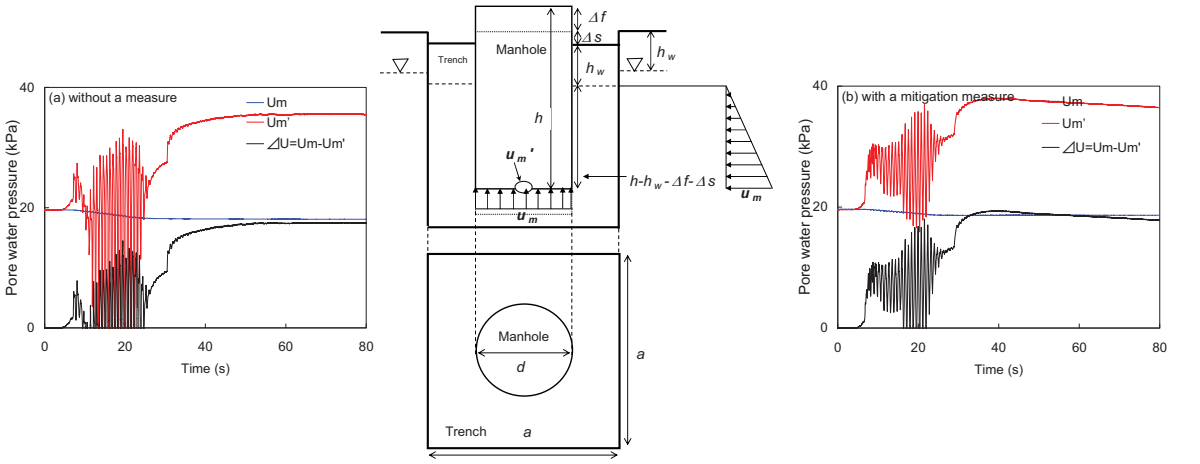
(a) without a measure
Um
Um'
⊿U=Um-Um'
Pore water pressure (kPa)
Time (s)
Trench
Manhole
Δf
Δs
h
h_w
u_m'
u_m
h-h_w-Δf-Δs
d
a
(b) with a mitigation measure

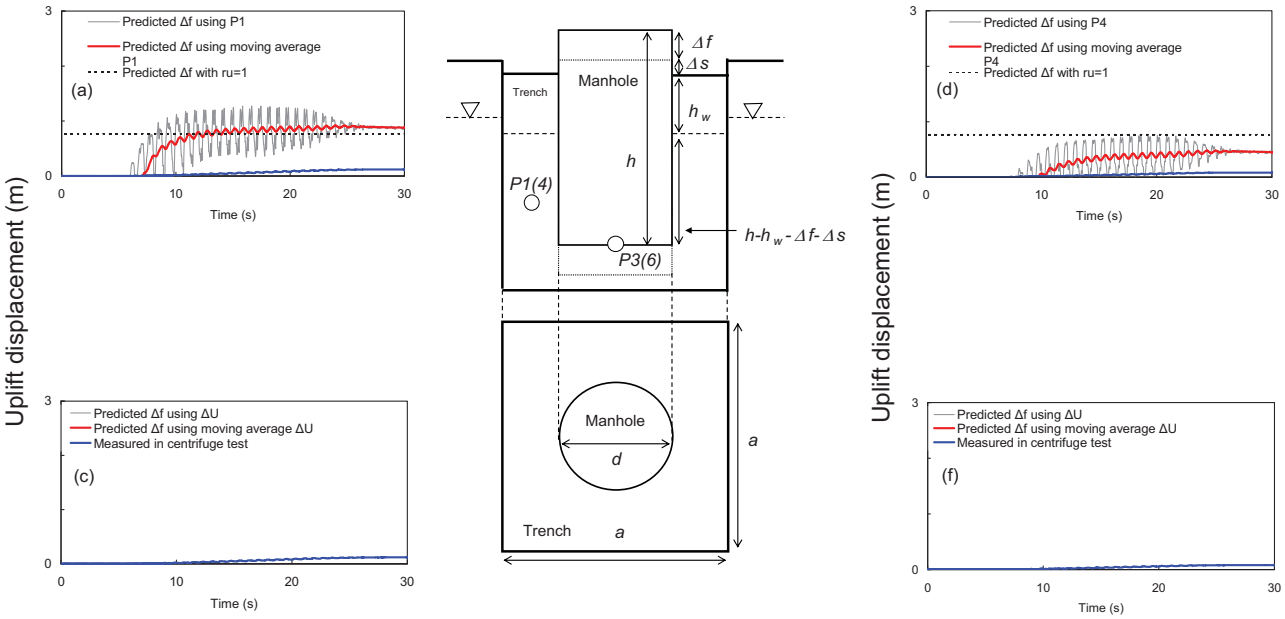
Uplift displacement (m)
Predicted Δf using P1
Predicted Δf using moving average
Predicted Δf with ru=1
(a)
Predicted Δf using ΔU
Predicted Δf using moving average ΔU
Measured in centrifuge test
(c)
Time (s)
Trench
Manhole
P1(4)
P3(6)
h
h_w
Δf
Δs
h-h_w-Δf-Δs
d
a
Predicted Δf using P4
(d)
(f)

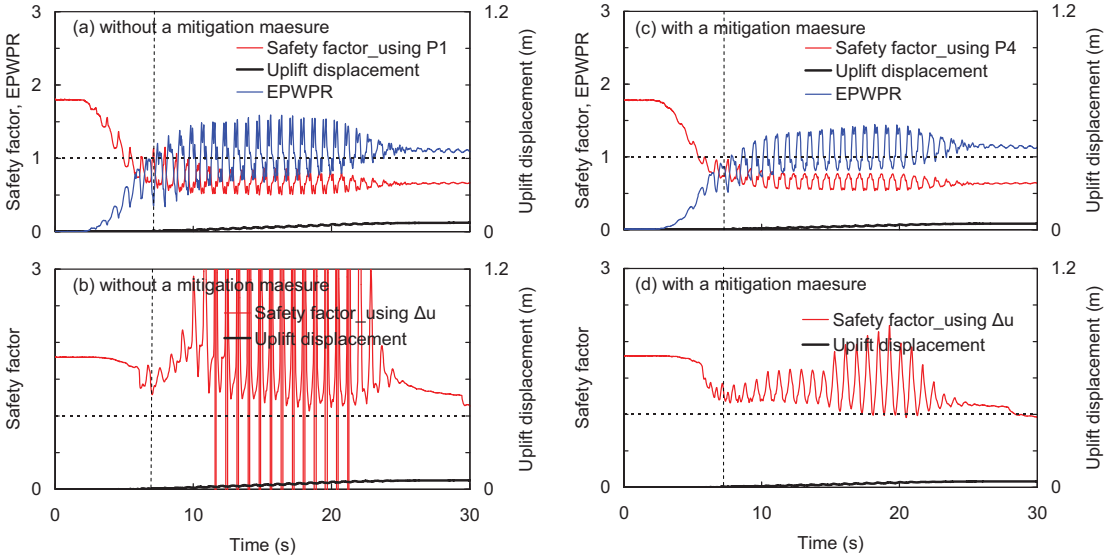
(a) without a mitigation maesure
Safety factor_using P1
Uplift displacement
EPWPR
Safety factor, EPWPR
Uplift displacement (m)
(c) with a mitigation maesure
Safety factor_using P4
(b) without a mitigation maesure
Safety factor_using Δu
Safety factor
(d) with a mitigation maesure
Time (s)

APPENDIX C
Viscotester (RION, VT-03F)

● Specifications

Measurement range	No. 4 rotor: 2 to 33 mPa·s No. 5 rotor: 15 to 150 mPa·s No. 3 rotor: 50 to 300 mPa·s
Sample fluid capacity	Approx. 460 mL (with Cup A or Cup B)
Measurement accuracy	Within ±5% of scale maximum (using supplied cup A or cup B) Scale calibrated acoording to JIS Z 8809: 2000 viscosity calibration standard
Rotor speed	62.5 rpm
Power requirements	6 V DC (four IEC R6P batteries) or AC adapter VA-05A or B*[1] Current consumption at maximum torque approx. 100mA
Dimensions	98 (W) × 181 (D) × 40 (H) mm (without protruding parts)
Weight	Approx. 570 g (without batteries)

*1 VA-05A, 120 V

● Rotors and Cups (unit: mm)

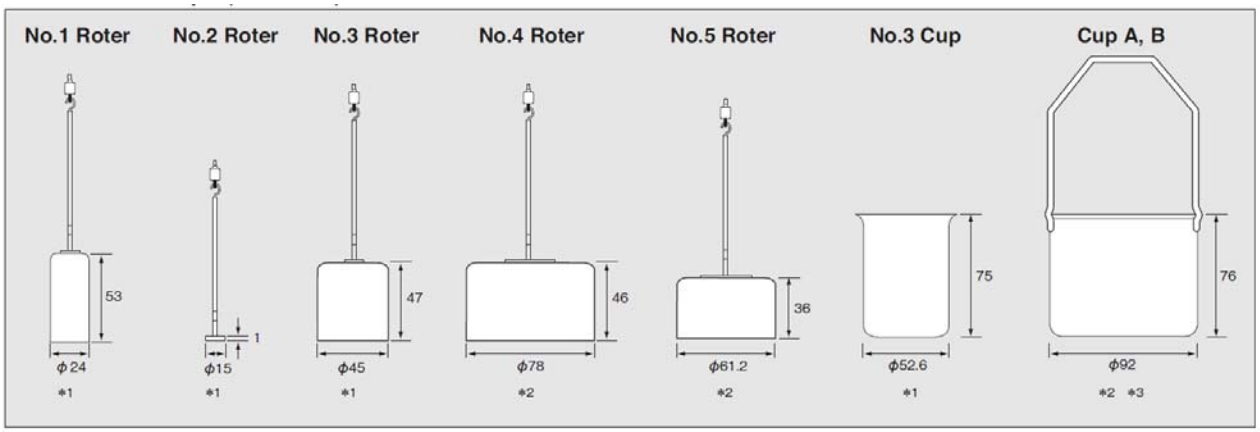

*1 Material: Stainless steel *2 Material: Aluminate *3 Cup B has a 30 mm diameter hole at the bottom. Use Cup B to measure viscosity by directly by dipping Rotor in the fluid.

Accelerometer (SSK, A6H-50)

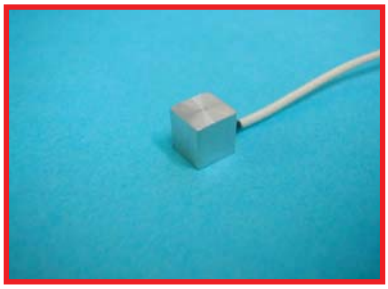

A6H

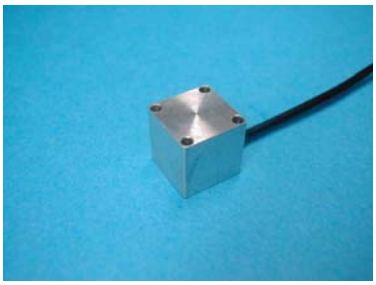

A10H

Features:
- Micro type
- High output(high sensitivity)
- High resolution
- From DC to high frequency
- Very small phase shift

Overview: The A-H series accelerometers are high G type accelerometers designed by integrated SSK transducer technology and used mainly for centrifugal loading test and also suitable for impact test in the engineering works and construction fields.

Specifications:

	±50G	±100G	±200G	±500G	±1000G	±2000G	±5000G
Model A6H	A6H-50	A6H-100	A6H-200	A6H-500	A6H-1000	A6H-2000	A6H-5000
Model A10H	A10H-50	A10H-100	A10H-200	A10H-500	A10H-1000	A10H-2000	A10H-5000
Natural oscillation Frequency	1KHz	1.4KHz	2KHz	3.2KHz	4.4KHz	6.2KHz	10KHz

Output voltage	100mVRO	option: An output for strain gauge of 5000μor 10,000μRO
Overlord	200%RO	is available.
Non-linearity(& hysteresis)	1%RO	
Reproducibility	0.2%RO	
Temperature characteristic	0.05%RO/℃(0 to 40℃)	option:0.02%RO/℃ is available.
Operating temperature range	-15℃ to +75℃	
Input/output resistance	500Ω	
Bridge voltage	6VDC(8VDC MAX)	
Cord length	3m with exposed ends	option: A type with a cord extension connector is available.

Measuring Blocks:

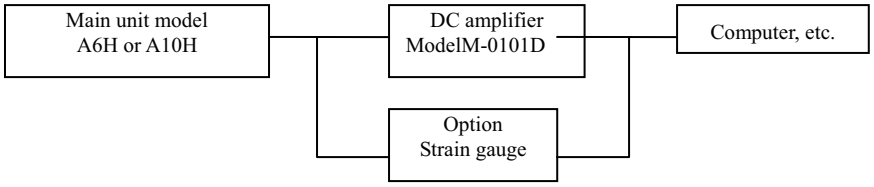

External View:

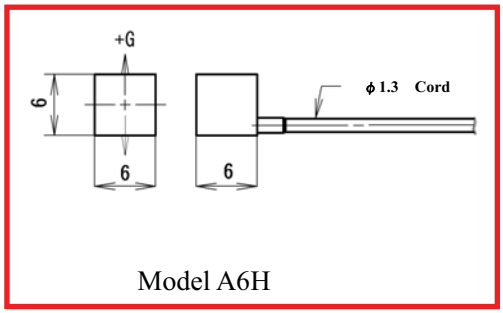

Model A6H

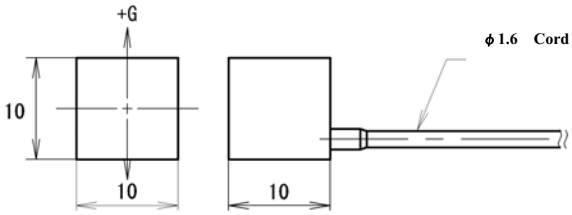

Model A10H

Laser displacement transducer (Keyence, LBP-080)

LB-080

仕様

種類		ロングレンジタイプ
型式	センサヘッド	LB-080
	アンプユニット	LB-1100
基準距離		80mm
測定範囲		±15mm
光源	種類	赤色半導体レーザ
	波長	670nm（可視光） JISクラス1M
	出力	最大2.5mW
スポット径（基準距離にて）		1×2mm
直線性（白紙にて）		0.25% of F.S.
分解能（白紙で基準距離にて）		8μm（LO時）
アナログ出力	電圧出力	±5V （3mm/V）
	インピーダンス	100Ω
	電流出力	4-20mA（適用負荷350ΩMAX）
アラーム出力		NPNオープンコレクタ最大100mA（40V以下） 残留電圧1V以下（N.C）
応答性		915Hz（HIGH時）/36Hz（MID時）/9Hz（LO時） 各－3dBにて
副機能		オートゼロ/応答性切換/オートレスポンスコントロール/相互干渉防止回路（30Hz）内蔵
定格	電源電圧	AC100～240V±10% 50/60Hz
	消費電力	約15VA
温度特性	センサヘッド	0.02% of F.S./℃
	アンプユニット	0.02% of F.S./℃
耐環境性	使用周囲照度	白熱ランプ・蛍光灯：2500lx以下
	使用周囲温度	アンプユニット0～＋50℃ センサヘッド0～＋45℃
	使用周囲湿度	35～85%RH（結露しないこと）
	耐振動	10～55Hz 複振幅1.5mm X、Y、Z各方向2時間

材質		センサヘッド：アルミダイキャスト アンプユニット：ポリカーボネート
質量（コード含む）	センサヘッド	約170g
	アンプユニット	約530g

外形寸法図

単位：mm

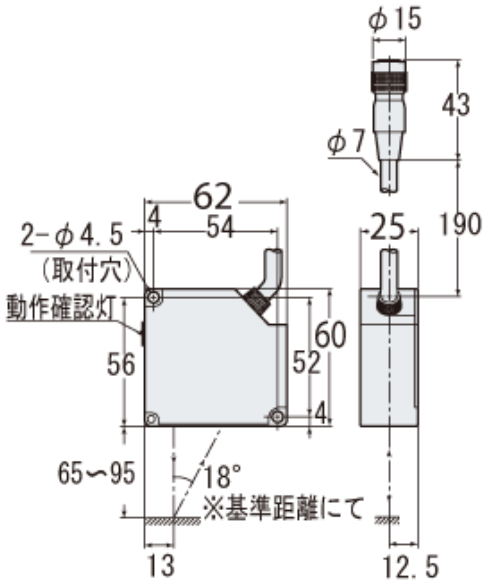

Pore water transducer (SSK, P306A-2 and P306AV-2)


P306A


P306AV


P306AVS

Features:
- Micro type
- Low capacity
- High output(high sensitivity)
- High response frequency
- Perfect waterproof structure

Overview: The pore water pressure transducer model P306A(model P306AV)is a pore water pressure transducer designed by integrated SSK transducer technology and provided with many features, being a typical transducer for mock-up experiments which have been widely used for liquefying test, centrifugal loading test, etc. in the engineering works and construction fields.

The standard filter is stainless steel #100 to #300. However, a ceramic filter is also available if desired.

Specifications:

	0.1Kgf/cm²	0.2Kgf/cm²	0.5Kgf/cm²	1Kgf/cm²	2Kgf/cm²	5Kgf/cm²	10Kgf/cm²	20Kgf/cm²
Model P306A	P306A-01	P306A-02	P306A-05	P306A-1	P306A-2	P306A-5	P306A-10	P306A-20
Model P306AV	P306AV-01	P306AV-02	P306AV-05	P306AV-1	P306AV-2	P306AV-5	P306AV-10	P306AV-20
Model P306AVS	P306AVS-01	P306AVS-02	P306AVS-05	P306AVS-1	P306AVS-2	P306AVS-5	P306AVS-10	P306AVS-20
Natural oscillation frequency	3.5KHz	4.9KHz	7.8KHz	11KHz	15KHz	24KHz	34KHz	48KHz

* A high rated capacity type is also available.(Consult with us.)

Output voltage	100mVRO	option: An output for strain gauge of 5000μor 10,000μRO
Overlord	150%RO	is available.
Non-linearity(& hysteresis)	0.5%RO	
Reproducibility	0.2%RO	
Temperature characteristic	0.05%RO/℃(0 to 40℃)	option:0.02%RO/℃ is available.
Operating temperature range	-15℃ to +75℃	
Input/output resistance	500Ω	
Bridge voltage	6VDC(8VDC MAX)	
Cord length	3m with exposed ends	option: A type with a cord extension connector is available.

Measuring Blocks:

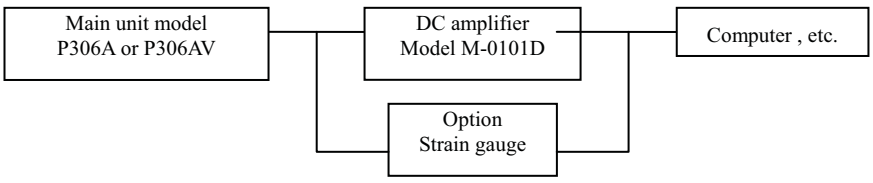

External View: